

Summer 2007

# A finite difference method for studying thermal deformation in a three-dimensional microsphere exposed to ultrashort-pulsed lasers

Xudong Du  
*Louisiana Tech University*

Follow this and additional works at: <https://digitalcommons.latech.edu/dissertations>



Part of the [Computer Sciences Commons](#), and the [Mechanical Engineering Commons](#)

---

## Recommended Citation

Du, Xudong, "" (2007). *Dissertation*. 491.  
<https://digitalcommons.latech.edu/dissertations/491>

This Dissertation is brought to you for free and open access by the Graduate School at Louisiana Tech Digital Commons. It has been accepted for inclusion in Doctoral Dissertations by an authorized administrator of Louisiana Tech Digital Commons. For more information, please contact [digitalcommons@latech.edu](mailto:digitalcommons@latech.edu).

A FINITE DIFFERENCE METHOD FOR STUDYING THERMAL  
DEFORMATION IN A 3D MICRO-SPHERE EXPOSED  
TO ULTRASHORT-PULSED LASERS

By  
Xudong Du, MS.

A Dissertation Presented in Partial Fulfillment  
of the Requirement for the Degree  
Doctor of Philosophy

COLLEGE OF ENGINEERING AND SCIENCE  
LOUISIANA TECH UNIVERSITY

August 2007

UMI Number: 3270942

### INFORMATION TO USERS

The quality of this reproduction is dependent upon the quality of the copy submitted. Broken or indistinct print, colored or poor quality illustrations and photographs, print bleed-through, substandard margins, and improper alignment can adversely affect reproduction.

In the unlikely event that the author did not send a complete manuscript and there are missing pages, these will be noted. Also, if unauthorized copyright material had to be removed, a note will indicate the deletion.

**UMI**<sup>®</sup>

---

UMI Microform 3270942

Copyright 2007 by ProQuest Information and Learning Company.

All rights reserved. This microform edition is protected against unauthorized copying under Title 17, United States Code.

ProQuest Information and Learning Company  
300 North Zeeb Road  
P.O. Box 1346  
Ann Arbor, MI 48106-1346

LOUISIANA TECH UNIVERSITY

THE GRADUATE SCHOOL

June 7th, 2007

Date

We hereby recommend that the dissertation prepared under our supervision  
by XUDONG DU

entitled A FINITE DIFFERENCE METHOD FOR STUDYING THERMAL  
DEFORMATION IN A 3D MICRO-SPHERE EXPOSED  
TO ULTRASHORT-PULSED LASERS

be accepted in partial fulfillment of the requirements for the Degree of  
DOCTOR OF PHILOSOPHY

Weizhong Dai

Supervisor of Dissertation Research

Richard J. Greechie

Head of Department

Computational Analysis Modeling  
Department

Recommendation concurred in:

Raja Harman

Richard J. Greechie

Adri P.

Advisory Committee

Approved:

Pankaj Suman  
Director of Graduate Studies

Approved:

Terry M. Connelly  
Dean of the Graduate School

Stan Nagp  
Dean of the College

## ABSTRACT

Ultrashort-pulsed lasers with pulse durations on the order of sub-picoseconds to femtoseconds possess the capabilities in limiting the undesirable spread of the thermal process zone in a heated sample which have been attracting worldwide interest in science and engineering. Success of ultrashort-pulsed lasers in real application relies on: (1) well characterized pulse width, intensity and experimental techniques; (2) reliable microscale heat transfer models; and (3) prevention of thermal damage. Laser damage by ultrashort-pulsed lasers occurs after the heating pulse is over since the pulse duration time is extremely short and the heat flux is essentially limited to the region within the electron thermal diffusion length. In contrast with long-pulse laser, laser damage is caused by melting temperature resulting from continuous pulse of energy. This dissertation investigates the mathematical model of heat transport phenomenon in a 3D micro-sphere exposed to ultrashort-pulsed lasers and presents a numerical method for studying thermal deformations. The method is obtained based on the parabolic two-step model and implicit finite difference schemes on a staggered grid. It accounts for the coupling effect between lattice temperature and strain rate, as well as for the hot electron blast effect in momentum transfer. In particular, a fourth-order compact scheme is developed for evaluating those stress derivatives in the dynamic equations of motion. It should be pointed out that micro-spheres are considered because they are of interest related to micro resonators in optical applications, such as ultra-low-threshold lasing, sensing,

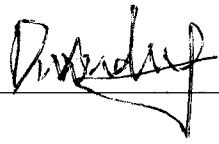
optoelectronic microdevices, cavity quantum electrodynamics and their potential in quantum information processing.

The numerical method is tested for its applicability by investigating the temperature rise and deformation in five examples, which are (1) a portion of the upper hemisphere is irradiated by a single-pulse laser, (2) portions of both the upper hemisphere and the lower hemisphere are irradiated by a single-pulse laser, (3) the upper hemisphere is irradiated by a single-pulse laser, (4) a portion of the upper hemisphere is irradiated by a double-pulse laser, and (5) portions of both the upper hemisphere and the lower hemisphere are irradiated by a double-pulse laser. Results show that no non-physical oscillations appear in the solutions and the micro-sphere expands when it is irradiated by ultrashort-pulsed lasers.

## APPROVAL FOR SCHOLARLY DISSEMINATION

The author grants to the Prescott Memorial Library of Louisiana Tech University the right to reproduce, by appropriate methods, upon request, any or all portions of this Dissertation. It is understood that "proper request" consists of the agreement, on the part of the requesting party, that said reproduction is for his personal use and that subsequent reproduction will not occur without written approval of the author of this Dissertation. Further, any portions of the Dissertation used in books, papers, and other works must be appropriately referenced to this Dissertation.

Finally, the author of this Dissertation reserves the right to publish freely, in the literature, at any time, any or all portions of this Dissertation.

Author 

Date 06/16/2007

## TABLE OF CONTENTS

ABSTRACT.....	iii
TABLE OF CONTENTS.....	vi
LIST OF TABLES.....	viii
LIST OF FIGURES.....	ix
NOMENCLATURE.....	xv
ACKNOWLEDGEMENTS.....	xix
CHAPTER ONE INTRODUCTION.....	1
1.1 Overview.....	1
1.2 Objective.....	3
1.3 Contents of This Dissertation.....	4
CHAPTER TWO BACKGROUND AND PREVIOUS WORK.....	6
2.1 Macroscopic Heat Transfer.....	6
2.2 Microscopic Heat Transfer.....	8
2.2.1 General Properties.....	8
2.2.2 Wave Nature of Microscale Heat Transfer.....	13
2.2.3 Dual Phase Lagging Behavior of Microscale Heat Transfer.....	14
2.2.4 Mathematical Model of Microscale Heat Transfer.....	15
2.3 Previous Work.....	21
CHAPTER THREE MATHEMATICAL MODEL.....	25
3.1 Problem Description.....	25
3.2 Model for a Micro-Sphere.....	26
3.2.1 Geometry Description.....	26
3.2.2 Governing Equations.....	27
3.2.3 Boundary Conditions and Initial Conditions.....	29
3.3 Conclusion.....	30
CHAPTER FOUR FINITE DIFFERENCE METHOD.....	31
4.1 Notations.....	31
4.2 Finite Difference Scheme and Algorithm.....	32



4.2.1 Conversions of the Governing Equations .....	32
4.2.2 Staggered Grid .....	33
4.2.3 Finite Difference Scheme .....	34
4.2.4 Algorithm.....	46
4.3 Conclusion .....	47
CHAPTER FIVE NUMERICAL EXAMPLES AND DISCUSSIONS .....	48
5.1 Description.....	48
5.2 Numerical Examples and Discussions .....	51
5.2.1 Example One.....	51
5.2.2 Example Two .....	68
5.2.3 Example Three .....	83
5.2.4 Example Four.....	98
5.2.5 Example Five .....	114
CHAPTER SIX CONCLUSION .....	129
APPENDIX SOURCE CODE OF THE NUMERICAL METHOD .....	130
REFERENCES .....	152

## LIST OF TABLES

Table 2.1 Phonon-electron coupling factor ( $G$ ), for some noble and transition metals [Tzou 1997].....	20
Table 5.1 Thermophysical properties for gold [Tzou 2002, Chen 2002a, Chen 2002b, Kaye 1973, Touloukian 1970a, Touloukian 1970b] .....	50

## LIST OF FIGURES

Fig. 2.1 Energy transport through phonon collision [Tzou 1997] .....	9
Fig. 2.2 Phonon interactions in a film of the same order of magnitude as the mean free path [Tzou 1997].....	13
Fig. 3.1 A 3D micro-sphere with three-dimensional coordinate systems.....	26
Fig. 4.1 A 3D staggered grid and locations of variables for a micro-sphere .....	34
Fig. 5.1 A 3D micro-sphere with radius $L = 0.1 \mu\text{m}$ .....	49
Fig. 5.2 Change in electron temperature $T_e$ at $r = 0.1 \mu\text{m}$ , $\theta = 0$ , $\varphi = 0$ versus time for various meshes with a laser fluence $J$ of $500 \text{ J/m}^2$ in example one.....	51
Fig. 5.3 Displacement $u_r$ at $r = 0.05 \mu\text{m}$ , $\theta = 0$ , $\varphi = 0$ versus time for various meshes with a laser fluence $J$ of $500 \text{ J/m}^2$ in example one .....	52
Fig. 5.4 Profiles of electron temperature ( $T_e$ ), and lattice temperature ( $T_l$ ) along $r$ -axis at $\varphi = 0$ and $\varphi = \pi$ for various times with a laser fluence $J$ of $500 \text{ J/m}^2$ and a mesh $60 \times 20 \times 20$ in example one .....	55
Fig. 5.5 Chen et al's method in [Chen 2002a] with regard to normal stress $\sigma_x$ with oscillations at two peaks .....	55
Fig. 5.6 Normal stress ( $\sigma_x$ ) along the diameter at $\varphi = 0$ and $\varphi = \pi$ at different times with three different laser fluences and a mesh of $60 \times 20 \times 20$ in example one.....	56
Fig. 5.7 Displacement ( $u_r$ ) along the diameter at $\varphi = 0$ and $\varphi = \pi$ at different times with three different laser fluences and a mesh of $60 \times 20 \times 20$ in example one.....	57
Fig. 5.8 Contours of electron temperature ( $T_e$ ) distributions in the cross section of $\theta = 0$ and $\theta = \pi$ at different times with a mesh of $60 \times 20 \times 20$ and a laser fluence $J$ of $500 \text{ J/m}^2$ in example one.....	59
Fig. 5.9 Contours of electron temperature ( $T_l$ ) distributions in the cross section of $\theta = 0$ and $\theta = \pi$ at different times with a mesh of $60 \times 20 \times 20$ and a laser fluence $J$ of $500 \text{ J/m}^2$ in example one.....	61

Fig. 5.10 Contours of displacement ( $u_r$ ) in the cross section of $\theta = 0$ and $\theta = \pi$ at different times with a mesh of $60 \times 20 \times 20$ and a laser fluence $J$ of $500 \text{ J/m}^2$ in example one .....	62
Fig. 5.11 Contours of displacement ( $u_\theta$ ) in the cross section of $\theta = 0$ and $\theta = \pi$ at different times with a mesh of $60 \times 20 \times 20$ and a laser fluence $J$ of $500 \text{ J/m}^2$ in example one .....	63
Fig. 5.12 Contours of displacement ( $u_\varphi$ ) in the cross section of $\theta = 0$ and $\theta = \pi$ at different times with a mesh of $60 \times 20 \times 20$ and a laser fluence $J$ of $500 \text{ J/m}^2$ in example one .....	64
Fig. 5.13 Contours of normal stress ( $\sigma_r$ ) in the cross section of $\theta = 0$ and $\theta = \pi$ at different times with a mesh of $60 \times 20 \times 20$ and a laser fluence $J$ of $500 \text{ J/m}^2$ in example one .....	65
Fig. 5.14 Contours of normal stress ( $\sigma_\theta$ ) in the cross section of $\theta = 0$ and $\theta = \pi$ at different times with a mesh of $60 \times 20 \times 20$ and a laser fluence $J$ of $500 \text{ J/m}^2$ in example one .....	66
Fig. 5.15 Contours of normal stress ( $\sigma_\varphi$ ) in the cross section of $\theta = 0$ and $\theta = \pi$ at different times with a mesh of $60 \times 20 \times 20$ and a laser fluence $J$ of $500 \text{ J/m}^2$ in example one .....	67
Fig. 5.16 Change in electron temperature $T_e$ at $r = 0.1 \text{ }\mu\text{m}$ , $\theta = 0$ , $\varphi = 0$ versus time for various meshes with a laser fluence $J$ of $500 \text{ J/m}^2$ in example two .....	68
Fig. 5.17 Displacement $u_r$ at $r = 0.05 \text{ }\mu\text{m}$ , $\theta = 0$ , $\varphi = 0$ versus time for various meshes with a laser fluence $J$ of $500 \text{ J/m}^2$ in example two .....	69
Fig. 5.18 Profiles of electron temperature ( $T_e$ ), and lattice temperature ( $T_l$ ) along $r$ -axis at $\varphi = 0$ and $\varphi = \pi$ for various times with a laser fluence $J$ of $500 \text{ J/m}^2$ and a mesh $60 \times 20 \times 20$ in example two .....	70
Fig. 5.19 Normal stress ( $\sigma_r$ ) along the diameter at $\varphi = 0$ and $\varphi = \pi$ at different times with three different laser fluences and a mesh of $60 \times 20 \times 20$ in example two.....	71
Fig. 5.20 Displacement ( $u_r$ ) along the diameter at $\varphi = 0$ and $\varphi = \pi$ at different times with three different laser fluences and a mesh of $60 \times 20 \times 20$ in example two.....	72
Fig. 5.21 Contours of electron temperature ( $T_e$ ) distributions in the cross section of $\theta = 0$ and $\theta = \pi$ at different times with a mesh of $60 \times 20 \times 20$ and a laser fluence $J$ of $500 \text{ J/m}^2$ in example two.....	74

Fig. 5.22 Contours of electron temperature ( $T_e$ ) distributions in the cross section of $\theta = 0$ and $\theta = \pi$ at different times with a mesh of $60 \times 20 \times 20$ and a laser fluence $J$ of $500 \text{ J/m}^2$ in example two.....	76
Fig. 5.23 Contours of displacement ( $u_r$ ) in the cross section of $\theta = 0$ and $\theta = \pi$ at different times with a mesh of $60 \times 20 \times 20$ and a laser fluence $J$ of $500 \text{ J/m}^2$ in example two.....	77
Fig. 5.24 Contours of displacement ( $u_\theta$ ) in the cross section of $\theta = 0$ and $\theta = \pi$ at different times with a mesh of $60 \times 20 \times 20$ and a laser fluence $J$ of $500 \text{ J/m}^2$ in example two.....	78
Fig. 5.25 Contours of displacement ( $u_\varphi$ ) in the cross section of $\theta = 0$ and $\theta = \pi$ at different times with a mesh of $60 \times 20 \times 20$ and a laser fluence $J$ of $500 \text{ J/m}^2$ in example two.....	79
Fig. 5.26 Contours of normal stress ( $\sigma_r$ ) in the cross section of $\theta = 0$ and $\theta = \pi$ at different times with a mesh of $60 \times 20 \times 20$ and a laser fluence $J$ of $500 \text{ J/m}^2$ in example two.....	80
Fig. 5.27 Contours of normal stress ( $\sigma_\theta$ ) in the cross section of $\theta = 0$ and $\theta = \pi$ at different times with a mesh of $60 \times 20 \times 20$ and a laser fluence $J$ of $500 \text{ J/m}^2$ in example two.....	81
Fig. 5.28 Contours of normal stress ( $\sigma_\varphi$ ) in the cross section of $\theta = 0$ and $\theta = \pi$ at different times with a mesh of $60 \times 20 \times 20$ and a laser fluence $J$ of $500 \text{ J/m}^2$ in example two.....	82
Fig. 5.29 Change in electron temperature $T_e$ at $r = 0.1 \text{ }\mu\text{m}$ , $\theta = 0$ , $\varphi = 0$ versus time for various meshes with a laser fluence $J$ of $500 \text{ J/m}^2$ in example three.....	83
Fig. 5.30 Displacement $u_r$ at $r = 0.05 \text{ }\mu\text{m}$ , $\theta = 0$ , $\varphi = 0$ versus time for various meshes with a laser fluence $J$ of $500 \text{ J/m}^2$ in example three.....	84
Fig. 5.31 Profiles of electron temperature ( $T_e$ ), and lattice temperature ( $T_l$ ) along $r$ -axis at $\varphi = 0$ and $\varphi = \pi$ for various times with a laser fluence $J$ of $500 \text{ J/m}^2$ and a mesh $60 \times 20 \times 20$ in example three.....	85
Fig. 5.32 Normal stress ( $\sigma_r$ ) along the diameter at $\varphi = 0$ and $\varphi = \pi$ at different times with three different laser fluences and a mesh of $60 \times 20 \times 20$ in example three.....	86
Fig. 5.33 Displacement ( $u_r$ ) along the diameter at $\varphi = 0$ and $\varphi = \pi$ at different times with three different laser fluences and a mesh of $60 \times 20 \times 20$ in example three.....	87

Fig. 5.34 Contours of electron temperature ( $T_e$ ) distributions in the cross section of $\theta = 0$ and $\theta = \pi$ at different times with a mesh of $60 \times 20 \times 20$ and a laser fluence $J$ of $500 \text{ J/m}^2$ in example three.....	89
Fig. 5.35 Contours of electron temperature ( $T_l$ ) distributions in the cross section of $\theta = 0$ and $\theta = \pi$ at different times with a mesh of $60 \times 20 \times 20$ and a laser fluence $J$ of $500 \text{ J/m}^2$ in example three.....	91
Fig. 5.36 Contours of displacement ( $u_r$ ) in the cross section of $\theta = 0$ and $\theta = \pi$ at different times with a mesh of $60 \times 20 \times 20$ and a laser fluence $J$ of $500 \text{ J/m}^2$ in example three.....	92
Fig. 5.37 Contours of displacement ( $u_\theta$ ) in the cross section of $\theta = 0$ and $\theta = \pi$ at different times with a mesh of $60 \times 20 \times 20$ and a laser fluence $J$ of $500 \text{ J/m}^2$ in example three.....	93
Fig. 5.38 Contours of displacement ( $u_\varphi$ ) in the cross section of $\theta = 0$ and $\theta = \pi$ at different times with a mesh of $60 \times 20 \times 20$ and a laser fluence $J$ of $500 \text{ J/m}^2$ in example three.....	94
Fig. 5.39 Contours of normal stress ( $\sigma_r$ ) in the cross section of $\theta = 0$ and $\theta = \pi$ at different times with a mesh of $60 \times 20 \times 20$ and a laser fluence $J$ of $500 \text{ J/m}^2$ in example three.....	95
Fig. 5.40 Contours of normal stress ( $\sigma_\theta$ ) in the cross section of $\theta = 0$ and $\theta = \pi$ at different times with a mesh of $60 \times 20 \times 20$ and a laser fluence $J$ of $500 \text{ J/m}^2$ in example three.....	96
Fig. 5.41 Contours of normal stress ( $\sigma_\varphi$ ) in the cross section of $\theta = 0$ and $\theta = \pi$ at different times with a mesh of $60 \times 20 \times 20$ and a laser fluence $J$ of $500 \text{ J/m}^2$ in example three.....	97
Fig. 5.42 Change in electron temperature $T_e$ at $r = 0.1 \text{ } \mu\text{m}$ , $\theta = 0$ , $\varphi = 0$ versus time for various meshes with a laser fluence $J$ of $500 \text{ J/m}^2$ in example four.....	99
Fig. 5.43 Displacement $u_r$ at $r = 0.05 \text{ } \mu\text{m}$ , $\theta = 0$ , $\varphi = 0$ versus time for various meshes with a laser fluence $J$ of $500 \text{ J/m}^2$ in example four.....	99
Fig. 5.44 Profiles of electron temperature ( $T_e$ ), and lattice temperature ( $T_l$ ) along $r$ -axis at $\varphi = 0$ and $\varphi = \pi$ for various times with a laser fluence $J$ of $500 \text{ J/m}^2$ and a mesh $60 \times 20 \times 20$ in example four.....	100
Fig. 5.45 Normal stress ( $\sigma_r$ ) along the diameter at $\varphi = 0$ and $\varphi = \pi$ at different times with three different laser fluences and a mesh of $60 \times 20 \times 20$ in example four.....	102

Fig. 5.46 Displacement ( $u_r$ ) along the diameter at $\varphi = 0$ and $\varphi = \pi$ at different times with three different laser fluences and a mesh of $60 \times 20 \times 20$ in example four .....	103
Fig. 5.47 Contours of electron temperature ( $T_e$ ) distributions in the cross section of $\theta = 0$ and $\theta = \pi$ at different times with a mesh of $60 \times 20 \times 20$ and a laser fluence $J$ of $500 \text{ J/m}^2$ in example four .....	105
Fig. 5.48 Contours of electron temperature ( $T_l$ ) distributions in the cross section of $\theta = 0$ and $\theta = \pi$ at different times with a mesh of $60 \times 20 \times 20$ and a laser fluence $J$ of $500 \text{ J/m}^2$ in example four .....	107
Fig. 5.49 Contours of displacement ( $u_r$ ) in the cross section of $\theta = 0$ and $\theta = \pi$ at different times with a mesh of $60 \times 20 \times 20$ and a laser fluence $J$ of $500 \text{ J/m}^2$ in example four .....	108
Fig. 5.50 Contours of displacement ( $u_\theta$ ) in the cross section of $\theta = 0$ and $\theta = \pi$ at different times with a mesh of $60 \times 20 \times 20$ and a laser fluence $J$ of $500 \text{ J/m}^2$ in example four .....	109
Fig. 5.51 Contours of displacement ( $u_\varphi$ ) in the cross section of $\theta = 0$ and $\theta = \pi$ at different times with a mesh of $60 \times 20 \times 20$ and a laser fluence $J$ of $500 \text{ J/m}^2$ in example four .....	110
Fig. 5.52 Contours of normal stress ( $\sigma_r$ ) in the cross section of $\theta = 0$ and $\theta = \pi$ at different times with a mesh of $60 \times 20 \times 20$ and a laser fluence $J$ of $500 \text{ J/m}^2$ in example four .....	111
Fig. 5.53 Contours of normal stress ( $\sigma_\theta$ ) in the cross section of $\theta = 0$ and $\theta = \pi$ at different times with a mesh of $60 \times 20 \times 20$ and a laser fluence $J$ of $500 \text{ J/m}^2$ in example four .....	112
Fig. 5.54 Contours of normal stress ( $\sigma_\varphi$ ) in the cross section of $\theta = 0$ and $\theta = \pi$ at different times with a mesh of $60 \times 20 \times 20$ and a laser fluence $J$ of $500 \text{ J/m}^2$ in example four .....	113
Fig. 5.55 Change in electron temperature $T_e$ at $r = 0.1 \text{ } \mu\text{m}$ , $\theta = 0$ , $\varphi = 0$ versus time for various meshes with a laser fluence $J$ of $500 \text{ J/m}^2$ in example five .....	115
Fig. 5.56 Displacement $u_r$ at $r = 0.05 \text{ } \mu\text{m}$ , $\theta = 0$ , $\varphi = 0$ versus time for various meshes with a laser fluence $J$ of $500 \text{ J/m}^2$ in example five .....	115
Fig. 5.57 Profiles of electron temperature ( $T_e$ ), and lattice temperature ( $T_l$ ) along $r$ -axis at $\varphi = 0$ and $\varphi = \pi$ for various times with a laser fluence $J$ of $500 \text{ J/m}^2$ and a mesh $60 \times 20 \times 20$ in example five .....	116

Fig. 5.58 Normal stress ( $\sigma_r$ ) along the diameter at $\varphi = 0$ and $\varphi = \pi$ at different times with three different laser fluences and a mesh of $60 \times 20 \times 20$ in example five.....	117
Fig. 5.59 Displacement ( $u_r$ ) along the diameter at $\varphi = 0$ and $\varphi = \pi$ at different times with three different laser fluences and a mesh of $60 \times 20 \times 20$ in example five.....	118
Fig. 5.60 Contours of electron temperature ( $T_e$ ) distributions in the cross section of $\theta = 0$ and $\theta = \pi$ at different times with a mesh of $60 \times 20 \times 20$ and a laser fluence $J$ of $500 \text{ J/m}^2$ in example five .....	120
Fig. 5.61 Contours of electron temperature ( $T_e$ ) distributions in the cross section of $\theta = 0$ and $\theta = \pi$ at different times with a mesh of $60 \times 20 \times 20$ and a laser fluence $J$ of $500 \text{ J/m}^2$ in example five .....	122
Fig. 5.62 Contours of displacement ( $u_r$ ) in the cross section of $\theta = 0$ and $\theta = \pi$ at different times with a mesh of $60 \times 20 \times 20$ and a laser fluence $J$ of $500 \text{ J/m}^2$ in example five.....	123
Fig. 5.63 Contours of displacement ( $u_\theta$ ) in the cross section of $\theta = 0$ and $\theta = \pi$ at different times with a mesh of $60 \times 20 \times 20$ and a laser fluence $J$ of $500 \text{ J/m}^2$ in example five.....	124
Fig. 5.64 Contours of displacement ( $u_\varphi$ ) in the cross section of $\theta = 0$ and $\theta = \pi$ at different times with a mesh of $60 \times 20 \times 20$ and a laser fluence $J$ of $500 \text{ J/m}^2$ in example five.....	125
Fig. 5.65 Contours of normal stress ( $\sigma_r$ ) in the cross section of $\theta = 0$ and $\theta = \pi$ at different times with a mesh of $60 \times 20 \times 20$ and a laser fluence $J$ of $500 \text{ J/m}^2$ in example five.....	126
Fig. 5.66 Contours of normal stress ( $\sigma_\theta$ ) in the cross section of $\theta = 0$ and $\theta = \pi$ at different times with a mesh of $60 \times 20 \times 20$ and a laser fluence $J$ of $500 \text{ J/m}^2$ in example five.....	127
Fig. 5.67 Contours of normal stress ( $\sigma_\varphi$ ) in the cross section of $\theta = 0$ and $\theta = \pi$ at different times with a mesh of $60 \times 20 \times 20$ and a laser fluence $J$ of $500 \text{ J/m}^2$ in example five.....	128



## NOMENCLATURE

$C_{e0}$	electron heat capacity, J/(m <sup>3</sup> K)
$C_p$	volumetric heat capacity
$C_l$	lattice heat capacity, J/(m <sup>3</sup> K)
$E$	modulus of elasticity, Pa
$G$	electron-lattice coupling factor, W/(m <sup>3</sup> K)
$J$	laser fluence, J/m <sup>2</sup>
$K$	bulk modulus, Pa
$k_e$	thermal conductivity, W/(mK)
$L$	radius of micro-sphere, m
$m_e$	electron mass, kg
$n_a$	atomic number density per unit volume, m <sup>-3</sup>
$n_e$	number density per unit volume, m <sup>-3</sup>
$N$	number of grid points
$Q$	volumetric heat source, W/m <sup>2</sup>
$\bar{q}$	heat flux, W/m <sup>2</sup>
$R$	surface reflectivity
$T$	absolute temperature, K

$T_e$	electron temperature, K
$T_l$	lattice temperature, K
$t$	time, s
$t_p$	laser pulse duration, s
$u_r$	displacement in the $r$ direction , m
$u_\theta$	displacement in the $\theta$ direction , m
$u_\varphi$	displacement in the $\varphi$ direction , m
$v_r$	velocity component in the $r$ direction , m/s
$v_\theta$	velocity component in the $\theta$ direction , m/s
$v_\varphi$	velocity component in the $\varphi$ direction , m/s
$v_s$	speed of sound , m/s
$r, \theta, \varphi$	spherical coordinates

### **Greek Symbols**

$\Delta t$	time increment, s
$\Delta r$	spatial grid size, m
$\Delta \theta$	spatial grid size, m
$\Delta \varphi$	spatial grid size, m
$\Delta_{-t}$	finite difference operator
$\zeta$	optical penetration depth, m
$\alpha_T$	thermal expansion coefficient
$\delta_r$	finite difference operator

$\delta_\theta$	finite difference operator
$\delta_\varphi$	finite difference operator
$\varepsilon_r$	normal strain in the $r$ direction
$\varepsilon_\theta$	normal strain in the $\theta$ direction
$\varepsilon_\varphi$	normal strain in the $\varphi$ direction
$\varepsilon_{r\theta}$	shear strain in the $r\theta$ direction
$\varepsilon_{r\varphi}$	shear strain in the $r\varphi$ direction
$\varepsilon_{\varphi\theta}$	shear strain in the $\varphi\theta$ direction
$\Lambda$	electron-blast coefficient, $\text{J}/(\text{m}^3 \text{K}^2)$
$\lambda$	Lame's constant, Pa
$\mu$	Lame's constant, Pa
$\rho$	density, $\text{kg}/\text{m}^3$
$\sigma$	Stefan-Boltzmann's constant
$\sigma_r$	normal stress in the $r$ direction
$\sigma_\theta$	normal stress in the $\theta$ direction
$\sigma_\varphi$	normal stress in the $\varphi$ direction
$\sigma_{r\theta}$	shear stress in the $r\theta$ direction
$\sigma_{r\varphi}$	shear stress in the $r\varphi$ direction
$\sigma_{\varphi\theta}$	shear stress in the $\varphi\theta$ direction

### Subscripts and Superscripts

0	initial value at $t = 0$
---	--------------------------

$D$	Debye temperature, K
$e$	electron
$i$	grid index in the $r$ direction
$j$	grid index in the $\theta$ direction
$k$	grid index in the $\varphi$ direction
$l$	lattice
$n$	time level

## ACKNOWLEDGEMENTS

This dissertation owes a lot of appreciation for the assistance, support and encouragement from my directors, my family, my relatives and my friends.

I am here to express my sincere gratitude to my advisor, Dr. Weizhong Dai, for his tireless guidance, endless encouragement and generous support throughout my graduate studies. Without his directions and suggestions, this dissertation could not be completed. I would like to thank Dr. Richard Greechie, who is a member of my committee, and also my advisor during my master studying period, for his long-term support and understanding throughout the years I have been at Louisiana Tech University. A special appreciation to Dr. Galen Turner is for his kindness in giving me the endless support in pursuing this Ph.D degree. Sincere acknowledgement is also extended to Dr. Raja Nassar and Dr. Andrei Paun for their teaching and directing me.

I owe a lot to my wife, my parents and my brother for their endless love and animation, especially to my mother, it is she who always told me there still exists hope. Finally, I would like to thank all my friends and relatives to make me confident when I faced difficulties. This dissertation is dedicated to all of you.

# CHAPTER ONE

## INTRODUCTION

### 1.1 Overview

Ultrafast lasers with pulse durations of the order of sub-picosecond to femtosecond domain possess exclusive capabilities in limiting the undesirable spread of the thermal process zone in the heated sample [Tzou 2002]. The application of ultrashort-pulsed lasers includes structural monitoring of thin metal films [Mandelis 1992, Opsal 1991], laser micromachining and patterning [Elliot 1989], structural tailoring of microfilms [Grigoropoulos 1994], and laser synthesis and processing in thin-film deposition [Narayan 1991]. Recent applications of ultrashort-pulsed lasers have been in different disciplines such as physics, chemistry, biology, medicine, and optical technology [Liu 2000, Shirk 1998]. The non-contact nature of femtosecond lasers has made them an ideal candidate for precise thermal processing of functional nanophase materials [Tzou 2002].

Success of high-energy ultrashort-pulsed lasers in real applications relies on three factors [Tzou 2002]: (1) well characterized pulse width, intensity and experimental techniques; (2) reliable microscale heat transfer models; and (3) prevention of thermal damage which is also the most important task in real applications. It should be pointed out here that ultrafast damage induced by sub-picosecond pulses is intrinsically different from that induced by long-pulse or continuous lasers. For the latter, laser damage is

caused by the elevated temperatures resulting from the continuous pumping of photon energy into the processed sample. The “damage threshold” termed in heating by long-pulse lasers, therefore, is often referred to as the laser intensity that drives the heated spot to the melting temperature. Thermal damage induced by ultrashort-pulsed lasers in the picosecond domain, on the other hand, occurs after the heating pulse is over [Wang 2007]. Field induced multi-photon ionization produces free electrons that are rapidly accelerated by the laser pulse. By absorbing energy from the impinging photons in the femtosecond domain, these free electrons mobilize and ionize neighboring atoms through high-frequency collisions, which generates more electrons. The hot electrons transmit thermal energy to photons through phonon-electron coupling, resulting in a new thermal property, called the electron-phonon coupling factor, for microscale heat transfer in metals [Wang 2007]. This process continues until a critical density of hot electrons is reached. Under a sufficiently high intensity of heating, in fact, experimental results have shown that the ultrafast damage involves shattering of a thin material layer (from the heated surface) without a clear signature of thermal damage by excessive temperature [Tzou 2002, Wang 2007]. Rather than the melting damage developed at high temperature, obviously, there exists a new driving force that brings about such ultrafast damage, probably in only a few picoseconds after heating is applied [Tzou 2002]. This is our motivation to study the thermal deformation induced by ultrashort-pulsed lasers because it is important in preventing thermal damage. Particularly, we are interested in the thermal deformation for micro-spheres because they are of interest related to micro resonators in optical applications, such as ultra-low-threshold lasing, sensing,

optoelectronic microdevices, cavity quantum electrodynamics and their potential in quantum information processing.

## 1.2 Objective

The research objective is to develop a new finite difference scheme to study the thermal deformation in a micro-sphere subjected to ultrashort-pulsed lasers based on the dynamic equations of motion related to two-step parabolic heat transport equations. Our coordinates of reference will be the spherical coordinates system. To achieve this objective, five steps should be followed:

- (1) Introduce velocity components into the model and re-write the dynamic equations of motion.
- (2) Construct a staggered grid.
- (3) Develop a fourth-order compact finite difference scheme for evaluating stress derivatives and share stress derivatives in the dynamic equations of motion. As such the third-order derivatives of stress and shear stress are disappeared and hence non-physical oscillations in the solutions are eliminated.
- (4) Develop a finite difference scheme for obtaining temperatures, displacements, stresses, and strains in a micro-sphere induced by ultrashort-pulsed lasers.
- (5) Apply the developed numerical scheme to investigate the temperature, displacement, stress, and strain distributions in a gold micro-sphere subjected to ultrashort-pulsed lasers, where a portion of the upper hemisphere is irradiated by a single-pulse laser, portions of both the upper hemisphere and the lower hemisphere are irradiated by a single-pulse laser, the upper hemisphere is irradiated by a single-pulse laser, a portion of the upper



hemisphere is irradiated by a double-pulse laser, and portions of both the upper hemisphere and the lower hemisphere are irradiated by a double-pulse laser.

Results of the research will provide a numerically efficient method without non-physical oscillations to solve the two-step parabolic heat transport in spherical coordinates and provide us a better understanding about the transport phenomenon in a micro-sphere. This research result will have an important impact on the development of short-pulse laser applications in the structural monitoring of thin metal films, laser patterning, structural tailoring of microfilms, and laser synthesis and processing in thin film deposition, as well as in other disciplines where high-energy short-pulse lasers are so important.

### **1.3 Contents of This Dissertation**

In Chapter Two, we will introduce the classical theory of heat transfer at the macro scale, and then we will discuss process of heat transfer in micro scale, the dual-phase-lagging behavior, as well as a review of previous work.

In Chapter Three, we will consider a gold micro-sphere irradiated by ultrashort pulsed lasers. The geometry mathematical model for thermal deformations will be set up.

In Chapter Four, we will develop a staggered finite difference scheme for solving the governing equation system and design the numerical algorithms for calculating the temperature, displacement, stress and strain distributions, respectively.

In Chapter Five, we will test the numerical results based on the developed numerical method for thermal deformation in a gold micro-sphere subjected to an ultrashort pulsed laser. Five cases including a portion of the upper hemisphere is irradiated by a single-pulse laser, portions of both the upper hemisphere and the lower hemisphere are

irradiated by a single-pulse laser, the upper hemisphere is irradiated by a single-pulse laser, a portion of the upper hemisphere is irradiated by a double-pulse laser, and portions of both the upper hemisphere and the lower hemisphere are irradiated by a double-pulse laser will be studied. Various mesh sizes will be chosen to test the convergence of the scheme. The electron temperatures, the lattice temperatures, the displacements, and the stresses will be calculated and discussed. And in Chapter Six, conclusions and future work will be discussed.

## **CHAPTER TWO**

### **BACKGROUND AND PREVIOUS WORK**

#### **2.1 Macroscopic Heat Transfer**

In thermodynamics, heat is defined as energy transfer due to temperature gradients or differences. Consistent with this viewpoint, only two modes of heat transfer are recognized: conduction and radiation. For example, heat transfer across a steel pipe is by conduction, whereas heat transfer from the sun to the earth is by radiation. These modes of transfer occur on a molecular or subatomic scale.

In the atmosphere at normal pressure, conduction is by molecules that travel a very short distance before colliding with another molecule and exchanging energy. On the other hand, radiation is by photons, which travel almost unimpeded through the air from one surface to another. Thus, an important distinction between conduction and radiation is that the energy carriers for conduction have a shorter mean free path, whereas for radiation, the carriers have a long mean free path. Additionally, a fluid, by virtue of its mass and velocity, can transport momentum, and by virtue of its temperature, it can transport energy. Therefore, convection is defined as the transport of energy by bulk motion of a medium. We will focus our discussion on the conduction mode of heat transfer.

On a microscopic level, the physical mechanisms of conduction are complex, ranging from molecular collisions in gases to lattice vibration in crystals, and flow of free electrons in metals. Heat conduction at the macro scale is a description of macroscopic conditions averaged over many grains. Thus, microscopic behaviors need to be aggregated over the domain by placing an emphasis on phenomenological laws, more suitable to the macroscopic level. In the classical theory of heat transfer, the heat conduction is governed by Fourier's law. It is a constitutive equation that depicts the way in which cause varies with effects. It is necessary along with the conservation of energy law to derive the heat transport equations. Regardless of the assumptions formulated in the constitutive equation, it must be admissible under the framework of the second law of thermodynamics [Kaba 2005].

Fourier's law of heat conduction can be expressed as follows [Kaba 2005, Wang 2007]

$$\vec{q}(\vec{r}, t) = -k\nabla T(\vec{r}, t), \quad (2.1)$$

where  $\vec{r}$  denotes the position vector of the material volume,  $k$  is the thermal conductivity of the material, and  $t$  is the physical time. The law states that the heat flux vector ( $\vec{q}$ ) and the temperature gradient ( $\nabla T$ ) across a material volume occur at the same instant of time. The energy equation derived from the first law of thermodynamics is [Kaba 2005, Wang 2007]

$$-\nabla \cdot \vec{q} = C_p \frac{\partial T}{\partial t} - Q, \quad (2.2)$$

where  $C_p$  is the volumetric heat capacity and  $Q$  is the heat source. Taking the divergence of Eq. (2.1) and substituting it into Eq. (2.2), we obtain the traditional

heat conduction equation [Kaba 2005, Wang 2007]

$$C_p \frac{\partial T}{\partial t} = \nabla \cdot (k \nabla T) + Q. \quad (2.3)$$

The immediate response dictated by Fourier's law results in an infinite speed of heat propagation, implying that a disturbance applied at a certain location in a solid medium is immediately sensed anywhere else in the medium. Because the heat flux vector and the temperature gradient are simultaneous, there is no difference between the cause and the effect of heat flow [Kaba 2004, Kaba 2005].

## **2.2 Microscopic Heat Transfer**

### **2.2.1 General Properties**

At the micro scale, the process of heat transfer is determined by phonon-electron interaction in metallic films and by phonon scattering in dielectric films, conductors and semiconductors [Tien 1998]. The classical theories established at the macro scale, such as heat conduction subjected to Fourier's law, are not expected to be informative at the micro scale as they describe macroscopic behavior aggregated over many grains. They break down further as the temporal domain becomes extremely small, say, on the order of picoseconds or femtoseconds. A typical case occurs in the ultrafast laser heating in the thermal processing of materials. For this case, the quasi-equilibrium assumption established in Fourier's law does not hold along with other macroscopic behaviors [Kaba 2004, Kaba 2005].

Regardless of the type of conducting medium, heat transport requires sufficient collisions among energy carriers. In metals, such energy carriers include electrons and phonons. In dielectric crystals, insulators and semiconductors, on the other hand, phonons are the primary energy carriers. The phonon gas can be viewed as a group of "mass

particles” that characterize the energy state of a metal lattice. For a metal lattice vibrating at a frequency  $\nu$  at a certain temperature  $T$ , the energy state of the metal lattice, and hence the energy state of the phonon, is [Tzou 1997]

$$E = h\nu, \quad (2.4)$$

with  $h$  being the Planck constant. The lattice frequency is of the order of tens of terahertz ( $10^{13}$  1/s) at room temperature. It is conceivable that the lattice frequency increases with the temperature of the metal lattice. Energy transport from one lattice to the other can thus be thought of as the consequence of a series of phonon collisions in time history, as illustrated in Fig. 2.1 [Tzou 1997, Kaba 2005].

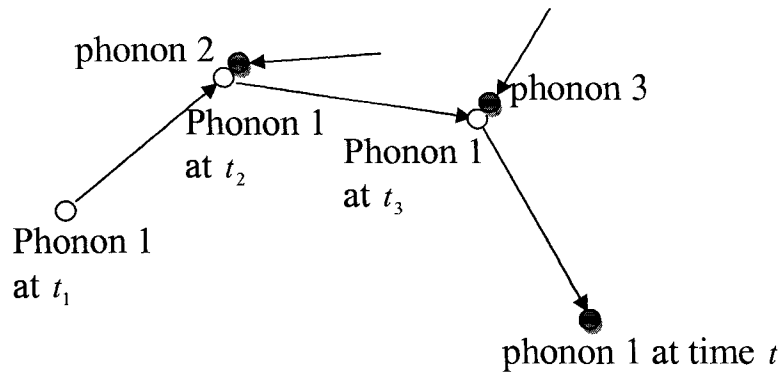


Fig. 2.1 Energy transport through phonon collision [Tzou 1997].

Bearing energy  $h\nu$  at time  $t_1$ , phonon 1 collides with phonon 2 at  $t_2$  and with phonon 3 at time  $t_3$ . In the course of each successive collision, energy is transferred from phonon 1 to phonons 2 and 3, causing a successive collision, and causing a successive change of vibrating frequency of phonon 1. To illustrate the phenomenon, the mean free path ( $d$  in space) is defined as the algebraic mean of the distance [Tzou 1997]

$$d = \frac{d_1 + d_2 + d_3}{3}, \quad (2.5a)$$

the mean free time  $\tau$  is defined similarly as the algebraic mean of the times traveled by phonon 1 between the two successive collisions with phonons 2 and 3 [Tzou 1997]

$$\tau = \frac{(\tau_2 - \tau_1) + (\tau_3 - \tau_2) + (t - \tau_3)}{3} = \frac{(t - \tau_1)}{3}, \quad (2.5b)$$

to simplify our analysis, two collisions were used in this example. In order to have a meaningful statistical ensemble space, of course, a “sufficient” number of collisions must be collected to determine the mean free path and the mean free time.

The macroscopic models assume the physical domain for heat transport is so large that it allows hundreds of thousands of phonon collisions before an observation or description is made for the process of heat transport. Since phonon collision requires a finite amount of time to occur, hundreds of thousands of those collisions would require a sufficiently long time for the process of heat transfer to occur. It is therefore clear that the macroscopic models not only require a sufficiently large physical domain for conducting heat (much larger than the mean free path), but also a sufficiently long time for heat conduction to take place (much longer than the mean free time). It should be pointed out that the sufficiently long time for the stabilization of energy transport by phonons should not be confused with the time required for the steady state to be reached. The sufficiently long time required in phonon collisions is to provide a statistically meaningful concept in regards to the mean free path and the mean free time. The heat transport phenomenon can still be time dependent after phonon transport becomes stabilized. In a phenomenological sense, the mean free time as illustrated in Fig. 2.1 is parallel to the characteristic time describing the relaxation behavior in the fast-transient process. For metals, the mean free time, or relaxation time, is of the order of picoseconds. In dielectrics crystals and insulators, the relaxation time is longer, roughly of the order of nanoseconds to

picoseconds. As a rough estimate, any response time being shorter than one nanosecond should be closely investigated. The fast-transient effect, such as wave behavior in heat conduction, may activate and introduce unexpected effects in heat transport. Such a threshold value of nanoseconds, however, depends on the combined effects of geometric configuration (of the specimen) and thermal loading imposed upon the system. It may vary by one order of magnitude if the system involves an abrupt change of geometric curvatures (specifically around a crack or notch tips), or be the subject to discontinuous thermal loading (irradiation of a short pulse laser, for instance) [Kaba 2005].

The mean free path for electrons is of the order of tens of nanometers ( $10^{-8}$  m) at room temperature. As a function of temperature, the mean free path's value may increase to the order of millimeters in the liquid helium temperature range, roughly 4 K. The mean free path in phonon collision or phonon scattering (from the boundaries of the grains) is much longer. For example, the mean free path is of the order of tenths of a micron ( $10^{-7}$  m) for a type IIa diamond film at room temperature [Majumdar 1993]. As an approximation, a physical device with a characteristic dimension in submicrons deserves special attention. The micro structural interaction effect, such as phonon-electron or phonon scattering, may dramatically enhance heat transfer in short times. Enhancement of heat transfer enlarges the thermal processing zone and increases temperature levels, which in turn may lead to early burnout of micro devices if not properly monitored.

Since the physical dimensions, under consideration at the micro scale, are of the same order of magnitude as the mean free path, and therefore the response time is of the same order of magnitude as the mean free time, the quantities derived from the concept of aggregation at the macro scale need to be reexamined for their meaning in a microscopic



environment. The temperature gradient, which has been simply derived in macro scale heat transfer, may lose its physical meaning for a thin film of thickness, the same order of magnitude as the mean free path. As illustrated in Fig. 2.2, while we can still divide the temperature difference  $T_2 - T_1$ , by the film thickness  $l$  ( $\cong d$ , the mean free path of phonon interaction/scattering) to obtain a “gradient like” quantity, the temperature gradient obtained in this fashion loses its usual physical meaning because of the lack of sufficient energy carriers between the two surfaces of the film and, consequently, the temperature field is discontinuous across the film thickness. Therefore, the concept of temperature gradient fails. Due to this failure, the macroscopic way of ascertaining the heat flux vector assuming Fourier’s law becomes questionable. Thus, there is an immediate ambiguity, which exists in both the concept of temperature gradient and the concept of heat flux, as we introduce the microscopic effects in space in the conventional theories of macro scale heat transfer [Tzou 1997].

A similar situation appears as the response time for the temperature is analyzed. The typical response time in the thin film is of the same order of magnitude as the mean free time, as a result of phonons traveling in the threshold of the mean free path. If the response time of primary concern (for the temperature or the heat flux vector) is of the same order of magnitude as the mean free time (relaxation time), the individual effects of phonon interaction and phonon scattering must be taken into account in the short time transient of heat transport. Thus, we have another situation that requires a closer look at the macroscopic assumptions of heat transfer [Tzou 1997].

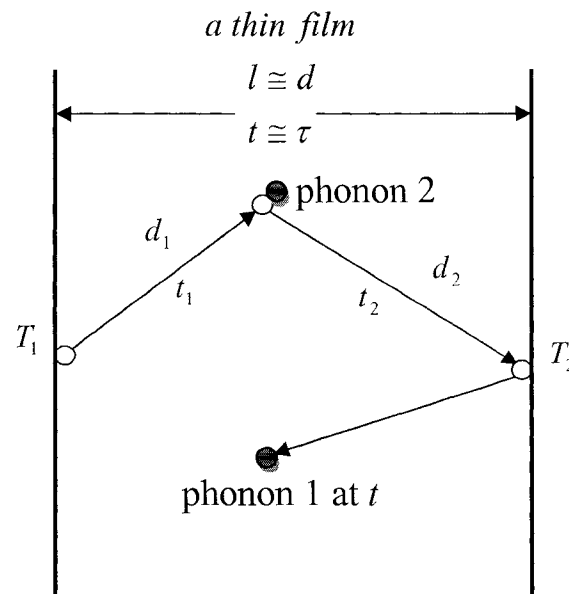


Fig. 2.2 Phonon interactions in a film of the same order of magnitude as the mean free path [Tzou 1997].

From Fig. 2.2, it is evident that the macro scale affect in space interfere with the macro scale effects in time. They cannot be separated and must be accounted for simultaneously in any framework seeking to develop a theory of heat transfer at the microscale. This becomes obvious as the finite speed of phonon transport in short time is considered. Phonons propagate at the speed of sound, on average, which is of the order of  $10^4$  to  $10^5$  m/s at room temperature, depending on the type of solid medium. A response time of the order of picoseconds ( $10^{-12}$  s) thus implies a traveling distance (the penetration depth of heat by phonon transport) of the order of submicrons ( $10^{-8}$  to  $10^{-7}$  m) [Tzou 1997, Kaba 2005].

### 2.2.2 Wave Nature of Microscale Heat Transfer

In solids that are not good electrical conductors, the principal mode of conduction heat transfer is that of vibrational energy transfer from one atom to its neighbors. Atoms

in solids are constantly at very high frequencies with relatively small amplitudes. The atomic vibrations of adjacent atoms are coupled through atomic bonding. These vibrations are coordinated in such a way that traveling lattice waves are produced, which propagate through the lattice at the speed of sound. A single quantum of vibrational energy is called a phonon.

However, in metals, the free electron mechanism of heat transport is much more efficient than the phonon mechanism, because phonons are more easily scattered than free electrons and because electrons have higher velocities.

The mean free path of an electron in a bulk material is typically on the order of 10 to 30 nm, where the electron-lattice is dominant. However, when the film thickness is on the order of the mean free path, boundary scattering becomes important [Tzou 1996]. Thin films are manufactured using a number of methods and a wide variety of conditions. The manufacturing method and environmental conditions during manufacture can have a serious influence on the microstructure of the film, which in turn influences defect and grain boundary scattering. Also, when heated by ultrashort pulses, the electron system becomes so hot that electron-electron scattering can become significant. Thus, microscale heat transfer requires consideration of the microscopic energy carriers and the full range of possible scattering mechanisms [Barron 2005].

### **2.2.3 Dual Phase Lagging Behavior of Microscale Heat Transfer**

Qiu and others [Qiu 1993c] have proposed a phase lag model to explain the wave-like propagation of heat on a microscale. This model expresses two primary phases for heat conduction. The first involves the deposition of energy on electrons while the second involves the transfer of this energy from electrons to the lattice of the material. As early

as 1957, Kaganov et al. proposed that free electrons can be heated to a temperature much higher than the lattice temperature in certain situations [Kaganov 1957]. This high heating results in a double phase heating of the material. According to Qiu's research, there exists two characteristic times for the transfer of heat: thermalization time and relaxation time [Qiu 1993c]. Thermalization time represents the time for electrons and the lattice to reach thermal equilibrium. It represents the time necessary to convert heat energy to the internal lattice. Relaxation time represents the time for electrons to change their states.

During a relatively slow heating process, the thermalization time can be thought of as instantaneous. This process is modeled well by a Fourier's law model. However, for very short laser-pulse heating, these assumptions are subject to question [Qiu 1993c]. In fact, because the physical dimension in microscale heat transfer is of the same order of magnitude as the electron free path, the response time is of this same magnitude. This fact indicates that the temperature gradient is not descriptive for a thin film of the same thickness as the mean free path [Tzou 1996].

#### **2.2.4 Mathematical Model of Microscale Heat Transfer**

The model in Eq. (2.3) can be described as a parabolic one-step equation because of the assumptions it makes that heat energy is converted to lattice energy instantaneously and that heat energy is assumed to be a diffusive process [Qiu 1993c]. Other non-Fourier models have been proposed to deal with the failings of the Fourier model on a microscale. One model is based on the modified flux law [Tzou 1993]

$$\vec{q} + \tau \frac{\partial \vec{q}}{\partial t} = -k \nabla T, \quad (2.6)$$

where  $\tau$  is the relaxation time and  $\vec{q}$  is the heat flux. The heat flux vector in this case maintains a memory of the time-history of the temperature gradient. Relaxation time is the effective mean free path  $l$ , divided by the phonon speed  $v_s$ . Mathematically,  $\tau = l/v_s$ . In the absence of relaxation time (or  $\tau = 0$ ), which implies a mathematical idealization from either a zero mean free path ( $l = 0$ ) or an infinite phonon speed ( $v \rightarrow \infty$ ) for phonon collisions, then Eq. (2.6) reduces to the classical Fourier rate equation. Therefore, an infinite speed of heat propagation is an assumption made in the classical theory of diffusion utilizing Fourier's law [Tzou 1993].

When Eq. (2.6) is combined with Eq. (2.3), we obtain the hyperbolic heat equation

$$C \frac{\partial T}{\partial t} = -\nabla \cdot \vec{q} + Q, \quad (2.7a)$$

$$\tau \frac{\partial \vec{q}}{\partial t} + k \nabla T + \vec{q} = 0. \quad (2.7b)$$

This equation is known as a hyperbolic equation because of the additional term that modifies the parabolic Fourier heat Eq. (2.3) [Tang 1996]. This modification predicts a finite speed of heat propagation because of the relaxation time  $\tau$ , associated with heat transfer. Typical wave speeds in metals are on the order of  $10^5$  m/s [Ozisik 1994].

While the hyperbolic model answers some issues arising from a microscale examination of heat transfer, it still leaves some questions. It is not based on the details of energy transport in the material, such as the interaction of electrons and phonons [Qiu 1993a]. Also, material properties may not be able to be regarded as constant. The relaxation time and thermal conductivity are generally temperature-dependent [Tzou

1993]. In addition, the value of thermal conductivity depends on processing parameters, such as laser pulse duration and intensity, during short-pulse laser heating [Qiu 1993b].

These considerations have led to the dual-phase lagging equation. This equation is derived from the lagging equation which holds a lag in heat flux behind the temperature gradient. Compared to the hyperbolic heat equation, this model has an additional mixed derivative term. Now, as with the hyperbolic model, the time lag associated with heat flux causes wavelike behavior. However, the additional time lag creates a mixed derivative term that renders the equation in the form of a parabolic equation. Thus, this parabolic dual phase equation is modeled as follows [Barron 2005, Wang 2007]

$$C_e(T_e) \frac{\partial T_e}{\partial t} = \nabla \cdot (k \nabla T_e) - G(T_e - T_l) + S, \quad (2.8a)$$

$$C_l(T_l) \frac{\partial T_l}{\partial t} = G(T_e - T_l). \quad (2.8b)$$

Here,  $C_e(T_e)$  and  $C_l(T_l)$  are the volumetric electron heat capacity and the volumetric lattice heat capacity, respectively, and  $G$  is the electron-lattice coupling factor. The coupling factor will be described in detail later. Qiu and Tien [Qiu 1993a] derived a model described as the hyperbolic two step model from the Boltzmann transport for electrons. Each of these models has functionality. Each is, however, contingent upon the interrelatedness of thermalization time and relaxation time.

The complexity of solutions for Eq. (2.8) lies in the temperature-dependent heat capacity of the electron gas. Tzou argues that for an electron gas temperature lower than the Fermi temperature, (of the order of  $10^4$  K), the electron heat capacity ( $C_e$ ) is proportional to the electron temperature [Tzou 1996]. This argument makes the equation

non-linear. In metals, the specific heat can be given by [Barron 1985]

$$C_e = \gamma_e T_e, \quad (2.9)$$

where  $\gamma_e$  is known as the electron specific heat coefficient and is experimentally obtainable.

In the parabolic dual-phase model, the energy exchange between phonons and electrons is characterized by the phonon-electron coupling factor  $G$  [Kaganov 1957]

$$G = \frac{\pi^2}{6} \frac{m_e n_e v_s^2}{\tau_e T_e} \quad \text{for } T_e \gg T_l, \quad (2.10)$$

where  $m_e$  represents the electron mass,  $n_e$  represents the number of density (concentration) of electrons per unit volume, and  $v_s$  represents the speed of sound

$$v_s = \frac{k}{2\pi\hbar} (6\pi^2 n_a)^{\frac{1}{3}} T_D, \quad (2.11)$$

with the quantity  $h$  being Planck's constant,  $k$  being Boltzmann constant,  $n_a$  being the atomic number density per unit volume, and  $T_D$  representing the Debye temperature. The electron temperature ( $T_e$ ) is much higher than the lattice temperature ( $T_l$ ) in the early time response. The condition  $T_e \gg T_l$  in Eq. (2.10) for the applicability of  $G$  is thus valid in the fast-transient process of electron-phonon dynamics. Within the limits of Wiedemann-Frenz's law, which states that for metals at moderate temperatures ( $T_l > 0.48T_D$ ), the ratio of the thermal conductivity to the electrical conductivity is proportional to the temperature and the constant of proportionality is independent of particular metal, the electron thermal conductivity can be expressed as [Kaganov 1957]

$$k_e = \frac{\pi^2 n_e k^2 \tau_e T_e}{3m_e}, \quad (2.12)$$

or simply

$$m_e = \frac{\pi^2 n_e k^2 \tau_e T_e}{3k_e}, \quad (2.13)$$

Substituting Eq. (2.12) into Eq. (2.10) for the electron mass yields

$$G = \frac{\pi^4 (n_e v k_s)^2}{18k}. \quad (2.14)$$

This coupling factor is dependent upon the thermal conductivity ( $k$ ) and the number density of the electron gas. The coupling factor does not show a strong dependence on temperature and is not affected by relaxation time [Tzou 1996].

In order to estimate the value of  $G$ , the number density of the electron gas is a key quantity. Qiu and Tien assumed one free electron per atom for noble metals and employed the s-band approximation for the valence electrons in transition metals [Qiu 1993c]. Thus, the value for number density of the electron gas is chosen as a fraction of the valence electrons. The phonon-electron coupling factor is calculated, and experimentally measured values are listed in Table 2.1 for comparison.



Table 2.1 Phonon-electron coupling factor ( $G$ ), for some noble and transition metals [Tzou 1997].

Metal	Calculated, $\times 10^{16}$ W/(m <sup>3</sup> K)	Measured, $\times 10^{16}$ W/(m <sup>3</sup> K)
Cu	14	$4.8 \pm 0.7$ (Brorson et al. 1990) 10 (Elsayed-Ali et al. 1987)
Ag	3.1	2.8 (Groeneveld et al. 1990)
Au	2.6	$2.8 \pm 0.5$ (Brorson et al. 1990)
Cr	45 ( $n_e/n_a = 0.5$ )	$42 \pm 5$ (Brorson et al. 1990)
W	27 ( $n_e/n_a = 1.0$ )	$26 \pm 3$ (Brorson et al. 1990)
V	648 ( $n_e/n_a = 2.0$ )	$523 \pm 37$ (Brorson et al. 1990)
Nb	138 ( $n_e/n_a = 2.0$ )	$387 \pm 36$ (Brorson et al. 1990)
Ti	202 ( $n_e/n_a = 1.0$ )	$185 \pm 16$ (Brorson et al. 1990)

Eq. (2.8a) is governed by diffusion in the electron gas and heat is transferred to the lattice in a lumped capacity sense through the coupling factor  $G$ . In other words, the rate of energy increase in the metal lattice is proportional to the temperature difference between the metal lattice and the electrons. By eliminating the electron gas temperature  $T_e$ , from Eq. (2.8) for constant thermal properties, one can show that [Barron 2005]

$$\frac{1}{\alpha_r} \frac{\partial T_l}{\partial t} + \frac{1}{C_r^2} \frac{\partial^2 T_l}{\partial t^2} = \nabla^2 T_l + \frac{\alpha_e}{C_r^2} \frac{\partial}{\partial t} (\nabla^2 T_l), \quad (2.15)$$

where  $\alpha_e$  is the thermal diffusivity of the electron gas and  $\alpha_r$  is the equivalent thermal diffusivity represented by

$$\alpha_T = \frac{k}{C_e + C_l}, \quad (2.16)$$

where  $C_T$  is the thermal wave speed and is represented by

$$C_T = \sqrt{\frac{kG}{C_e C_l}}. \quad (2.17)$$

However, for simplicity of discussion and ease of numerical analysis, this single equation form is seldom utilized. In this work, Eq. (2.8) is used.

Researchers determined the parabolic two-step model to be a good estimate [Qiu 1992]. To compare experimental results with a numerical model, the normalized temperature change in the electron gas is identical to the normalized reflectivity change on the film surface

$$\frac{\Delta R}{(\Delta R)_{\max}} = \frac{\Delta T_e}{(\Delta T_e)_{\max}} \quad (2.18)$$

where  $R$  denotes the reflectivity. The left side of Eq. (2.18) can be measured by the front-surface-pump and back-surface-probe technique [Tzou 1996]. The right hand side of Eq. (2.18) represents the solution to the numerical model for estimating heat propagation.

### 2.3 Previous Work

Till now, there are many researchers studying heat transfer models related to ultrashort-pulsed lasers [Tzou 1994, 1995a, 1995b, 1995c, 1995d, 1997, 1999, 2000a, 2000b, 2001, 2002] [Ozisik 1994] [Chiffell 1994] [Wang 2000, 2001a, 2001b, 2002] [Antaki 1998, 2000, 2002] [Dai 1999, 2000a, 2000b, 2000c, 2001a, 2001b, 2004a, 2004b] [Qiu 1992, 1993, 1994a, 1994b] [Joshi 1993] [Chen 1999a, 1999b, 2000a, 2000b, 2001, 2003] [Al-Nimr 1997a, 1997b, 1999, 2000a, 2000b, 2000c, 2001, 2003] [Ho 1995,

2003] [Tsai 2003]. Among these, Tzou and Ozisik [Tzou 1994] considered the heat equation in only one dimension. They studied the lagging behavior by solving over a semi-infinite interval. Their solutions were obtained using the Laplace transform method and the Reimann-sum approximation for the inversion.

Ozisik's [Ozisik 1994] work gives a thorough overview of the thermal wave theory emphasizing its applications in the field of engineering applications. Special features in the thermal wave propagation such as the sharp wavefront and rate effects, the thermal shock phenomenon, the thermal resonance phenomenon, and reflections of thermal waves across a material interface were discussed. Joshi and Majumdar [Joshi 1993] obtained numerical solutions using the explicit upstream difference method. Antaki and others [Antaki 1998, 2000, 2002] investigated the heat conduction in a semi-infinite slab. Tang and Araki [Tang 1999] derived an analytic solution in finite rigid slabs by using Green's formula and a finite integral transform technique. Ho and colleagues [Ho 1995, 2003] studied heat transfer in a multilayered structure using the lattice Boltzmann method. Tsai and Hung [Tsai 2003] studied thermal wave propagation in a bi-layered composite sphere using the dual-phase-lagging heat transport equation. Recently, Dai and Nassar [Dai 2004b] have developed a finite difference scheme for solving the parabolic two-step heat transport equations in a 3D double-layered rectangular thin film. Tzou and Qiu [Tzou 2001] studied thermal lagging in ultrafast laser heating. This study was implemented to describe the experimental data of femtosecond (fs) laser heating of gold films. Wang and associates [Wang 2001b, 2002] showed the dual-phase heat conduction equation has a unique solution under certain boundary conditions. Al-Nimr and Arpaci [Al-Nimr 1997a, 1997b, 1999, 2000a, 2000b, 2001, 2003] proposed an approach based

on the physical decoupling of the hyperbolic two-step model, to describe the thermal behavior of a thin metal film exposed to picosecond thermal pulse. This approach was based upon the assumption that the metal film thermal behavior occurs in two distinct stages. In the first phase, the electron gas transmits its energy to the lattice through electron-phonon coupling. In the second phase, the electron gas and lattice are at thermal equilibrium. In this phase diffusion dominates the transfer of energy within the system. This method, which eliminates the coupling of energy equations to simplify the system, applies to metal films with the parameter  $\frac{GL^2}{k_e}$  much less than one. Chen and Beraun [Chen 1999a, 1999b, 2000a, 2000b, 2001, 2003] used a corrective smoothed particle method to find a numerical solution to the interaction of short laser bursts and thin metallic films. Dai and Nassar [Dai 1999, 2001, 2002, 2004] have developed many finite difference models for examining a numerical solution for a dual thin film system irradiated by an ultrashort laser burst.

Thus, there is considerable research covering the dual-phase model for heat conduction. However, only a few mathematical models for studying thermal deformation induced by ultrashort-pulsed lasers have been developed [Tzou 2002, Chen2002a, Chen 2002c, Chen 2003]. Tzou and his colleagues [Tzou 2002] presented a one-dimensional model in a double-layered thin film. The model was solved using a differential-difference approach. Chen and his colleagues [Chen 2002a] considered a two-dimensional axisymmetric cylindrical thin film and proposed an explicit finite difference method by adding an artificial viscosity term to eliminate numerical oscillations, and in [Chen 2002c] they applied the method developed in [Chen 2002a] to investigate the deformation of metals subjected to ultrashort-pulsed laser heating, and in [Chen 2003] they developed

a combined finite difference/finite element method to solve the coupled thermomechanical equations. Recently, Dai and Wang [Wang 2006a, Wang 2006b] have developed a finite difference method for studying thermal deformation in 2D thin films exposed to ultrashort pulsed lasers. However, thermal deformation in a 3D micro-sphere has not been studied yet since micro-spheres are of interest related to micro resonators in optical applications, such as ultra-low-threshold lasing, sensing, optoelectronic microdevices, cavity quantum electrodynamics and their potential in quantum information processing. Thus, in this dissertation, we will study thermal deformation about a 3D micro-sphere exposed to ultrashort pulsed lasers by developing a fourth-order compact finite difference scheme for solving the dynamic equations of motion to eliminate non-physical oscillation.

## **CHAPTER THREE**

### **MATHEMATICAL MODEL**

#### **3.1 Problem Description**

In this chapter, we will investigate the mathematical model of heat transport phenomenon in a micro-sphere subjected to an ultrashort-pulsed laser. As described in Chapter Two, the hot-electron blast is found to be significant under intensified heating, and thus ultrafast deformation needs to be addressed in non-equilibrium heating of electrons and phonons. Because the magnitude of deformation may easily reach a fraction of the micro-sphere's thickness on the microscopic level, it is important to investigate the thermal deformation and stress in the microscale levels. And from a microfabrication standpoint, a micro-sphere is an important component in the fabrication of microelectronic devices, and understanding the temperature, displacement, stress distribution at the sub-atomic level as well as in the metal lattice is the subject of important investigations. Geometrically, since the dimensions of a micro-sphere relate favorably to those of elementary physical particles, the micro-sphere can be used to model the heat transport phenomenon in physical particles. Thus, a clear understanding of the temperature, displacement, stress distribution in this microelectronic device is of vital importance. To the end, the well-posedness of the problem is investigated; the numerical

schemes are proposed to solve the governing equations.

### 3.2 Model for a Micro-Sphere

#### 3.2.1 Geometry Description

Figure 3.1 shows a micro-sphere in a three-dimensional coordinates system which is exposed to ultrashort-pulsed lasers. Consider the spherical coordinates system, the point P is defined by the following spherical coordinates:  $r, \theta, \varphi$ , where  $r$  is the length of OP, ranging from 0 to  $\infty$ ;  $\theta$  is the angle between the projection of OP on the XY-plane with the positive X-axis ranging from 0 to  $2\pi$ ;  $\varphi$  is the angle between OP and the positive Z-axis ranging from 0 to  $\pi$ .

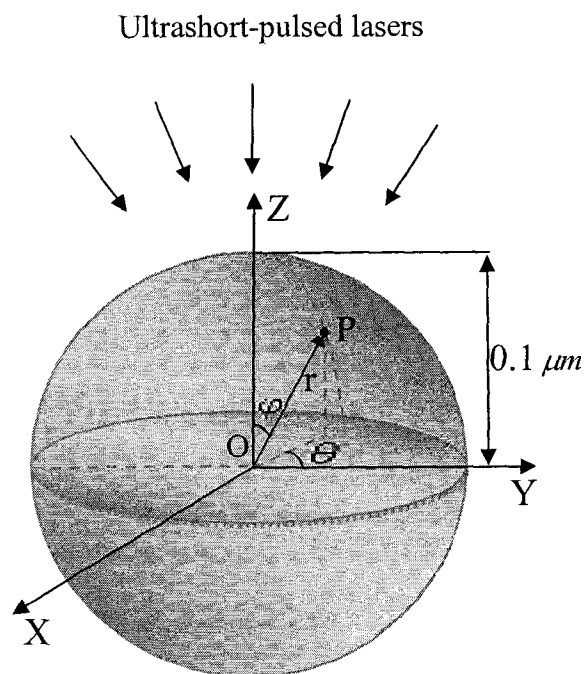


Fig. 3.1 A 3D micro-sphere with three-dimensional coordinate systems

### 3.2.2 Governing Equations

The governing equations for studying thermal deformation in the micro-sphere can be expressed as follows:

(1) Dynamic equations of motion [Tzou 2002, Chen 2002a, Brorson 1987, Wang 2006a, Reismann 1980]:

$$\rho \frac{\partial^2 u_r}{\partial t^2} = \frac{\partial \sigma_r}{\partial r} + \frac{1}{r} \frac{\partial \sigma_{r\varphi}}{\partial \varphi} + \frac{1}{r \sin \varphi} \frac{\partial \sigma_{r\theta}}{\partial \theta} + \frac{1}{r} (2\sigma_r - \sigma_\varphi - \sigma_\theta + \sigma_{r\varphi} \cot \varphi) + 2\Lambda T_e \frac{\partial T_e}{\partial r}, \quad (3.1)$$

$$\rho \frac{\partial^2 u_\varphi}{\partial t^2} = \frac{\partial \sigma_{r\varphi}}{\partial r} + \frac{1}{r} \frac{\partial \sigma_\varphi}{\partial \varphi} + \frac{1}{r \sin \varphi} \frac{\partial \sigma_{\varphi\theta}}{\partial \theta} + \frac{1}{r} [(\sigma_\varphi - \sigma_\theta) \cot \varphi + 3\sigma_{r\varphi}] + 2\Lambda T_e \frac{1}{r} \frac{\partial T_e}{\partial \varphi}, \quad (3.2)$$

$$\rho \frac{\partial^2 u_\theta}{\partial t^2} = \frac{\partial \sigma_{r\theta}}{\partial r} + \frac{1}{r} \frac{\partial \sigma_{\varphi\theta}}{\partial \varphi} + \frac{1}{r \sin \varphi} \frac{\partial \sigma_\theta}{\partial \theta} + \frac{1}{r} (2\sigma_{\varphi\theta} \cot \varphi + 3\sigma_{r\theta}) + 2\Lambda T_e \frac{1}{r \sin \varphi} \frac{\partial T_e}{\partial \theta}, \quad (3.3)$$

$$\sigma_r = \lambda(\varepsilon_r + \varepsilon_\varphi + \varepsilon_\theta) + 2\mu\varepsilon_r - (3\lambda + 2\mu)\alpha_T(T_l - T_0), \quad (3.4)$$

$$\sigma_\varphi = \lambda(\varepsilon_r + \varepsilon_\varphi + \varepsilon_\theta) + 2\mu\varepsilon_\varphi - (3\lambda + 2\mu)\alpha_T(T_l - T_0), \quad (3.5)$$

$$\sigma_\theta = \lambda(\varepsilon_r + \varepsilon_\varphi + \varepsilon_\theta) + 2\mu\varepsilon_\theta - (3\lambda + 2\mu)\alpha_T(T_l - T_0), \quad (3.6)$$

$$\sigma_{r\varphi} = 2\mu\varepsilon_{r\varphi}, \sigma_{r\theta} = 2\mu\varepsilon_{r\theta}, \sigma_{\varphi\theta} = 2\mu\varepsilon_{\varphi\theta}, \quad (3.7)$$

$$\varepsilon_r = \frac{\partial u_r}{\partial r}, \quad (3.8)$$

$$\varepsilon_\varphi = \frac{1}{r} \left( u_r + \frac{\partial u_\varphi}{\partial \varphi} \right), \quad (3.9)$$

$$\varepsilon_\theta = \frac{1}{r \sin \varphi} \left( \frac{\partial u_\theta}{\partial \theta} + \sin \varphi u_r + \cos \varphi u_\varphi \right), \quad (3.10)$$

$$\varepsilon_{r\varphi} = \frac{1}{2} \left( \frac{1}{r} \frac{\partial u_r}{\partial \varphi} + \frac{\partial u_\varphi}{\partial r} - \frac{u_\varphi}{r} \right), \quad (3.11)$$



$$\varepsilon_{\varphi\theta} = \frac{1}{2r} \left( \frac{1}{\sin\varphi} \frac{\partial u_\varphi}{\partial\theta} + \frac{\partial u_\theta}{\partial\varphi} - u_\theta \cot\varphi \right), \quad (3.12)$$

$$\varepsilon_{r\theta} = \frac{1}{2} \left( \frac{1}{r \sin\varphi} \frac{\partial u_r}{\partial\theta} + \frac{\partial u_\theta}{\partial r} - \frac{u_\theta}{r} \right). \quad (3.13)$$

Here,  $u_r, u_\theta, u_\varphi$  are the displacements in the  $r, \theta, \varphi$  directions, respectively;  $\varepsilon_r, \varepsilon_\theta, \varepsilon_\varphi$  are the normal strains in the  $r, \theta, \varphi$  directions, respectively;  $\varepsilon_{r\varphi}$  is the shear strain in the  $r\varphi$  direction,  $\varepsilon_{r\theta}$  is the shear strain in the  $r\theta$  direction, and  $\varepsilon_{\varphi\theta}$  is the shear strain in the  $\varphi\theta$  direction;  $\sigma_r, \sigma_\theta, \sigma_\varphi$  are the normal stresses in the  $r, \theta, \varphi$  directions, respectively;  $\sigma_{r\varphi}$  is the shear stress in the  $r\varphi$  direction,  $\sigma_{r\theta}$  is the shear stress in the  $r\theta$  direction, and  $\sigma_{\varphi\theta}$  is the shear stress in the  $\varphi\theta$  direction;  $T_e$  and  $T_l$  are electron and lattice temperatures, respectively;  $T_0$  is the initial temperature;  $\rho$  is density;  $\Lambda$  is the electron-blast coefficient;  $\lambda = K - \frac{2}{3}\mu$  [Reismann 1980] and  $\mu$  are Lamé's coefficients;  $K$  is bulk modulus; and  $\alpha_T$  is the thermal expansion coefficient.

(2) Energy equations [Tzou 2002, Kaba 2005, Chen 2005, Qiu 1992, Tzou 1996]:

$$\begin{aligned} C_e(T_e) \frac{\partial T_e}{\partial t} &= \frac{1}{r^2} \frac{\partial}{\partial r} (k_e(T_e, T_l) r^2 \frac{\partial T_e}{\partial r}) + \frac{1}{r^2 \sin^2 \varphi} \frac{\partial}{\partial \theta} (k_e(T_e, T_l) \frac{\partial T_e}{\partial \theta}) \\ &+ \frac{1}{r^2 \sin \varphi} \frac{\partial}{\partial \varphi} (k_e(T_e, T_l) \sin \varphi \frac{\partial T_e}{\partial \varphi}) - G(T_e - T_l) + Q, \end{aligned} \quad (3.14)$$

$$C_l \frac{\partial T_l}{\partial t} = G(T_e - T_l) - (3\lambda + 2\mu) \alpha_T \frac{\partial}{\partial t} (\varepsilon_r + \varepsilon_\varphi + \varepsilon_\theta), \quad (3.15)$$

where the heat source is given by

$$Q(r, \theta, \varphi, t) = 0.94J \frac{1-R}{t_p \zeta} \exp\left[-\frac{L-r}{\zeta} - 2.77 \left(\frac{t-2t_p}{t_p}\right)^2\right] \cos\varphi. \quad (3.16)$$

Here,  $C_e(T_e) = C_{e0} \left( \frac{T_e}{T_0} \right)$  is the electron heat capacity,  $k_e(T_e, T_l) = k_0 \left( \frac{T_e}{T_l} \right)$  is the thermal conductivity,  $G$  is the electron–lattice coupling factor,  $C_l$  is the lattice heat capacity, respectively;  $Q$  is the energy absorption rate;  $J$  is laser fluence;  $R$  is surface reflectivity;  $t_p$  is laser pulse duration;  $L$  is the radius of the micro-sphere;  $\zeta$  is the optical penetration depth; Eqs. (3.14) and (3.15) are often referred to as the parabolic two-step heat transport equations.

### 3.2.3 Boundary Conditions and Initial Conditions

The boundary conditions are assumed to be stress free and thermally insulated [Tzou 2002, Chen 2002]:

$$\sigma_r = 0, \quad \sigma_{r\varphi} = 0, \quad \sigma_{r\theta} = 0 \quad \text{at } r = L \quad (3.17)$$

$$\sigma_\theta = \sigma_{\theta+2\pi}, \quad \sigma_{r\theta} = \sigma_{r\theta+2\pi}, \quad \sigma_{\varphi\theta} = \sigma_{\varphi\theta+2\pi} \quad (3.18)$$

$$\frac{\partial T_e}{\partial r} = 0, \quad \frac{\partial T_l}{\partial r} = 0 \quad \text{at } r = L \quad (3.19)$$

$$T_e(r, \theta, \varphi, t) = T_e(r, \theta + 2\pi, \varphi, t), \quad T_l(r, \theta, \varphi, t) = T_l(r, \theta + 2\pi, \varphi, t) \quad (3.20)$$

Without loss of generality, we assume for simplicity:

$$\frac{\partial \sigma_r}{\partial r} = 0, \quad \frac{\partial \sigma_{r\theta}}{\partial r} = 0, \quad \frac{\partial \sigma_{r\varphi}}{\partial r} = 0, \quad \frac{\partial T_e}{\partial r} = 0, \quad \frac{\partial T_l}{\partial r} = 0 \quad \text{at } r = 0 \quad (3.21)$$

$$\frac{\partial \sigma_\varphi}{\partial \varphi} = 0, \quad \frac{\partial \sigma_{\varphi\theta}}{\partial \varphi} = 0, \quad \frac{\partial \sigma_{r\varphi}}{\partial \varphi} = 0, \quad \frac{\partial T_e}{\partial \varphi} = 0, \quad \frac{\partial T_l}{\partial \varphi} = 0 \quad \text{at } \varphi = 0, \pi \quad (3.22)$$

It should be pointed out that insulated boundaries are imposed due to the assumption that there are no heat losses from the sphere surfaces in the short time response [Tzou 1996].

The initial conditions are assumed to be:

$$T_e = T_l = T_0, u_r = u_\varphi = u_\theta = 0, \frac{\partial u_r}{\partial t} = \frac{\partial u_\theta}{\partial t} = \frac{\partial u_\varphi}{\partial t} = 0 \quad \text{at } t = 0. \quad (3.23)$$

### 3.3 Conclusion

In this chapter, we have set up the governing equations for the model of a micro-sphere for studying thermal deformation. However, the mathematical complexity of the coupled, nonlinear, transient governing Eqs. (3.1) – (3.16) make it impossible to derive closed-form solutions to the present model because of the temperature-dependent thermophysical properties such as  $C_e(T_e)$ ,  $C_l(T_l)$ ,  $k_e(T_e, T_l)$  and because of the nonlinear hot-electron blast force. Hence, the numerical methods are needed to find out for solving these mathematical models.

## CHAPTER FOUR

### FINITE DIFFERENCE METHOD

In this chapter, we will develop finite difference methods for solving those governing equations set up in the previous chapter. In view of the fact that the numerical difficulty caused by a grid mesh having a high aspect ratio is less for finite difference methods than for finite element methods, the hyperbolic-parabolic partial differential equation system combined with the initial and boundary conditions is solved with finite difference methods.

#### 4.1 Notations

We denote  $u_r^n(i+1/2, j, k)$ ,  $u_\theta^n(i, j+1/2, k)$ , and  $u_\varphi^n(i, j, k+1/2)$  as numerical approximations of  $u_r((i+1/2)\Delta r, j\Delta\theta, k\Delta\varphi, n\Delta t)$ ,  $u_\theta(i\Delta r, (j+1/2)\Delta\theta, k\Delta\varphi, n\Delta t)$ , and  $u_\varphi(i\Delta r, j\Delta\theta, (k+1/2)\Delta\varphi, n\Delta t)$ , respectively, where  $\Delta t, \Delta r, \Delta\theta$  and  $\Delta\varphi$  are time increment and spatial grid sizes, respectively. And  $i, j, k$  are indices with  $1 \leq i \leq N_r + 1$ ,  $1 \leq j \leq N_\theta + 1$  and  $1 \leq k \leq N_\varphi + 1$  so that  $N_r\Delta r = L$ ,  $N_\theta\Delta\theta = 2\pi$  and  $N_\varphi\Delta\varphi = \pi$ . Similar notations are used for other variables. Furthermore, we introduce the finite difference operators  $\Delta_{-t}$ ,  $\delta_r$ ,  $\delta_\theta$  and  $\delta_\varphi$  as follows:

$$\Delta_{-t}u^n(i, j, k) = u^n(i, j, k) - u^{n-1}(i, j, k), \quad (4.1)$$

$$\delta_r u^n(i, j, k) = u^n(i+1/2, j, k) - u^n(i-1/2, j, k), \quad (4.2)$$

$$\delta_\theta u^n(i, j, k) = u^n(i, j + 1/2, k) - u^n(i, j - 1/2, k), \quad (4.3)$$

$$\delta_\varphi u^n(i, j, k) = u^n(i, j, k + 1/2) - u^n(i, j, k - 1/2), \quad (4.4)$$

## 4.2 Finite Difference Scheme and Algorithm

### 4.2.1 Conversion of the Governing Equations

In order to prevent the solution from oscillations, using a similar argument as that in [Wang 2006a, Wang 2006b], we introduce three velocity components  $v_r$ ,  $v_\theta$  and  $v_\varphi$  into the model and re-write the dynamic equations of motion, Eqs. (3.1) – (3.13) as follows:

$$v_r = \frac{\partial u_r}{\partial t}, \quad v_\theta = \frac{\partial u_\theta}{\partial t}, \quad v_\varphi = \frac{\partial u_\varphi}{\partial t}, \quad (4.5)$$

$$\rho \frac{\partial v_r}{\partial t} = \frac{\partial \sigma_r}{\partial r} + \frac{1}{r} \frac{\partial \sigma_{r\varphi}}{\partial \varphi} + \frac{1}{r \sin \varphi} \frac{\partial \sigma_{r\theta}}{\partial \theta} + \frac{1}{r} (2\sigma_r - \sigma_\varphi - \sigma_\theta + \sigma_{r\varphi} \cot \varphi) + 2\Lambda T_e \frac{\partial T_e}{\partial r}, \quad (4.6)$$

$$\rho \frac{\partial v_\varphi}{\partial t} = \frac{\partial \sigma_{r\varphi}}{\partial r} + \frac{1}{r} \frac{\partial \sigma_\varphi}{\partial \varphi} + \frac{1}{r \sin \varphi} \frac{\partial \sigma_{\varphi\theta}}{\partial \theta} + \frac{1}{r} [(\sigma_\varphi - \sigma_\theta) \cot \varphi + 3\sigma_{r\varphi}] + 2\Lambda T_e \frac{1}{r} \frac{\partial T_e}{\partial \varphi}, \quad (4.7)$$

$$\rho \frac{\partial v_\theta}{\partial t} = \frac{\partial \sigma_{r\theta}}{\partial r} + \frac{1}{r} \frac{\partial \sigma_{\varphi\theta}}{\partial \varphi} + \frac{1}{r \sin \varphi} \frac{\partial \sigma_\theta}{\partial \theta} + \frac{1}{r} (2\sigma_{\varphi\theta} \cot \varphi + 3\sigma_{r\theta}) + 2\Lambda T_e \frac{1}{r \sin \varphi} \frac{\partial T_e}{\partial \theta}, \quad (4.8)$$

$$\sigma_r = \lambda(\varepsilon_r + \varepsilon_\varphi + \varepsilon_\theta) + 2\mu\varepsilon_r - (3\lambda + 2\mu)\alpha_T(T_l - T_0), \quad (4.9)$$

$$\sigma_\varphi = \lambda(\varepsilon_r + \varepsilon_\varphi + \varepsilon_\theta) + 2\mu\varepsilon_\varphi - (3\lambda + 2\mu)\alpha_T(T_l - T_0), \quad (4.10)$$

$$\sigma_\theta = \lambda(\varepsilon_r + \varepsilon_\varphi + \varepsilon_\theta) + 2\mu\varepsilon_\theta - (3\lambda + 2\mu)\alpha_T(T_l - T_0), \quad (4.11)$$

$$\sigma_{r\varphi} = 2\mu\varepsilon_{r\varphi}, \quad \sigma_{r\theta} = 2\mu\varepsilon_{r\theta}, \quad \sigma_{\varphi\theta} = 2\mu\varepsilon_{\varphi\theta}, \quad (4.12)$$

$$\frac{\partial \varepsilon_r}{\partial t} = \frac{\partial v_r}{\partial r}, \quad (4.13)$$

$$\frac{\partial \varepsilon_\varphi}{\partial t} = \frac{1}{r} (v_r + \frac{\partial v_\varphi}{\partial \varphi}), \quad (4.14)$$

$$\frac{\partial \varepsilon_\theta}{\partial t} = \frac{1}{r \sin \varphi} \left( \frac{\partial v_\theta}{\partial \theta} + v_r \sin \varphi + v_\varphi \cos \varphi \right), \quad (4.15)$$

$$\frac{\partial \varepsilon_{r\varphi}}{\partial t} = \frac{1}{2} \left( \frac{1}{r} \frac{\partial v_r}{\partial \varphi} + \frac{\partial v_\varphi}{\partial r} - \frac{v_\varphi}{r} \right), \quad (4.16)$$

$$\frac{\partial \varepsilon_{\varphi\theta}}{\partial t} = \frac{1}{2r} \left( \frac{1}{\sin \varphi} \frac{\partial v_\varphi}{\partial \theta} + \frac{\partial v_\theta}{\partial \varphi} - v_\theta \cot \varphi \right), \quad (4.17)$$

$$\frac{\partial \varepsilon_{r\theta}}{\partial t} = \frac{1}{2} \left( \frac{1}{r \sin \varphi} \frac{\partial v_r}{\partial \theta} + \frac{\partial v_\theta}{\partial r} - \frac{v_\theta}{r} \right). \quad (4.18)$$

#### 4.2.2 Staggered Grid

To develop the finite difference schemes, we need to construct a staggered grid shown as Fig. 4.1, where  $v_r$  and  $u_r$  are placed at  $(r_{i+1/2}, \theta_j, \varphi_k)$ ,  $v_\theta$  and  $u_\theta$  are placed at  $(r_i, \theta_{j+1/2}, \varphi_k)$ ,  $v_\varphi$  and  $u_\varphi$  are placed at  $(r_i, \theta_j, \varphi_{k+1/2})$ ,  $\varepsilon_{r\theta}$  and  $\sigma_{r\theta}$  are placed at  $(r_{i+1/2}, \theta_{j+1/2}, \varphi_k)$ ,  $\varepsilon_{r\varphi}$  and  $\sigma_{r\varphi}$  are placed at  $(r_{i+1/2}, \theta_j, \varphi_{k+1/2})$ ,  $\varepsilon_{\varphi\theta}$  and  $\sigma_{\varphi\theta}$  are placed at  $(r_i, \theta_{j+1/2}, \varphi_{k+1/2})$ , while  $\varepsilon_r, \varepsilon_\theta, \varepsilon_\varphi, \sigma_r, \sigma_\theta, \sigma_\varphi, T_e$  and  $T_l$  are at  $(r_i, \theta_j, \varphi_k)$ . Here, we denote  $v_r''(i+1/2, j, k)$ ,  $v_\theta''(i, j+1/2, k)$  and  $v_\varphi''(i, j, k+1/2)$  as numerical approximations of  $v_r((i+1/2)\Delta r, j\Delta\theta, k\Delta\varphi, n\Delta t)$ ,  $v_\theta(i\Delta r, (j+1/2)\Delta\theta, k\Delta\varphi, n\Delta t)$  and  $v_\varphi(i\Delta r, j\Delta\theta, (k+1/2)\Delta\varphi, n\Delta t)$ , respectively.

It should be pointed out that the staggered-grid method is often employed in computational fluid dynamics to prevent the solution from oscillation [Patankar 1980]. For example, if  $v_r$  and  $\varepsilon_r$  in Eq. (4.13) are placed at a same location, implying a central finite difference scheme may produce a velocity component  $v_r$ , a wave solution, implying oscillation.

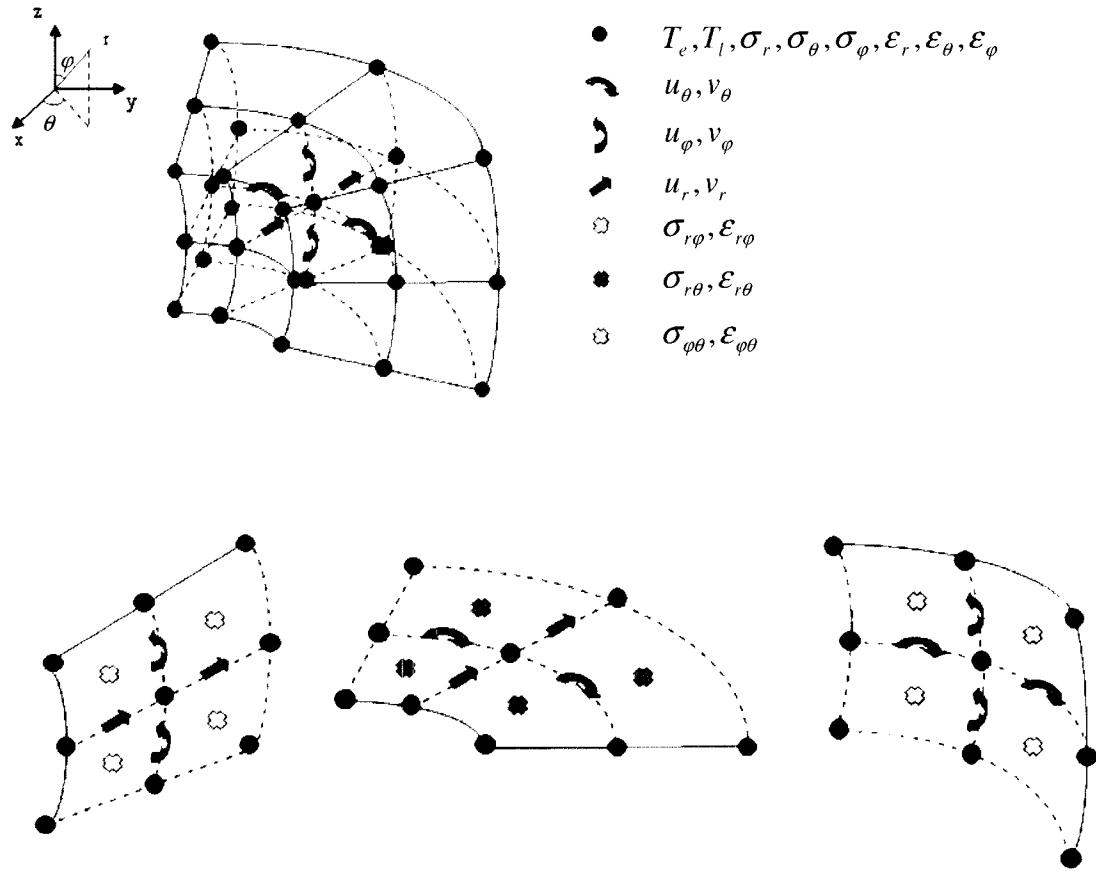


Fig. 4.1 A 3D staggered grid and locations of variables for a micro-sphere.

### 4.2.3 Finite Difference Scheme

Now we begin to develop the finite difference methods for solving the above governing equations. To avoid non-physical oscillations in the solution, we further develop a fourth-order compact finite difference scheme for evaluating stress derivatives

and shear stress derivatives  $\frac{\partial \sigma_r}{\partial r}$ ,  $\frac{\partial \sigma_{r\phi}}{\partial \phi}$ ,  $\frac{\partial \sigma_{\phi\theta}}{\partial \theta}$  and etc. in Eqs. (4.6) – (4.8). To this end,

we let

$$a \frac{\partial \sigma_r(i-1)}{\partial r} + b \frac{\partial \sigma_r(i)}{\partial r} + a \frac{\partial \sigma_r(i+1)}{\partial r} = \frac{\sigma_r(i+1/2) - \sigma_r(i-1/2)}{\Delta r}, \quad 2 + \frac{1}{2} \leq i \leq N_r - \frac{1}{2}, \quad (4.19)$$

where a and b are unknown constants. Here, we omit indices  $j, k$  and  $n$  for simplicity.

Using the Taylor series expansion, we obtain

$$\sigma_r(i+1/2) = \sigma_r(i) + \frac{\Delta r}{2} \frac{\partial \sigma_r(i)}{\partial r} + \frac{\Delta r^2}{2!2^2} \frac{\partial^2 \sigma_r(i)}{\partial r^2} + \frac{\Delta r^3}{3!2^3} \frac{\partial^3 \sigma_r(i)}{\partial r^3} + \frac{\Delta r^4}{4!2^4} \frac{\partial^4 \sigma_r(i)}{\partial r^4} + O(\Delta r^5), \quad (4.20a)$$

$$\sigma_r(i-1/2) = \sigma_r(i) - \frac{\Delta r}{2} \frac{\partial \sigma_r(i)}{\partial r} + \frac{\Delta r^2}{2!2^2} \frac{\partial^2 \sigma_r(i)}{\partial r^2} - \frac{\Delta r^3}{3!2^3} \frac{\partial^3 \sigma_r(i)}{\partial r^3} + \frac{\Delta r^4}{4!2^4} \frac{\partial^4 \sigma_r(i)}{\partial r^4} + O(\Delta r^5), \quad (4.20b)$$

$$\frac{\partial \sigma_r(i+1)}{\partial r} = \frac{\partial \sigma_r(i)}{\partial r} + \Delta r \frac{\partial^2 \sigma_r(i)}{\partial r^2} + \frac{\Delta r^2}{2} \frac{\partial^3 \sigma_r(i)}{\partial r^3} + \frac{\Delta r^3}{3!} \frac{\partial^4 \sigma_r(i)}{\partial r^4} + O(\Delta r^4), \quad (4.20c)$$

$$\frac{\partial \sigma_r(i-1)}{\partial r} = \frac{\partial \sigma_r(i)}{\partial r} - \Delta r \frac{\partial^2 \sigma_r(i)}{\partial r^2} + \frac{\Delta r^2}{2} \frac{\partial^3 \sigma_r(i)}{\partial r^3} - \frac{\Delta r^3}{3!} \frac{\partial^4 \sigma_r(i)}{\partial r^4} + O(\Delta r^4), \quad (4.20d)$$

substituting Eqs. (4.20a) – (4.20d) into Eq. (4.19), and comparing the corresponding terms, we obtain

$$2a + b = \frac{1}{2}, \quad a = \frac{1}{24}, \quad b = \frac{5}{12}, \quad (4.21)$$

with truncation error of  $O(\Delta r^4)$ . It should be pointed out that the dissipative term

$\frac{\partial^3 \sigma_r(i)}{\partial r^3}$  has been eliminated from the truncation error. Hence,  $\frac{\partial \sigma_r(i)}{\partial r}$  can be obtained

by solving the following tridiagonal system

$$\frac{1}{24} \frac{\partial \sigma_r(i-1)}{\partial r} + \frac{5}{12} \frac{\partial \sigma_r(i)}{\partial r} + \frac{1}{24} \frac{\partial \sigma_r(i+1)}{\partial r} = \frac{\sigma_r(i+1/2) - \sigma_r(i-1/2)}{\Delta r}, \quad 2 + \frac{1}{2} \leq i \leq N_r - \frac{1}{2}, \quad (4.22)$$

where

$$\frac{\partial \sigma_r(3/2)}{\partial r} = \frac{\sigma_r(2) - \sigma_r(1)}{\Delta r}, \quad \frac{\partial \sigma_r(N_r + 1/2)}{\partial r} = \frac{\sigma_r(N_r + 1) - \sigma_r(N_r)}{\Delta r}. \quad (4.23)$$



Using the similar argument, we can evaluate other stress derivatives and shear stress derivatives in Eqs. (4.6) – (4.8). Then to Eq. (4.6), by using Taylor series expansion we can obtain following equations at point  $(i + \frac{1}{2}, j, k)$

$$v_r^n(i+1/2, j, k) = v_r^{n+1}(i+1/2, j, k) - \Delta t \frac{\partial v_r^{n+1}(i+1/2, j, k)}{\partial t} + \frac{\Delta t^2}{2} \frac{\partial^2 v_r^{n+1}(i+1/2, j, k)}{\partial t^2} + O(\Delta t^3),$$

thus,

$$\frac{\partial v_r^{n+1}(i+1/2, j, k)}{\partial t} = \frac{v_r^{n+1}(i+1/2, j, k) - v_r^n(i+1/2, j, k)}{\Delta t} + O(\Delta t), \quad (4.24a)$$

and then by  $\frac{\partial f(u)}{\partial x} = \frac{df}{du} \cdot \frac{\partial u}{\partial x}$ , we can obtain

$$2\Lambda T_e \frac{\partial T_e}{\partial r} = \Lambda \frac{\partial T_e^2}{\partial r}, \quad (4.24b)$$

from Eq. (4.24b), by using Taylor series expansion again we can obtain

$$(T_e^2)^{n+1}(i+1, j, k) = (T_e^2)^{n+1}(i+1/2, j, k) + \frac{\Delta r}{2} \frac{\partial (T_e^2)^{n+1}(i+1/2, j, k)}{\partial r} + \frac{\Delta r^2}{8} \frac{\partial^2 (T_e^2)^{n+1}(i+1/2, j, k)}{\partial r^2} + O(\Delta r^3),$$

$$(T_e^2)^{n+1}(i, j, k) = (T_e^2)^{n+1}(i+1/2, j, k) - \frac{\Delta r}{2} \frac{\partial (T_e^2)^{n+1}(i+1/2, j, k)}{\partial r} + \frac{\Delta r^2}{8} \frac{\partial^2 (T_e^2)^{n+1}(i+1/2, j, k)}{\partial r^2} + O(\Delta r^3),$$

which is

$$\frac{\partial (T_e^2)^{n+1}(i+1/2, j, k)}{\partial r} = \frac{(T_e^2)^{n+1}(i+1, j, k) - (T_e^2)^{n+1}(i, j, k)}{\Delta r} + O(\Delta r^2), \quad (4.24c)$$

substituting Eqs. (4.24a) – (4.24c) into Eq. (4.6), we obtain

$$\begin{aligned}
& \rho \frac{1}{\Delta t} \Delta_{-t} v_r^{n+1}(i+1/2, j, k) \\
&= \frac{\partial \sigma_r(i+1/2, j, k)}{\partial r} + \frac{1}{r_{i+1/2}} \frac{\partial \sigma_{r\varphi}(i+1/2, j, k)}{\partial \varphi} + \frac{1}{r_{i+1/2} \sin \varphi_k} \frac{\partial \sigma_{r\theta}(i+1/2, j, k)}{\partial \theta} \\
&+ \frac{1}{r_{i+1/2}} \left[ 2 \frac{\sigma_r^{n+1}(i, j, k) + \sigma_r^{n+1}(i+1, j, k)}{2} - \frac{\sigma_\varphi^{n+1}(i, j, k) + \sigma_\varphi^{n+1}(i+1, j, k)}{2} \right. \\
&- \left. \frac{\sigma_\theta^{n+1}(i, j, k) + \sigma_\theta^{n+1}(i+1, j, k)}{2} + \frac{\sigma_{r\varphi}^{n+1}(i+1/2, j, k+1/2) + \sigma_{r\varphi}^{n+1}(i+1/2, j, k-1/2)}{2} \cot \varphi_k \right] \\
&+ \Lambda \frac{1}{\Delta r} \delta_r (T_e^2)^{n+1}(i+1/2, j, k).
\end{aligned} \tag{4.24}$$

Similarly to Eqs. (4.7) and (4.8), we can obtain following equations at point  $(i, j, k + \frac{1}{2})$

and point  $(i, j + \frac{1}{2}, k)$ , respectively

$$\begin{aligned}
& \rho \frac{1}{\Delta t} \Delta_{-t} v_\varphi^{n+1}(i, j, k+1/2) \\
&= \frac{\partial \sigma_{r\varphi}(i, j, k+1/2)}{\partial r} + \frac{1}{r_i} \frac{\partial \sigma_\varphi(i, j, k+1/2)}{\partial \varphi} + \frac{1}{r_i \sin \varphi_{k+1/2}} \frac{\partial \sigma_{\varphi\theta}(i, j, k+1/2)}{\partial \theta} \\
&+ \frac{1}{r_i} \left[ \left( \frac{\sigma_\varphi^{n+1}(i, j, k+1) + \sigma_\varphi^{n+1}(i, j, k)}{2} - \frac{\sigma_\theta^{n+1}(i, j, k+1) + \sigma_\theta^{n+1}(i, j, k)}{2} \right) \cot \varphi_{k+1/2} \right. \\
&+ \left. 3 \frac{\sigma_{r\varphi}^{n+1}(i+1/2, j, k+1/2) + \sigma_{r\varphi}^{n+1}(i-1/2, j, k+1/2)}{2} \right] \\
&+ \Lambda \frac{1}{r_i \Delta \varphi} \delta_\varphi (T_e^2)^{n+1}(i, j, k+1/2),
\end{aligned} \tag{4.25}$$

$$\begin{aligned}
& \rho \frac{1}{\Delta t} \Delta_{-t} v_{\theta}^{n+1}(i, j+1/2, k) \\
&= \frac{\partial \sigma_{r\theta}(i, j+1/2, k)}{\partial r} + \frac{1}{r_i} \frac{\partial \sigma_{\varphi\theta}(i, j+1/2, k)}{\partial \varphi} + \frac{1}{r_i \sin \varphi_k} \frac{\partial \sigma_{\theta}(i, j+1/2, k)}{\partial \theta} \\
&+ \frac{1}{r_i} \left[ 2 \frac{\sigma_{\varphi\theta}^{n+1}(i, j+1/2, k+1/2) + \sigma_{\varphi\theta}^{n+1}(i, j+1/2, k-1/2)}{2} \right] \cot \varphi_k \\
&+ 3 \frac{\sigma_{r\theta}^{n+1}(i+1/2, j+1/2, k) + \sigma_{r\theta}^{n+1}(i-1/2, j+1/2, k)}{2} \\
&+ \Lambda \frac{1}{r_i \sin \varphi_k \Delta \theta} \delta_{\theta} (T_e^2)^{n+1}(i, j+1/2, k).
\end{aligned} \tag{4.26}$$

To Eqs. (4.9) – (4.12) we obtain following equations at point  $(i, j, k)$

$$\begin{aligned}
\sigma_r^{n+1}(i, j, k) &= \lambda [\varepsilon_r^{n+1}(i, j, k) + \varepsilon_{\varphi}^{n+1}(i, j, k) + \varepsilon_{\theta}^{n+1}(i, j, k)] + 2\mu \varepsilon_r^{n+1}(i, j, k) \\
&\quad - (3\lambda + 2\mu) \alpha_r [T_l^{n+1}(i, j, k) - T_0],
\end{aligned} \tag{4.27}$$

$$\begin{aligned}
\sigma_{\varphi}^{n+1}(i, j, k) &= \lambda [\varepsilon_r^{n+1}(i, j, k) + \varepsilon_{\varphi}^{n+1}(i, j, k) + \varepsilon_{\theta}^{n+1}(i, j, k)] + 2\mu \varepsilon_{\varphi}^{n+1}(i, j, k) \\
&\quad - (3\lambda + 2\mu) \alpha_r [T_l^{n+1}(i, j, k) - T_0],
\end{aligned} \tag{4.28}$$

$$\begin{aligned}
\sigma_{\theta}^{n+1}(i, j, k) &= \lambda [\varepsilon_r^{n+1}(i, j, k) + \varepsilon_{\varphi}^{n+1}(i, j, k) + \varepsilon_{\theta}^{n+1}(i, j, k)] + 2\mu \varepsilon_{\theta}^{n+1}(i, j, k) \\
&\quad - (3\lambda + 2\mu) \alpha_r [T_l^{n+1}(i, j, k) - T_0],
\end{aligned} \tag{4.29}$$

$$\sigma_{r\varphi}^{n+1}(i+1/2, j, k+1/2) = 2\mu \varepsilon_{r\varphi}^{n+1}(i+1/2, j, k+1/2), \tag{4.30}$$

$$\sigma_{r\theta}^{n+1}(i+1/2, j+1/2, k) = 2\mu \varepsilon_{r\theta}^{n+1}(i+1/2, j+1/2, k), \tag{4.31}$$

$$\sigma_{\varphi\theta}^{n+1}(i, j+1/2, k+1/2) = 2\mu \varepsilon_{\varphi\theta}^{n+1}(i, j+1/2, k+1/2). \tag{4.32}$$

To discretize Eq. (4.13), by using Taylor series expansion at point  $(i, j, k)$  we obtain

$$\varepsilon_r^n(i, j, k) = \varepsilon_r^{n+1}(i, j, k) - \Delta t \frac{\partial \varepsilon_r^{n+1}(i, j, k)}{\partial t} + \frac{\Delta t^2}{2} \frac{\partial^2 \varepsilon_r^{n+1}(i, j, k)}{\partial t^2} + O(\Delta t^3),$$

that is,

$$\frac{\partial \varepsilon_r^{n+1}(i, j, k)}{\partial t} = \frac{\varepsilon_r^{n+1}(i, j, k) - \varepsilon_r^n(i, j, k)}{\Delta t} + O(\Delta t), \tag{4.33a}$$

$$v_r^{n+1}(i+1/2, j, k) = v_r^{n+1}(i, j, k) + \frac{\Delta r}{2} \frac{\partial v_r^{n+1}(i, j, k)}{\partial r} + \frac{\Delta r^2}{8} \frac{\partial^2 v_r^{n+1}(i, j, k)}{\partial r^2} + O(\Delta r^3),$$

$$v_r^{n+1}(i-1/2, j, k) = v_r^{n+1}(i, j, k) - \frac{\Delta r}{2} \frac{\partial v_r^{n+1}(i, j, k)}{\partial r} + \frac{\Delta r^2}{8} \frac{\partial^2 v_r^{n+1}(i, j, k)}{\partial r^2} + O(\Delta r^3),$$

that is,

$$\frac{\partial v_r^{n+1}(i, j, k)}{\partial r} = \frac{v_r^{n+1}(i+1/2, j, k) - v_r^{n+1}(i-1/2, j, k)}{\Delta r} + O(\Delta r^2), \quad (4.33b)$$

substituting Eqs. (4.33a) and (4.33b) into Eq. (4.13), we obtain

$$\frac{1}{\Delta t} \Delta_{-r} \varepsilon_r^{n+1}(i, j, k) = \frac{1}{\Delta r} \delta_r v_r^{n+1}(i, j, k). \quad (4.33)$$

Similarly to discretize Eqs. (4.14) and (4.15) we obtain

$$\frac{1}{\Delta t} \Delta_{-r} \varepsilon_\varphi^{n+1}(i, j, k) = \frac{1}{r_i} \left[ \frac{v_r^{n+1}(i+1/2, j, k) + v_r^{n+1}(i-1/2, j, k)}{2} + \frac{1}{\Delta \varphi} \delta_\varphi v_\varphi^{n+1}(i, j, k) \right], \quad (4.34)$$

$$\begin{aligned} \frac{1}{\Delta t} \Delta_{-r} \varepsilon_\theta^{n+1}(i, j, k) &= \frac{1}{r_i \sin \varphi_k} \left[ \frac{v_r^{n+1}(i+1/2, j, k) + v_r^{n+1}(i-1/2, j, k)}{2} \sin \varphi_k \right. \\ &\quad \left. + \frac{v_\varphi^{n+1}(i, j, k+1/2) + v_\varphi^{n+1}(i, j, k-1/2)}{2} \cos \varphi_k + \frac{1}{\Delta \theta} \delta_\theta v_\theta^{n+1}(i, j, k) \right]. \end{aligned} \quad (4.35)$$

To Eq. (4.16), we obtain at point  $(i + \frac{1}{2}, j, k + \frac{1}{2})$

$$\begin{aligned} \varepsilon_{r\varphi}^n(i+1/2, j, k+1/2) &= \varepsilon_{r\varphi}^{n+1}(i+1/2, j, k+1/2) - \frac{\Delta t}{2} \frac{\partial \varepsilon_{r\varphi}^{n+1}(i+1/2, j, k+1/2)}{\partial t} \\ &\quad + \frac{\Delta t^2}{8} \frac{\partial^2 \varepsilon_{r\varphi}^{n+1}(i+1/2, j, k+1/2)}{\partial t^2} + O(\Delta t^3), \end{aligned}$$

that is

$$\frac{\partial \varepsilon_{r\varphi}^{n+1}(i+1/2, j, k+1/2)}{\partial t} = \frac{\varepsilon_{r\varphi}^{n+1}(i+1/2, j, k+1/2) - \varepsilon_{r\varphi}^n(i+1/2, j, k+1/2)}{\Delta t} + O(\Delta t), \quad (4.36a)$$

$$v_r^{n+1}(i+1/2, j, k+1) = v_r^{n+1}(i+1/2, j, k+1/2) + \frac{\Delta\varphi}{2} \frac{\partial v_r^{n+1}(i+1/2, j, k+1/2)}{\partial\varphi} \\ + \frac{\Delta\varphi^2}{8} \frac{\partial^2 v_r^{n+1}(i+1/2, j, k+1/2)}{\partial\varphi^2} + O(\Delta\varphi^3),$$

$$v_r^{n+1}(i+1/2, j, k) = v_r^{n+1}(i+1/2, j, k+1/2) - \frac{\Delta\varphi}{2} \frac{\partial v_r^{n+1}(i+1/2, j, k+1/2)}{\partial\varphi} \\ + \frac{\Delta\varphi^2}{8} \frac{\partial^2 v_r^{n+1}(i+1/2, j, k+1/2)}{\partial\varphi^2} + O(\Delta\varphi^3),$$

that is

$$\frac{\partial v_r^{n+1}(i+1/2, j, k+1/2)}{\partial\varphi} = \frac{v_r^{n+1}(i+1/2, j, k+1) - v_r^{n+1}(i+1/2, j, k)}{\Delta\varphi} + O(\Delta\varphi^2), \quad (4.36b)$$

$$v_\varphi^{n+1}(i+1, j, k+1/2) = v_\varphi^{n+1}(i+1/2, j, k+1/2) + \frac{\Delta r}{2} \frac{\partial v_\varphi^{n+1}(i+1/2, j, k+1/2)}{\partial r} \\ + \frac{\Delta r^2}{8} \frac{\partial^2 v_\varphi^{n+1}(i+1/2, j, k+1/2)}{\partial r^2} + O(\Delta r^3),$$

$$v_\varphi^{n+1}(i, j, k+1/2) = v_\varphi^{n+1}(i+1/2, j, k+1/2) - \frac{\Delta r}{2} \frac{\partial v_\varphi^{n+1}(i+1/2, j, k+1/2)}{\partial r} \\ + \frac{\Delta r^2}{8} \frac{\partial^2 v_\varphi^{n+1}(i+1/2, j, k+1/2)}{\partial r^2} + O(\Delta r^3),$$

that is

$$\frac{\partial v_\varphi^{n+1}(i+1/2, j, k+1/2)}{\partial r} = \frac{v_\varphi^{n+1}(i+1, j, k+1/2) - v_\varphi^{n+1}(i, j, k+1/2)}{\Delta r} + O(\Delta r^2), \quad (4.36c)$$

then substituting Eqs. (4.36a) - (4.36c) into Eq. (4.16), we obtain

$$\frac{1}{\Delta t} \Delta_{-t} \varepsilon_{r\varphi}^{n+1}(i+1/2, j, k+1/2) \\ = \frac{1}{2} \left[ \frac{1}{r_{i+1/2} \Delta\varphi} \delta_\varphi v_r^{n+1}(i+1/2, j, k+1/2) + \frac{1}{\Delta r} \delta_r v_\varphi^{n+1}(i+1/2, j, k+1/2) \right. \\ \left. - \frac{1}{r_{i+1/2}} \frac{v_\varphi^{n+1}(i+1, j, k+1/2) + v_\varphi^{n+1}(i, j, k+1/2)}{2} \right]. \quad (4.36)$$

Using similar argument to discretize Eqs. (4.17) and (4.18), we obtain

$$\begin{aligned} & \frac{1}{\Delta t} \Delta_{-t} \varepsilon_{\varphi\theta}^{n+1}(i, j+1/2, k+1/2) \\ &= \frac{1}{2r_i} \left[ \frac{1}{\sin \varphi_{k+1/2} \Delta\theta} \delta_{\theta} v_{\varphi}^{n+1}(i, j+1/2, k+1/2) + \frac{1}{\Delta\varphi} \delta_{\varphi} v_{\theta}^{n+1}(i, j+1/2, k+1/2) \right. \\ & \quad \left. - \frac{v_{\theta}^{n+1}(i, j+1/2, k+1) + v_{\theta}^{n+1}(i, j+1/2, k)}{2} \cot \varphi_{k+1/2} \right], \end{aligned} \quad (4.37)$$

$$\begin{aligned} & \frac{1}{\Delta t} \Delta_{-t} \varepsilon_{r\theta}^{n+1}(i+1/2, j+1/2, k) \\ &= \frac{1}{2} \left[ \frac{1}{r_{i+1/2} \sin \varphi_k \Delta\theta} \delta_{\theta} v_r^{n+1}(i+1/2, j+1/2, k) + \frac{1}{\Delta r} \delta_r v_{\theta}^{n+1}(i+1/2, j+1/2, k) \right. \\ & \quad \left. - \frac{1}{r_{i+1/2}} \frac{v_{\theta}^{n+1}(i+1, j+1/2, k) + v_{\theta}^{n+1}(i, j+1/2, k)}{2} \right]. \end{aligned} \quad (4.38)$$

To discretize the energy equation Eq. (3.14) presented in the previous chapter at point  $(i, j, k)$ , we obtain following equations

$$\begin{aligned} T_e^{n+1}(i, j, k) &= T_e^{n+1/2}(i, j, k) + \frac{\Delta t}{2} \frac{\partial T_e^{n+1/2}(i, j, k)}{\partial t} + \frac{\Delta t^2}{8} \frac{\partial^2 T_e^{n+1/2}(i, j, k)}{\partial t^2} + O(\Delta t^3), \\ T_e^n(i, j, k) &= T_e^{n+1/2}(i, j, k) - \frac{\Delta t}{2} \frac{\partial T_e^{n+1/2}(i, j, k)}{\partial t} + \frac{\Delta t^2}{8} \frac{\partial^2 T_e^{n+1/2}(i, j, k)}{\partial t^2} + O(\Delta t^3), \end{aligned}$$

that is

$$T_e^{n+1/2}(i, j, k) = \frac{T_e^{n+1}(i, j, k) + T_e^n(i, j, k)}{2} + O(\Delta t^2),$$

and

$$\frac{\partial T_e^{n+1/2}(i, j, k)}{\partial t} = \frac{T_e^{n+1}(i, j, k) - T_e^n(i, j, k)}{\Delta t} + O(\Delta t^2),$$

so we can get

$$C_e(T_e) \frac{\partial T_e^{n+1/2}(i, j, k)}{\partial t} = C_{e0} \frac{T_e^{n+1}(i, j, k) + T_e^n(i, j, k)}{2T_0} \cdot \frac{T_e^{n+1}(i, j, k) - T_e^n(i, j, k)}{\Delta t}, \quad (4.39a)$$

then by using Crank-Nicolson method which use both explicit scheme and implicit

scheme together, to discretize three conservative items  $\frac{\partial}{\partial r}(k_e(T_e, T_l)r^2 \frac{\partial T_e}{\partial r})$ ,

$\frac{\partial}{\partial \theta}(k_e(T_e, T_l) \frac{\partial T_e}{\partial \theta})$ ,  $\frac{\partial}{\partial \varphi}(k_e(T_e, T_l) \sin \varphi \frac{\partial T_e}{\partial \varphi})$  as follows

$$\begin{aligned}
& \frac{1}{r^2} \frac{\partial}{\partial r} (k_e^{n+1/2}(i, j, k) r^2 \frac{\partial T_e^{n+1/2}(i, j, k)}{\partial r}) \\
&= \frac{1}{r_i^2} \cdot \frac{r_{i+1/2}^2 [k_e^{n+1}(i+1, j, k) T_e^{n+1}(i+1, j, k) - k_e^{n+1}(i, j, k) T_e^{n+1}(i, j, k)]}{2\Delta r^2} \\
&- \frac{1}{r_i^2} \cdot \frac{r_{i-1/2}^2 [k_e^{n+1}(i, j, k) T_e^{n+1}(i, j, k) - k_e^{n+1}(i-1, j, k) T_e^{n+1}(i-1, j, k)]}{2\Delta r^2} \\
&+ \frac{1}{r_i^2} \cdot \frac{r_{i+1/2}^2 [k_e^n(i+1, j, k) T_e^n(i+1, j, k) - k_e^n(i, j, k) T_e^n(i, j, k)]}{2\Delta r^2} \\
&- \frac{1}{r_i^2} \cdot \frac{r_{i-1/2}^2 [k_e^n(i, j, k) T_e^n(i, j, k) - k_e^n(i-1, j, k) T_e^n(i-1, j, k)]}{2\Delta r^2},
\end{aligned} \tag{4.39b}$$

$$\begin{aligned}
& \frac{1}{r^2 \sin^2 \varphi} \frac{\partial}{\partial \theta} (k_e^{n+1/2}(i, j, k) \frac{\partial T_e^{n+1/2}(i, j, k)}{\partial \theta}) \\
&= \frac{1}{r_i^2 \sin^2 \varphi_k} \cdot \frac{[k_e^{n+1}(i, j+1, k) T_e^{n+1}(i, j+1, k) - k_e^{n+1}(i, j, k) T_e^{n+1}(i, j, k)]}{2\Delta \theta^2} \\
&- \frac{1}{r_i^2 \sin^2 \varphi_k} \cdot \frac{[k_e^{n+1}(i, j, k) T_e^{n+1}(i, j, k) - k_e^{n+1}(i, j-1, k) T_e^{n+1}(i, j-1, k)]}{2\Delta \theta^2} \\
&+ \frac{1}{r_i^2 \sin^2 \varphi_k} \cdot \frac{[k_e^n(i, j+1, k) T_e^n(i, j+1, k) - k_e^n(i, j, k) T_e^n(i, j, k)]}{2\Delta \theta^2} \\
&- \frac{1}{r_i^2 \sin^2 \varphi_k} \cdot \frac{[k_e^n(i, j, k) T_e^n(i, j, k) - k_e^n(i, j-1, k) T_e^n(i, j-1, k)]}{2\Delta \theta^2},
\end{aligned} \tag{4.39c}$$

$$\begin{aligned}
& \frac{1}{r^2 \sin \varphi} \frac{\partial}{\partial \varphi} \left( k_e^{n+1/2}(i, j, k) \sin \varphi \frac{\partial T_e^{n+1/2}(i, j, k)}{\partial \varphi} \right) \\
&= \frac{1}{r_i^2 \sin \varphi_k} \cdot \frac{[k_e^{n+1}(i, j, k+1) \sin \varphi_{k+1} T_e^{n+1}(i, j, k+1) - k_e^{n+1}(i, j, k) \sin \varphi_k T_e^{n+1}(i, j, k)]}{2\Delta\varphi^2} \\
&- \frac{1}{r_i^2 \sin \varphi_k} \cdot \frac{[k_e^{n+1}(i, j, k) \sin \varphi_k T_e^{n+1}(i, j, k) - k_e^{n+1}(i, j, k-1) \sin \varphi_{k-1} T_e^{n+1}(i, j, k-1)]}{2\Delta\varphi^2} \\
&+ \frac{1}{r_i^2 \sin \varphi_k} \cdot \frac{[k_e^n(i, j, k+1) \sin \varphi_{k+1} T_e^n(i, j, k+1) - k_e^n(i, j, k) \sin \varphi_k T_e^n(i, j, k)]}{2\Delta\varphi^2} \\
&- \frac{1}{r_i^2 \sin \varphi_k} \cdot \frac{[k_e^n(i, j, k) \sin \varphi_k T_e^n(i, j, k) - k_e^n(i, j, k-1) \sin \varphi_{k-1} T_e^n(i, j, k-1)]}{2\Delta\varphi^2}, \tag{4.39d}
\end{aligned}$$

and

$$G(T_e^{n+1/2}(i, j, k) - T_i^{n+1/2}(i, j, k)) = G\left[\frac{T_e^{n+1}(i, j, k) + T_e^n(i, j, k)}{2} - \frac{T_i^{n+1}(i, j, k) - T_i^n(i, j, k)}{2}\right], \tag{4.39e}$$

substituting Eqs. (4.39a) - (4.39e) into Eq. (3.14), we obtain

$$\begin{aligned}
& C_{e0} \left[ \frac{T_e^{n+1}(i, j, k) + T_e^n(i, j, k)}{2T_0} \right] \frac{1}{\Delta t} \Delta_{-t} T_e^{n+1}(i, j, k) \\
&= \frac{r_{i+1/2}^2}{2r_i^2 \Delta r^2} [k_e^{n+1}(i+1/2, j, k) \delta_r T_e^{n+1}(i+1/2, j, k) + k_e^n(i+1/2, j, k) \delta_r T_e^n(i+1/2, j, k)] \\
&- \frac{r_{i-1/2}^2}{2r_i^2 \Delta r^2} [k_e^{n+1}(i-1/2, j, k) \delta_r T_e^{n+1}(i-1/2, j, k) + k_e^n(i-1/2, j, k) \delta_r T_e^n(i-1/2, j, k)] \\
&+ \frac{1}{2r_i^2 \Delta \theta^2 \sin^2 \varphi_k} [k_e^{n+1}(i, j+1/2, k) \delta_\theta T_e^{n+1}(i, j+1/2, k) + k_e^n(i, j+1/2, k) \delta_\theta T_e^n(i, j+1/2, k)] \\
&- \frac{1}{2r_i^2 \Delta \theta^2 \sin^2 \varphi_k} [k_e^{n+1}(i, j-1/2, k) \delta_\theta T_e^{n+1}(i, j-1/2, k) + k_e^n(i, j-1/2, k) \delta_\theta T_e^n(i, j-1/2, k)] \\
&+ \frac{\sin \varphi_{k+1/2}}{2r_i^2 \Delta \varphi^2 \sin \varphi_k} [k_e^{n+1}(i, j, k+1/2) \delta_\varphi T_e^{n+1}(i, j, k+1/2) + k_e^n(i, j, k+1/2) \delta_\varphi T_e^n(i, j, k+1/2)] \\
&- \frac{\sin \varphi_{k-1/2}}{2r_i^2 \Delta \varphi^2 \sin \varphi_k} [k_e^{n+1}(i, j, k-1/2) \delta_\varphi T_e^{n+1}(i, j, k-1/2) + k_e^n(i, j, k-1/2) \delta_\varphi T_e^n(i, j, k-1/2)] \\
&- G \left[ \frac{T_e^{n+1}(i, j, k) + T_e^n(i, j, k)}{2} - \frac{T_i^{n+1}(i, j, k) + T_i^n(i, j, k)}{2} \right] + Q^{n+1/2}(i, j, k). \tag{4.39}
\end{aligned}$$



To discretize Eq. (3.15) at point  $(i, j, k)$  we obtain

$$\begin{aligned}
& C_1 \frac{1}{\Delta t} \Delta_{-t} T_l^{n+1}(i, j, k) \\
&= G \left[ \frac{T_e^{n+1}(i, j, k) + T_e^n(i, j, k)}{2} - \frac{T_l^{n+1}(i, j, k) + T_l^n(i, j, k)}{2} \right] \\
&\quad - (3\lambda + 2\mu) \alpha_T \frac{1}{\Delta} [\Delta_{-t} \varepsilon_r^{n+1}(i, j, k) + \Delta_{-t} \varepsilon_\theta^{n+1}(i, j, k) + \Delta_{-t} \varepsilon_\varphi^{n+1}(i, j, k)].
\end{aligned} \tag{4.40}$$

Finally to discretize the displacement equation Eq. (4.5) at point  $(i + \frac{1}{2}, j, k)$ ,  $(i, j + \frac{1}{2}, k)$ ,

$(i, j, k + \frac{1}{2})$  by Euler backward scheme, respectively, we obtain

$$\frac{1}{\Delta} \Delta_{-t} u_r^{n+1}(i+1/2, j, k) = v_r^{n+1}(i+1/2, j, k), \tag{4.41}$$

$$\frac{1}{\Delta} \Delta_{-t} u_\theta^{n+1}(i, j+1/2, k) = v_\theta^{n+1}(i, j+1/2, k), \tag{4.42}$$

$$\frac{1}{\Delta} \Delta_{-t} u_\varphi^{n+1}(i, j, k+1/2) = v_\varphi^{n+1}(i, j, k+1/2). \tag{4.43}$$

To complete the formulation of our numerical method, we now turn our attention to the approximation of boundary and initial conditions from Eqs. (3.17) – (3.23):

$$\sigma_r^n(N_r + 1, j, k) = 0, \quad 1 \leq j \leq N_\theta + 1, 1 \leq k \leq N_\varphi + 1, \tag{4.44a}$$

$$\sigma_r^n(1, j, k) = \sigma_r^n(2, j, k), \quad 1 \leq j \leq N_\theta + 1, 1 \leq k \leq N_\varphi + 1, \tag{4.44b}$$

$$\sigma_{r\theta}^n(N_r + 1/2, j + 1/2, k) = 0, \quad 1 \leq j \leq N_\theta, 1 \leq k \leq N_\varphi + 1, \tag{4.44c}$$

$$\sigma_{r\theta}^n(1 + 1/2, j + 1/2, k) = \sigma_{r\theta}^n(2 + 1/2, j + 1/2, k), \quad 1 \leq j \leq N_\theta, 1 \leq k \leq N_\varphi + 1, \tag{4.44d}$$

$$\sigma_{r\varphi}^n(N_r + 1/2, j, k + 1/2) = 0, \quad 1 \leq j \leq N_\theta + 1, 1 \leq k \leq N_\varphi, \tag{4.44e}$$

$$\sigma_{r\varphi}^n(1 + 1/2, j, k + 1/2) = \sigma_{r\varphi}^n(2 + 1/2, j, k + 1/2), \quad 1 \leq j \leq N_\theta + 1, 1 \leq k \leq N_\varphi, \tag{4.44f}$$

$$\sigma_{\theta}^n(i, j, k) = \sigma_{\theta}^n(i, j + N_{\theta}, k), \quad 1 \leq i \leq N_r + 1, 1 \leq k \leq N_{\varphi} + 1, \quad (4.45a)$$

$$\sigma_{r\theta}^n(i + 1/2, j + 1/2, k) = \sigma_{r\theta}^n(i + 1/2, j + N_{\theta} + 1/2, k), \quad 1 \leq i \leq N_r, 1 \leq k \leq N_{\varphi} + 1, \quad (4.45b)$$

$$\sigma_{\varphi\theta}^n(i, j + 1/2, k + 1/2) = \sigma_{\varphi\theta}^n(i, j + N_{\theta} + 1/2, k + 1/2), \quad 1 \leq i \leq N_r + 1, 1 \leq k \leq N_{\varphi}, \quad (4.45c)$$

$$\sigma_{\varphi}^n(i, j, 1) = \sigma_{\varphi}^n(i, j, 2), \quad 1 \leq i \leq N_r + 1, 1 \leq j \leq N_{\theta} + 1, \quad (4.46a)$$

$$\sigma_{\varphi}^n(i, j, N_{\varphi} + 1) = \sigma_{\varphi}^n(i, j, N_{\varphi}), \quad 1 \leq i \leq N_r + 1, 1 \leq j \leq N_{\theta} + 1, \quad (4.46b)$$

$$\sigma_{r\varphi}^n(i + 1/2, j, 1 + 1/2) = \sigma_{r\varphi}^n(i + 1/2, j, 2 + 1/2), \quad 1 \leq i \leq N_r, 1 \leq j \leq N_{\theta} + 1, \quad (4.46c)$$

$$\sigma_{r\varphi}^n(i + 1/2, j, N_{\varphi} + 1/2) = \sigma_{r\varphi}^n(i + 1/2, j, N_{\varphi} - 1/2), \quad 1 \leq i \leq N_r, 1 \leq j \leq N_{\theta} + 1, \quad (4.46d)$$

$$\sigma_{\varphi\theta}^n(i, j + 1/2, 1 + 1/2) = \sigma_{\varphi\theta}^n(i, j + 1/2, 2 + 1/2), \quad 1 \leq i \leq N_r + 1, 1 \leq j \leq N_{\theta}, \quad (4.46e)$$

$$\sigma_{\varphi\theta}^n(i, j + 1/2, N_{\varphi} + 1/2) = \sigma_{\varphi\theta}^n(i, j + 1/2, N_{\varphi} - 1/2), \quad 1 \leq i \leq N_r + 1, 1 \leq j \leq N_{\theta}, \quad (4.46f)$$

$$T_e^n(1, j, k) = T_e^n(2, j, k), T_e^n(N_r + 1, j, k) = T_e^n(N_r, j, k), \quad 1 \leq j \leq N_{\theta} + 1, 1 \leq k \leq N_{\varphi} + 1, \quad (4.47a)$$

$$T_e^n(i, j, k) = T_e^n(i, j + N_{\theta}, k), \quad 1 \leq i \leq N_r + 1, 1 \leq k \leq N_{\varphi} + 1, \quad (4.47b)$$

$$T_e^n(i, j, 1) = T_e^n(i, j, 2), T_e^n(i, j, N_{\varphi} + 1) = T_e^n(i, j, N_{\varphi}), \quad 1 \leq i \leq N_r + 1, 1 \leq j \leq N_{\theta} + 1, \quad (4.47c)$$

$$T_l^n(1, j, k) = T_l^n(2, j, k), T_l^n(N_r + 1, j, k) = T_l^n(N_r, j, k), \quad 1 \leq j \leq N_{\theta} + 1, 1 \leq k \leq N_{\varphi} + 1, \quad (4.48a)$$

$$T_l^n(i, j, k) = T_l^n(i, j + N_{\theta}, k), \quad 1 \leq i \leq N_r + 1, 1 \leq k \leq N_{\varphi} + 1, \quad (4.48b)$$

$$T_l^n(i, j, 1) = T_l^n(i, j, 2), T_l^n(i, j, N_{\varphi} + 1) = T_l^n(i, j, N_{\varphi}), \quad 1 \leq i \leq N_r + 1, 1 \leq j \leq N_{\theta} + 1, \quad (4.48c)$$

where  $1 \leq i \leq N_r + 1, 1 \leq j \leq N_{\theta} + 1, 1 \leq k \leq N_{\varphi} + 1$  for any time level  $n$ . The initial conditions

are approximated as

$$u_r^0(i + 1/2, j, k) = u_{\theta}^0(i, j + 1/2, k) = u_{\varphi}^0(i, j, k + 1/2) = 0, \quad (4.49a)$$

$$v_r^0(i + 1/2, j, k) = v_{\theta}^0(i, j + 1/2, k) = v_{\varphi}^0(i, j, k + 1/2) = 0, \quad (4.49b)$$

$$T_e^0(i, j, k) = T_l^0(i, j, k) = T_0, \quad (4.49c)$$

$$\varepsilon_r^0(i, j, k) = \varepsilon_\theta^0(i, j, k) = \varepsilon_\varphi^0(i, j, k) = 0, \quad (4.49d)$$

$$\sigma_r^0(i, j, k) = \sigma_\theta^0(i, j, k) = \sigma_\varphi^0(i, j, k) = 0, \quad (4.49e)$$

$$\sigma_{r\theta}^0(i+1/2, j+1/2, k) = \varepsilon_{r\theta}^0(i+1/2, j+1/2, k) = 0, \quad (4.49f)$$

$$\sigma_{r\varphi}^0(i+1/2, j, k+1/2) = \varepsilon_{r\varphi}^0(i+1/2, j, k+1/2) = 0, \quad (4.49g)$$

$$\sigma_{\varphi\theta}^0(i, j+1/2, k+1/2) = \varepsilon_{\varphi\theta}^0(i, j+1/2, k+1/2) = 0. \quad (4.49h)$$

It can be seen that the truncation error of Eqs. (4.24)–(4.26) is  $O(\Delta t + \Delta r^2 + \Delta\varphi^4 + \Delta\theta^4)$ ,  $O(\Delta t + \Delta r^4 + \Delta\varphi^2 + \Delta\theta^4)$ ,  $O(\Delta t + \Delta r^4 + \Delta\varphi^4 + \Delta\theta^2)$ , respectively; the truncation error of Eqs. (4.33)–(4.35) is  $O(\Delta t + \Delta r^2)$ ,  $O(\Delta t + \Delta\varphi^2)$ ,  $O(\Delta t + \Delta\theta^2)$ , respectively; and the truncation error of Eqs. (4.36)–(4.38) is  $O(\Delta t + \Delta r^2 + \Delta\varphi^2)$ ,  $O(\Delta t + \Delta r^2 + \Delta\theta^2)$ ,  $O(\Delta t + \Delta\theta^2 + \Delta\varphi^2)$ , respectively; the truncation error of Eqs. (4.39), (4.40) is  $O(\Delta t^2 + \Delta r^2 + \Delta\theta^2 + \Delta\varphi^2)$ . It should be pointed out that Eqs. (4.24)–(4.26) are nonlinear since the terms  $\delta_r(T_e^2)^{n+1}(i+1/2, j, k)$ ,  $\delta_\theta(T_e^2)^{n+1}(i, j+1/2, k)$  and  $\delta_\varphi(T_e^2)^{n+1}(i, j, k+1/2)$  are nonlinear. Also, it can be seen that Eq. (4.39) is nonlinear. Therefore, the above schemes must be solved iteratively.

#### 4.2.4 Algorithm

An iterative method for solving the above schemes at time level  $n+1$  is developed as follows:

Step 1. Set the values  $\varepsilon_r^{n+1}$ ,  $\varepsilon_\theta^{n+1}$ ,  $\varepsilon_\varphi^{n+1}$ ,  $\varepsilon_{r\varphi}^{n+1}$ ,  $\varepsilon_{r\theta}^{n+1}$  and  $\varepsilon_{\varphi\theta}^{n+1}$ , solve Eqs. (4.39), (4.40) iteratively for  $T_e^{n+1}$  and  $T_l^{n+1}$ .

Step 2. Solve for  $\sigma_r^{n+1}, \sigma_\theta^{n+1}, \sigma_\varphi^{n+1}, \sigma_{r\varphi}^{n+1}, \sigma_{r\theta}^{n+1}$  and  $\sigma_{\varphi\theta}^{n+1}$  using Eqs. (4.27)–(4.32).

Step 3. Solve for derivatives of  $\sigma_r^{n+1}, \sigma_\theta^{n+1}, \sigma_\varphi^{n+1}, \sigma_{r\varphi}^{n+1}, \sigma_{r\theta}^{n+1}$  and  $\sigma_{\varphi\theta}^{n+1}$  using Eqs. (4.22), (4.23) or similar equations.

Step 4. Solve for  $v_r^{n+1}, v_\theta^{n+1}$  and  $v_\varphi^{n+1}$  using Eqs. (4.24)–(4.26).

Step 5. Update  $\varepsilon_r^{n+1}, \varepsilon_\theta^{n+1}, \varepsilon_\varphi^{n+1}, \varepsilon_{r\varphi}^{n+1}, \varepsilon_{r\theta}^{n+1}$  and  $\varepsilon_{\varphi\theta}^{n+1}$  using Eqs. (4.33)–(4.38).

Given the required accuracy  $E_1$  (for temperature) and  $E_2$  (for strain), repeat the above steps until a convergent solution is obtained based on the following criteria:

$$\begin{aligned} |T_e^{n+1(new)}(i, j, k) - T_e^{n+1(old)}(i, j, k)| &\leq E_1, \\ |\varepsilon_r^{n+1(new)}(i, j, k) - \varepsilon_r^{n+1(old)}(i, j, k)| &\leq E_2, & |\varepsilon_\theta^{n+1(new)}(i, j, k) - \varepsilon_\theta^{n+1(old)}(i, j, k)| &\leq E_2, \\ |\varepsilon_\varphi^{n+1(new)}(i, j, k) - \varepsilon_\varphi^{n+1(old)}(i, j, k)| &\leq E_2, & |\varepsilon_{r\theta}^{n+1(new)}(i, j, k) - \varepsilon_{r\theta}^{n+1(old)}(i, j, k)| &\leq E_2, \\ |\varepsilon_{r\varphi}^{n+1(new)}(i, j, k) - \varepsilon_{r\varphi}^{n+1(old)}(i, j, k)| &\leq E_2, & |\varepsilon_{\varphi\theta}^{n+1(new)}(i, j, k) - \varepsilon_{\varphi\theta}^{n+1(old)}(i, j, k)| &\leq E_2. \end{aligned}$$

### 4.3 Conclusion

In this chapter, we developed finite difference methods for solving those governing equations set up in the previous chapter. And to avoid non-physical oscillations in the solution, we further developed a fourth-order compact finite difference scheme for evaluating stress derivatives and shear stress derivatives  $\frac{\partial \sigma_r}{\partial r}, \frac{\partial \sigma_{r\varphi}}{\partial \varphi}, \frac{\partial \sigma_{\varphi\theta}}{\partial \theta}$  and etc. In

the next chapter, we will test our numerical methods by five cases.

## CHAPTER FIVE

### NUMERICAL EXAMPLES AND DISCUSSIONS

In this chapter, we will show the numerical examples based on the developed numerical schemes for thermal deformation in a gold micro-sphere subjected to an ultrashort pulsed laser. Five examples will be used for testing the numerical schemes. In example one, the laser irradiates a portion ( $0 \leq \varphi \leq \pi/4$ ) of the upper hemisphere; in example two, the laser irradiates the whole upper hemisphere; and in example three, the laser irradiates both the top portion ( $0 \leq \varphi \leq \pi/4$ ) and the bottom portion ( $3\pi/4 \leq \varphi \leq \pi$ ); in example four and example five, we will change the heat source to the laser with double-pulse which irradiates the top portion ( $0 \leq \varphi \leq \pi/4$ ) and irradiates both the top portion ( $0 \leq \varphi \leq \pi/4$ ) and the bottom portion ( $3\pi/4 \leq \varphi \leq \pi$ ), respectively. For each example, the electron temperature, the lattice temperature, the displacement and the stress will be calculated and discussed.

#### 5.1 Description

To test the applicability of the developed numerical schemes, we will investigate the temperature rise and thermal deformation in a micro-sphere with the radius  $0.1 \mu\text{m}$ , as shown in Fig. 5.1.

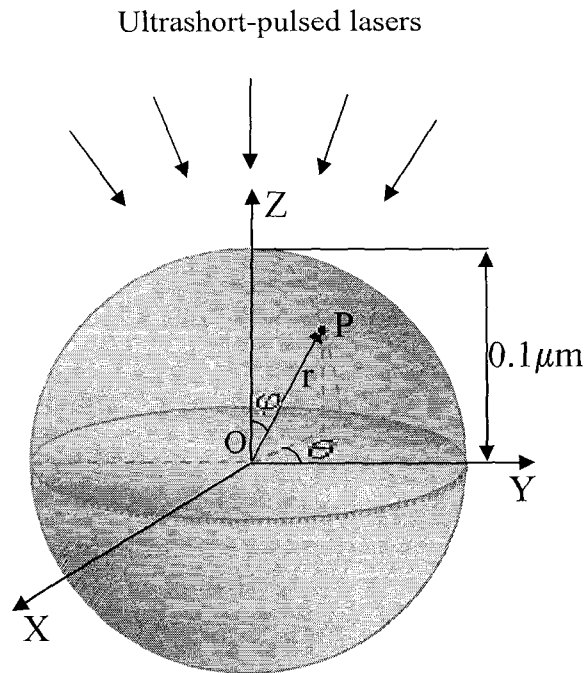


Fig. 5.1 A 3D micro-sphere with radius  $L = 0.1 \mu\text{m}$ .

The thermophysical properties for gold are listed in Table 5.1 [Tzhou 2002, Chen 2002a, Chen 2002b]. Four meshes of  $60 \times 20 \times 20$ ,  $40 \times 20 \times 20$ ,  $30 \times 20 \times 40$ , and  $20 \times 30 \times 40$  were chosen in order to test the convergence of the solution. The time increment was chosen to be 0.005 ps, and  $T_0$  was set to be 300 K. Three different values of laser fluence ( $J = 500 \text{ J/m}^2$ ,  $1,000 \text{ J/m}^2$ ,  $2,000 \text{ J/m}^2$ ) were chosen to study the hot electron blast force. The convergence criteria were chosen to be  $E_1 = 10^{-5}$  for temperature and  $E_2 = 10^{-12}$  for deformation.

Table 5.1 Thermophysical properties for gold [Tzou 2002, Chen 2002a, Chen 2002b]

Properties	Unit	Value
$\rho$	kg/m <sup>3</sup>	19,300
$\Lambda$	J/(m <sup>-3</sup> K <sup>-2</sup> )	70
$K$	Pa	$217 \times 10^9$
$\mu$	Pa	$27 \times 10^9$
$\alpha_T$	K <sup>-1</sup>	$14.2 \times 10^{-6}$
$C_{e0}$	J/(m <sup>3</sup> K)	$2.1 \times 10^4$
$C_l$	J/(m <sup>3</sup> K)	$2.5 \times 10^6$
$G$	W/(m <sup>3</sup> K)	$2.6 \times 10^{16}$
$K_e$	W/(mK)	315
$R$		0.93
$t_p$	s	$0.1 \times 10^{-12}$
$\zeta$	m	$15.3 \times 10^{-9}$
$L$	m	$1.0 \times 10^{-7}$
$J$	J/m <sup>2</sup>	500; 1,000; 2,000

## 5.2 Numerical Examples and Discussions

### 5.2.1 Example One

In this case, the laser irradiates a portion ( $0 \leq r \leq L, 0 \leq \theta \leq 2\pi, 0 \leq \varphi \leq \pi/4$ ).

Fig. 5.2 shows the change in electron temperature ( $\Delta T_e / (\Delta T_e)_{\max}$ ) at the point ( $r = L, \varphi = 0, \theta = 0$ ) for various meshes ( $60 \times 20 \times 20$ ,  $40 \times 20 \times 20$ ,  $30 \times 20 \times 40$ ,  $20 \times 30 \times 40$ ) with laser fluence  $J = 500 \text{ J/m}^2$ . The maximum temperature rise of  $T_e$  (i.e.  $(\Delta T_e)_{\max}$ ) is about 3931.22 K, which is close to that obtained in [Qiu 1994]. Fig. 5.3 shows the displacement  $u_r$  at the point ( $r = L/2, \varphi = 0, \theta = 0$ ) versus time.

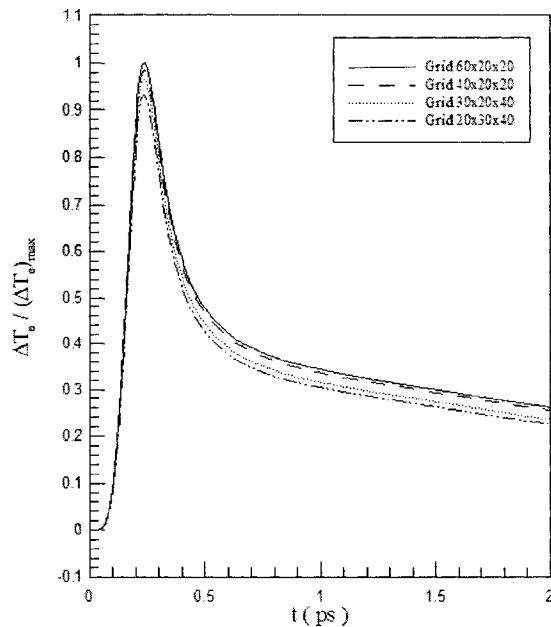


Fig. 5.2 Change in electron temperature  $T_e$  at  $r = 0.1 \text{ } \mu\text{m}$ ,  $\theta = 0$ ,  $\varphi = 0$  versus time for various meshes with a laser fluence  $J$  of  $500 \text{ J/m}^2$ .



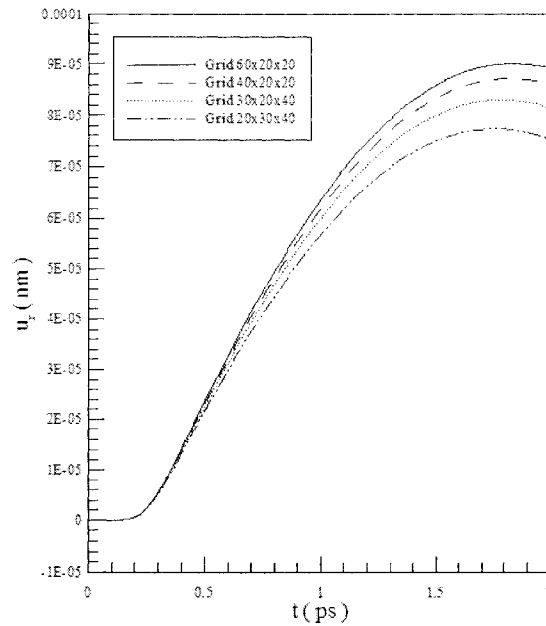


Fig. 5.3 Displacement  $u_r$  at  $r = 0.05 \mu\text{m}$ ,  $\theta = 0$ ,  $\varphi = 0$  versus time for various meshes with a laser fluence  $J$  of  $500 \text{ J/m}^2$ .

It can be seen from both figures above that the grid size has no significant effect on the solution and hence the solution is convergent.

Fig. 5.4 shows profiles of electron temperature and lattice temperature along the diameter at  $\varphi = 0$  and  $\varphi = \pi$  with laser fluence  $J = 500 \text{ J/m}^2$  and a mesh of  $60 \times 20 \times 20$  at different times (a)  $t = 0.25 \text{ ps}$ , (b)  $t = 0.5 \text{ ps}$ , (c)  $t = 1 \text{ ps}$ , (d)  $t = 5 \text{ ps}$  and (e)  $t = 20 \text{ ps}$ , respectively. It can be seen that the electron temperature rises to its maximum at the beginning and then decreases while the lattice temperature rises gradually with time to a uniform temperature distribution at  $t = 20 \text{ ps}$ . Electron temperature decreases rapidly with time and lattice temperature rises gradually with time in the gold sphere because of the effect of the heat diffusion in the electron gas and the constant heat flow from hot electrons to metal lattices. The uniform electron and lattice temperature are probably due

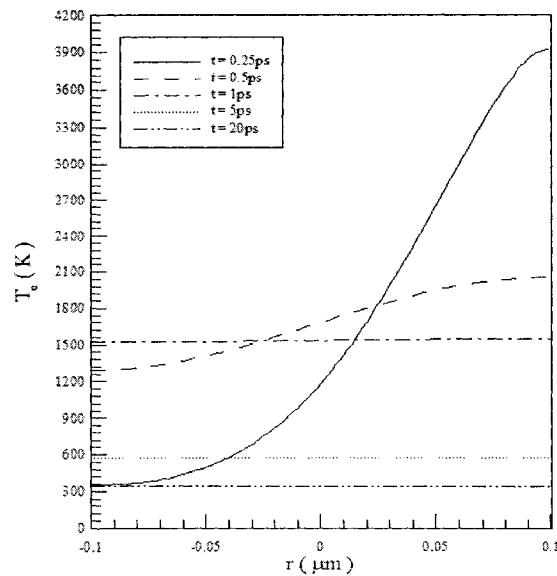
to an increased rate of collision between electrons and phonons in the gold layer as boundary is thermally insulated.

Fig. 5.6 shows normal stress  $\sigma_r$  along the diameter at  $\varphi = 0$  and  $\varphi = \pi$  at different times (a)  $t = 5$  ps, (b)  $t = 10$  ps, (c)  $t = 15$  ps, (d)  $t = 20$  ps with a mesh of  $60 \times 20 \times 20$  and three different laser fluences ( $J = 500 \text{ J/m}^2$ ,  $1,000 \text{ J/m}^2$ ,  $2,000 \text{ J/m}^2$ ). Usually, numerical oscillations appear near the peak of the curve, as shown in Fig. 5.5 [Chen 2002a]. It can be seen from Fig. 5.6 (particularly Fig. 5.5(b)–Fig. 5.5(d)) that the normal stress does not show non-physical oscillations near the two peaks of the curve. And also from Fig. 5.5 we can see, with the time increasing, the two peaks become closer and closer, and finally they will meet together. It shows that the energy is transferred from the surface of the micro-sphere to the center along the  $r$  direction.

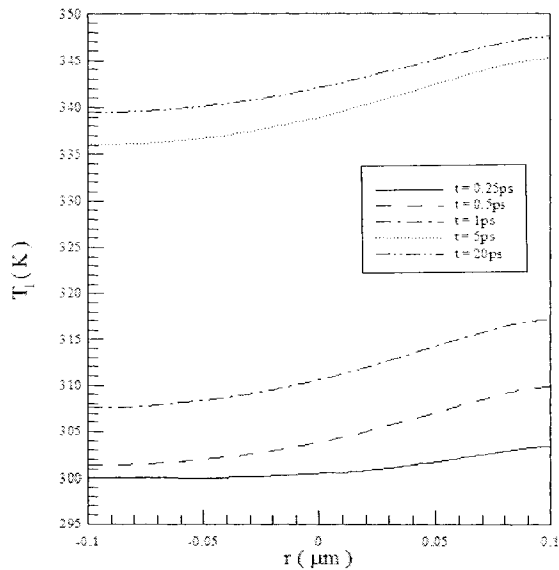
Fig. 5.7 shows displacement  $u_r$  along the diameter at  $\varphi = 0$  and  $\varphi = \pi$  at different times (a)  $t = 5$  ps, (b)  $t = 10$  ps, (c)  $t = 15$  ps, and (d)  $t = 20$  ps with a mesh of  $60 \times 20 \times 20$  and three different laser fluences ( $J = 500 \text{ J/m}^2$ ,  $1,000 \text{ J/m}^2$ ,  $2,000 \text{ J/m}^2$ ). From the figures, we can see the displacement along the  $r$  direction. So it shows the fact again that the thermal energy is transferred along the  $r$  direction from the surface of the micro-sphere to the center along the  $r$  direction.

Figs. 5.8–5.15 were plotted based on the results obtained in a mesh of  $60 \times 20 \times 20$  with a laser fluence  $J = 500 \text{ J/m}^2$ . Figs. 5.8 and 5.9 show contours of electron temperature distributions and lattice temperature distributions in the cross section of  $\theta = 0$  and  $\theta = \pi$  at different times (a)  $t = 0.25$  ps, (b)  $t = 0.5$  ps, (c)  $t = 1$  ps, (d)  $t = 5$  ps, (e)  $t = 10$  ps, and (f)  $t = 20$  ps, respectively. It can be seen from both figures that the heat is mainly transferred from top surface to bottom. Figs. 5.10–5.15 show

contours of displacement ( $u_r, u_\theta, u_\varphi$ ) and normal stress ( $\sigma_r, \sigma_\theta, \sigma_\varphi$ ) in the cross section of  $\theta = 0$  and  $\theta = \pi$  at different times (a)  $t = 5$  ps, (b)  $t = 10$  ps, (c)  $t = 15$  ps, and (d)  $t = 20$  ps, respectively. It can be seen from Fig. 5.10 that the sphere is expanding along the  $r$  direction and the top portion of the sphere expands much more as compared with the bottom. This is because the laser irradiates from the top portion of the sphere. From Figs. 5.13–5.15 we can see that the blasting forces produce compressive stresses at first, then as the wave of stress propagates along  $r$  direction, severe stresses alteration appear in the gold sphere. Since metal including gold is weaker in general when resisting tension, the tensile region of the sphere will be more detrimental. For this reason, it is too hard for a gold sphere to resist the damage induced by ultrashort laser heating.



(a)



(b)

Fig. 5.4 Profiles of (a) electron temperature ( $T_e$ ), and (b) lattice temperature ( $T_l$ ) along  $r$ -axis at  $\varphi = 0$  and  $\varphi = \pi$  for various times with a laser fluence  $J$  of  $500 \text{ J/m}^2$  and a mesh  $60 \times 20 \times 20$ .

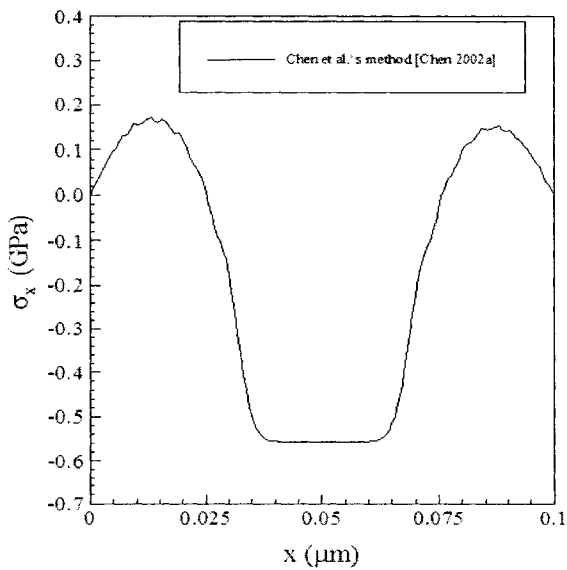


Fig. 5.5 Chen et al.'s method in [Chen 2002a] with regard to normal stress  $\sigma_x$  with oscillations at two peaks.

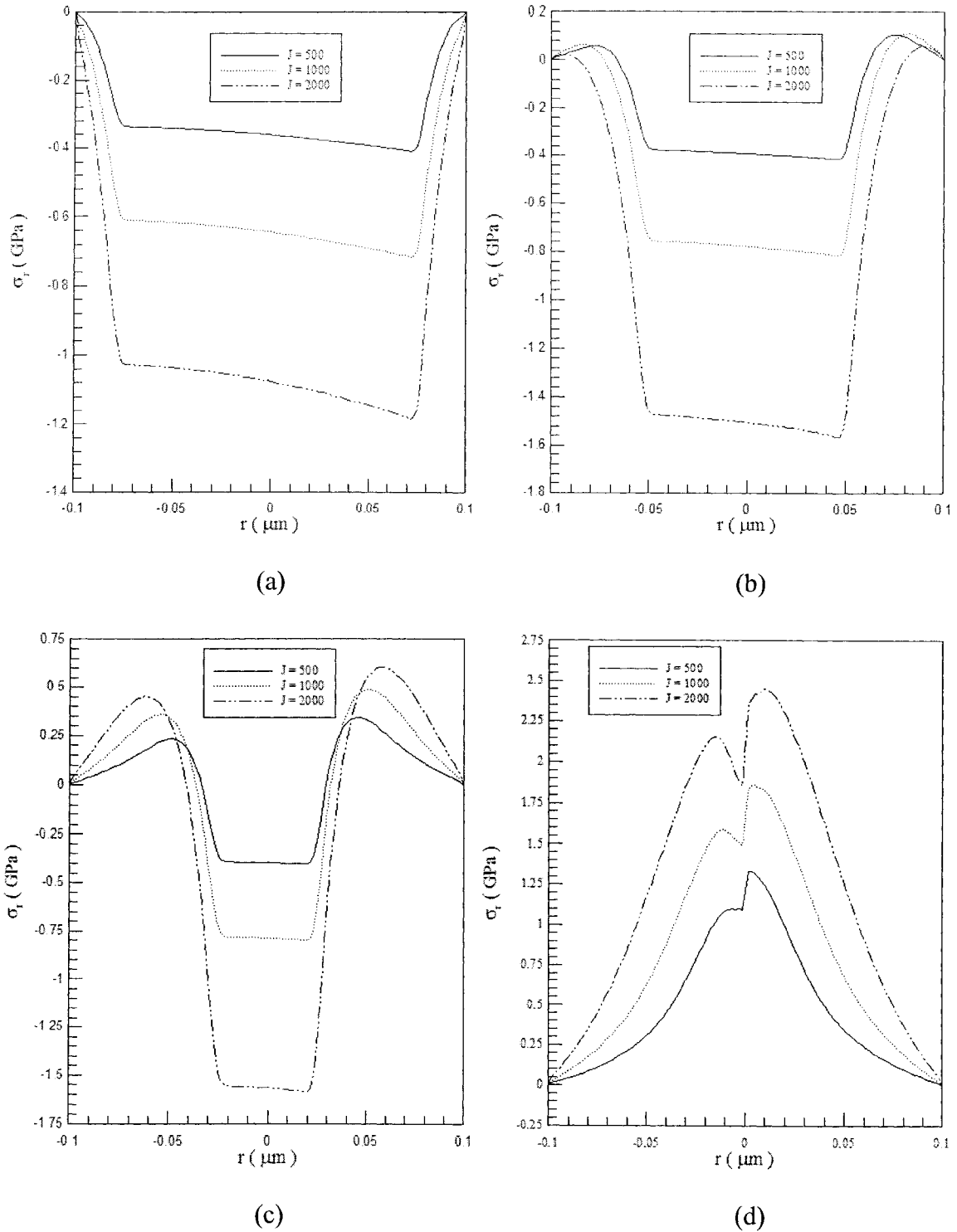


Fig. 5.6 Normal stress ( $\sigma_r$ ) along the diameter at  $\varphi = 0$  and  $\varphi = \pi$  at different times (a)  $t = 5$  ps, (b)  $t = 10$  ps, (c)  $t = 15$  ps, and (d)  $t = 20$  ps with three different laser fluences and a mesh of  $60 \times 20 \times 20$ .

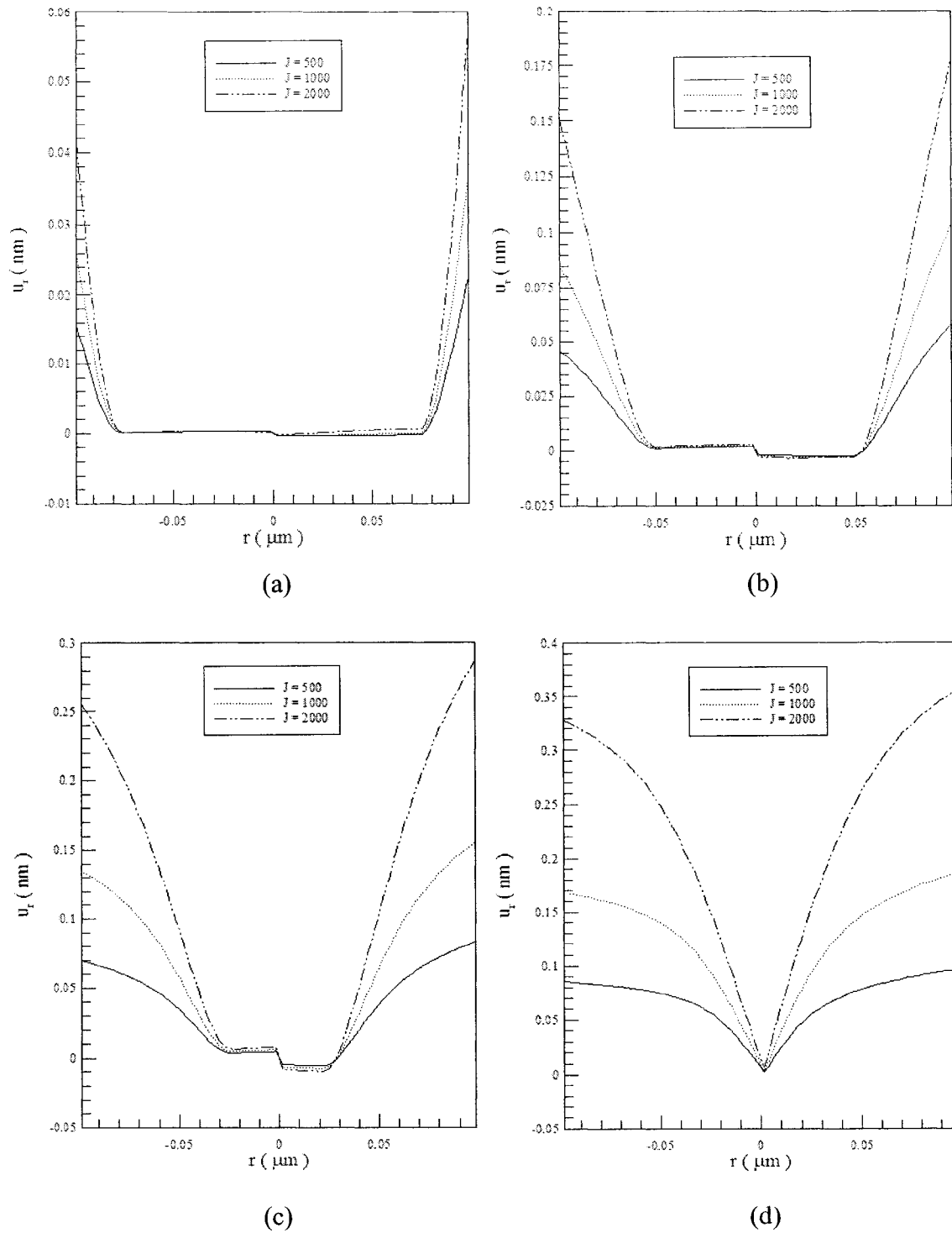
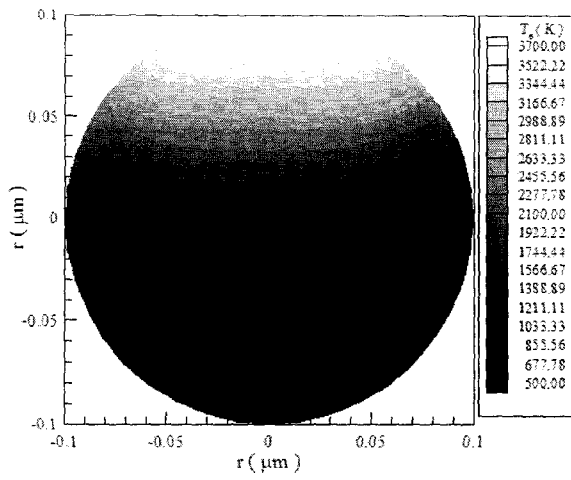
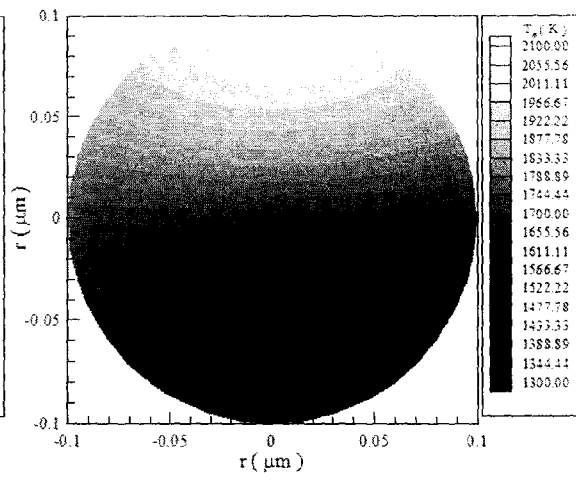


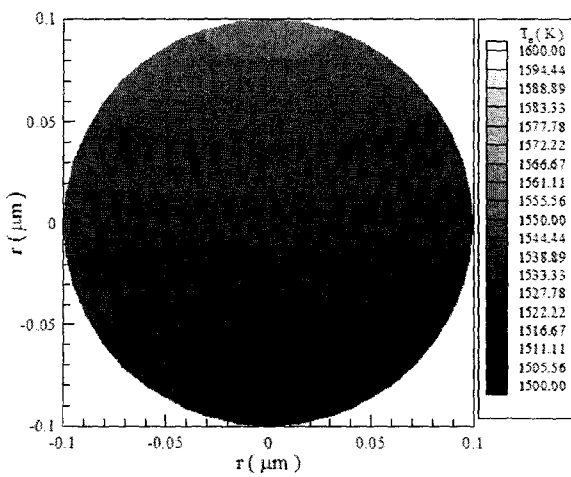
Fig. 5.7 Displacement ( $u_r$ ) along the diameter at  $\varphi = 0$  and  $\varphi = \pi$  at different times (a)  $t = 5$  ps, (b)  $t = 10$  ps, (c)  $t = 15$  ps, and (d)  $t = 20$  ps with three different laser fluences and a mesh of  $60 \times 20 \times 20$ .



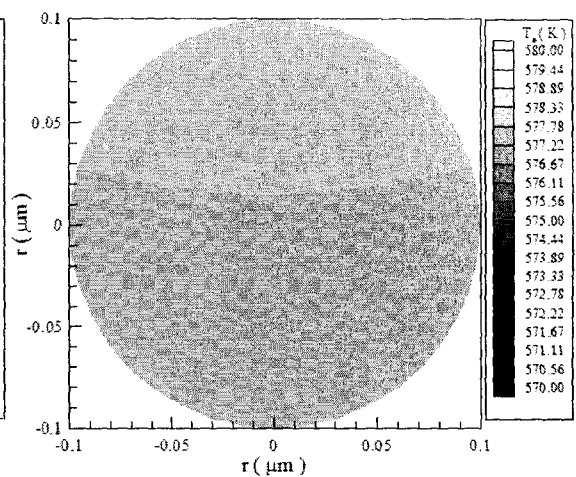
(a)



(b)



(c)



(d)

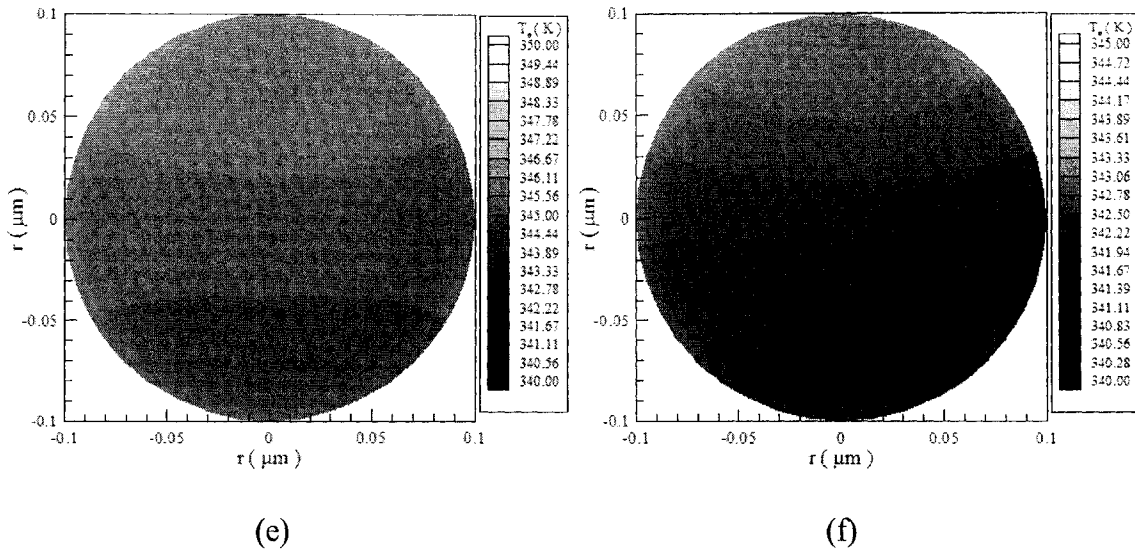
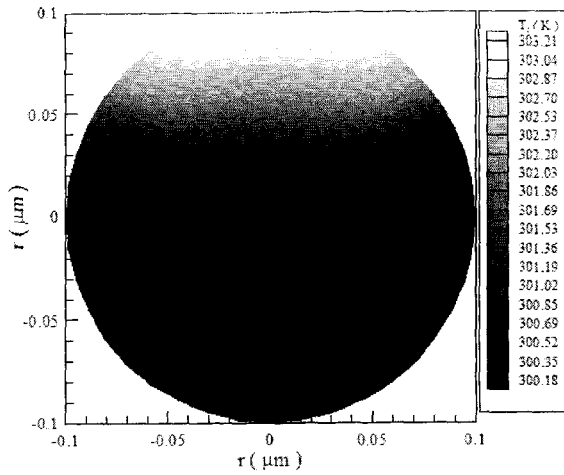
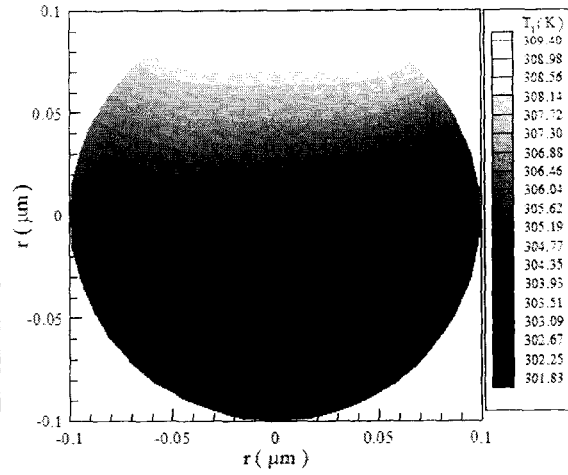


Fig. 5.8 Contours of electron temperature ( $T_e$ ) distributions in the cross section of  $\theta = 0$  and  $\theta = \pi$  at different times (a)  $t = 0.25$  ps, (b)  $t = 0.5$  ps, (c)  $t = 1$  ps, (d)  $t = 5$  ps, (e)  $t = 10$  ps, and (f)  $t = 20$  ps with a mesh of  $60 \times 20 \times 20$  and a laser fluence  $J$  of  $500 \text{ J/m}^2$ .

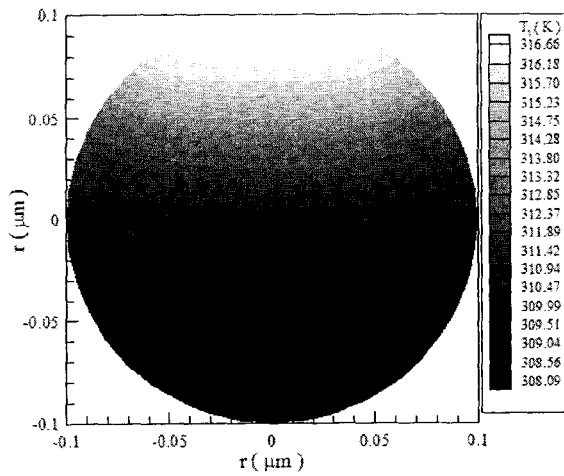




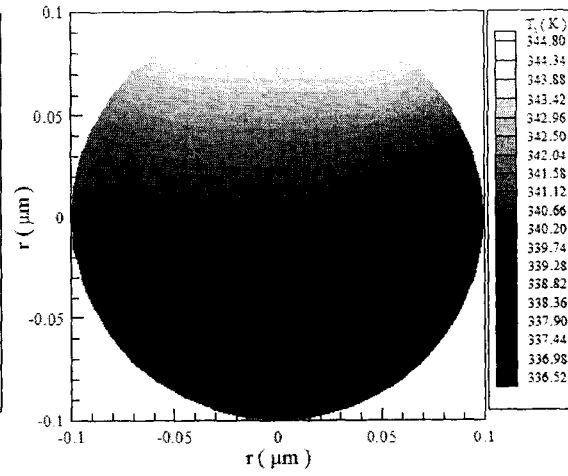
(a)



(b)



(c)



(d)

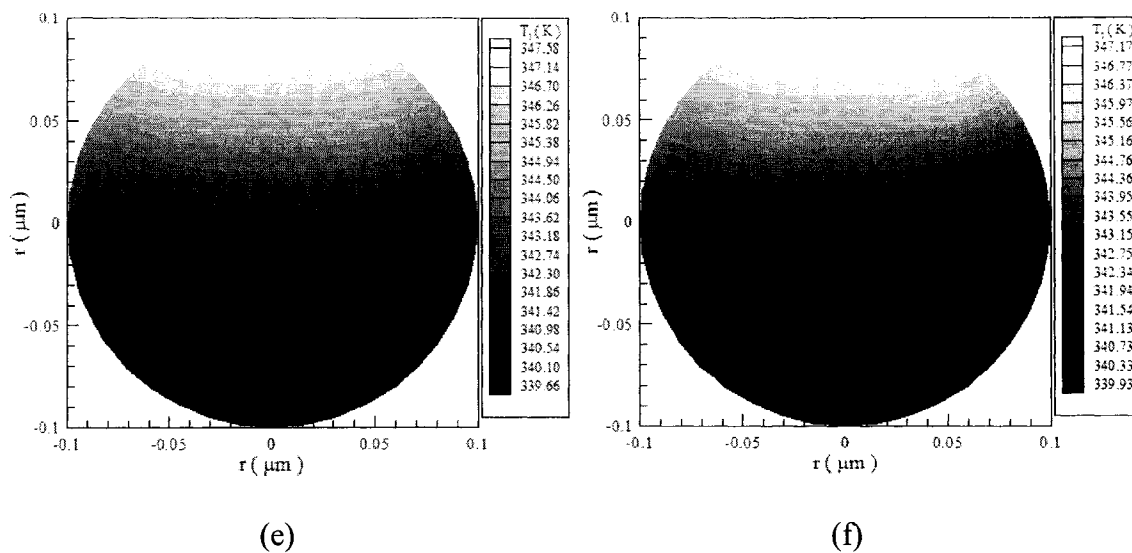


Fig. 5.9 Contours of lattice temperature ( $T_l$ ) distributions in the cross section of  $\theta = 0$  and  $\theta = \pi$  at different times (a)  $t = 0.25$  ps, (b)  $t = 0.5$  ps, (c)  $t = 1$  ps, (d)  $t = 5$  ps, (e)  $t = 10$  ps, and (f)  $t = 20$  ps with a mesh of  $60 \times 20 \times 20$  and a laser fluence  $J$  of  $500 \text{ J/m}^2$ .

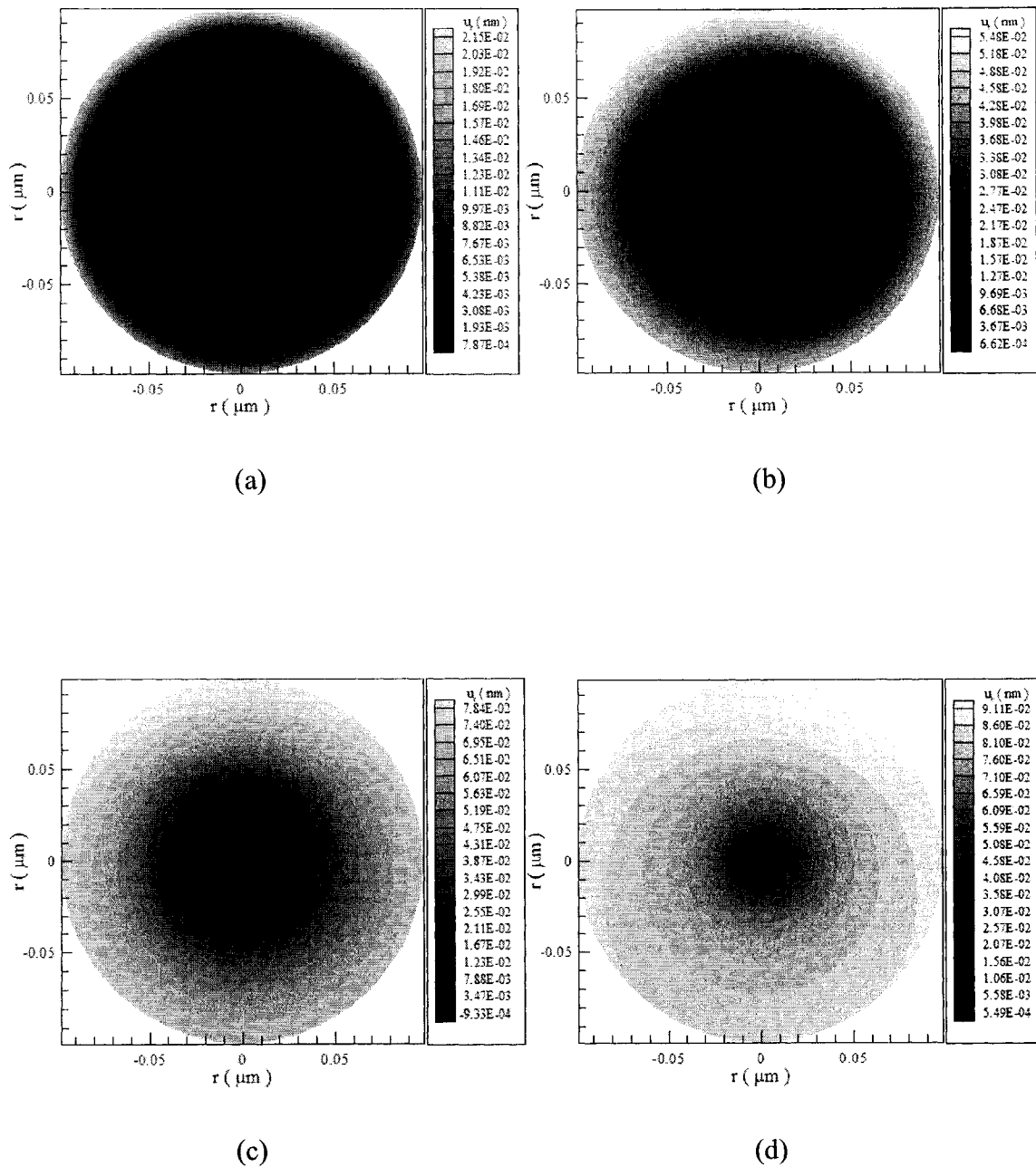


Fig. 5.10 Contours of displacement ( $u_r$ ) distributions in the cross section of  $\theta = 0$  and  $\theta = \pi$  at different times (a)  $t = 5$  ps, (b)  $t = 10$  ps, (c)  $t = 15$  ps, and (d)  $t = 20$  ps with a mesh of  $60 \times 20 \times 20$  and a laser fluence  $J$  of  $500 \text{ J/m}^2$ .

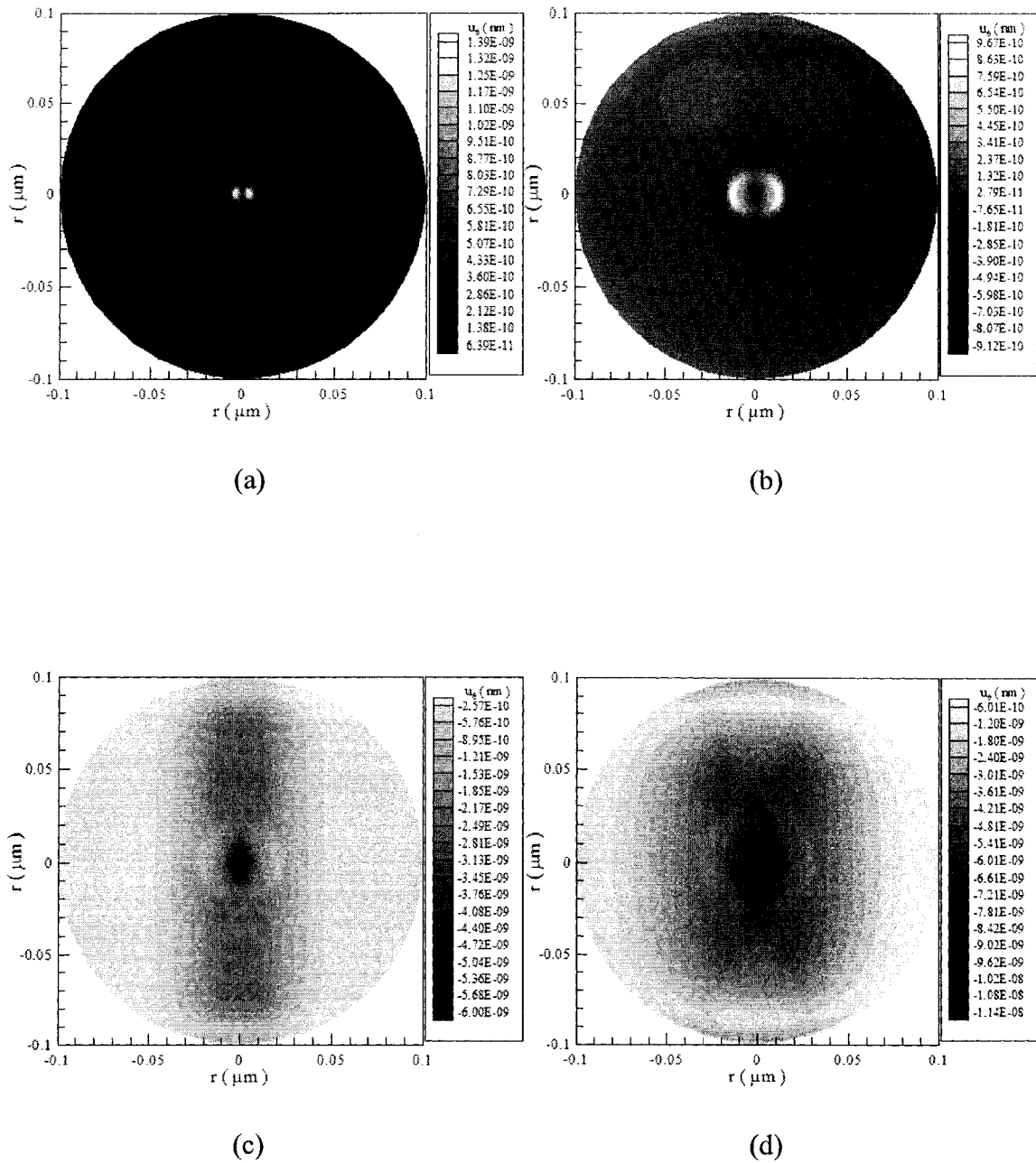


Fig. 5.11 Contours of displacement ( $u_\theta$ ) distributions in the cross section of  $\theta = 0$  and  $\theta = \pi$  at different times (a)  $t = 5$  ps, (b)  $t = 10$  ps, (c)  $t = 15$  ps, and (d)  $t = 20$  ps with a mesh of  $60 \times 20 \times 20$  and a laser fluence  $J$  of  $500 \text{ J/m}^2$ .

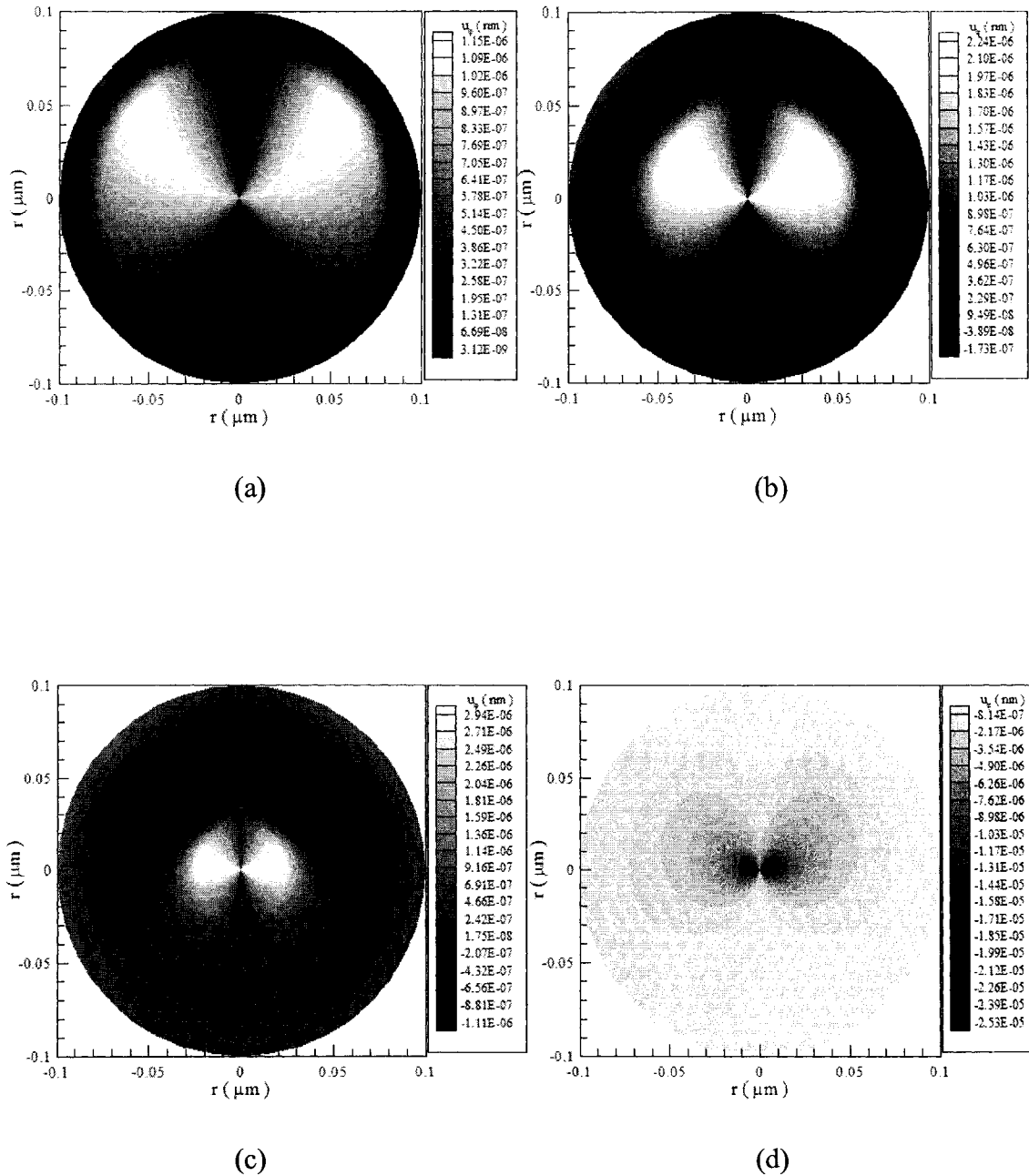


Fig. 5.12 Contours of displacement ( $u_\varphi$ ) distributions in the cross section of  $\theta = 0$  and  $\theta = \pi$  at different times (a)  $t = 5$  ps, (b)  $t = 10$  ps, (c)  $t = 15$  ps, and (d)  $t = 20$  ps with a mesh of  $60 \times 20 \times 20$  and a laser fluence  $J$  of  $500 \text{ J/m}^2$ .

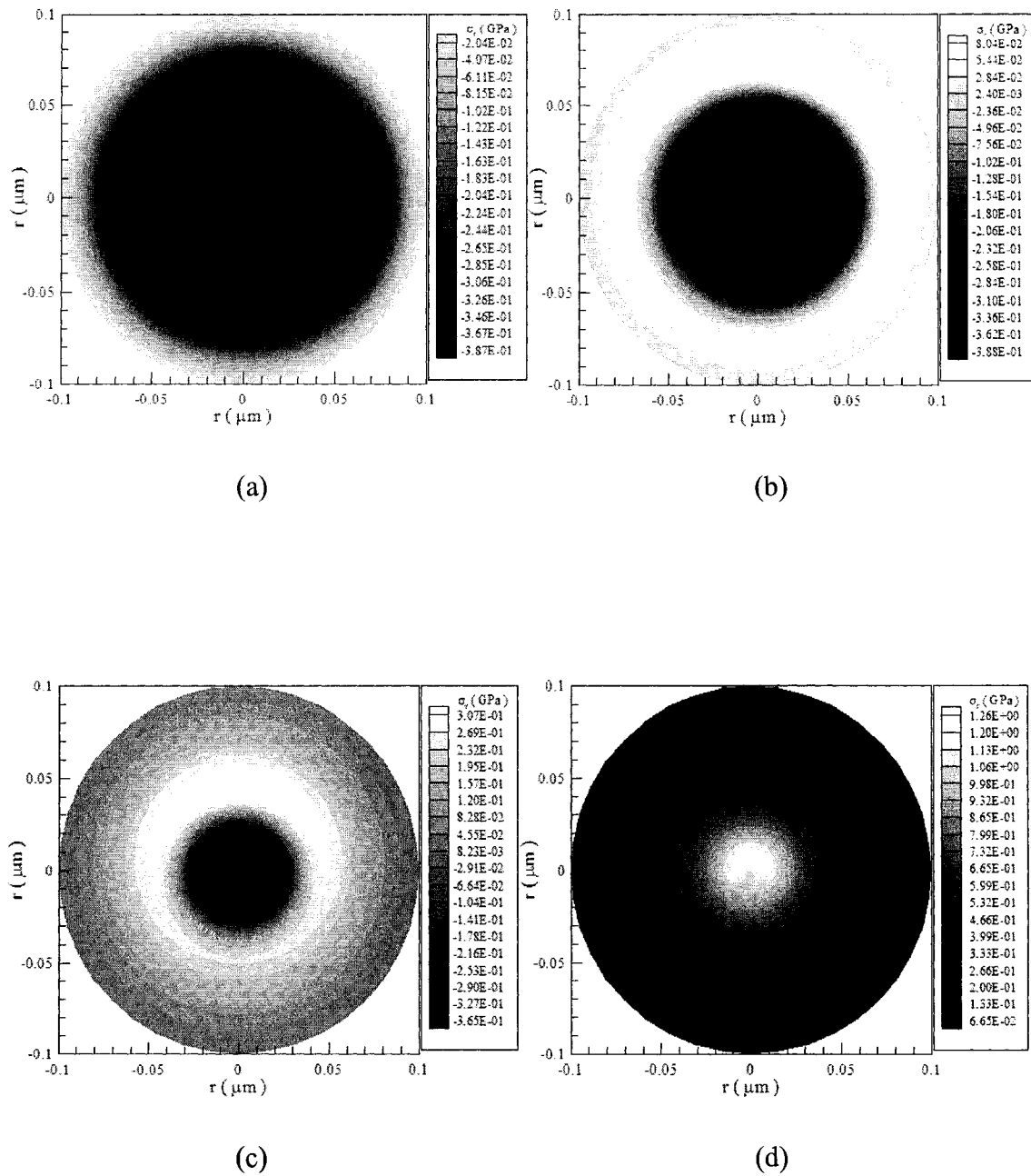


Fig. 5.13 Contours of normal stress ( $\sigma_r$ ) distributions in the cross section of  $\theta = 0$  and  $\theta = \pi$  at different times (a)  $t = 5$  ps, (b)  $t = 10$  ps, (c)  $t = 15$  ps, and (d)  $t = 20$  ps with a mesh of  $60 \times 20 \times 20$  and a laser fluence  $J$  of  $500 \text{ J/m}^2$ .

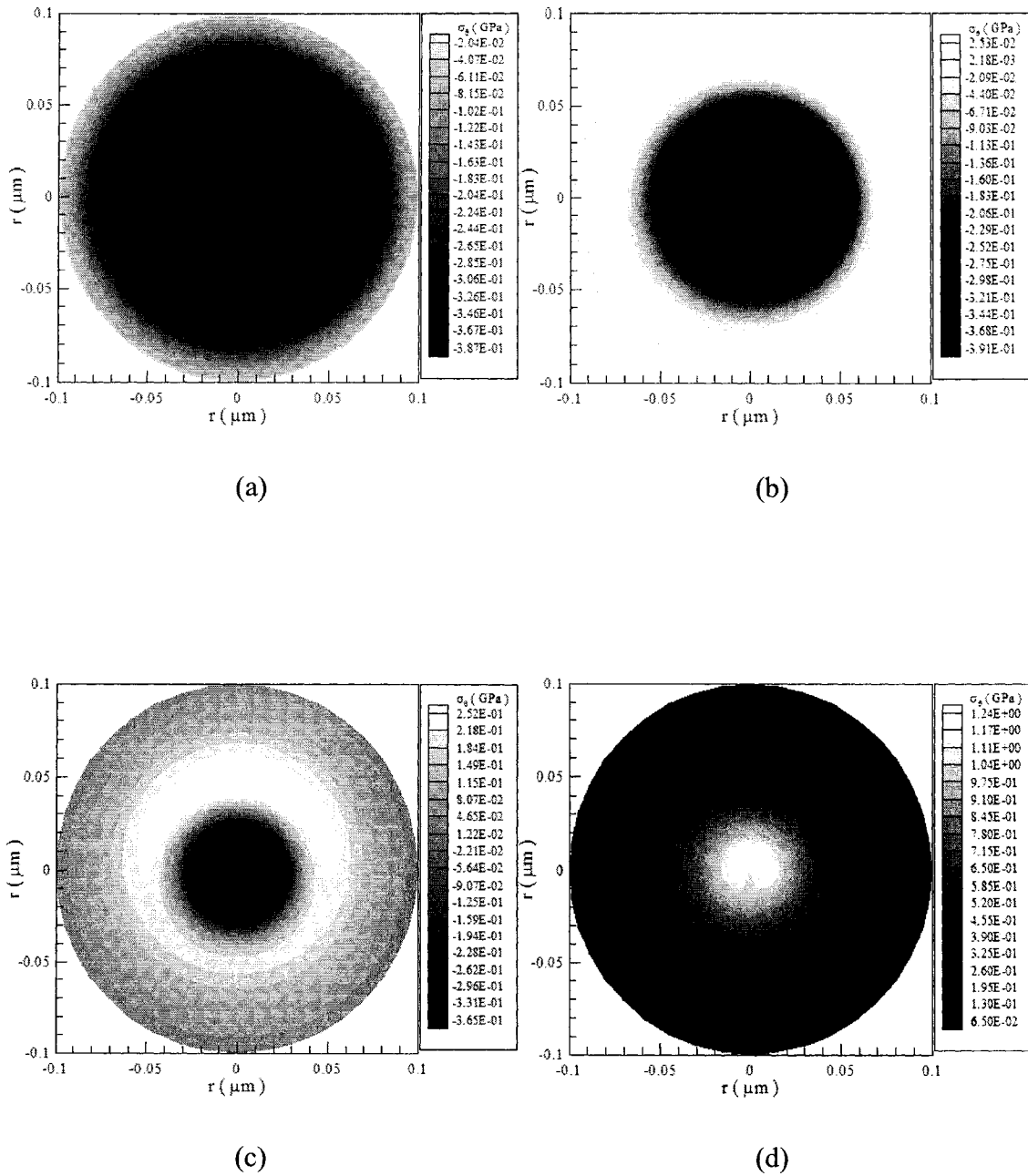


Fig. 5.14 Contours of normal stress ( $\sigma_\theta$ ) distributions in the cross section of  $\theta = 0$  and  $\theta = \pi$  at different times (a)  $t = 5$  ps, (b)  $t = 10$  ps, (c)  $t = 15$  ps, and (d)  $t = 20$  ps with a mesh of  $60 \times 20 \times 20$  and a laser fluence  $J$  of  $500 \text{ J/m}^2$ .

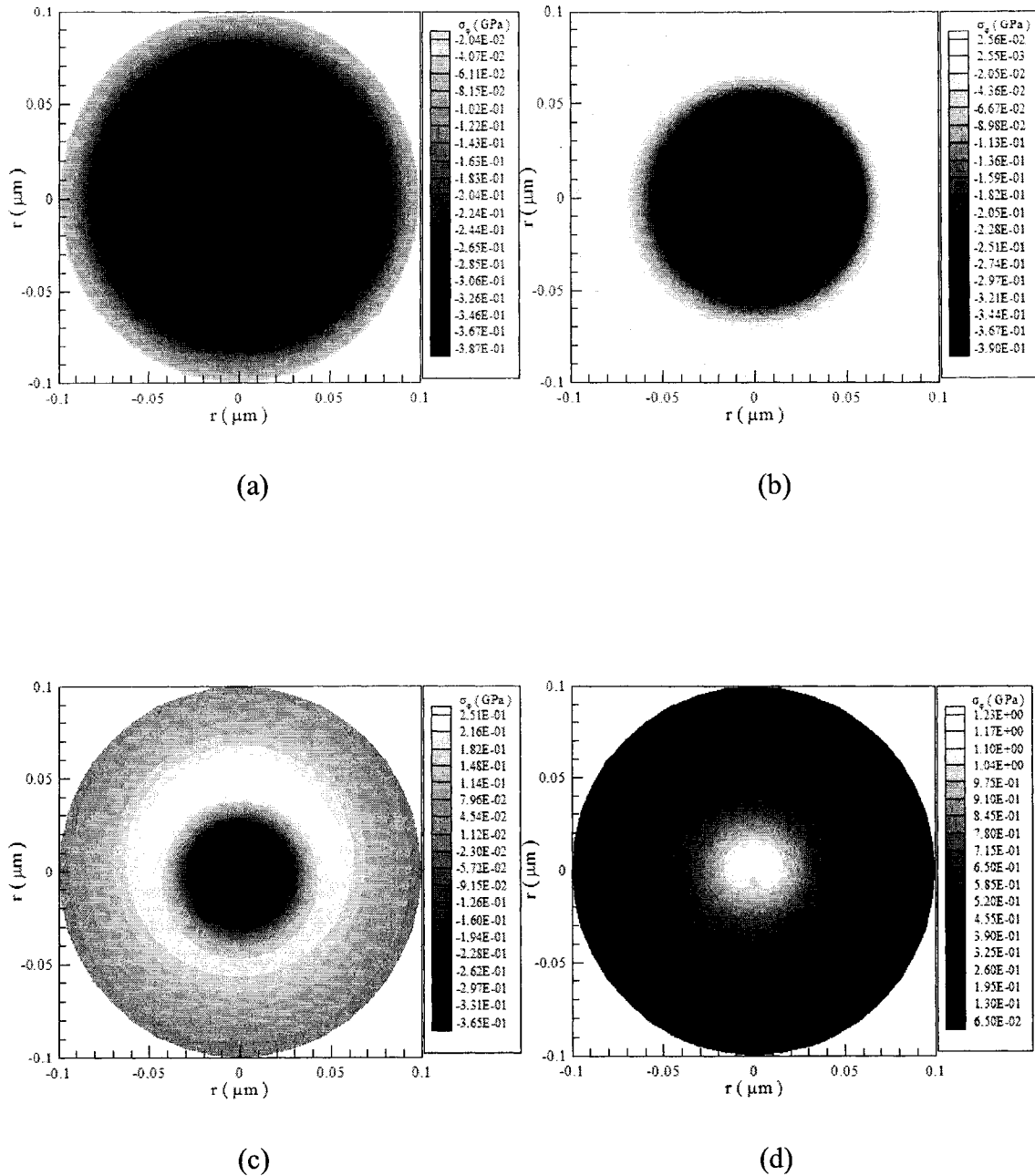


Fig. 5.15 Contours of normal stress ( $\sigma_\varphi$ ) distributions in the cross section of  $\theta = 0$  and  $\theta = \pi$  at different times (a)  $t = 5$  ps, (b)  $t = 10$  ps, (c)  $t = 15$  ps, and (d)  $t = 20$  ps with a mesh of  $60 \times 20 \times 20$  and a laser fluence  $J$  of  $500 \text{ J/m}^2$ .



### 5.2.2 Example Two

In this case, the laser irradiates both the top portion ( $0 \leq r \leq L, 0 \leq \theta \leq 2\pi, 0 \leq \varphi \leq \pi/4$ ) and the bottom portion ( $0 \leq r \leq L, 0 \leq \theta \leq 2\pi, 3\pi/4 \leq \varphi \leq \pi$ ).

Fig. 5.16 shows the change in electron temperature ( $\Delta T_e / (\Delta T_e)_{\max}$ ) at the point ( $r = L, \varphi = 0, \theta = 0$ ) for various meshes ( $60 \times 20 \times 20$ ,  $40 \times 20 \times 20$ ,  $30 \times 20 \times 40$ , and  $20 \times 30 \times 40$ ) with laser fluence  $J = 500 \text{ J/m}^2$ . The result is similar to that in Fig. 5.2 except that the temperature is higher since in this case the laser irradiates from both top and bottom. The maximum temperature rise of  $T_e$  is about 3935 K. And Fig. 5.17 shows the displacement  $u_r$  at the point ( $r = L/2, \varphi = 0, \theta = 0$ ) versus time. It shows again the solution is convergent.

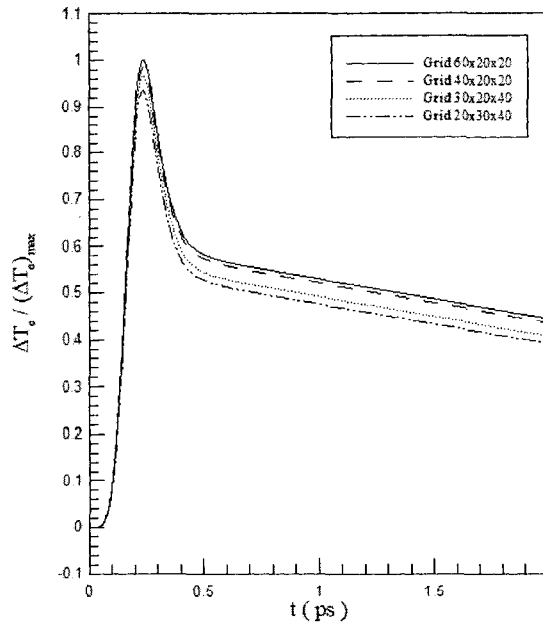


Fig. 5.16 Change in electron temperature  $T_e$  at  $r = 0.1 \text{ } \mu\text{m}$ ,  $\theta = 0$ ,  $\varphi = 0$  versus time for various meshes with a laser fluence  $J$  of  $500 \text{ J/m}^2$ .

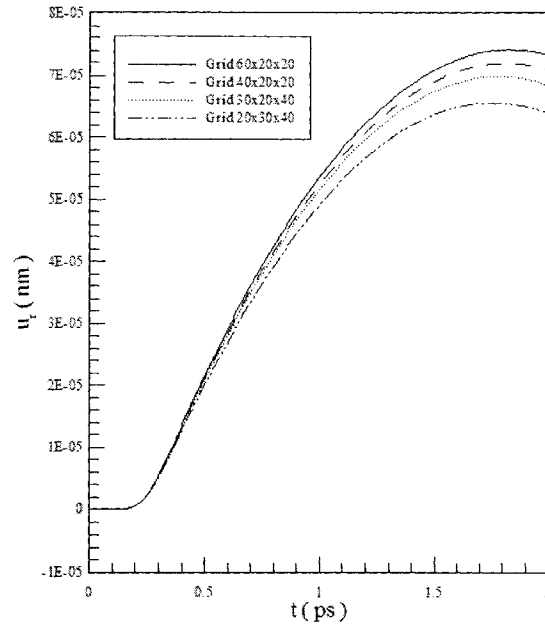
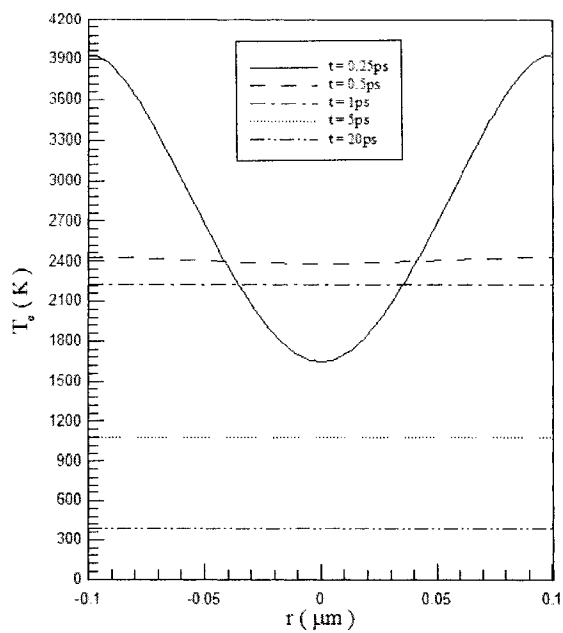
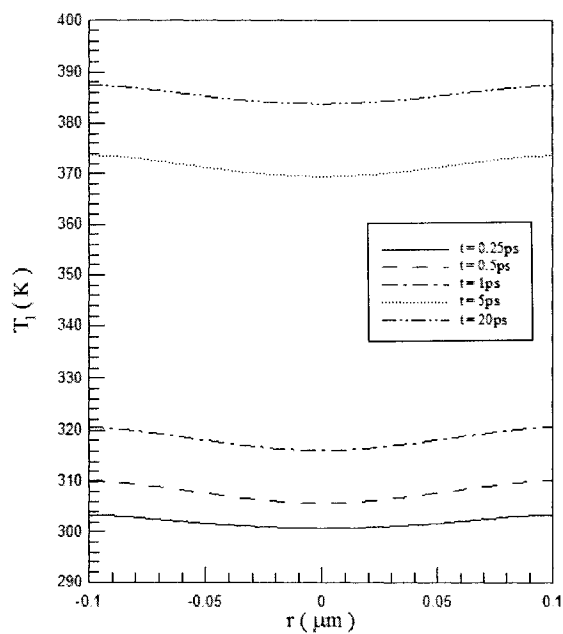


Fig. 5.17 Displacement  $u_r$ , at  $r = 0.05 \mu\text{m}$ ,  $\theta = 0$ ,  $\varphi = 0$  versus time for various meshes with a laser fluence  $J$  of  $500 \text{ J/m}^2$ .

Fig. 5.18 shows profiles of electron temperature and lattice temperature along the diameter at  $\varphi = 0$  and  $\varphi = \pi$  with laser fluence  $J = 500 \text{ J/m}^2$  and a mesh of  $60 \times 20 \times 20$  at different times (a)  $t = 0.25 \text{ ps}$ , (b)  $t = 0.5 \text{ ps}$ , (c)  $t = 1 \text{ ps}$ , (d)  $t = 5 \text{ ps}$ , and (e)  $t = 20 \text{ ps}$ , respectively. Figs. 5.19 and 5.20 show normal stress  $\sigma_r$  and displacement  $u_r$  along the diameter at  $\varphi = 0$  and  $\varphi = \pi$  at different times (a)  $t = 5 \text{ ps}$ , (b)  $t = 10 \text{ ps}$ , (c)  $t = 15 \text{ ps}$ , and (d)  $t = 20 \text{ ps}$  with a mesh of  $60 \times 20 \times 20$  and three different laser fluences ( $J = 500 \text{ J/m}^2$ ,  $1,000 \text{ J/m}^2$ ,  $2,000 \text{ J/m}^2$ ). It can be seen from these figures that all profiles are symmetric with respect to the original point and no numerical oscillations appear in the normal stress  $\sigma_r$ .



(a)



(b)

Fig. 5.18 Profiles of (a) electron temperature ( $T_e$ ), and (b) lattice temperature ( $T_l$ ) along  $r$ -axis at  $\varphi = 0$  and  $\varphi = \pi$  for various times with a laser fluence  $J$  of  $500\text{ J/m}^2$  and a mesh  $60 \times 20 \times 20$ .

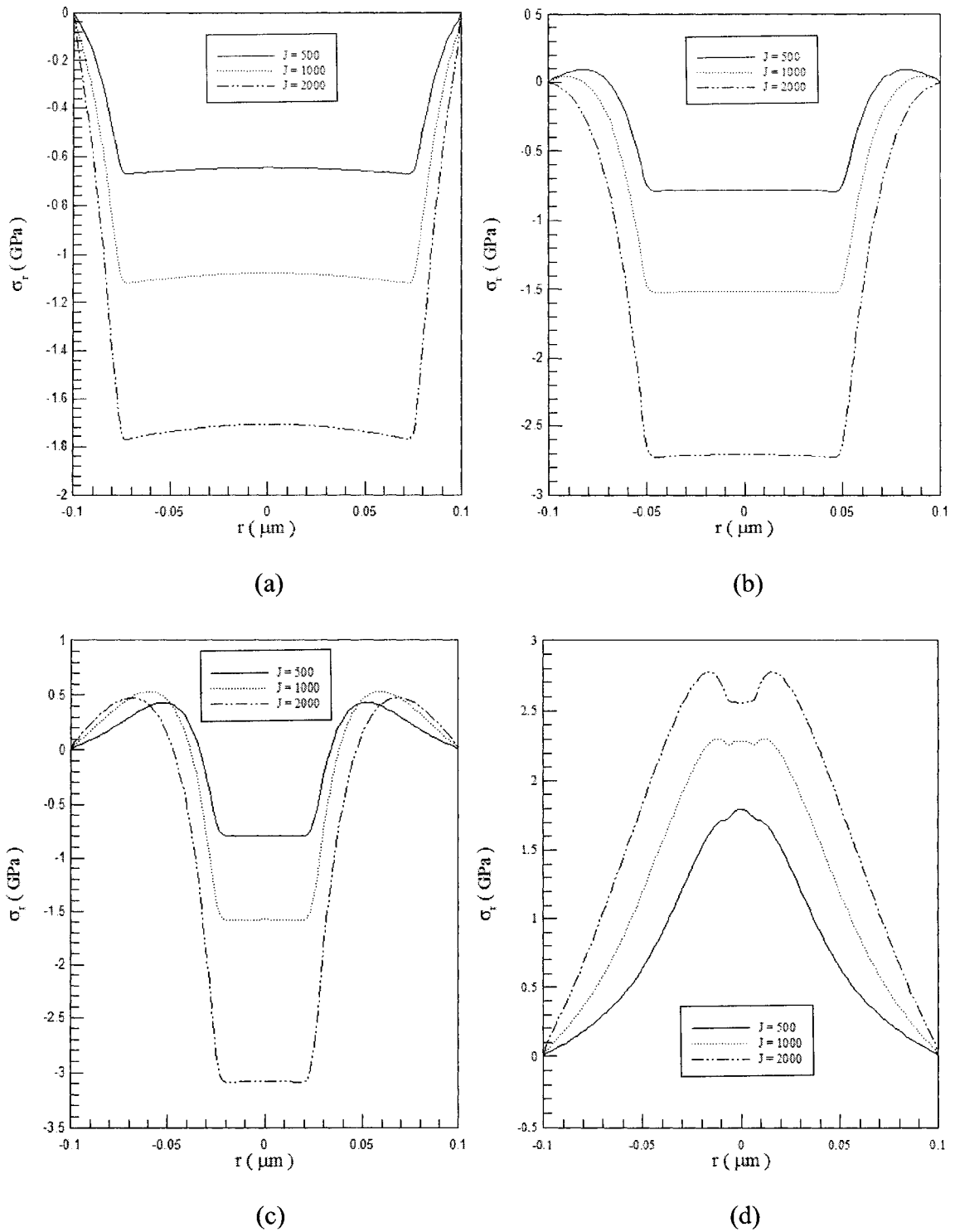


Fig. 5.19 Normal stress ( $\sigma_r$ ) along the diameter at  $\varphi = 0$  and  $\varphi = \pi$  at different times (a)  $t = 5$  ps, (b)  $t = 10$  ps, (c)  $t = 15$  ps, and (d)  $t = 20$  ps with three different laser fluences and a mesh of  $60 \times 20 \times 20$ .

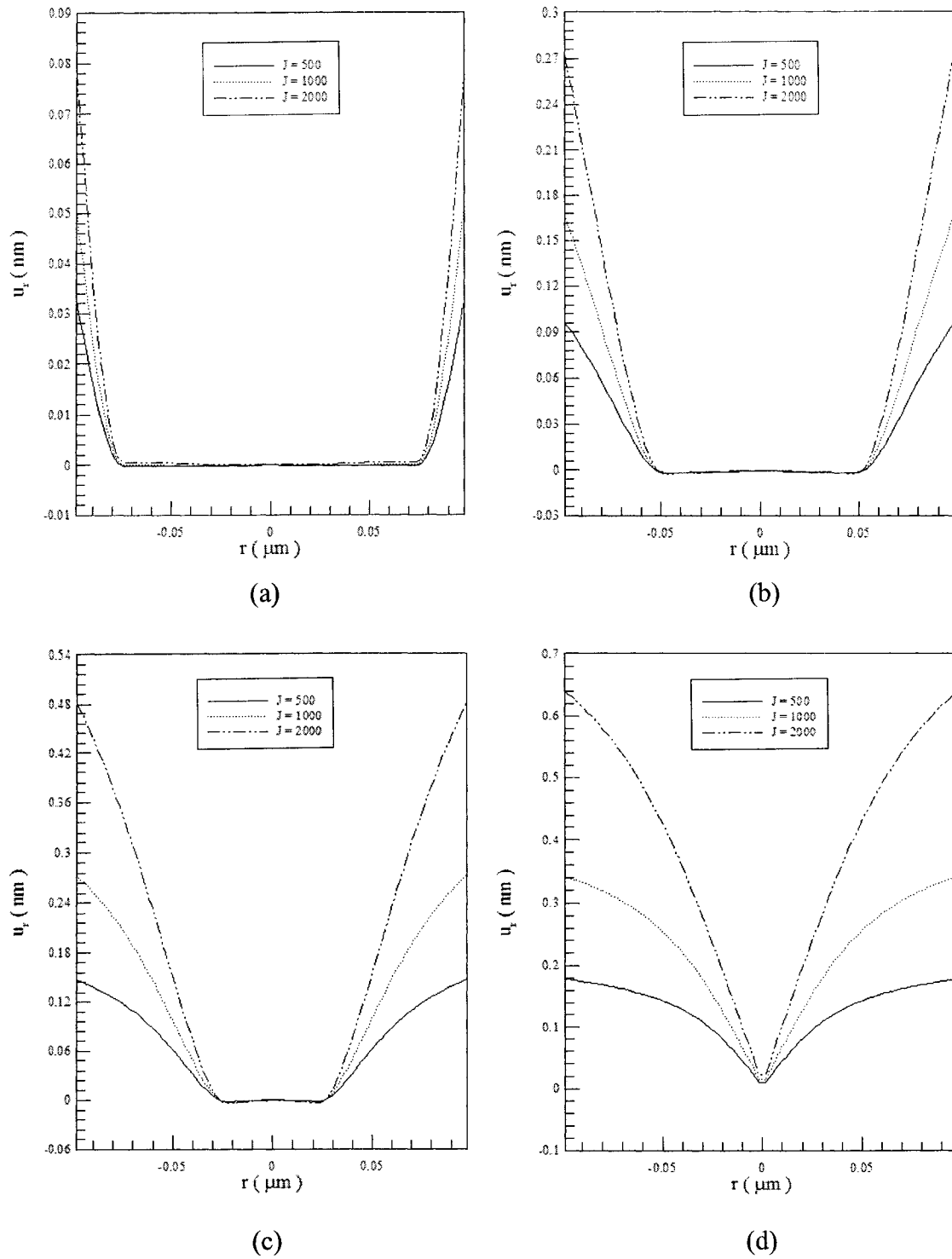
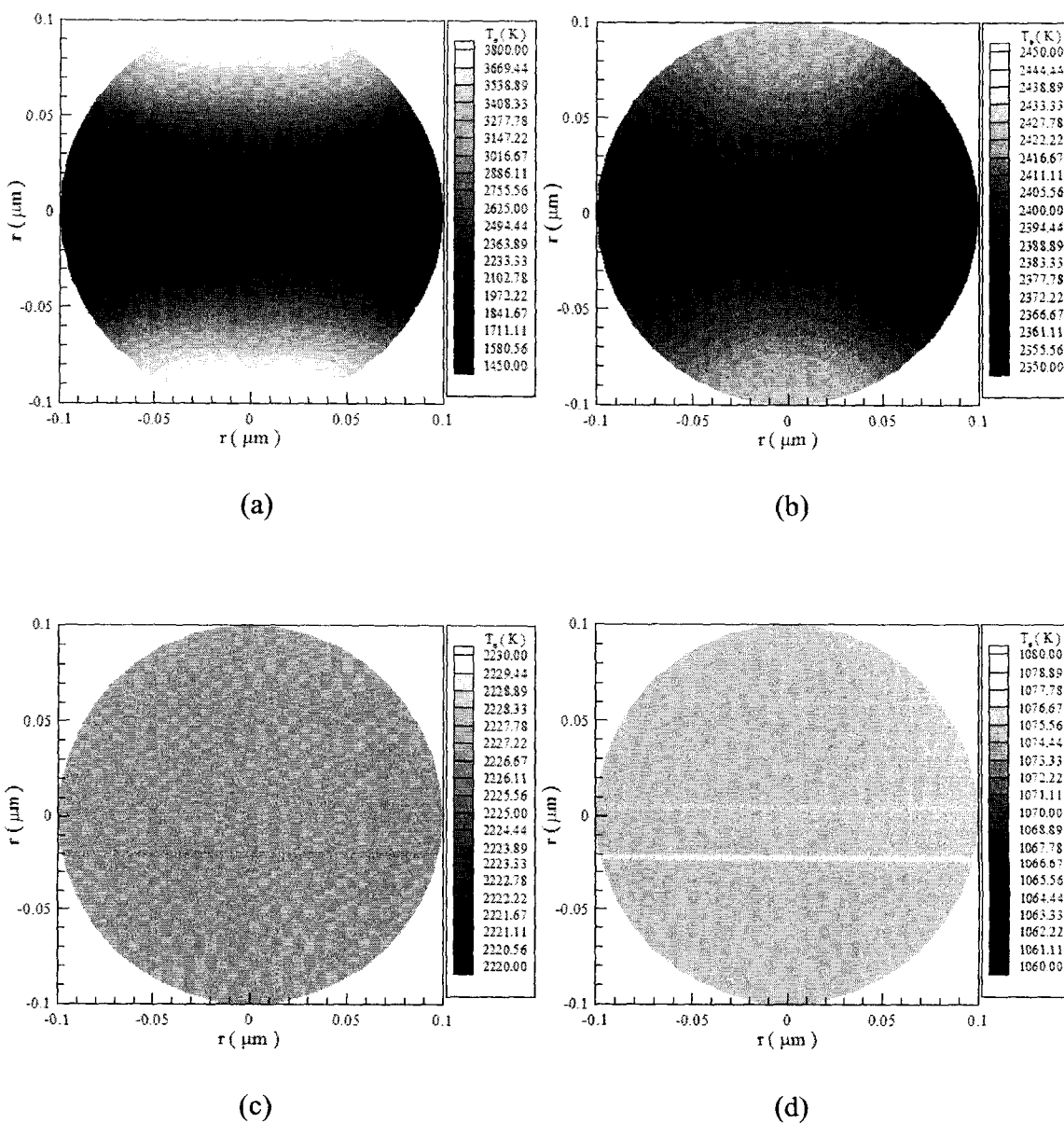


Fig. 5.20 Displacement ( $u_r$ ) along the diameter at  $\varphi = 0$  and  $\varphi = \pi$  at different times (a)  $t = 5$  ps, (b)  $t = 10$  ps, (c)  $t = 15$  ps, and (d)  $t = 20$  ps with three different laser fluences and a mesh of  $60 \times 20 \times 20$ .

Figs. 5.21–5.28 were plotted based on the results obtained in a mesh of  $60 \times 20 \times 20$  with a laser fluence  $J = 500 \text{ J/m}^2$ . Figs. 5.21 and 5.22 show contours of electron temperature distributions and lattice temperature distributions in the cross section of  $\theta = 0$  and  $\theta = \pi$  at different times (a)  $t = 0.25 \text{ ps}$ , (b)  $t = 0.5 \text{ ps}$ , (c)  $t = 1 \text{ ps}$ , (d)  $t = 5 \text{ ps}$ , (e)  $t = 10 \text{ ps}$ , and (f)  $t = 20 \text{ ps}$ , respectively. It can be seen from both figures that the heat is mainly transferred from both the top and the bottom to the center.



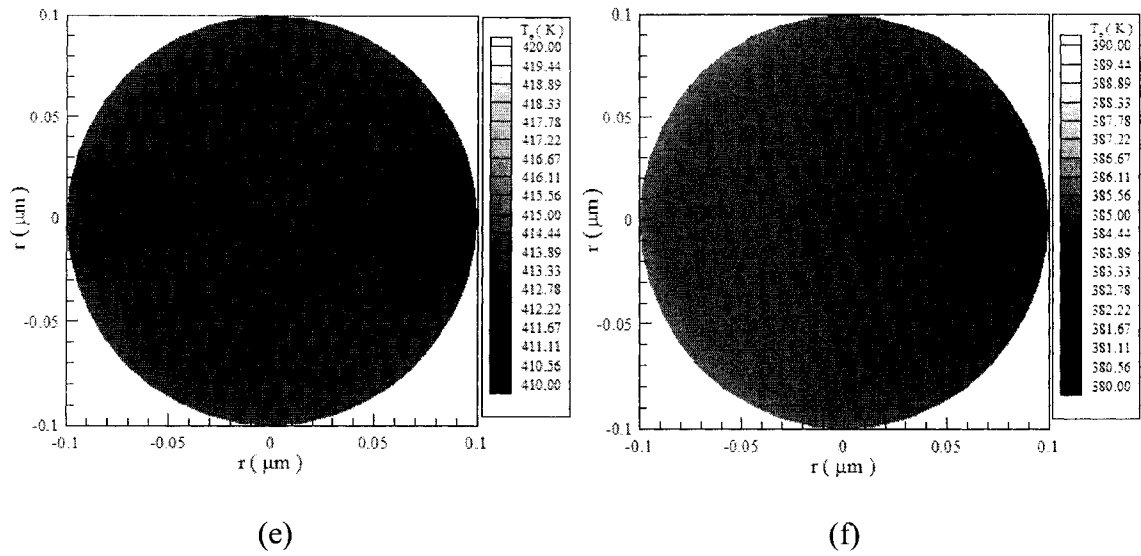
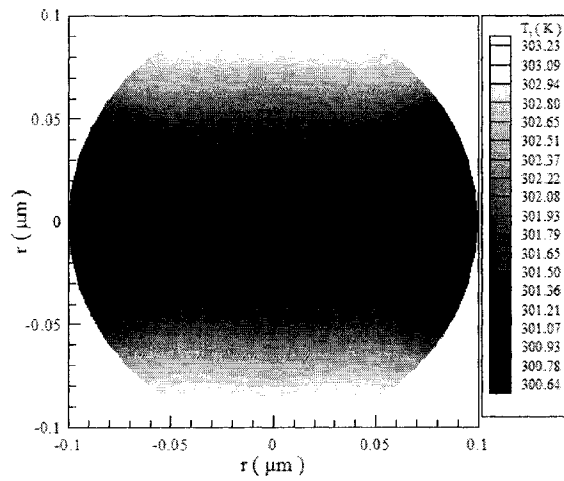
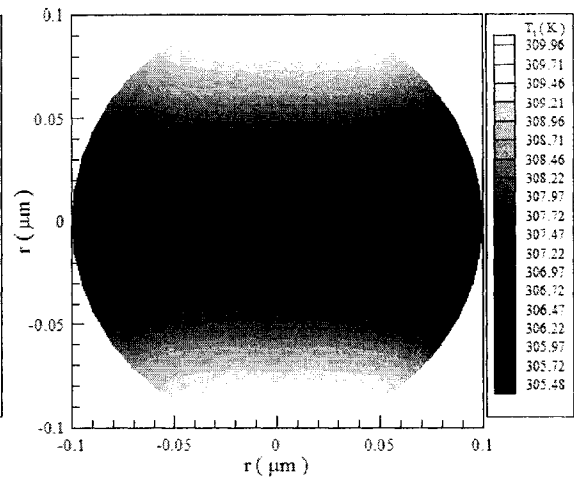


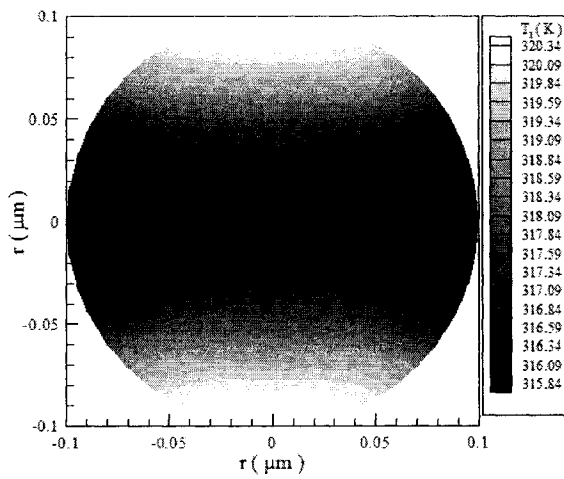
Fig. 5.21 Contours of electron temperature ( $T_e$ ) distributions in the cross section of  $\theta = 0$  and  $\theta = \pi$  at different times (a)  $t = 0.25$  ps, (b)  $t = 0.5$  ps, (c)  $t = 1$  ps, (d)  $t = 5$  ps, (e)  $t = 10$  ps, and (f)  $t = 20$  ps with a mesh of  $60 \times 20 \times 20$  and a laser fluence  $J$  of  $500 \text{ J/m}^2$ .



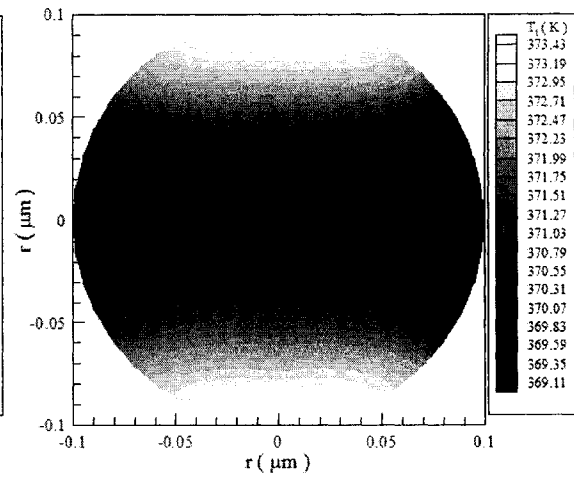
(a)



(b)



(c)



(d)



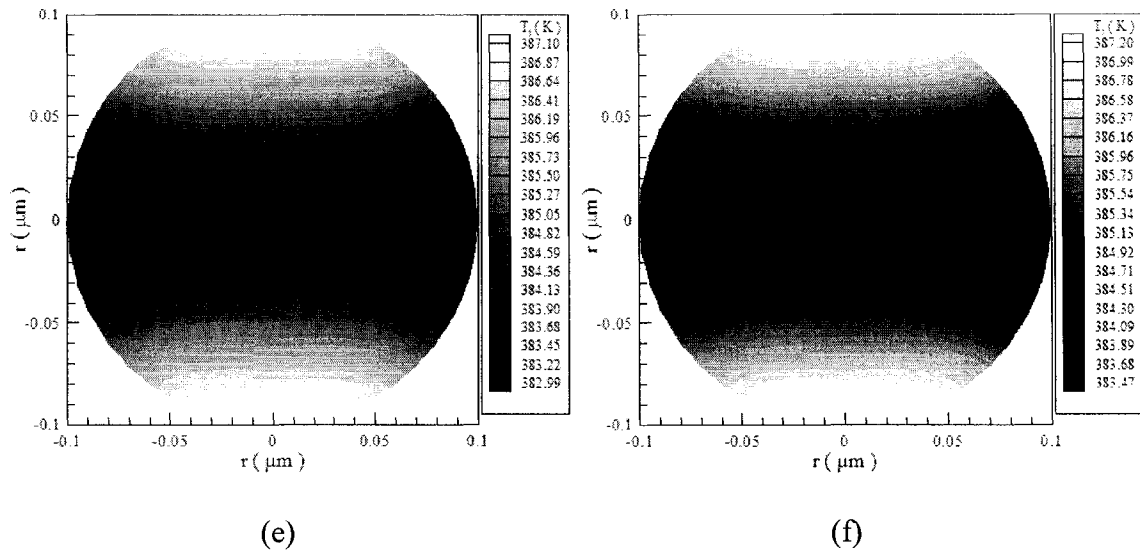


Fig. 5.22 Contours of lattice temperature ( $T_l$ ) distributions in the cross section of  $\theta = 0$  and  $\theta = \pi$  at different times (a)  $t = 0.25$  ps, (b)  $t = 0.5$  ps, (c)  $t = 1$  ps, (d)  $t = 5$  ps, (e)  $t = 10$  ps, and (f)  $t = 20$  ps with a mesh of  $60 \times 20 \times 20$  and a laser fluence  $J$  of  $500 \text{ J/m}^2$ .

Figs. 5.23–5.28 show contours of displacement ( $u_r, u_\theta, u_\phi$ ) and normal stress ( $\sigma_r, \sigma_\theta, \sigma_\phi$ ) in the cross section of  $\theta = 0$  and  $\theta = \pi$  at different times (a)  $t = 5$  ps, (b)  $t = 10$  ps, (c)  $t = 15$  ps, (d)  $t = 20$  ps, respectively. It can be seen from Fig. 5.23 that the upper hemisphere and the lower hemisphere expanding symmetrically along  $r$  direction.

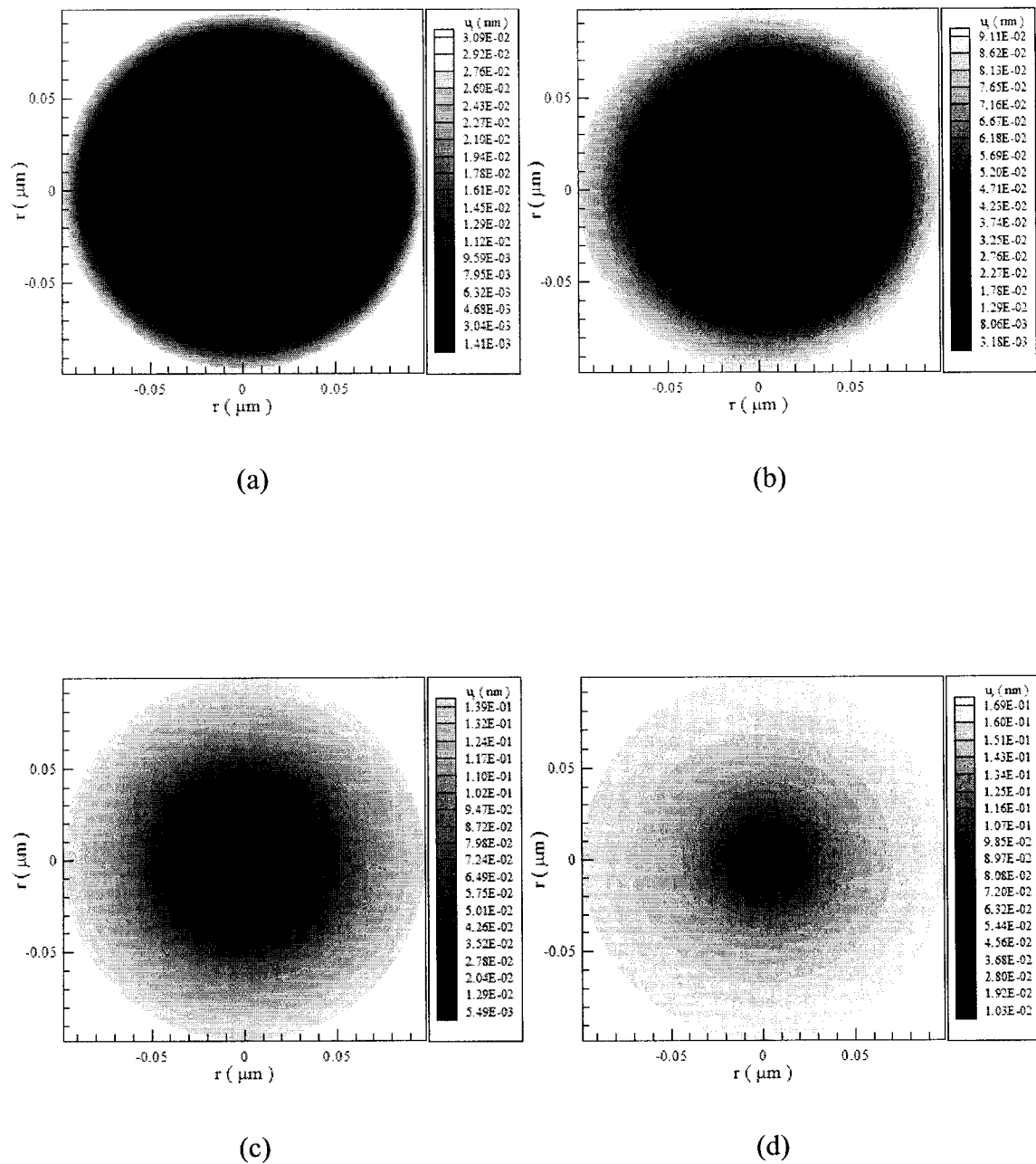


Fig. 5.23 Contours of displacement ( $u_r$ ) distributions in the cross section of  $\theta = 0$  and  $\theta = \pi$  at different times (a)  $t = 5$  ps, (b)  $t = 10$  ps, (c)  $t = 15$  ps, and (d)  $t = 20$  ps with a mesh of  $60 \times 20 \times 20$  and a laser fluence  $J$  of  $500 \text{ J/m}^2$ .

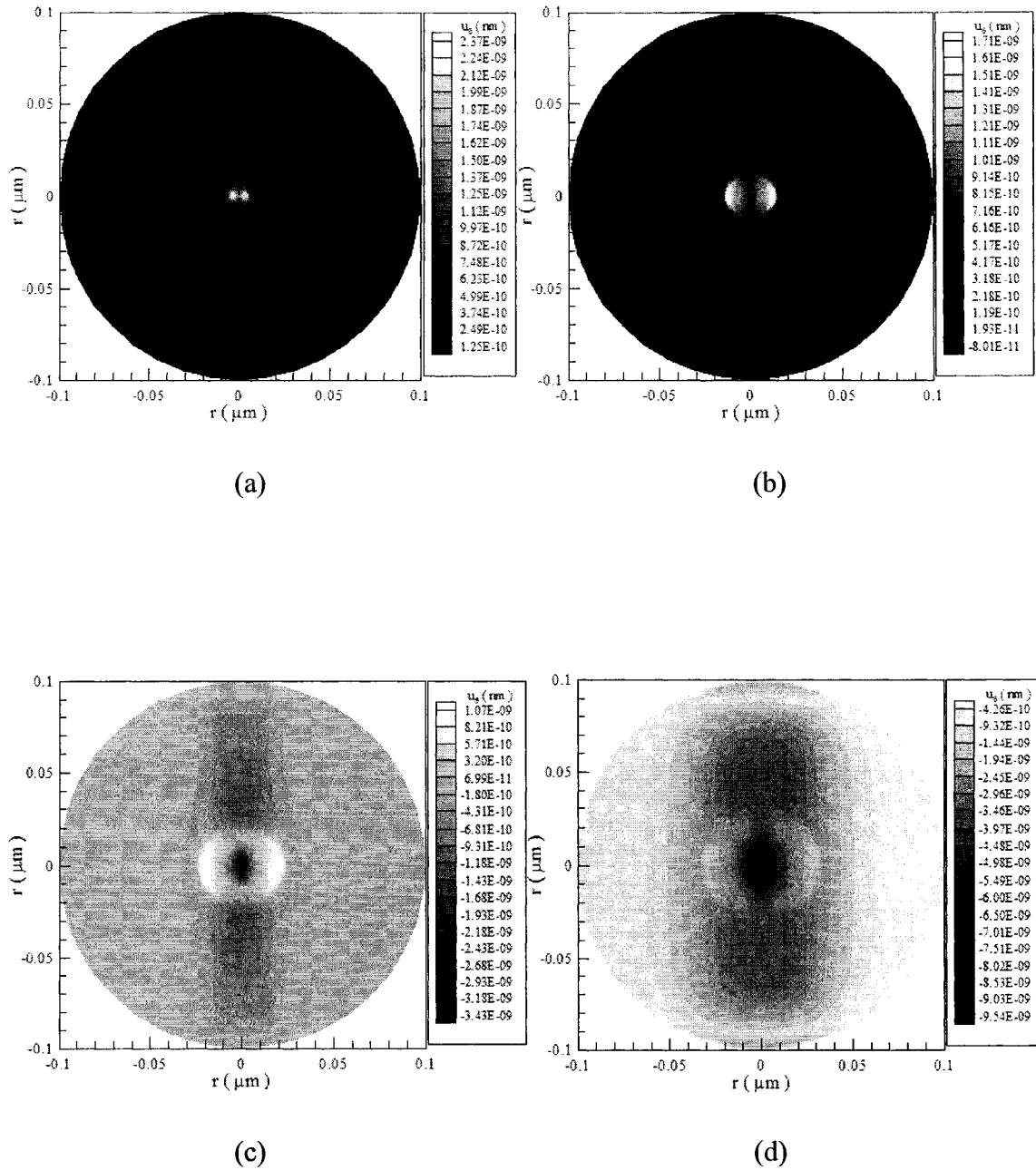


Fig. 5.24 Contours of displacement ( $u_\theta$ ) distributions in the cross section of  $\theta = 0$  and  $\theta = \pi$  at different times (a)  $t = 5$  ps, (b)  $t = 10$  ps, (c)  $t = 15$  ps, and (d)  $t = 20$  ps with a mesh of  $60 \times 20 \times 20$  and a laser fluence  $J$  of  $500 \text{ J/m}^2$ .

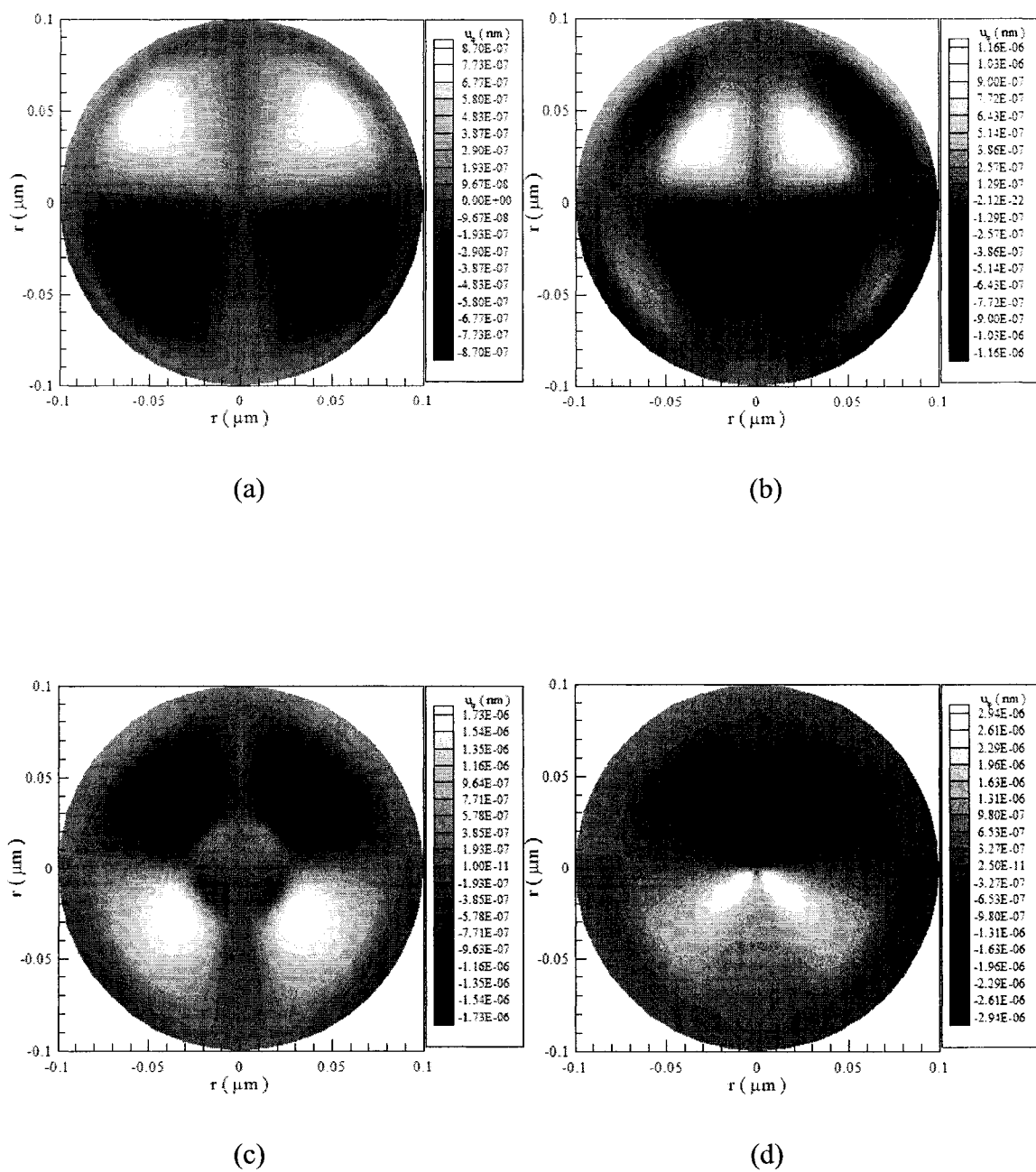


Fig. 5.25 Contours of displacement ( $u_\varphi$ ) distributions in the cross section of  $\theta = 0$  and  $\theta = \pi$  at different times (a)  $t = 5$  ps, (b)  $t = 10$  ps, (c)  $t = 15$  ps, and (d)  $t = 20$  ps with a mesh of  $60 \times 20 \times 20$  and a laser fluence  $J$  of  $500 \text{ J/m}^2$ .

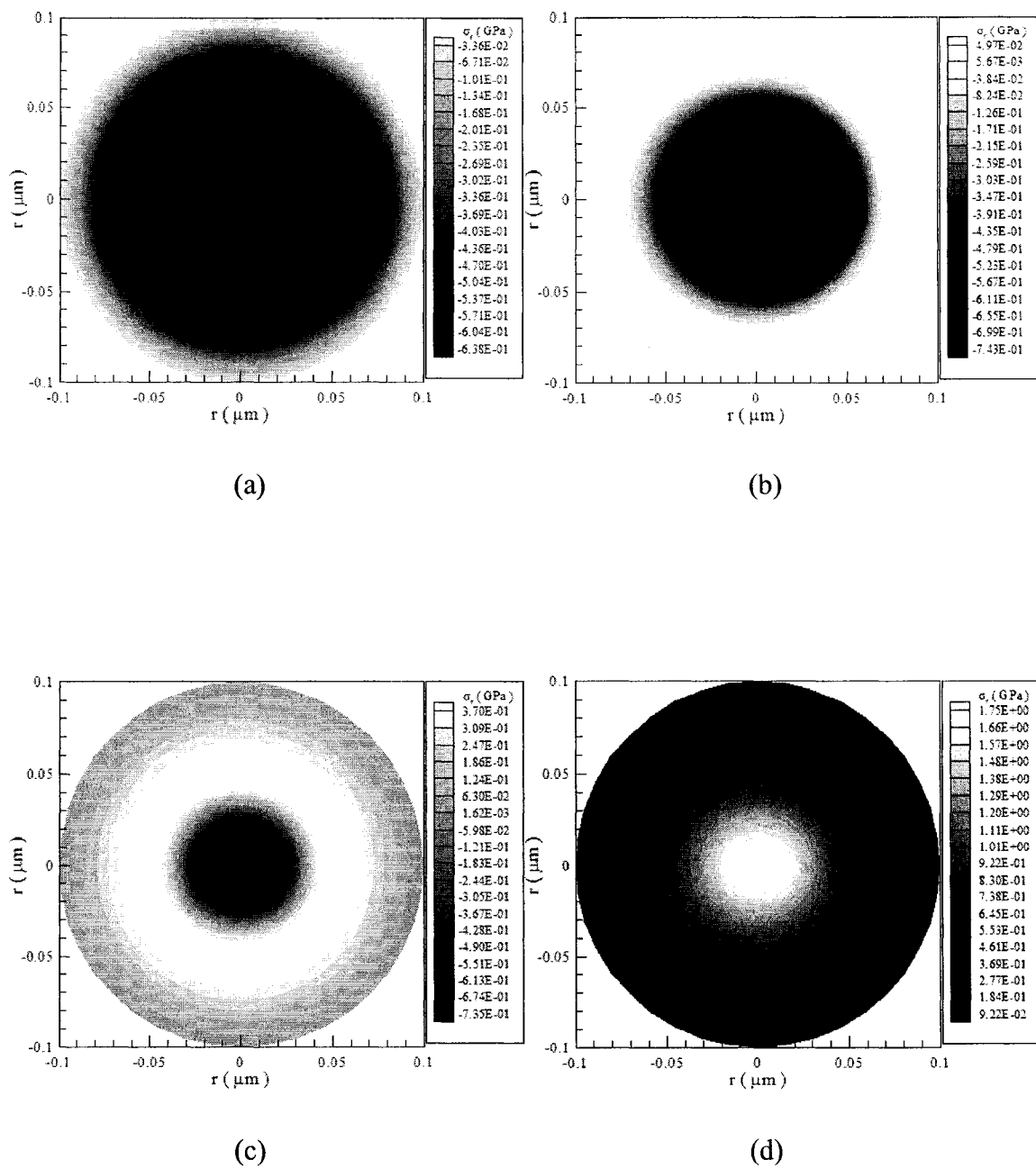


Fig. 5.26 Contours of normal stress ( $\sigma_r$ ) distributions in the cross section of  $\theta = 0$  and  $\theta = \pi$  at different times (a)  $t = 5$  ps, (b)  $t = 10$  ps, (c)  $t = 15$  ps, and (d)  $t = 20$  ps with a mesh of  $60 \times 20 \times 20$  and a laser fluence  $J$  of  $500 \text{ J/m}^2$ .

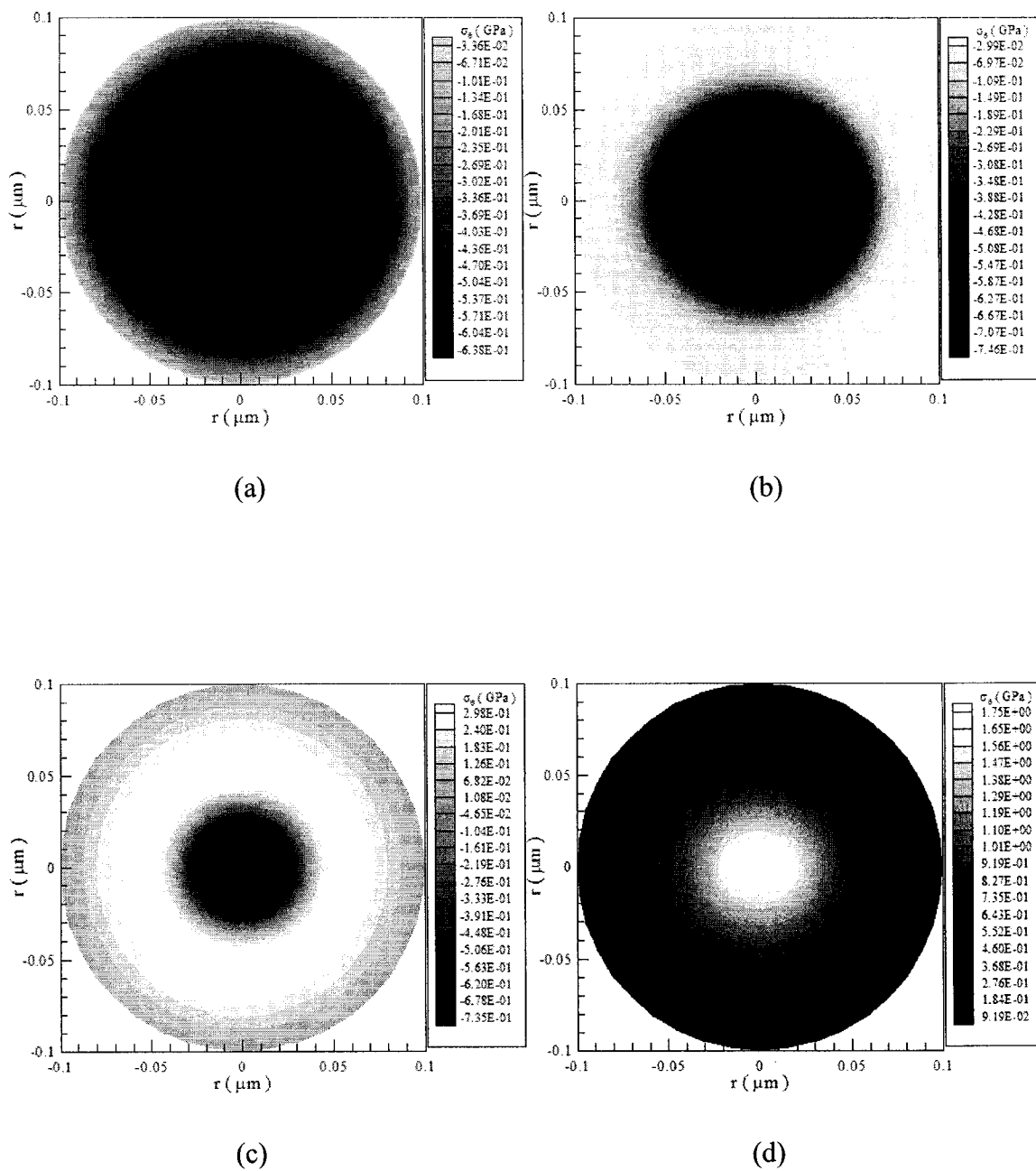


Fig. 5.27 Contours of normal stress ( $\sigma_\theta$ ) distributions in the cross section of  $\theta = 0$  and  $\theta = \pi$  at different times (a)  $t = 5$  ps, (b)  $t = 10$  ps, (c)  $t = 15$  ps, and (d)  $t = 20$  ps with a mesh of  $60 \times 20 \times 20$  and a laser fluence  $J$  of  $500 \text{ J/m}^2$ .

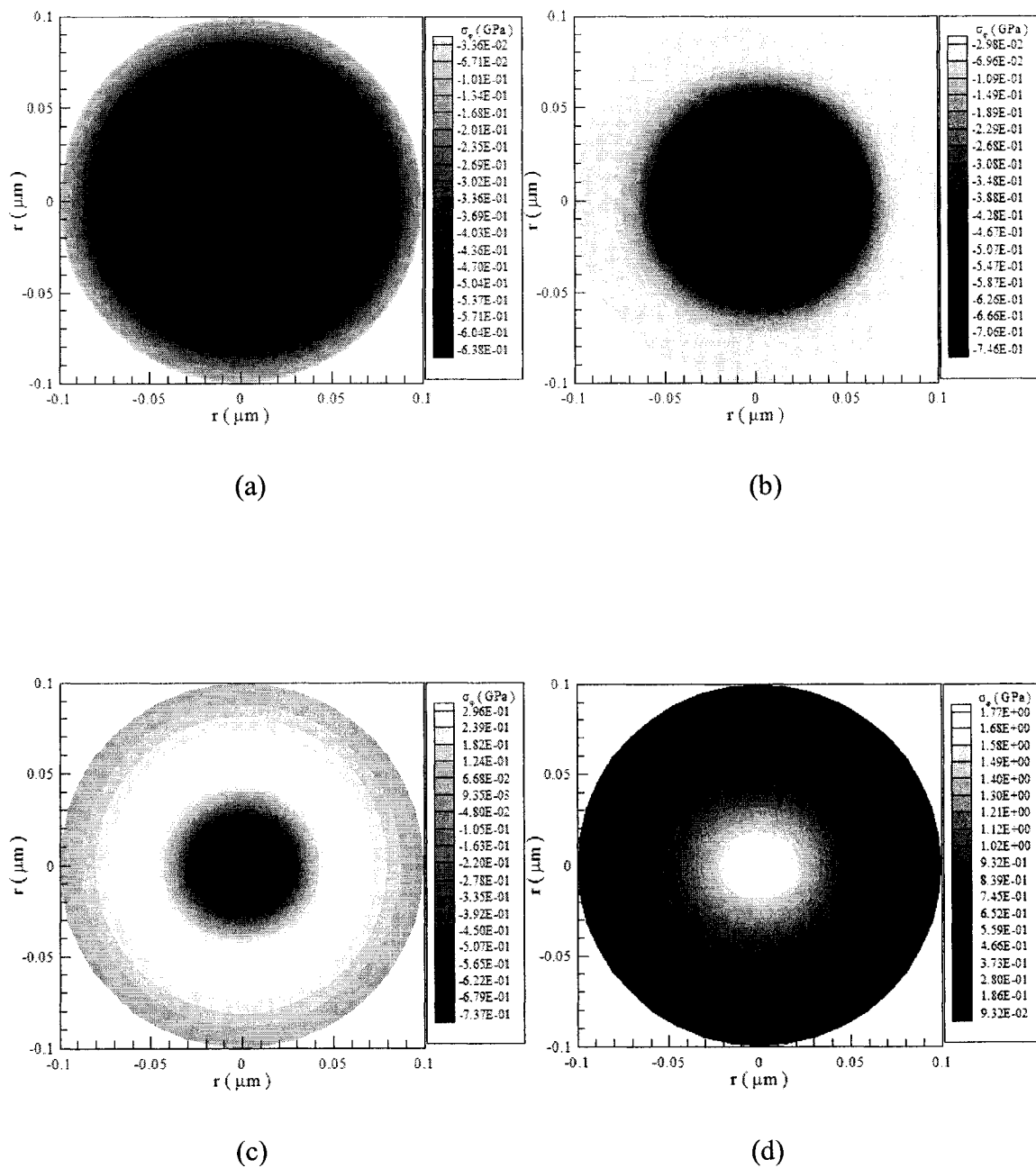


Fig. 5.28 Contours of normal stress ( $\sigma_\phi$ ) distributions in the cross section of  $\theta = 0$  and  $\theta = \pi$  at different times (a)  $t = 5$  ps, (b)  $t = 10$  ps, (c)  $t = 15$  ps, and (d)  $t = 20$  ps with a mesh of  $60 \times 20 \times 20$  and a laser fluence  $J$  of  $500 \text{ J/m}^2$ .

### 5.2.3 Example Three

In this case, the laser irradiates the top hemisphere ( $0 \leq r \leq L$ ,  $0 \leq \theta \leq 2\pi$ ,  $0 \leq \varphi \leq \pi/2$ ).

Fig. 5.29 shows the change in electron temperature ( $\Delta T_e / (\Delta T_e)_{\max}$ ) at the point ( $r = L$ ,  $\varphi = 0$ ,  $\theta = 0$ ) for various meshes ( $60 \times 20 \times 20$ ,  $40 \times 20 \times 20$ ,  $30 \times 20 \times 40$ , and  $20 \times 30 \times 40$ ) with laser fluence  $J = 500 \text{ J/m}^2$ . The result is similar to that in Figs. 5.2 and 5.16 except that the temperature is higher. The maximum temperature rise of  $T_e$  is about 4119 K. And Fig. 5.30 shows the displacement  $u_r$  at the point ( $r = L/2$ ,  $\varphi = 0$ ,  $\theta = 0$ ) versus time.

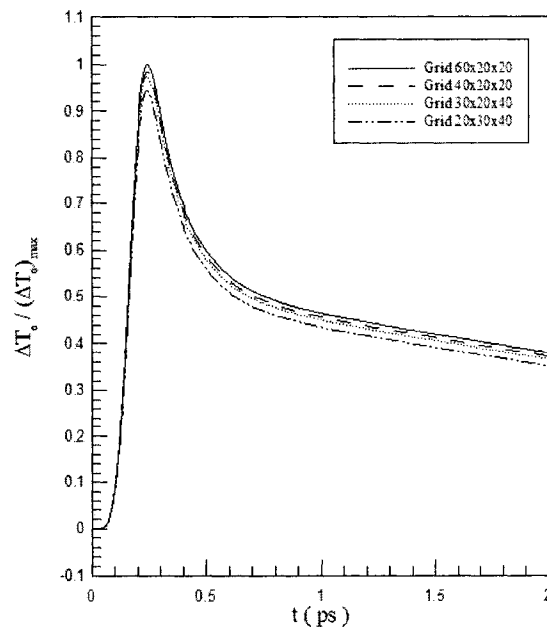


Fig. 5.29 Change in electron temperature  $T_e$  at  $r = 0.1 \text{ } \mu\text{m}$ ,  $\theta = 0$ ,  $\varphi = 0$  versus time for various meshes with a laser fluence  $J$  of  $500 \text{ J/m}^2$ .



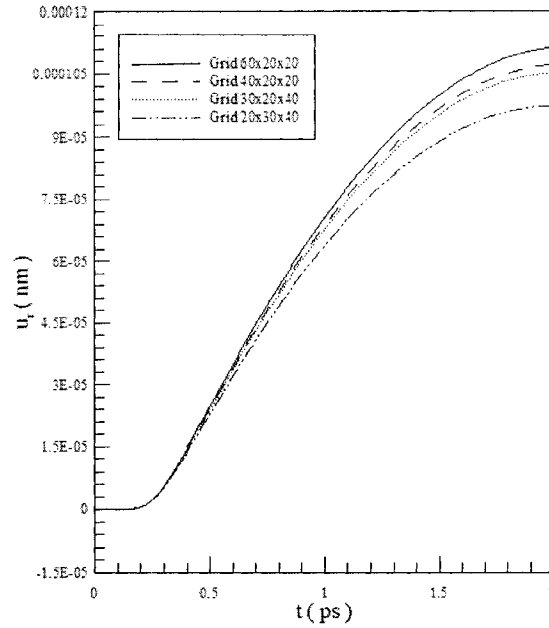
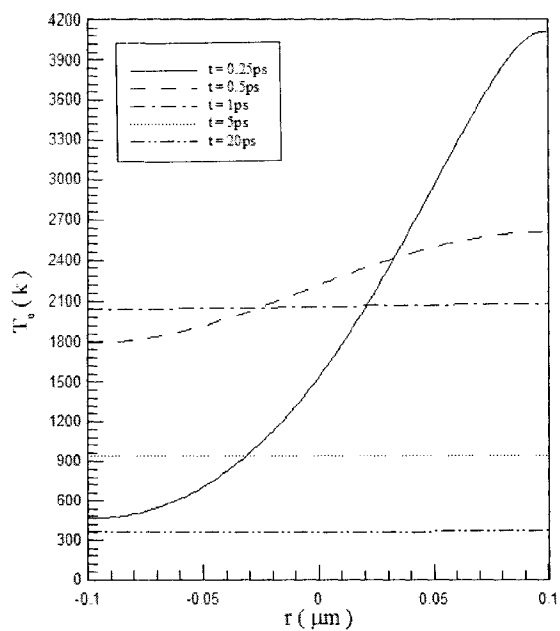
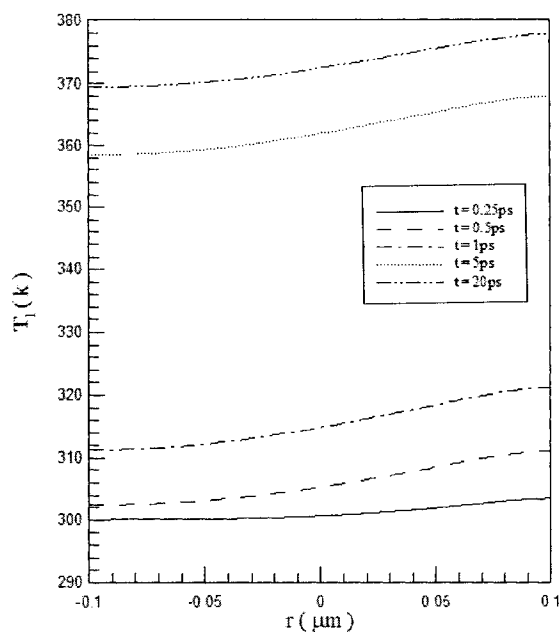


Fig. 5.30 Displacement  $u_r$  at  $r = 0.05 \mu\text{m}$ ,  $\theta = 0$ ,  $\varphi = 0$  versus time for various meshes with a laser fluence  $J$  of  $500 \text{ J/m}^2$ .

Fig. 5.31 shows profiles of electron temperature and lattice temperature along the diameter at  $\varphi = 0$  and  $\varphi = \pi$  with laser fluence  $J = 500 \text{ J/m}^2$  and a mesh of  $60 \times 20 \times 20$  at different times (a)  $t = 0.25 \text{ ps}$ , (b)  $t = 0.5 \text{ ps}$ , (c)  $t = 1 \text{ ps}$ , (d)  $t = 5 \text{ ps}$ , and (e)  $t = 20 \text{ ps}$ , respectively. Figs. 5.32 and 5.33 show normal stress  $\sigma_r$  and displacement  $u_r$  along the diameter at  $\varphi = 0$  and  $\varphi = \pi$  at different times (a)  $t = 5 \text{ ps}$ , (b)  $t = 10 \text{ ps}$ , (c)  $t = 15 \text{ ps}$ , and (d)  $t = 20 \text{ ps}$  with a mesh of  $60 \times 20 \times 20$  and three different laser fluences ( $J = 500 \text{ J/m}^2$ ,  $1,000 \text{ J/m}^2$ ,  $2,000 \text{ J/m}^2$ ). It can be seen from these figures that the heat is transferred from the top to the bottom along the  $r$  direction.



(a)



(b)

Fig. 5.31 Profiles of (a) electron temperature ( $T_e$ ), and (b) lattice temperature ( $T_l$ ) along  $r$ -axis at  $\varphi = 0$  and  $\varphi = \pi$  for various times with a laser fluence  $J$  of  $500 \text{ J/m}^2$  and a mesh  $60 \times 20 \times 20$ .

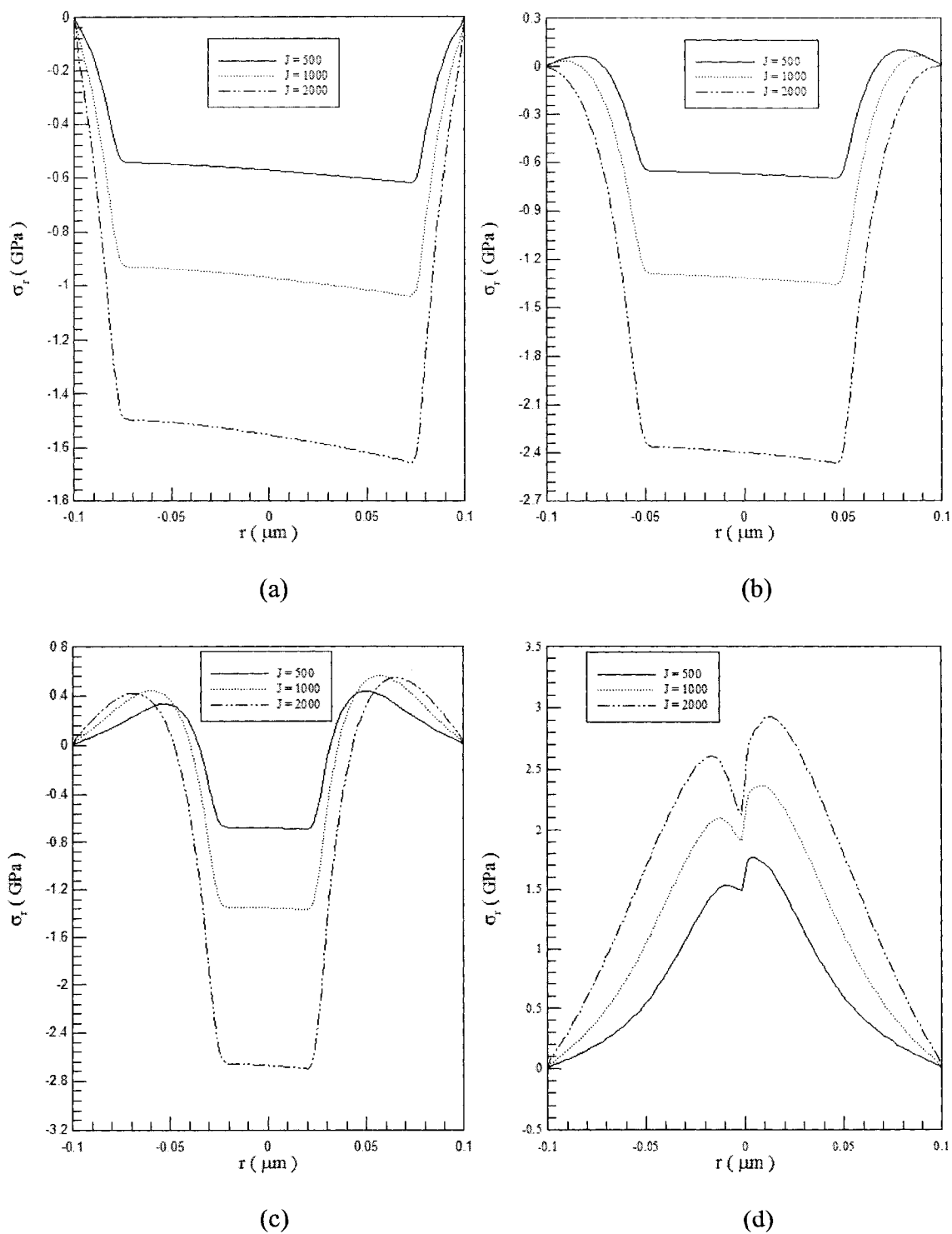


Fig. 5.32 Normal stress ( $\sigma_r$ ) along the diameter at  $\varphi = 0$  and  $\varphi = \pi$  at different times (a)  $t = 5$  ps, (b)  $t = 10$  ps, (c)  $t = 15$  ps, and (d)  $t = 20$  ps with three different laser fluences and a mesh of  $60 \times 20 \times 20$ .

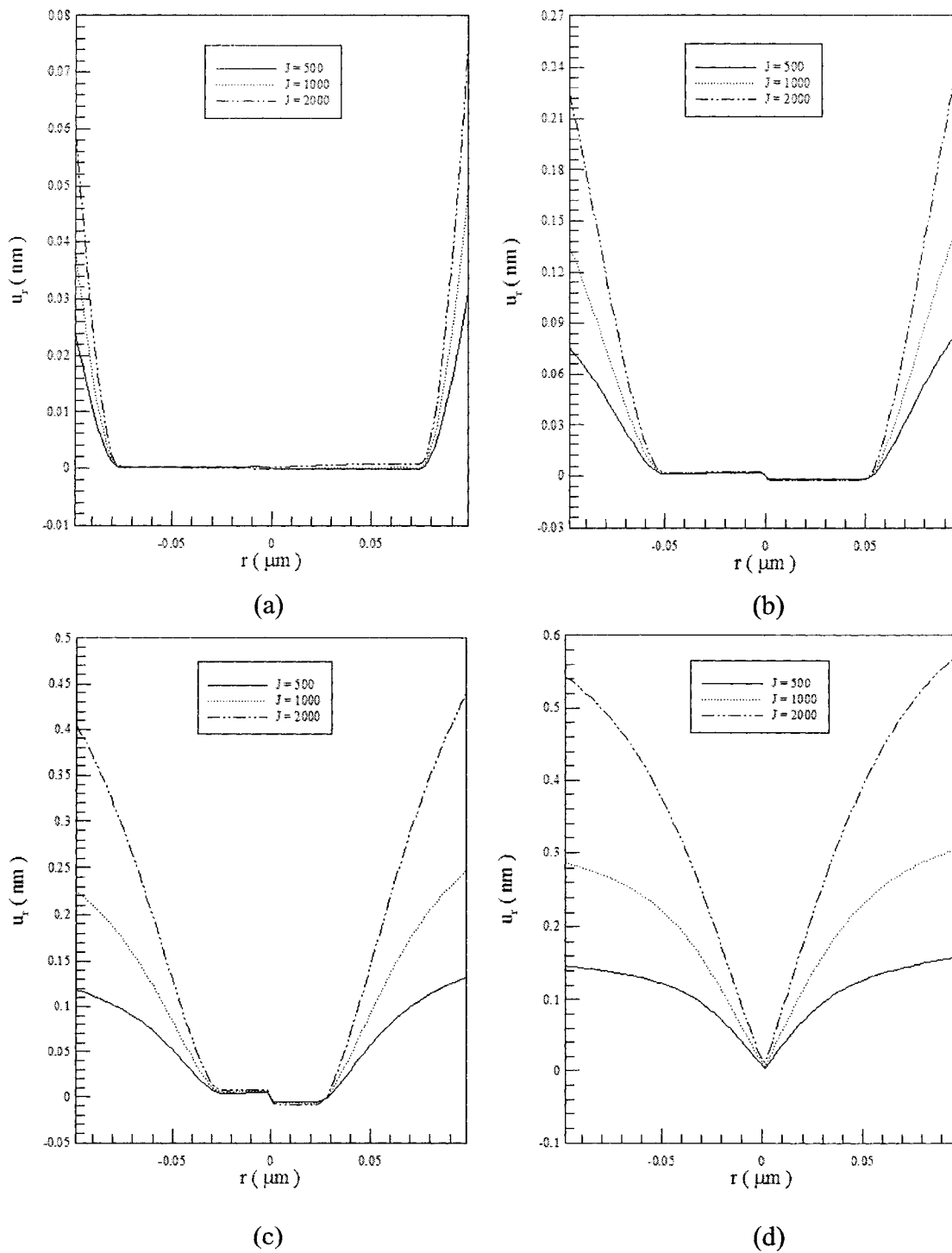
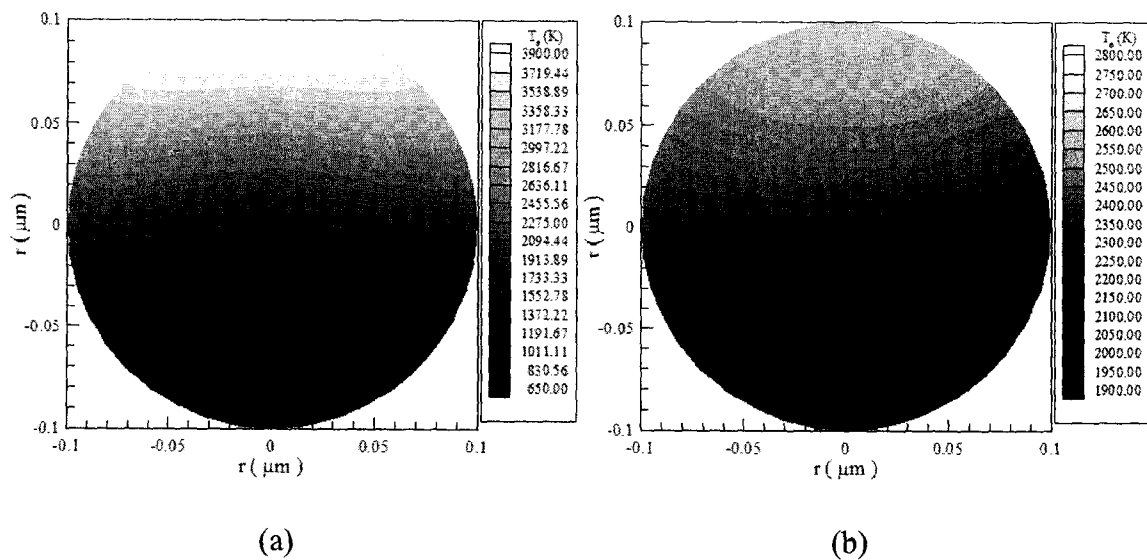


Fig. 5.33 Displacement ( $u_r$ ) along the diameter at  $\varphi = 0$  and  $\varphi = \pi$  at different times (a)  $t = 5$  ps, (b)  $t = 10$  ps, (c)  $t = 15$  ps, and (d)  $t = 20$  ps with three different laser fluences and a mesh of  $60 \times 20 \times 20$ .

Figs. 5.34–5.41 were plotted based on the results obtained in a mesh of  $60 \times 20 \times 20$  with a laser fluence  $J = 500 \text{ J/m}^2$ . Figs. 5.34 and 5.35 show contours of electron temperature distributions and lattice temperature distributions in the cross section of  $\theta = 0$  and  $\theta = \pi$  at different times (a)  $t = 0.25 \text{ ps}$ , (b)  $t = 0.5 \text{ ps}$ , (c)  $t = 1 \text{ ps}$ , (d)  $t = 5 \text{ ps}$ , (e)  $t = 10 \text{ ps}$ , and (f)  $t = 20 \text{ ps}$ , respectively. It can be seen from both figures that the heat is mainly transferred from top to bottom along  $r$  direction. Figs. 5.36 – 5.41 show contours of displacement ( $u_r, u_\theta, u_\phi$ ) and normal stress ( $\sigma_r, \sigma_\theta, \sigma_\phi$ ) in the cross section of  $\theta = 0$  and  $\theta = \pi$  at different times (a)  $t = 5 \text{ ps}$ , (b)  $t = 10 \text{ ps}$ , (c)  $t = 15 \text{ ps}$ , and (d)  $t = 20 \text{ ps}$ , respectively.



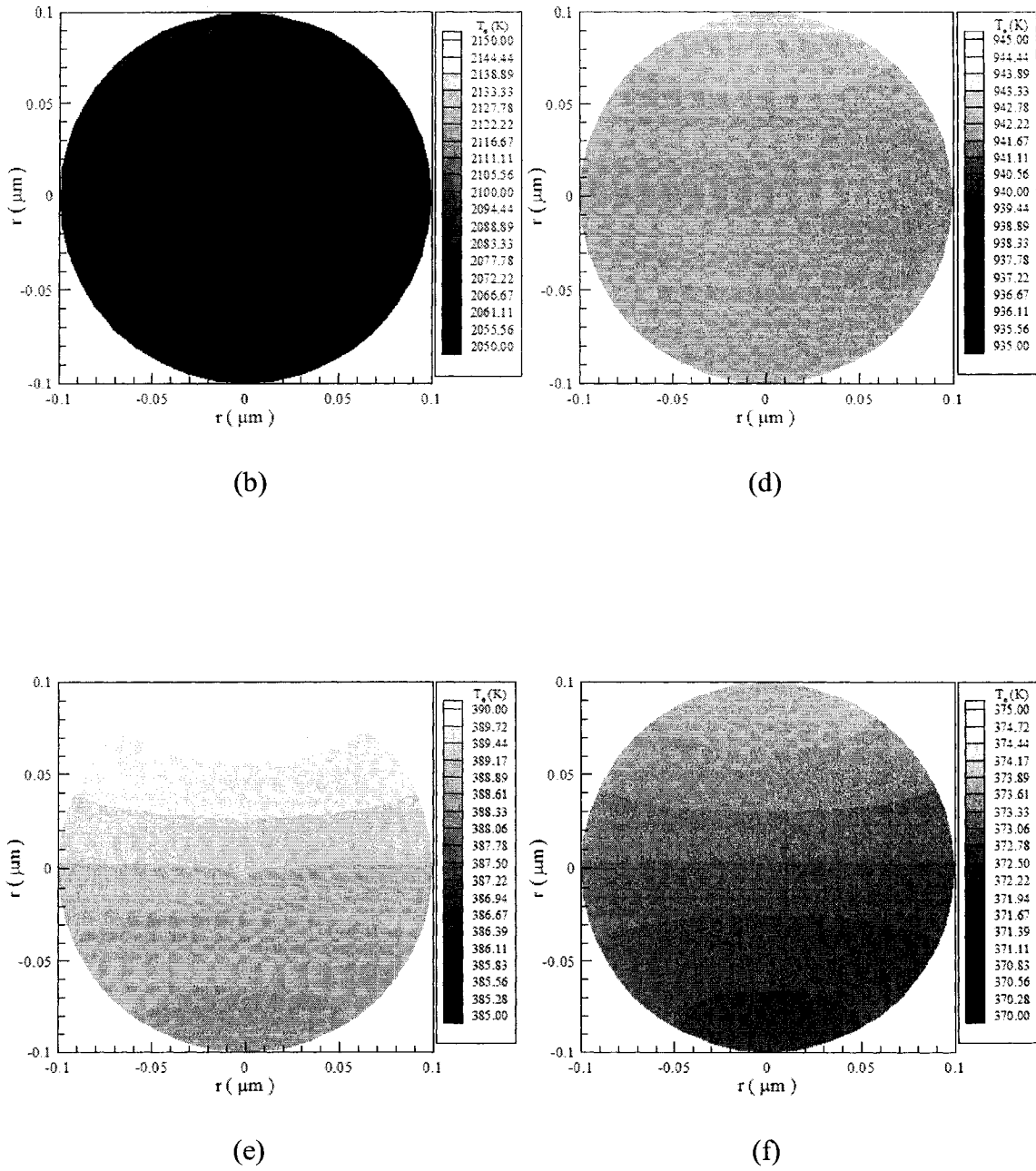
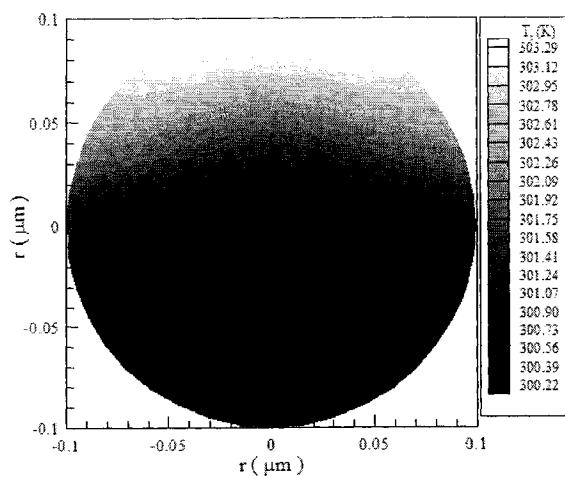
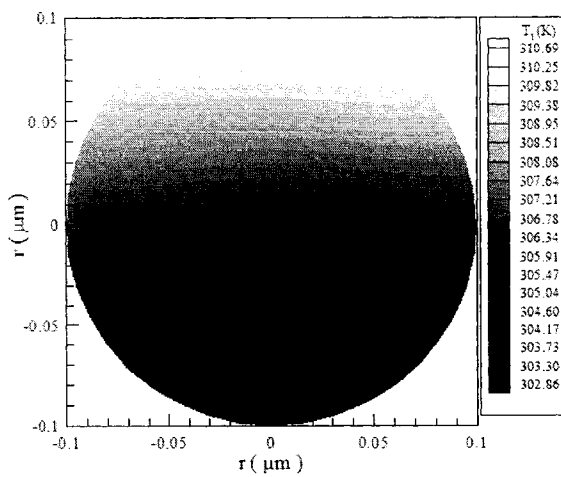


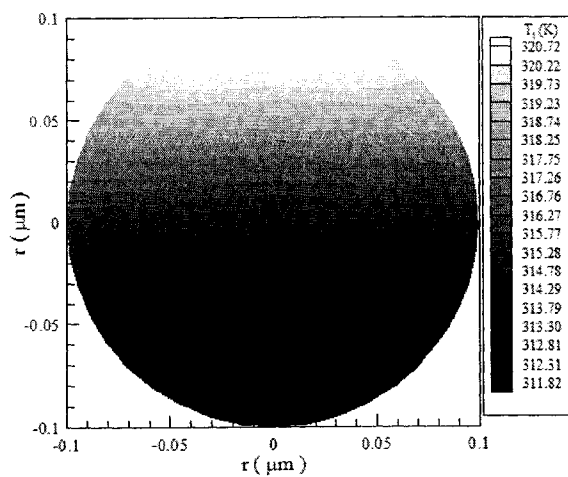
Fig. 5.34 Contours of electron temperature ( $T_e$ ) distributions in the cross section of  $\theta = 0$  and  $\theta = \pi$  at different times (a)  $t = 0.25$  ps, (b)  $t = 0.5$  ps, (c)  $t = 1$  ps, (d)  $t = 5$  ps, (e)  $t = 10$  ps, and (f)  $t = 20$  ps with a mesh of  $60 \times 20 \times 20$  and a laser fluence  $J$  of  $500 \text{ J/m}^2$ .



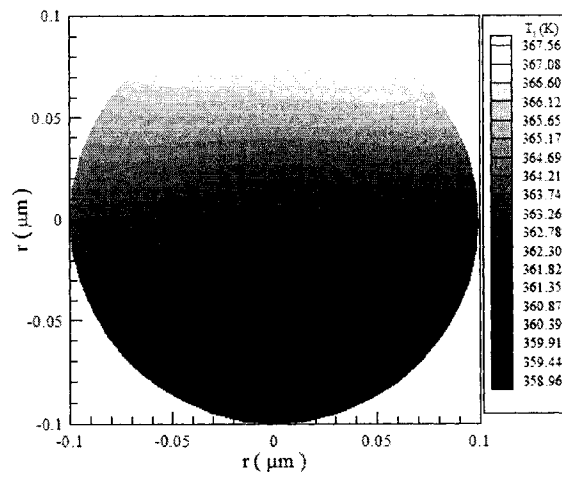
(a)



(b)



(c)



(d)

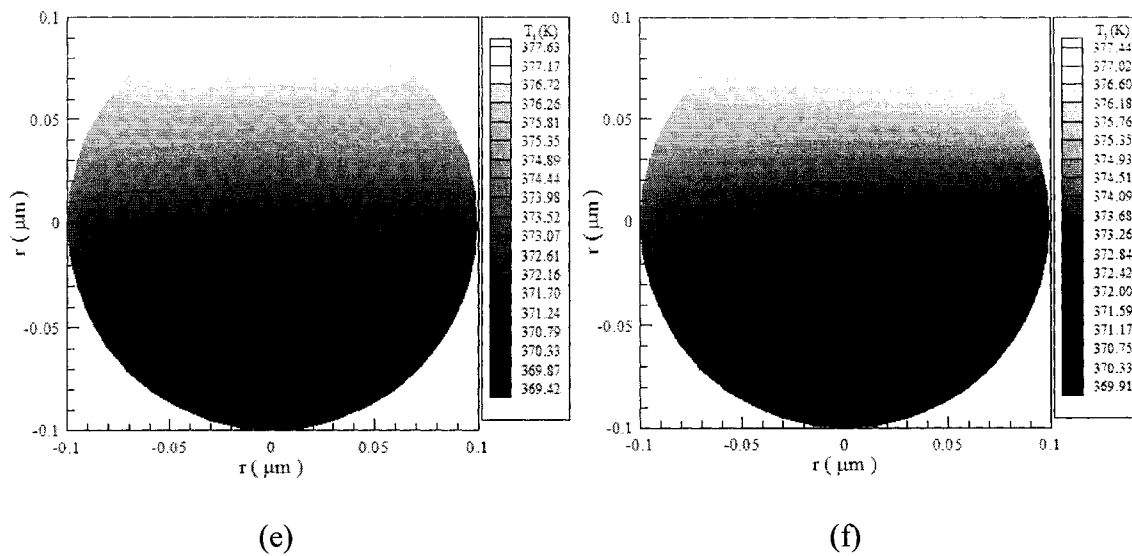


Fig. 5.35 Contours of lattice temperature ( $T_l$ ) distributions in the cross section of  $\theta = 0$  and  $\theta = \pi$  at different times (a)  $t = 0.25$  ps, (b)  $t = 0.5$  ps, (c)  $t = 1$  ps, (d)  $t = 5$  ps, (e)  $t = 10$  ps, and (f)  $t = 20$  ps with a mesh of  $60 \times 20 \times 20$  and a laser fluence  $J$  of  $500 \text{ J/m}^2$ .



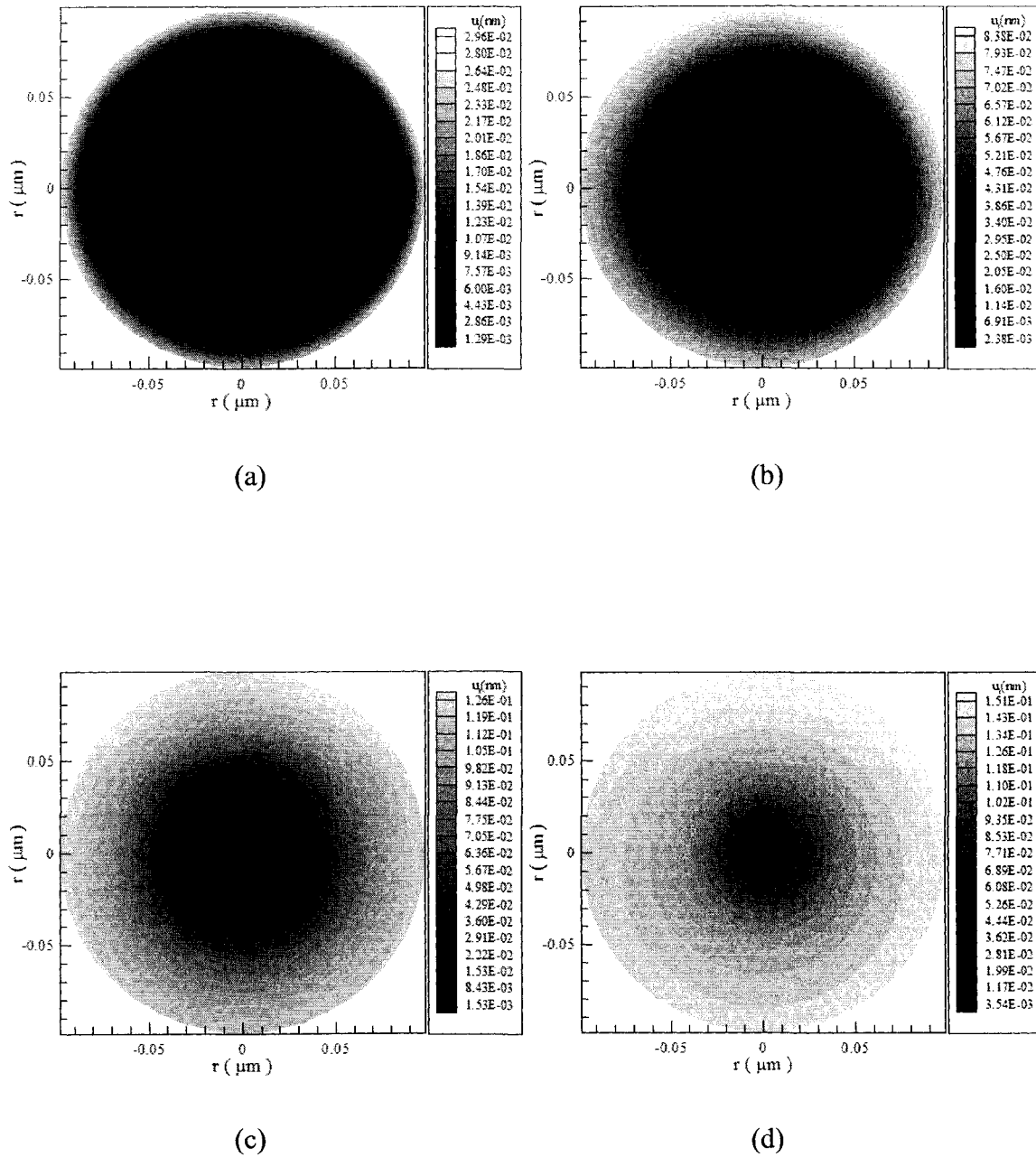


Fig. 5.36 Contours of displacement ( $u_r$ ) distributions in the cross section of  $\theta = 0$  and  $\theta = \pi$  at different times (a)  $t = 5$  ps, (b)  $t = 10$  ps, (c)  $t = 15$  ps, and (d)  $t = 20$  ps with a mesh of  $60 \times 20 \times 20$  and a laser fluence  $J$  of  $500 \text{ J/m}^2$ .

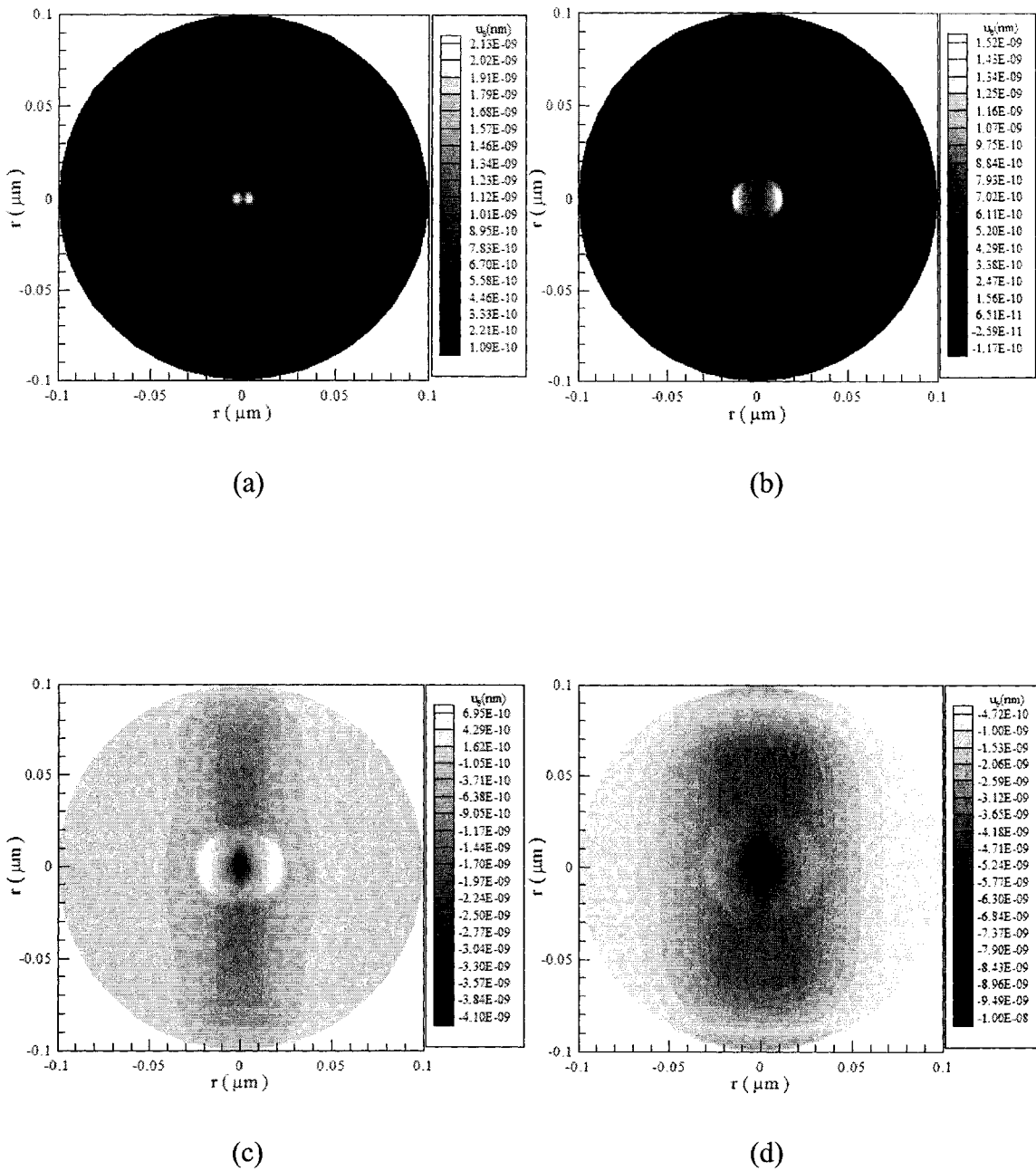


Fig. 5.37 Contours of displacement ( $u_\theta$ ) distributions in the cross section of  $\theta = 0$  and  $\theta = \pi$  at different times (a)  $t = 5$  ps, (b)  $t = 10$  ps, (c)  $t = 15$  ps, and (d)  $t = 20$  ps with a mesh of  $60 \times 20 \times 20$  and a laser fluence  $J$  of  $500 \text{ J/m}^2$ .

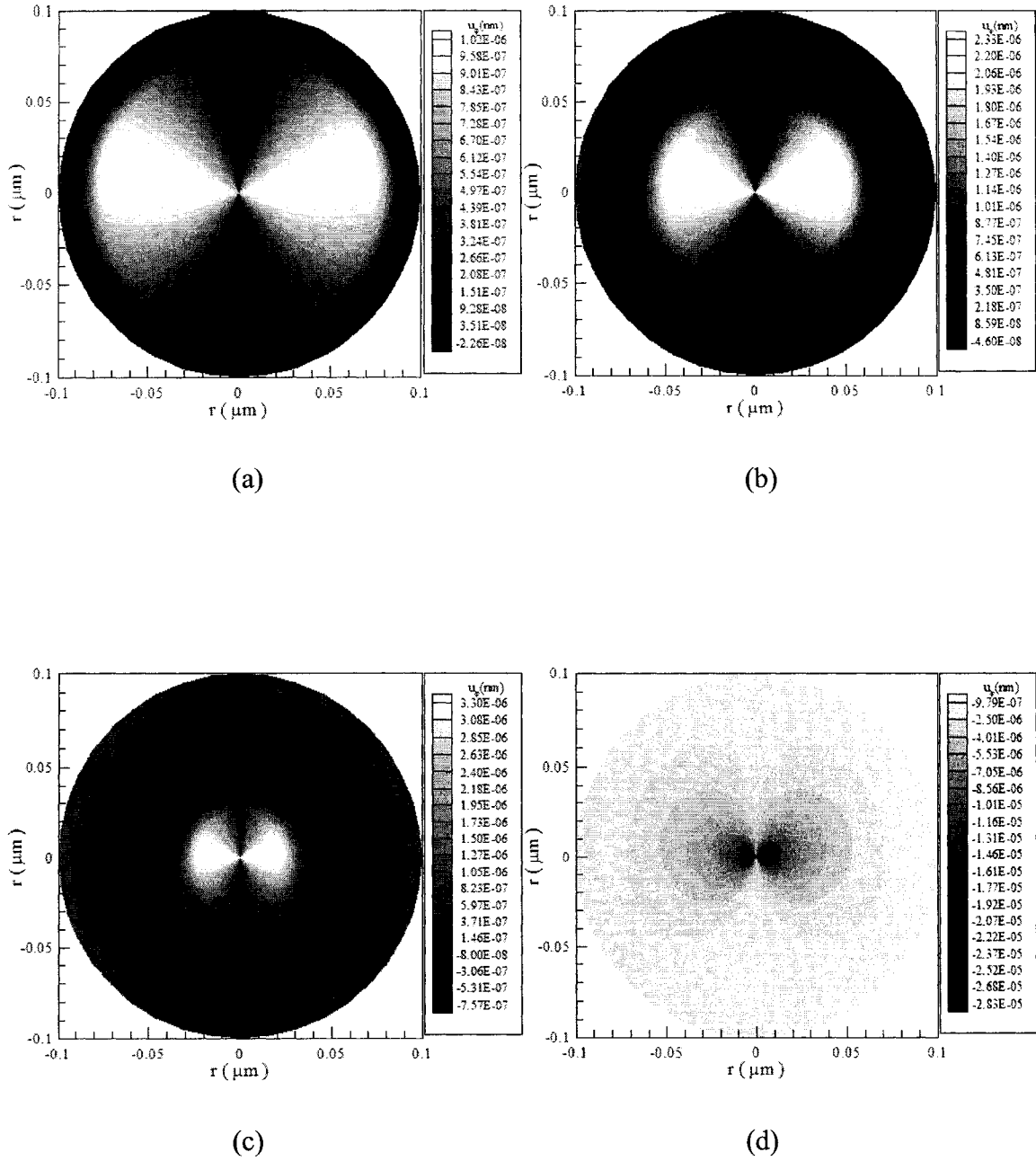


Fig. 5.38 Contours of displacement ( $u_\varphi$ ) distributions in the cross section of  $\theta = 0$  and  $\theta = \pi$  at different times (a)  $t = 5$  ps, (b)  $t = 10$  ps, (c)  $t = 15$  ps, and (d)  $t = 20$  ps with a mesh of  $60 \times 20 \times 20$  and a laser fluence  $J$  of  $500 \text{ J/m}^2$ .

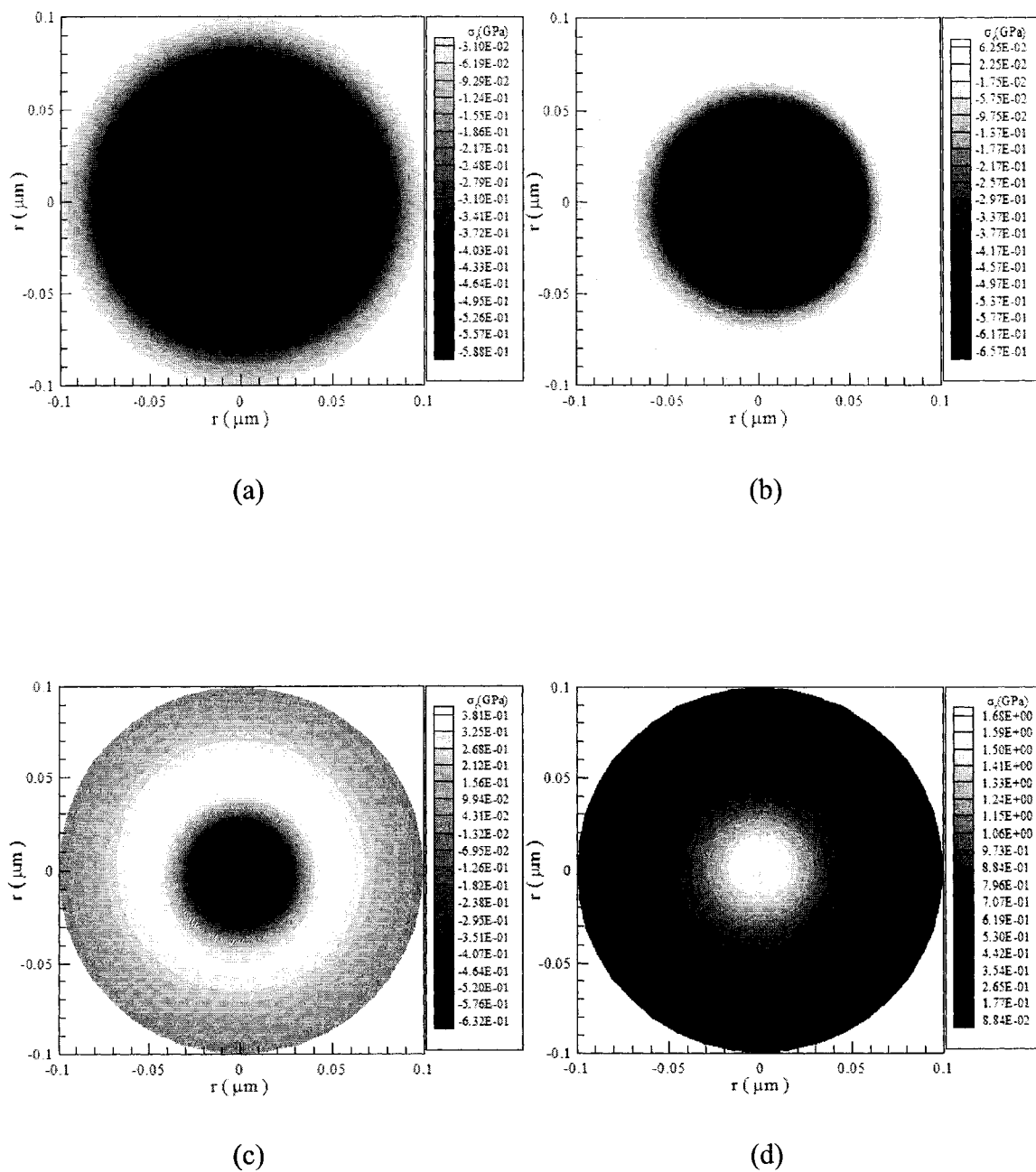


Fig. 5.39 Contours of normal stress ( $\sigma_r$ ) distributions in the cross section of  $\theta = 0$  and  $\theta = \pi$  at different times (a)  $t = 5$  ps, (b)  $t = 10$  ps, (c)  $t = 15$  ps, and (d)  $t = 20$  ps with a mesh of  $60 \times 20 \times 20$  and a laser fluence  $J$  of  $500 \text{ J/m}^2$ .

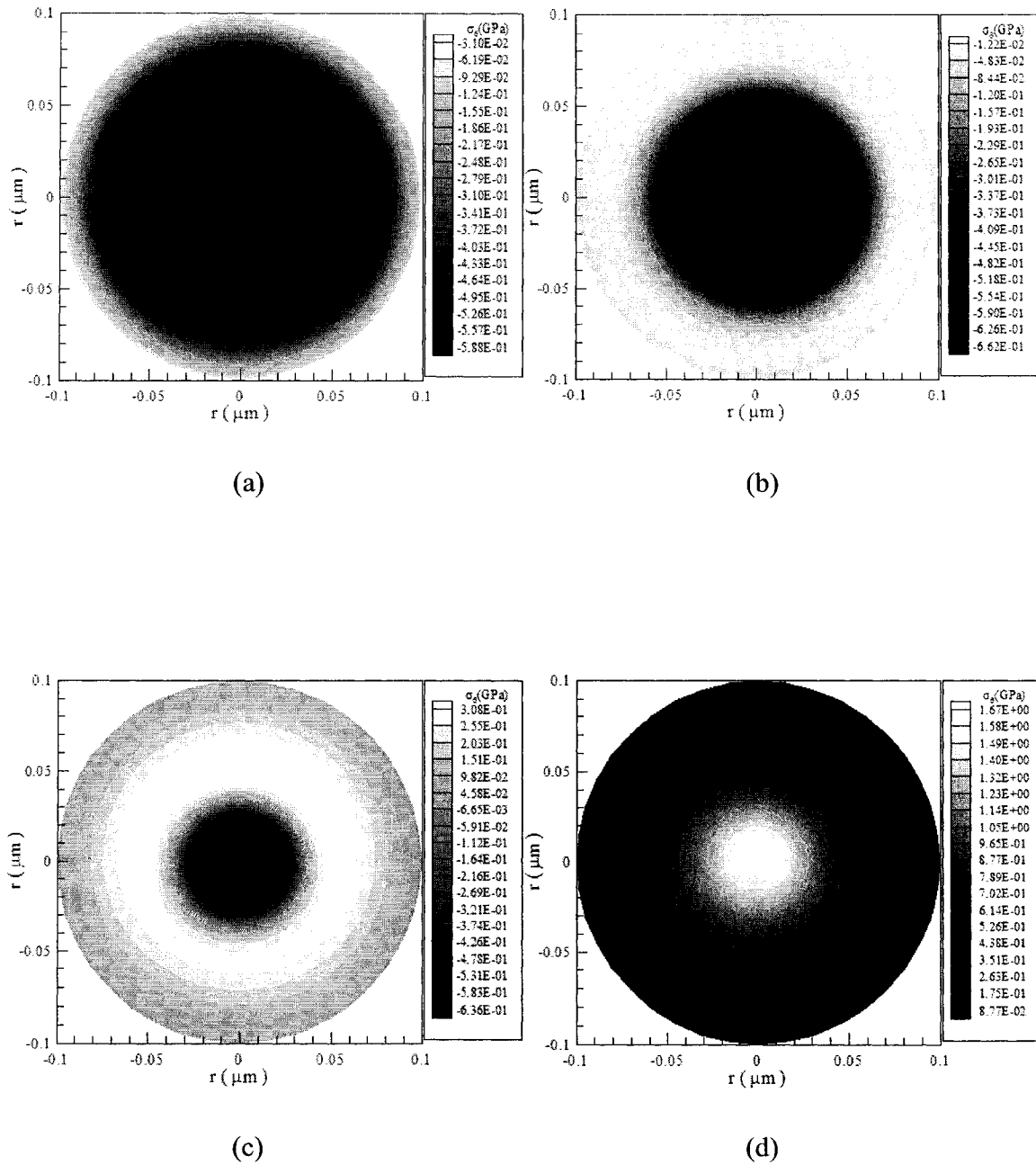


Fig. 5.40 Contours of normal stress ( $\sigma_\theta$ ) distributions in the cross section of  $\theta = 0$  and  $\theta = \pi$  at different times (a)  $t = 5$  ps, (b)  $t = 10$  ps, (c)  $t = 15$  ps, and (d)  $t = 20$  ps with a mesh of  $60 \times 20 \times 20$  and a laser fluence  $J$  of  $500 \text{ J/m}^2$ .

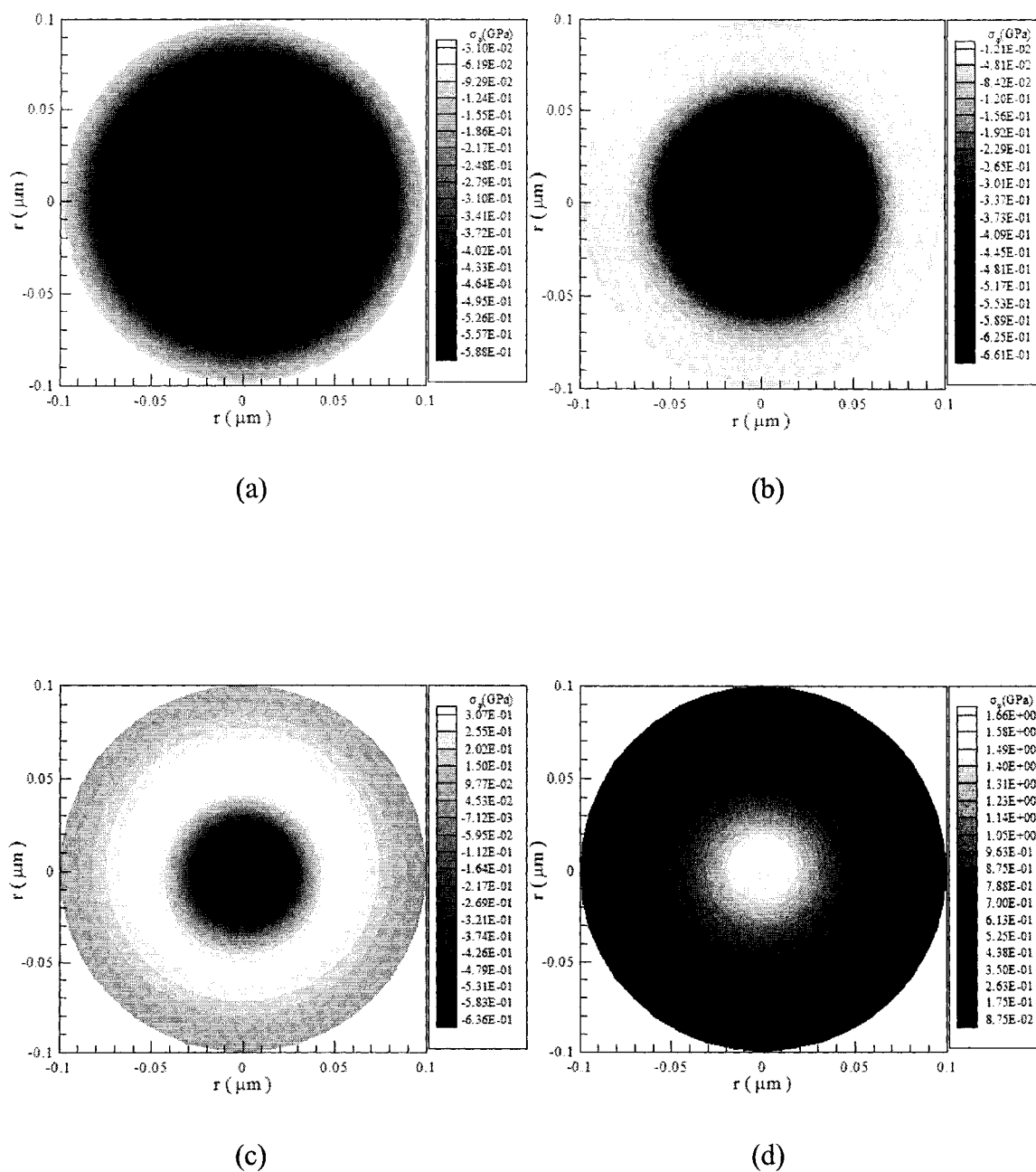


Fig. 5.41 Contours of normal stress ( $\sigma_\varphi$ ) distributions in the cross section of  $\theta = 0$  and  $\theta = \pi$  at different times (a)  $t = 5$  ps, (b)  $t = 10$  ps, (c)  $t = 15$  ps, and (d)  $t = 20$  ps with a mesh of  $60 \times 20 \times 20$  and a laser fluence  $J$  of  $500 \text{ J/m}^2$ .

### 5.2.4 Example Four

Now we change the laser from a single-pulse to double-pulse. Thus, the heat source equation becomes [Kaba 2004]

$$Q(r, \theta, \varphi, t) = 0.94J \frac{1-R}{t_p \zeta} e^{-\frac{L-r}{\zeta}} \cdot [e^{-2.77(\frac{t-2t_p}{t_p})^2} + e^{-2.77(\frac{t-4t_p}{t_p})^2}] \cos\varphi. \quad (5.1)$$

In this case, we let the double-pulse laser irradiates a top portion ( $0 \leq r \leq L$ ,  $0 \leq \theta \leq 2\pi$ ,  $0 \leq \varphi \leq \pi/2$ ).

Fig. 5.42 shows the change in electron temperature ( $\Delta T_e / (\Delta T_e)_{\max}$ ) at the point ( $r = L$ ,  $\varphi = 0$ ,  $\theta = 0$ ) for various meshes ( $60 \times 20 \times 20$ ,  $40 \times 20 \times 20$ ,  $30 \times 20 \times 40$ , and  $20 \times 30 \times 40$ ) with laser fluence  $J = 500 \text{ J/m}^2$ . It can be seen from Fig 5.42 there are two peaks in electron temperature distribution due to the repetitive pulse heating. The maximum temperature rise of  $T_e$  at the first peak is about 3931.58 K, which is almost the same with the maximum temperature in example one. And the maximum temperature rise of  $T_e$  at the second peak is about 4540.33 K, which is a little higher than that at the first peak. And Fig. 5.43 shows the displacement  $u_r$  at the point ( $r = L/2$ ,  $\varphi = 0$ ,  $\theta = 0$ ) versus time.

Fig. 5.44 shows profiles of electron temperature and lattice temperature along the diameter at  $\varphi = 0$  and  $\varphi = \pi$  with laser fluence  $J = 500 \text{ J/m}^2$  and a mesh of  $60 \times 20 \times 20$  at different times (a)  $t = 0.25 \text{ ps}$ , (b)  $t = 0.5 \text{ ps}$ , (c)  $t = 1 \text{ ps}$ , (d)  $t = 5 \text{ ps}$ , and (e)  $t = 20 \text{ ps}$ , respectively. The temperature distribution is similar to those shown in Figs. 5.4 and 5.31.

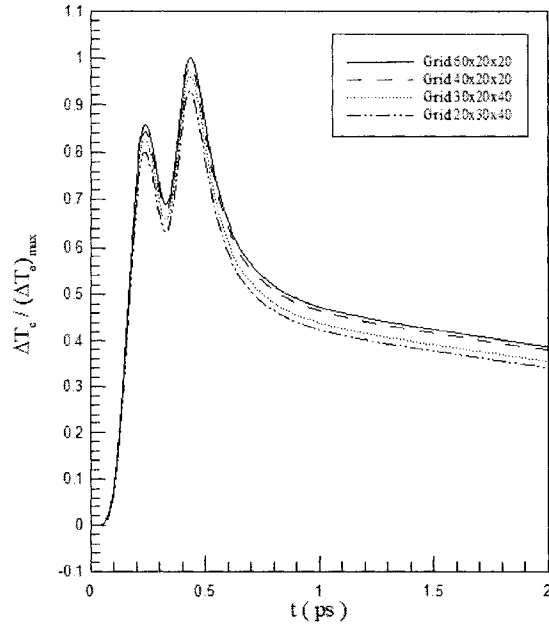


Fig. 5.42 Change in electron temperature  $T_e$  at  $r = 0.1 \mu\text{m}$ ,  $\theta = 0$ ,  $\varphi = 0$  versus time for various meshes with a laser fluence  $J$  of  $500 \text{ J/m}^2$ .

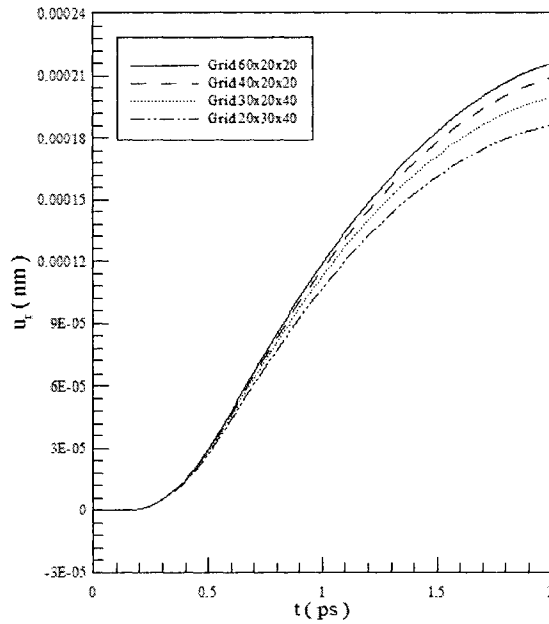
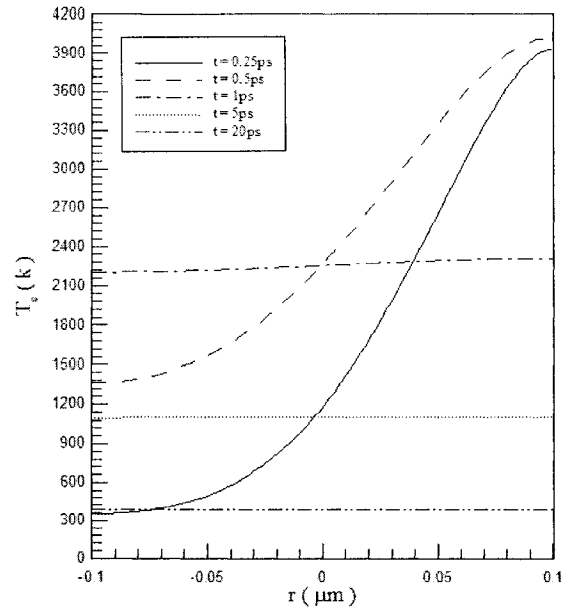
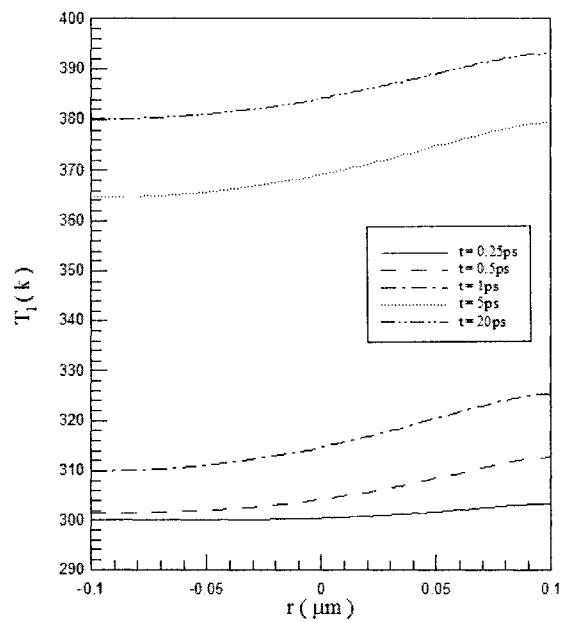


Fig. 5.43 Displacement  $u_t$  at  $r = 0.05 \mu\text{m}$ ,  $\theta = 0$ ,  $\varphi = 0$  versus time for various meshes with a laser fluence  $J$  of  $500 \text{ J/m}^2$ .





(a)



(b)

Fig. 5.44 Profiles of (a) electron temperature ( $T_e$ ), and (b) lattice temperature ( $T_l$ ) along  $r$ -axis at  $\varphi = 0$  and  $\varphi = \pi$  for various times with a laser fluence  $J$  of  $500 \text{ J/m}^2$  and a mesh of  $60 \times 20 \times 20$ .

Figs. 5.45 and 5.46 show normal stress  $\sigma_r$  and displacement  $u_r$  along the diameter at  $\varphi = 0$  and  $\varphi = \pi$  at different times (a)  $t = 5$  ps, (b)  $t = 10$  ps, (c)  $t = 15$  ps, and (d)  $t = 20$  ps with a mesh of  $60 \times 20 \times 20$  and three different laser fluences ( $J = 500 \text{ J/m}^2$ ,  $1,000 \text{ J/m}^2$ ,  $2,000 \text{ J/m}^2$ ). It can be seen from these figures that the heat is transferred from top to bottom along the  $r$  direction which is similar to those in examples one and three. And from Fig. 5.45 it can be seen that it does not show any non-physical oscillation.

Figs. 5.47–5.54 were plotted based on the results obtained in a mesh of  $60 \times 20 \times 20$  with a laser fluence  $J = 500 \text{ J/m}^2$ . Figs. 5.47 and 5.48 show contours of electron temperature distributions and lattice temperature distributions in the cross section of  $\theta = 0$  and  $\theta = \pi$  at different times (a)  $t = 0.25$  ps, (b)  $t = 0.5$  ps, (c)  $t = 1$  ps, (d)  $t = 5$  ps, (e)  $t = 10$  ps, and (f)  $t = 20$  ps, respectively. It can be seen from both figures that the heat is mainly transferred from top to bottom along  $r$  direction. Figs. 5.49–5.54 show contours of displacement ( $u_r, u_\theta, u_\varphi$ ) and normal stress ( $\sigma_r, \sigma_\theta, \sigma_\varphi$ ) in the cross section of  $\theta = 0$  and  $\theta = \pi$  at different times (a)  $t = 5$  ps, (b)  $t = 10$  ps, (c)  $t = 15$  ps, and (d)  $t = 20$  ps, respectively.

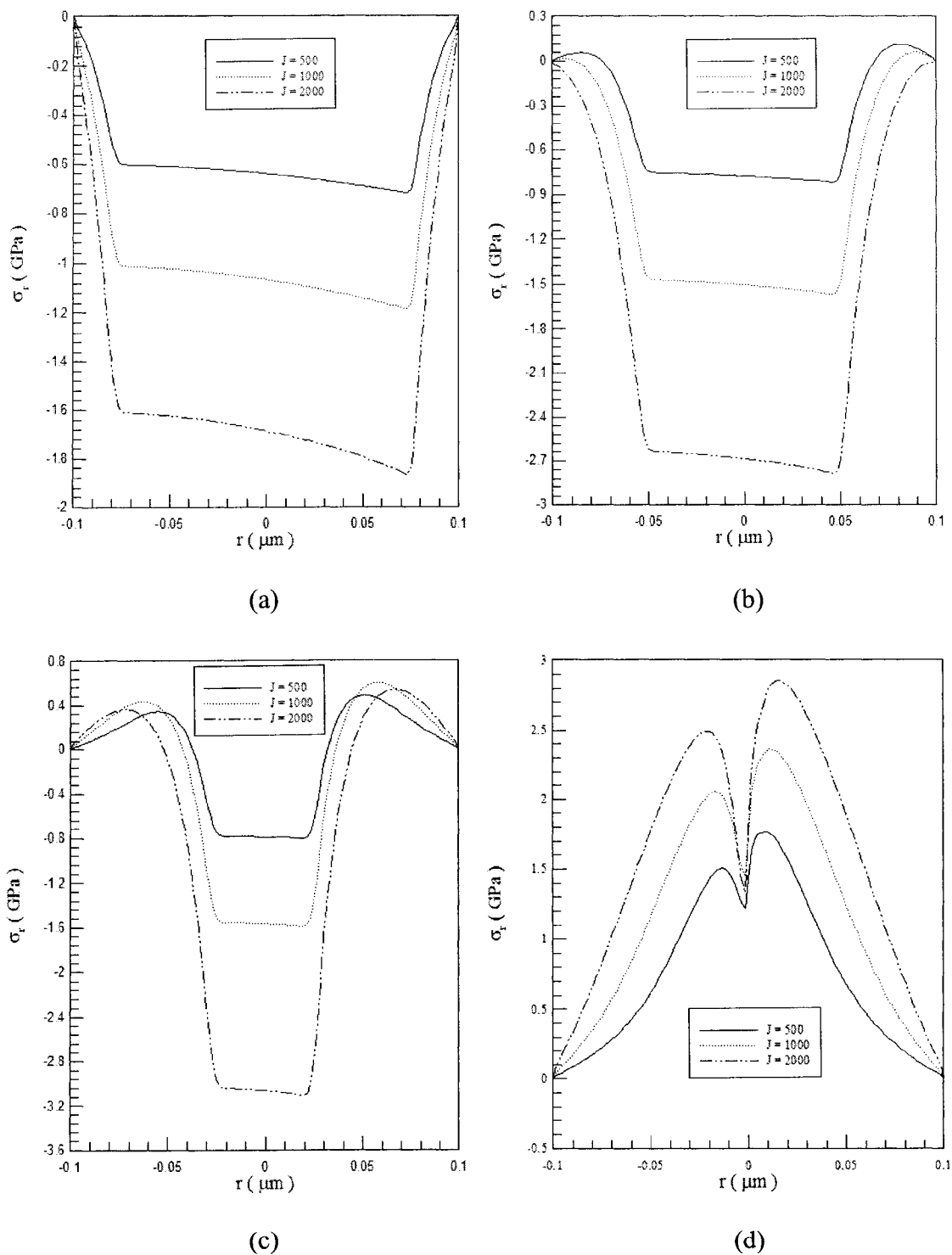


Fig. 5.45 Normal stress ( $\sigma_r$ ) along the diameter at  $\varphi = 0$  and  $\varphi = \pi$  at different times (a)  $t = 5$  ps, (b)  $t = 10$  ps, (c)  $t = 15$  ps, and (d)  $t = 20$  ps with three different laser fluences and a mesh of  $60 \times 20 \times 20$ .

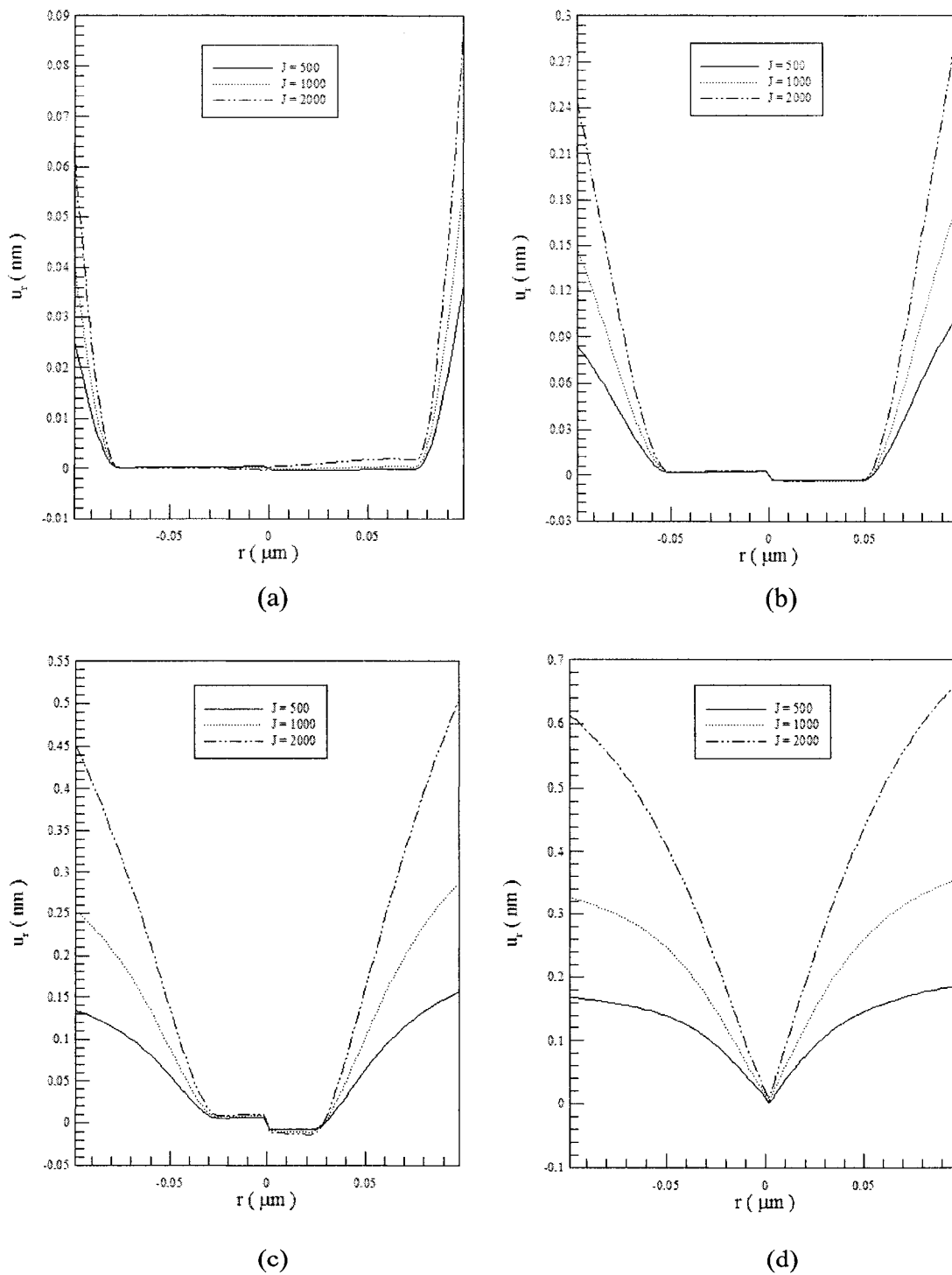
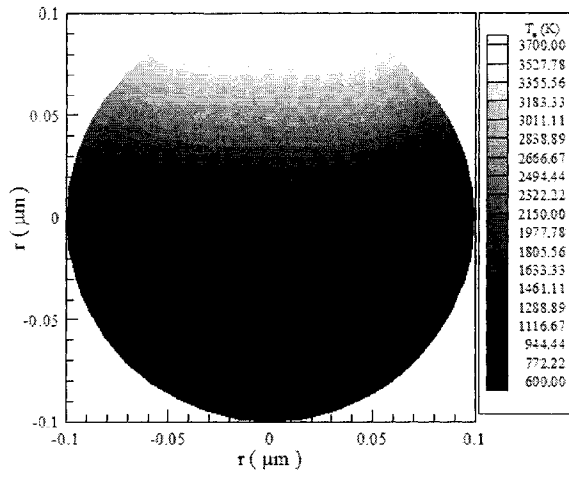
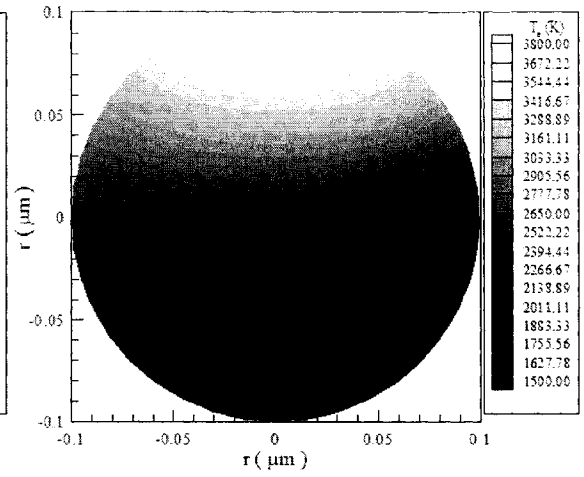


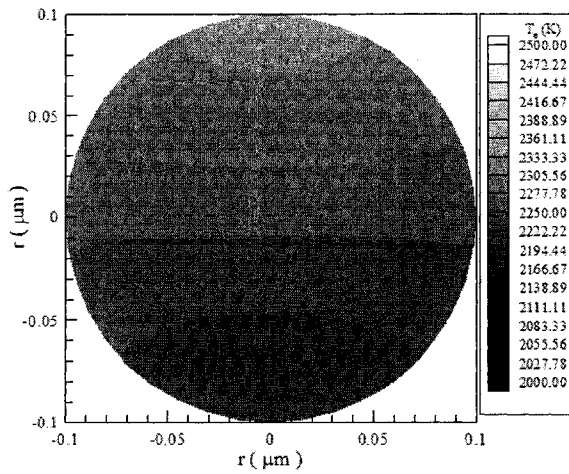
Fig. 5.46 Displacement ( $u_r$ ) along the diameter at  $\varphi = 0$  and  $\varphi = \pi$  at different times (a)  $t = 5$  ps, (b)  $t = 10$  ps, (c)  $t = 15$  ps, and (d)  $t = 20$  ps with three different laser fluences and a mesh of  $60 \times 20 \times 20$ .



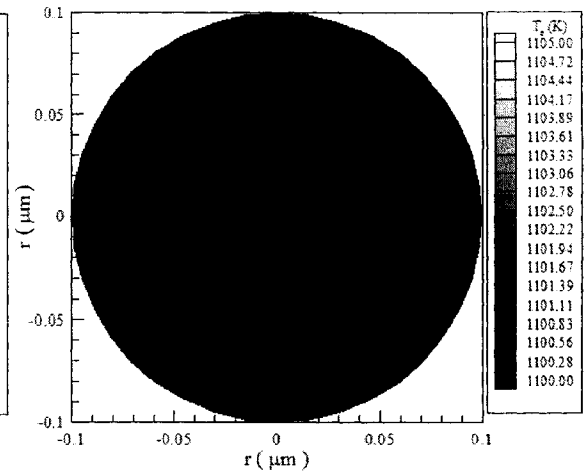
(a)



(b)



(c)



(d)

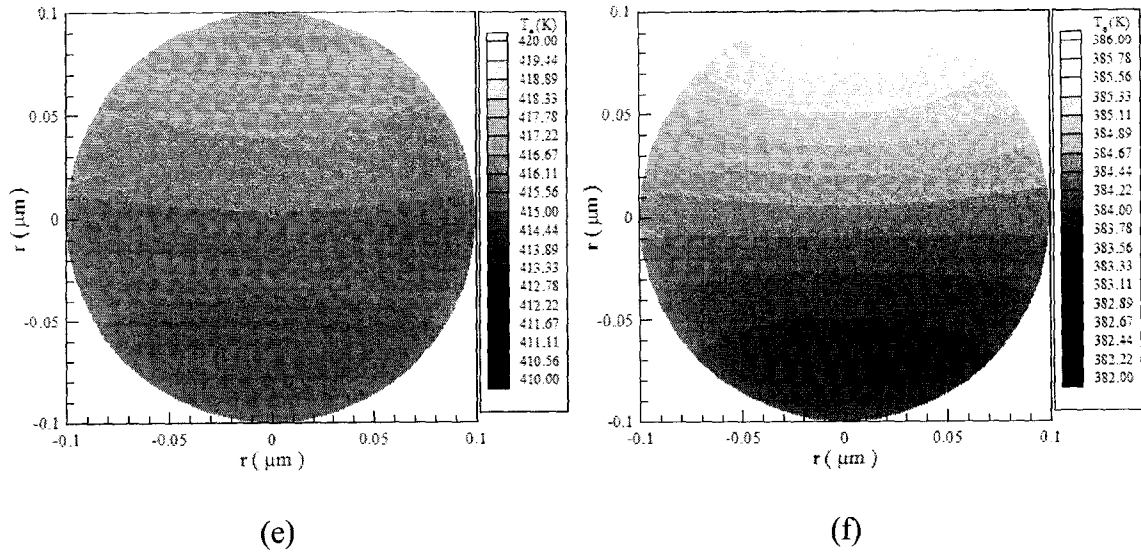
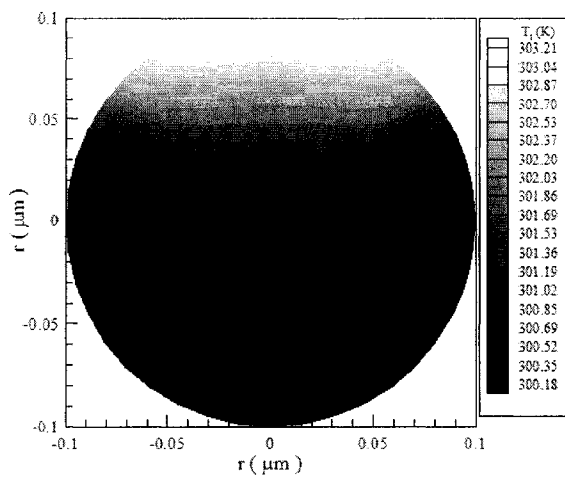
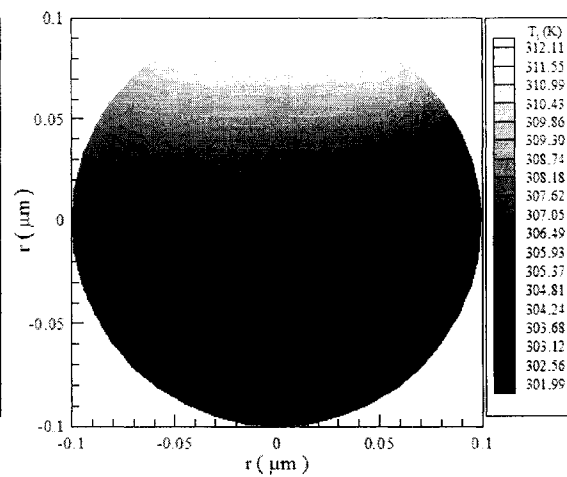


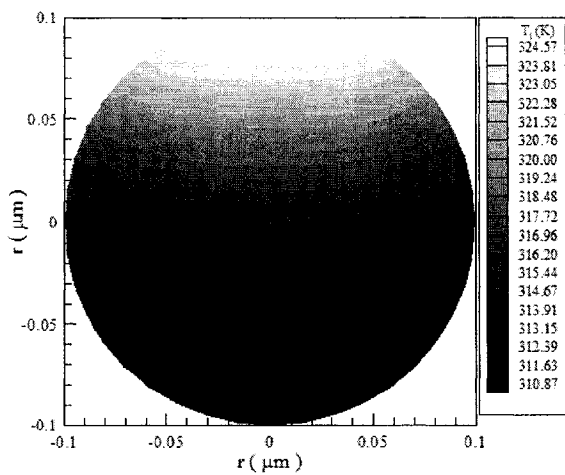
Fig. 5.47 Contours of electron temperature ( $T_e$ ) distributions in the cross section of  $\theta = 0$  and  $\theta = \pi$  at different times (a)  $t = 0.25$  ps, (b)  $t = 0.5$  ps, (c)  $t = 1$  ps, (d)  $t = 5$  ps, (e)  $t = 10$  ps, and (f)  $t = 20$  ps with a mesh of  $60 \times 20 \times 20$  and a laser fluence  $J$  of  $500 \text{ J/m}^2$ .



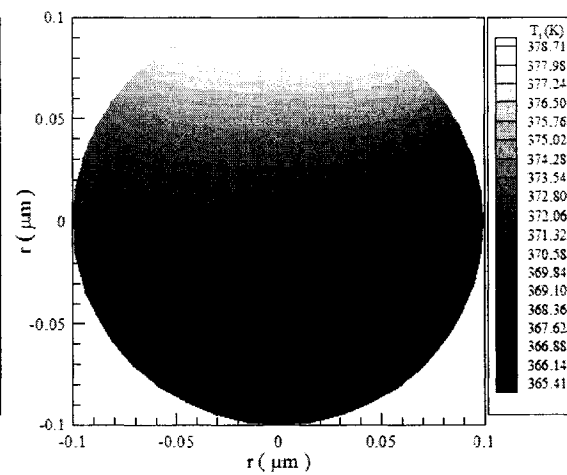
(a)



(b)



(c)



(d)

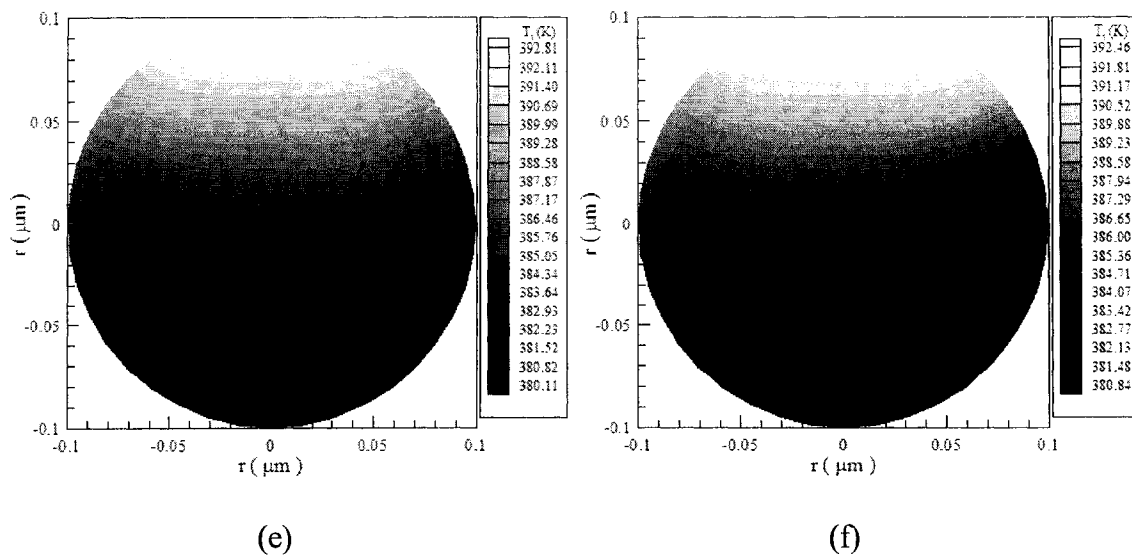


Fig. 5.48 Contours of lattice temperature ( $T_1$ ) distributions in the cross section of  $\theta = 0$  and  $\theta = \pi$  at different times (a)  $t = 0.25$  ps, (b)  $t = 0.5$  ps, (c)  $t = 1$  ps, (d)  $t = 5$  ps, (e)  $t = 10$  ps, and (f)  $t = 20$  ps with a mesh of  $60 \times 20 \times 20$  and a laser fluence  $J$  of  $500 \text{ J/m}^2$ .



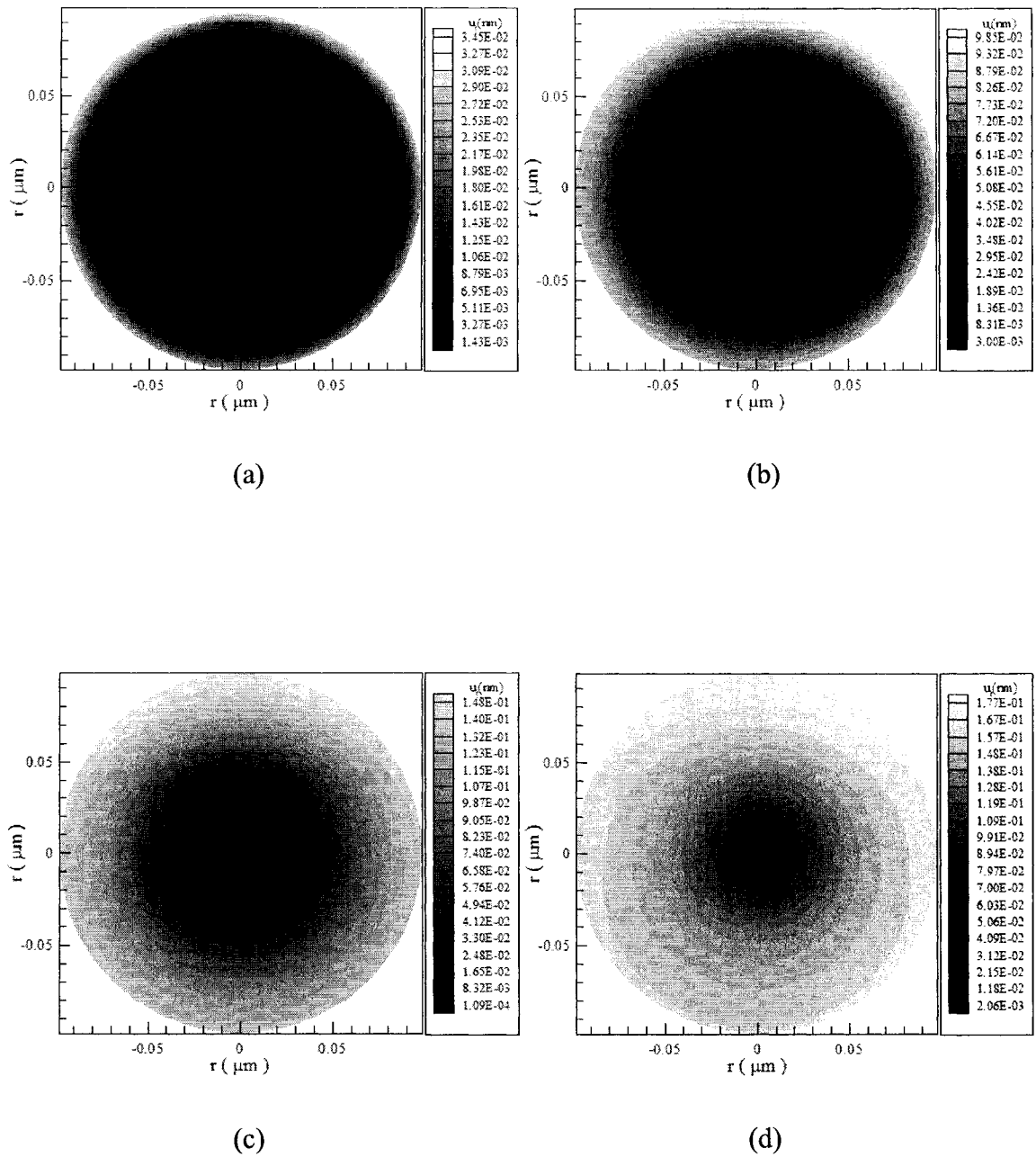


Fig. 5.49 Contours of displacement ( $u_r$ ) distributions in the cross section of  $\theta = 0$  and  $\theta = \pi$  at different times (a)  $t = 5$  ps, (b)  $t = 10$  ps, (c)  $t = 15$  ps, and (d)  $t = 20$  ps with a mesh of  $60 \times 20 \times 20$  and a laser fluence  $J$  of  $500 \text{ J/m}^2$ .

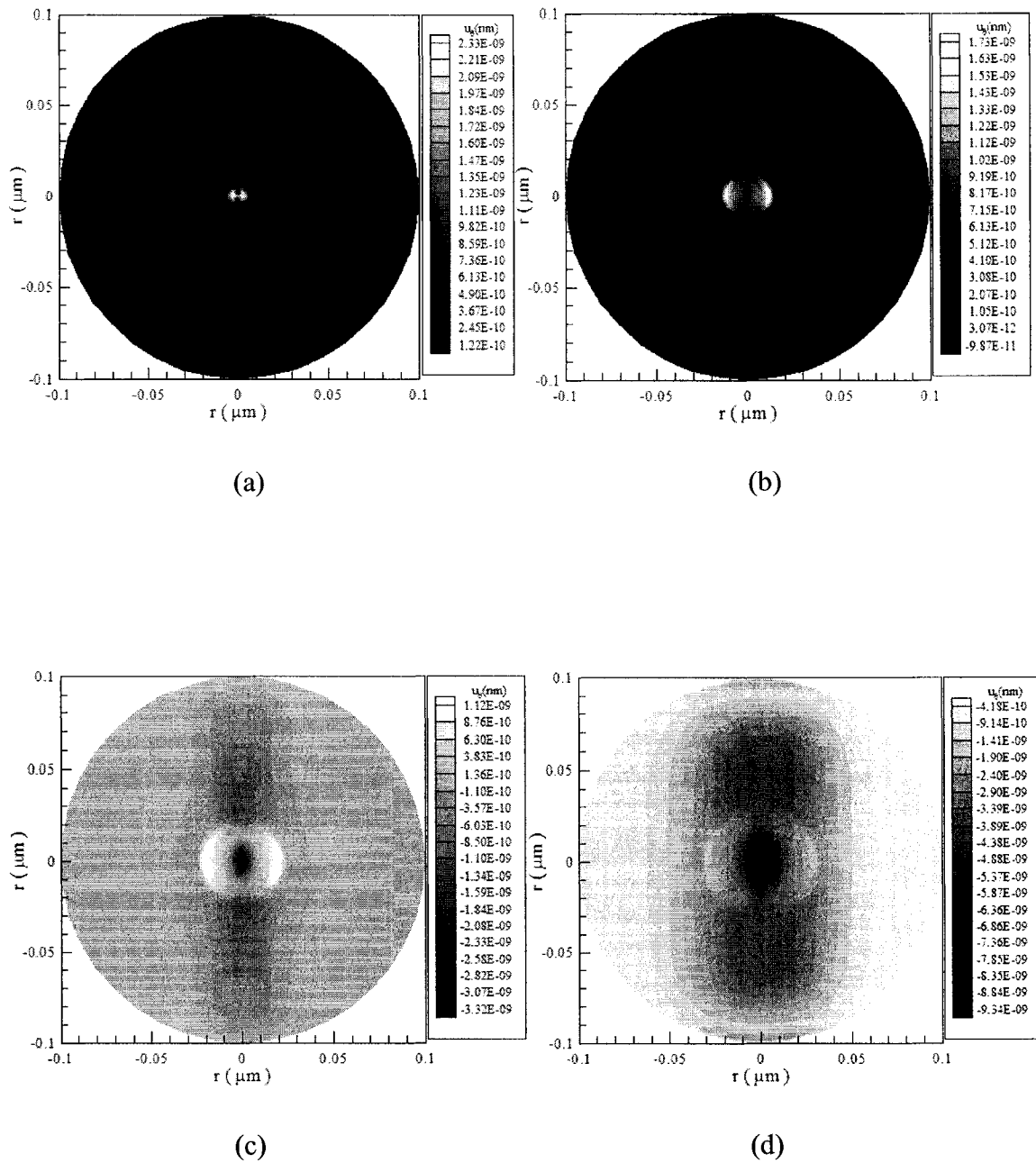


Fig. 5.50 Contours of displacement ( $u_\theta$ ) distributions in the cross section of  $\theta = 0$  and  $\theta = \pi$  at different times (a)  $t = 5$  ps, (b)  $t = 10$  ps, (c)  $t = 15$  ps, and (d)  $t = 20$  ps with a mesh of  $60 \times 20 \times 20$  and a laser fluence  $J$  of  $500 \text{ J/m}^2$ .

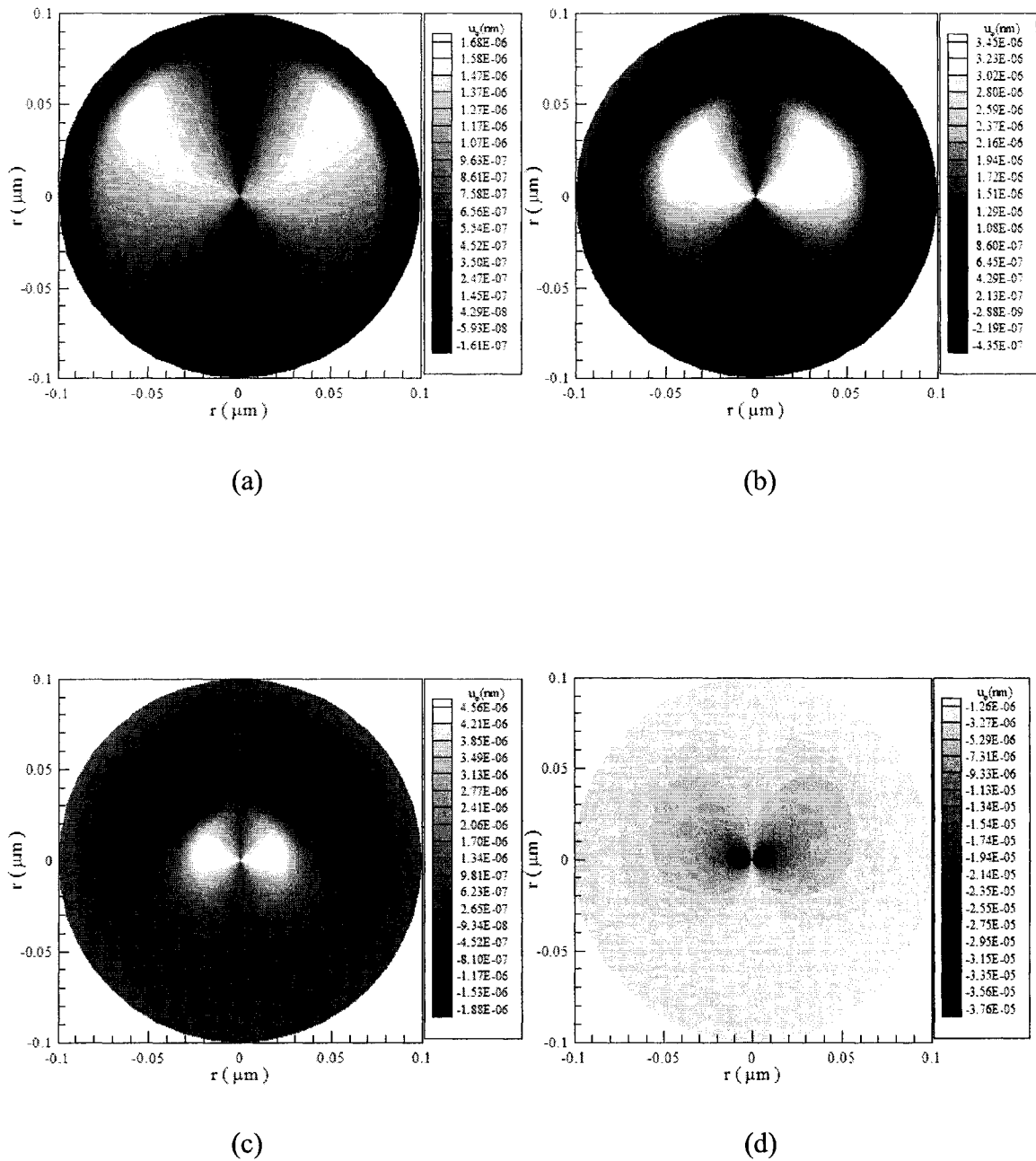


Fig. 5.51 Contours of displacement ( $u_\varphi$ ) distributions in the cross section of  $\theta = 0$  and  $\theta = \pi$  at different times (a)  $t = 5$  ps, (b)  $t = 10$  ps, (c)  $t = 15$  ps, and (d)  $t = 20$  ps with a mesh of  $60 \times 20 \times 20$  and a laser fluence  $J$  of  $500 \text{ J/m}^2$ .

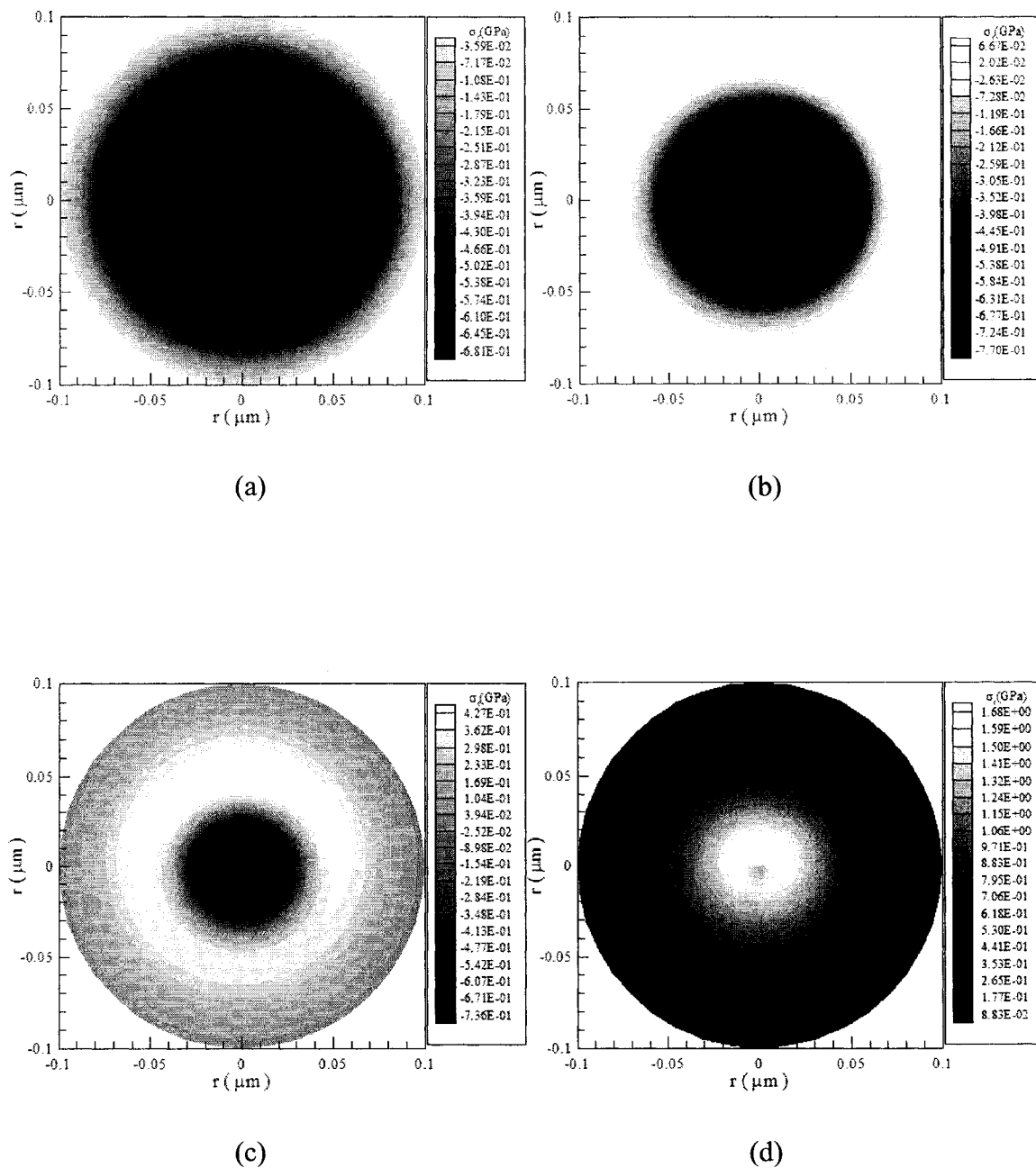


Fig. 5.52 Contours of normal stress ( $\sigma_r$ ) distributions in the cross section of  $\theta = 0$  and  $\theta = \pi$  at different times (a)  $t = 5$  ps, (b)  $t = 10$  ps, (c)  $t = 15$  ps, and (d)  $t = 20$  ps with a mesh of  $60 \times 20 \times 20$  and a laser fluence  $J$  of  $500 \text{ J/m}^2$ .

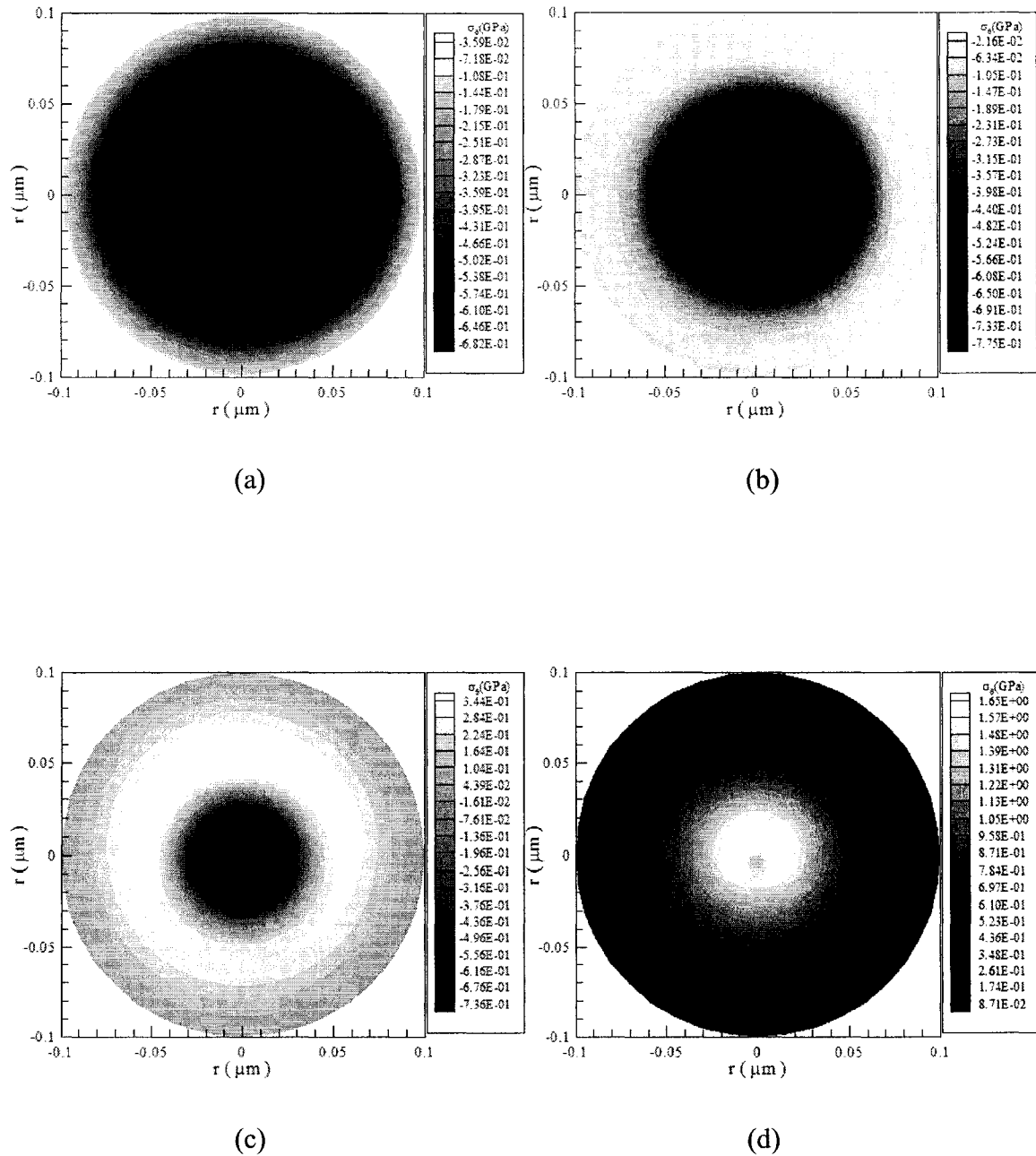


Fig. 5.53 Contours of normal stress ( $\sigma_\theta$ ) distributions in the cross section of  $\theta = 0$  and  $\theta = \pi$  at different times (a)  $t = 5$  ps, (b)  $t = 10$  ps, (c)  $t = 15$  ps, and (d)  $t = 20$  ps with a mesh of  $60 \times 20 \times 20$  and a laser fluence  $J$  of  $500 \text{ J/m}^2$ .

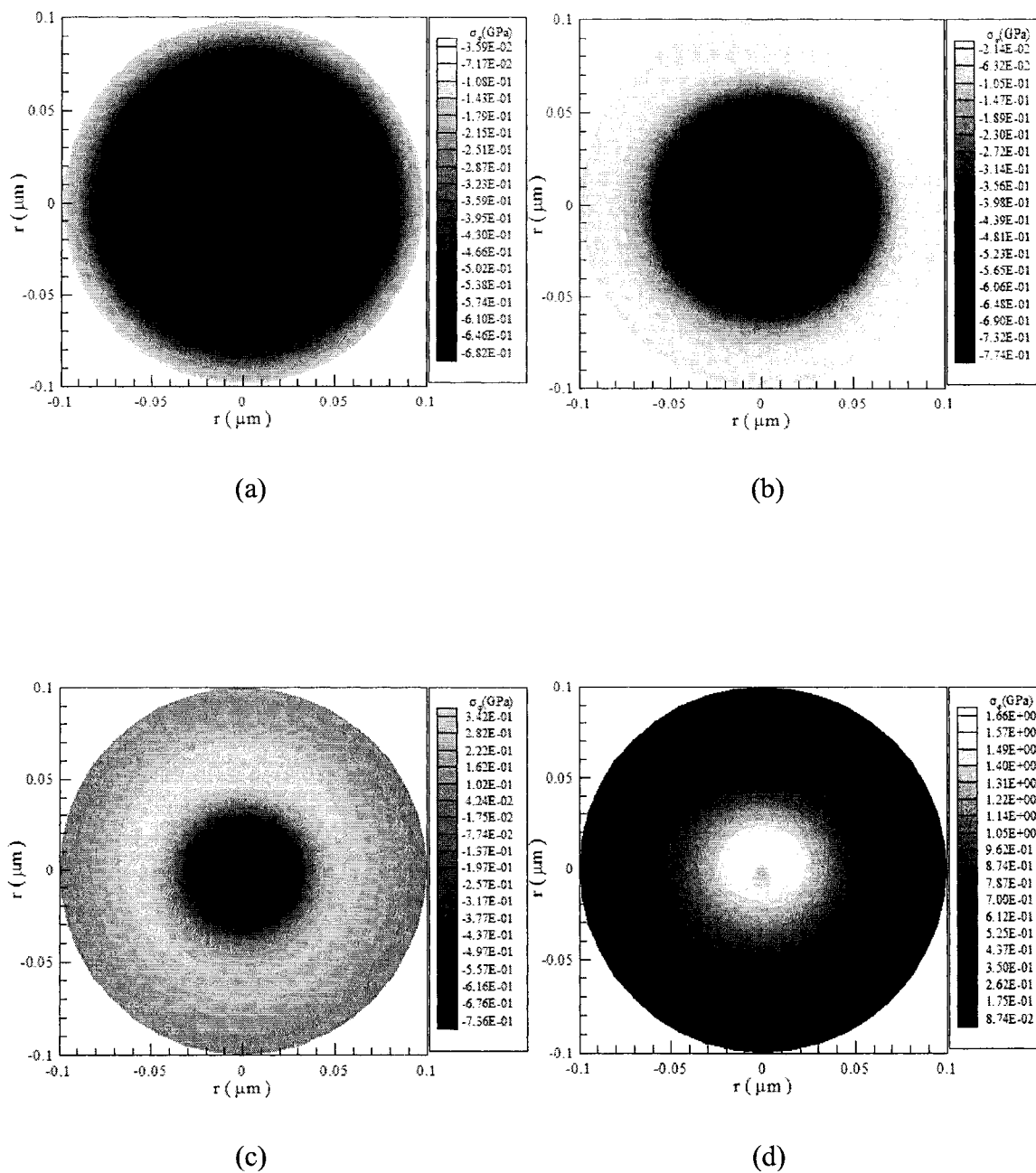


Fig. 5.54 Contours of normal stress ( $\sigma_r$ ) distributions in the cross section of  $\theta = 0$  and  $\theta = \pi$  at different times (a)  $t = 5$  ps, (b)  $t = 10$  ps, (c)  $t = 15$  ps, and (d)  $t = 20$  ps with a mesh of  $60 \times 20 \times 20$  and a laser fluence  $J$  of  $500 \text{ J/m}^2$ .

### 5.2.5 Example Five

Finally, we will study the case that the laser with double-pulse irradiates both the top portion ( $0 \leq r \leq L$ ,  $0 \leq \theta \leq 2\pi$ ,  $0 \leq \varphi \leq \pi/4$ ) and the bottom portion ( $0 \leq r \leq L$ ,  $0 \leq \theta \leq 2\pi$ ,  $3\pi/4 \leq \varphi \leq \pi$ ).

Fig. 5.55 shows the change in electron temperature ( $\Delta T_e / (\Delta T_e)_{\max}$ ) at the point ( $r = L$ ,  $\varphi = 0$ ,  $\theta = 0$ ) for various meshes ( $60 \times 20 \times 20$ ,  $40 \times 20 \times 20$ ,  $30 \times 20 \times 40$ , and  $20 \times 30 \times 40$ ) with laser fluence  $J = 500 \text{ J/m}^2$ . The result is similar to that in Fig. 5.42 except that the temperature is higher. The maximum temperature rise of  $T_e$  at the first peak is about 3935.41 K, which is very close to the maximum temperature in example two. And the maximum temperature rise of  $T_e$  at the second peak is about 4680.57 K, which is higher than that at the first peak. And Fig. 5.56 shows the displacement  $u_r$  at the point ( $r = L/2$ ,  $\varphi = 0$ ,  $\theta = 0$ ) versus time.

Fig. 5.57 shows profiles of electron temperature and lattice temperature along the diameter at  $\varphi = 0$  and  $\varphi = \pi$  with laser fluence  $J = 500 \text{ J/m}^2$  and a mesh of  $60 \times 20 \times 20$  at different times (a)  $t = 0.25 \text{ ps}$ , (b)  $t = 0.5 \text{ ps}$ , (c)  $t = 1 \text{ ps}$ , (d)  $t = 5 \text{ ps}$ , and (e)  $t = 20 \text{ ps}$ , respectively. Figs. 5.58 and 5.59 show normal stress  $\sigma_r$  and displacement  $u_r$  along the diameter at  $\varphi = 0$  and  $\varphi = \pi$  at different times (a)  $t = 5 \text{ ps}$ , (b)  $t = 10 \text{ ps}$ , (c)  $t = 15 \text{ ps}$ , and (d)  $t = 20 \text{ ps}$  with a mesh of  $60 \times 20 \times 20$  and three different laser fluences ( $J = 500 \text{ J/m}^2$ ,  $1,000 \text{ J/m}^2$ ,  $2,000 \text{ J/m}^2$ ). It can be seen from these figures that all profiles are symmetric with respect to the center point which is similar to those in example two. And there is no numerical oscillations appear in the normal stress  $\sigma_r$ .

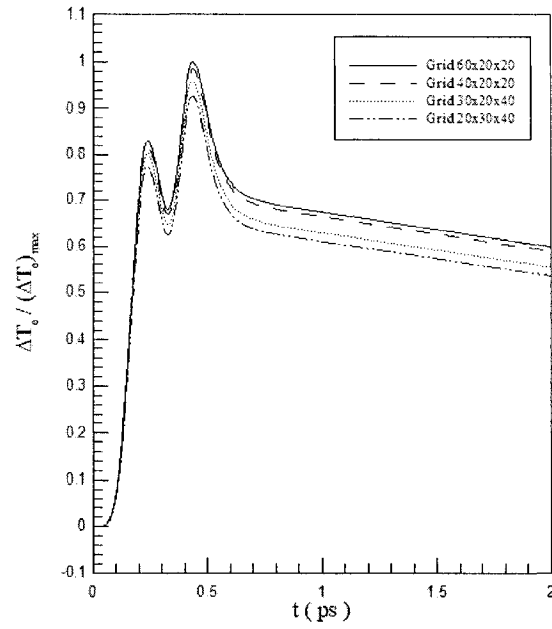


Fig. 5.55 Change in electron temperature  $T_e$  at  $r = 0.1 \mu\text{m}$ ,  $\theta = 0$ ,  $\varphi = 0$  versus time for various meshes with a laser fluence  $J$  of  $500 \text{ J/m}^2$ .

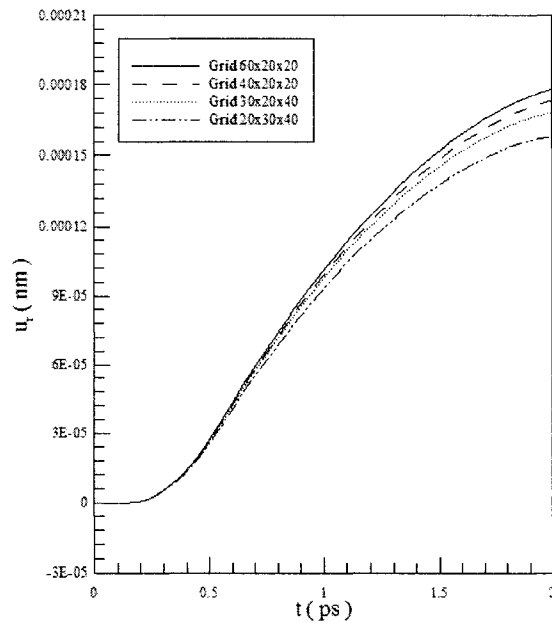
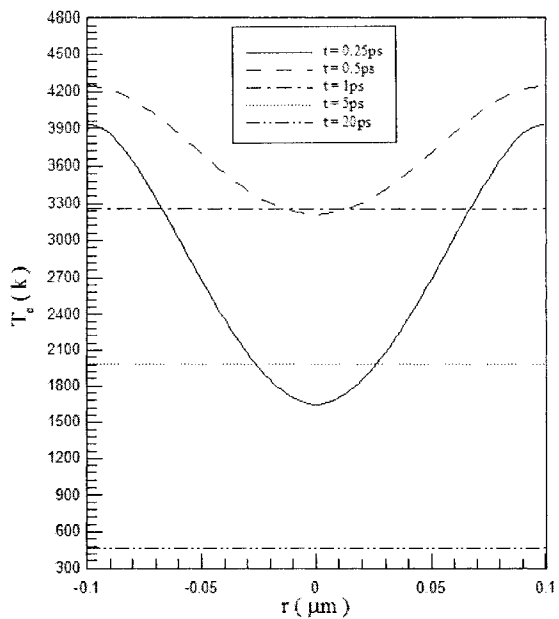
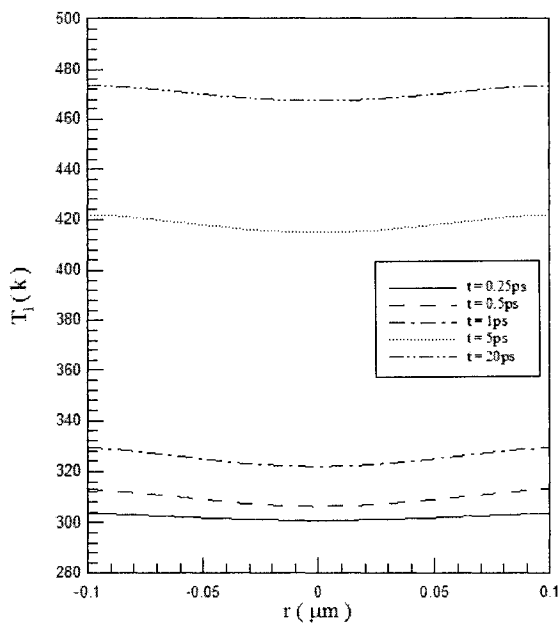


Fig. 5.56 Displacement  $u_r$  at  $r = 0.05 \mu\text{m}$ ,  $\theta = 0$ ,  $\varphi = 0$  versus time for various meshes with a laser fluence  $J$  of  $500 \text{ J/m}^2$ .





(a)



(b)

Fig. 5.57 Profiles of (a) electron temperature ( $T_e$ ), and (b) lattice temperature ( $T_l$ ) along  $r$ -axis at  $\varphi = 0$  and  $\varphi = \pi$  for various times with a laser fluence  $J$  of  $500 \text{ J/m}^2$  and a mesh of  $60 \times 20 \times 20$ .

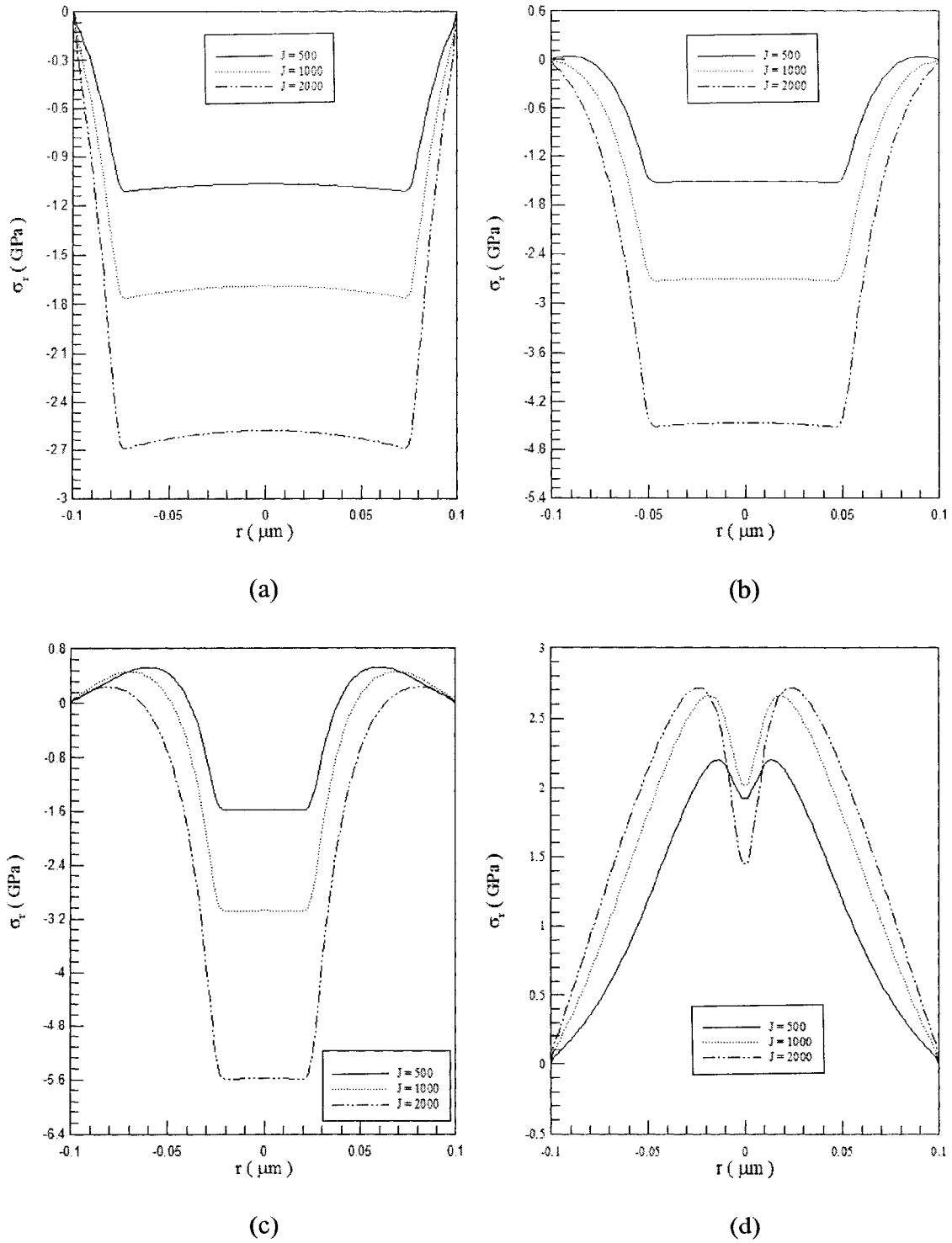


Fig. 5.58 Normal stress ( $\sigma_r$ ) along the diameter at  $\varphi = 0$  and  $\varphi = \pi$  at different times (a)  $t = 5$  ps, (b)  $t = 10$  ps, (c)  $t = 15$  ps, and (d)  $t = 20$  ps with three different laser fluences and a mesh of  $60 \times 20 \times 20$ .

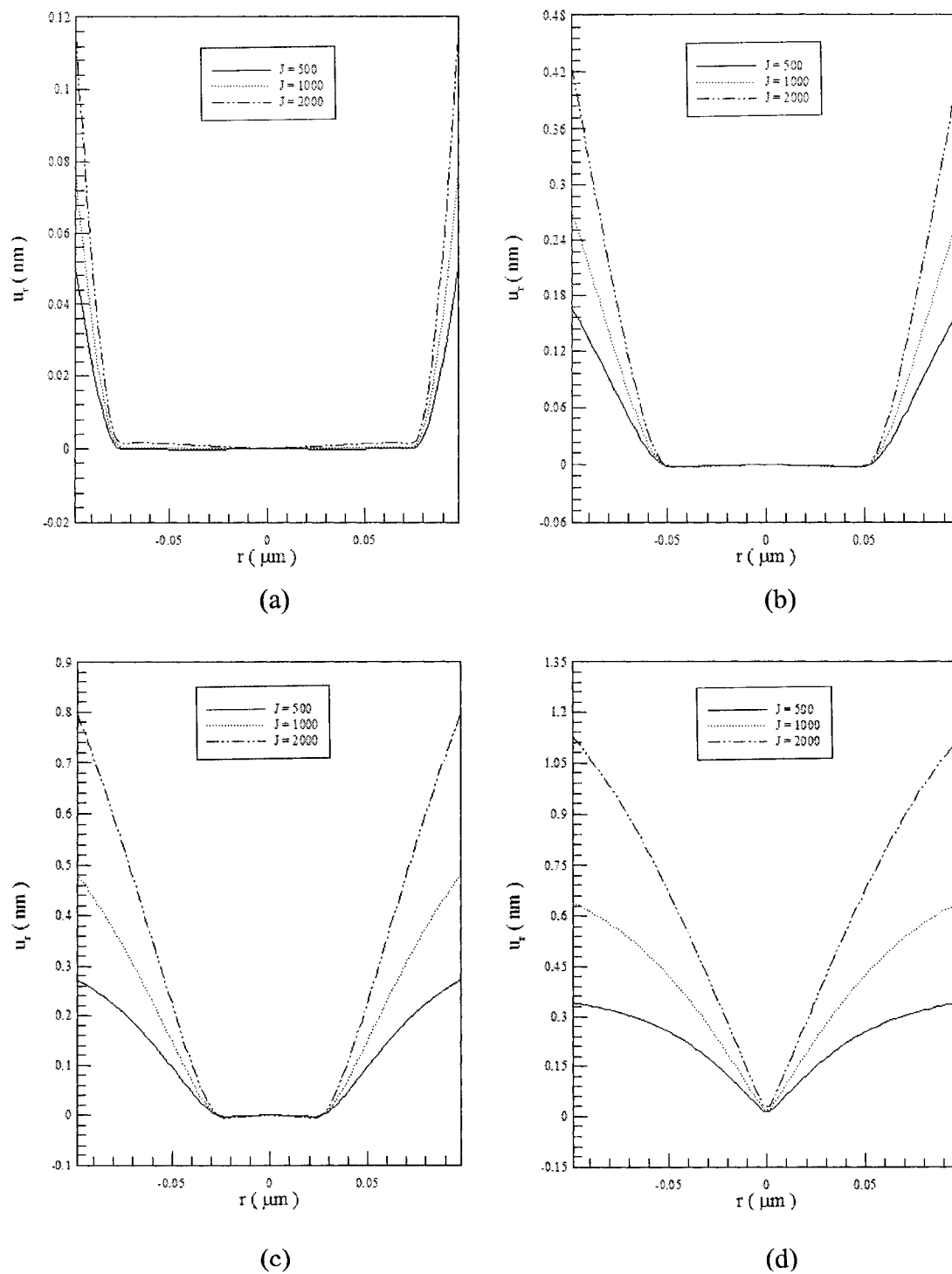
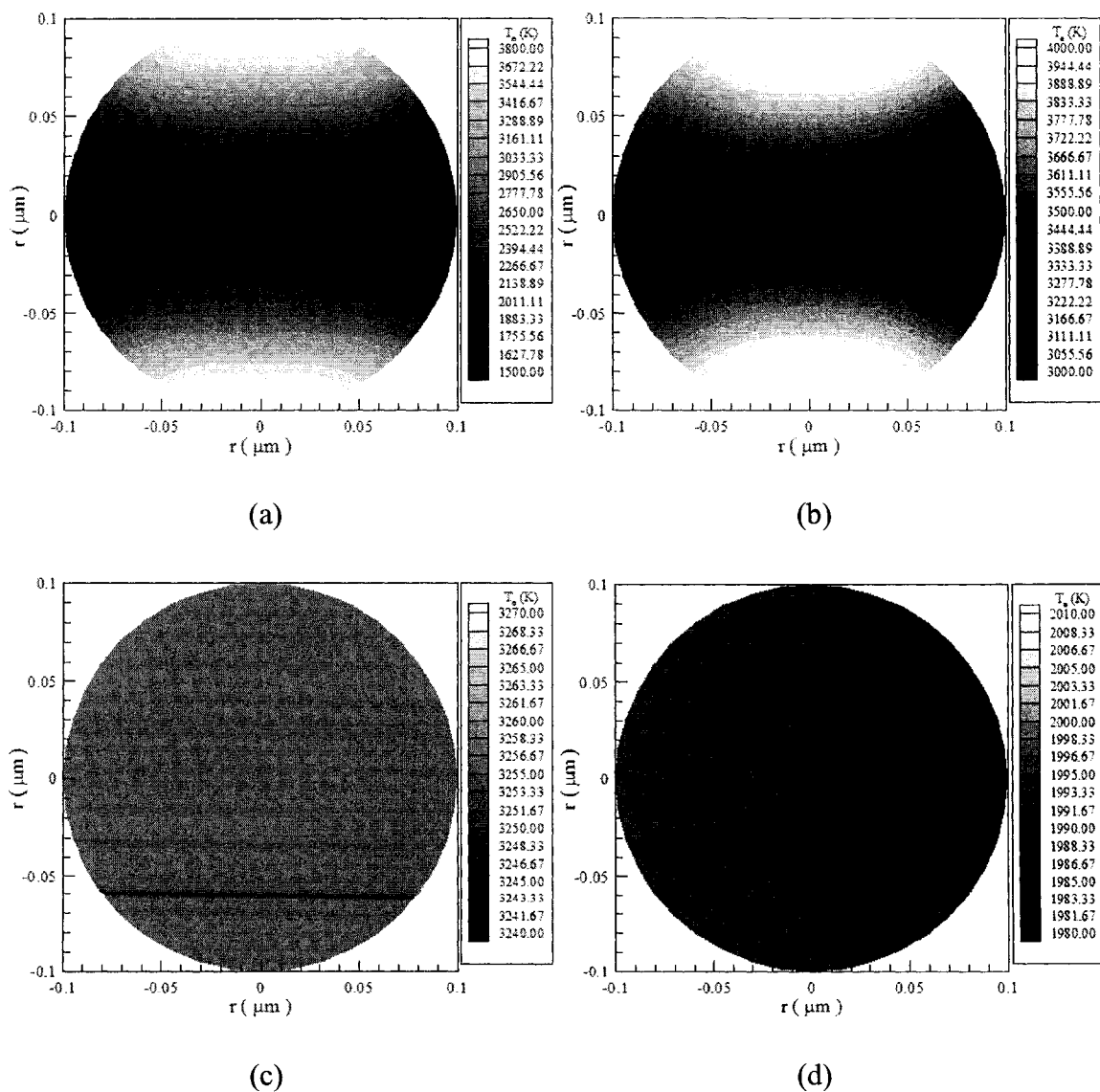


Fig. 5.59 Displacement ( $u_r$ ) along the diameter at  $\varphi = 0$  and  $\varphi = \pi$  at different times (a)  $t = 5$  ps, (b)  $t = 10$  ps, (c)  $t = 15$  ps, and (d)  $t = 20$  ps with three different laser fluences and a mesh of  $60 \times 20 \times 20$ .

Figs. 5.60–5.67 were plotted based on the results obtained in a mesh of  $60 \times 20 \times 20$  with a laser fluence  $J = 500 \text{ J/m}^2$ . Figs. 5.60 and 5.61 show contours of electron temperature distributions and lattice temperature distributions in the cross section of  $\theta = 0$  and  $\theta = \pi$  at different times (a)  $t = 0.25 \text{ ps}$ , (b)  $t = 0.5 \text{ ps}$ , (c)  $t = 1 \text{ ps}$ , (d)  $t = 5 \text{ ps}$ , (e)  $t = 10 \text{ ps}$ , and (f)  $t = 20 \text{ ps}$ , respectively. It can be seen from both figures that the heat is mainly transferred from both the top surface and the bottom surface to the center.



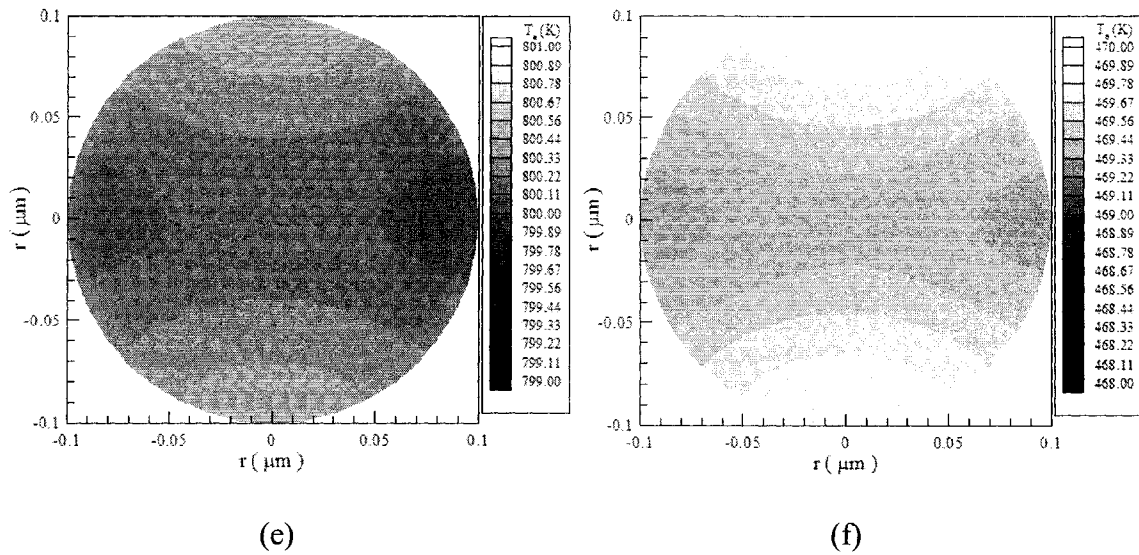
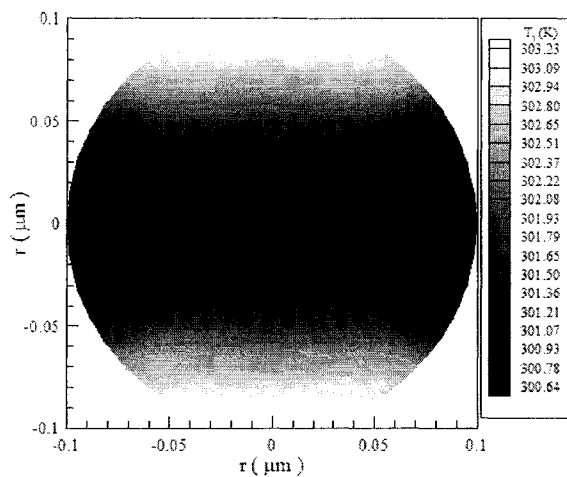
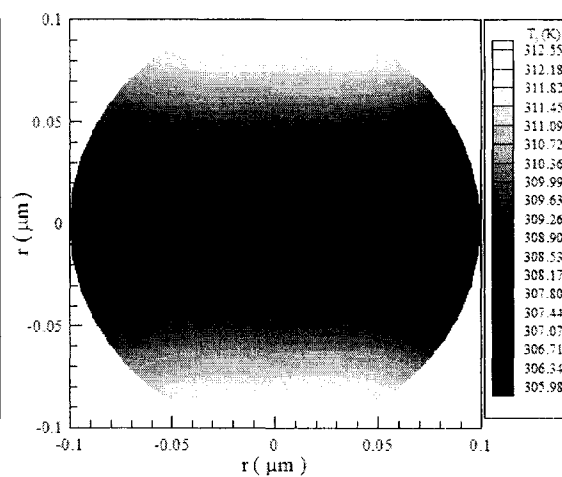


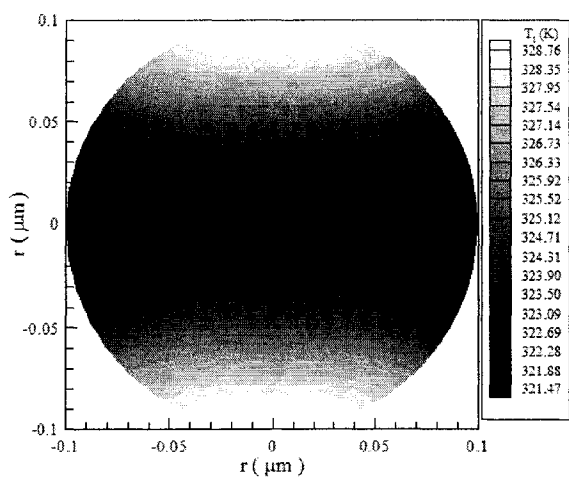
Fig. 5.60 Contours of electron temperature ( $T_e$ ) distributions in the cross section of  $\theta = 0$  and  $\theta = \pi$  at different times (a)  $t = 0.25$  ps, (b)  $t = 0.5$  ps, (c)  $t = 1$  ps, (d)  $t = 5$  ps, (e)  $t = 10$  ps, and (f)  $t = 20$  ps with a mesh of  $60 \times 20 \times 20$  and a laser fluence  $J$  of  $500 \text{ J/m}^2$ .



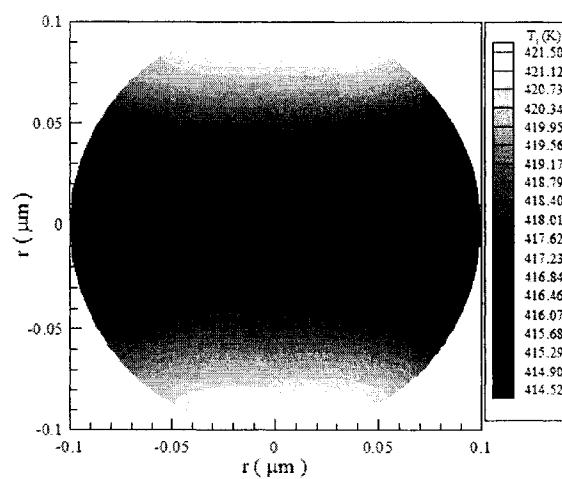
(a)



(b)



(c)



(d)

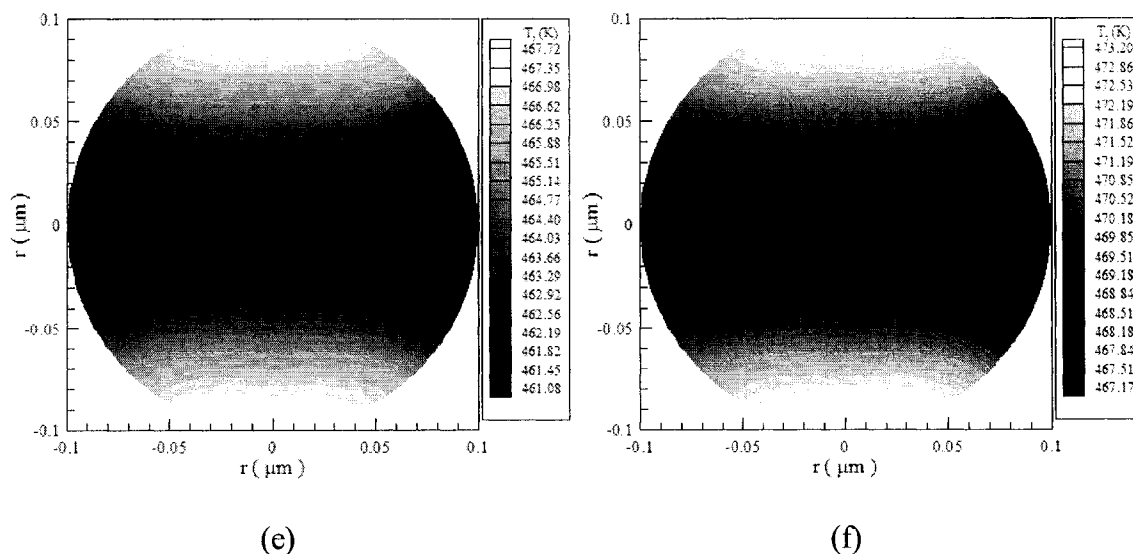


Fig. 5.61 Contours of lattice temperature ( $T_1$ ) distributions in the cross section of  $\theta = 0$  and  $\theta = \pi$  at different times (a)  $t = 0.25$  ps, (b)  $t = 0.5$  ps, (c)  $t = 1$  ps, (d)  $t = 5$  ps, (e)  $t = 10$  ps, and (f)  $t = 20$  ps with a mesh of  $60 \times 20 \times 20$  and a laser fluence  $J$  of  $500 \text{ J/m}^2$ .

Figs. 5.62–5.67 show contours of displacement ( $u_r, u_\theta, u_\phi$ ) and normal stress ( $\sigma_r, \sigma_\theta, \sigma_\phi$ ) in the cross section of  $\theta = 0$  and  $\theta = \pi$  at different times (a)  $t = 5$  ps, (b)  $t = 10$  ps, (c)  $t = 15$  ps, and (d)  $t = 20$  ps, respectively. It can be seen from Fig. 5.62 that the upper hemisphere and the lower hemisphere expanding symmetrically along  $r$  direction which is similar to Fig. 5.23.

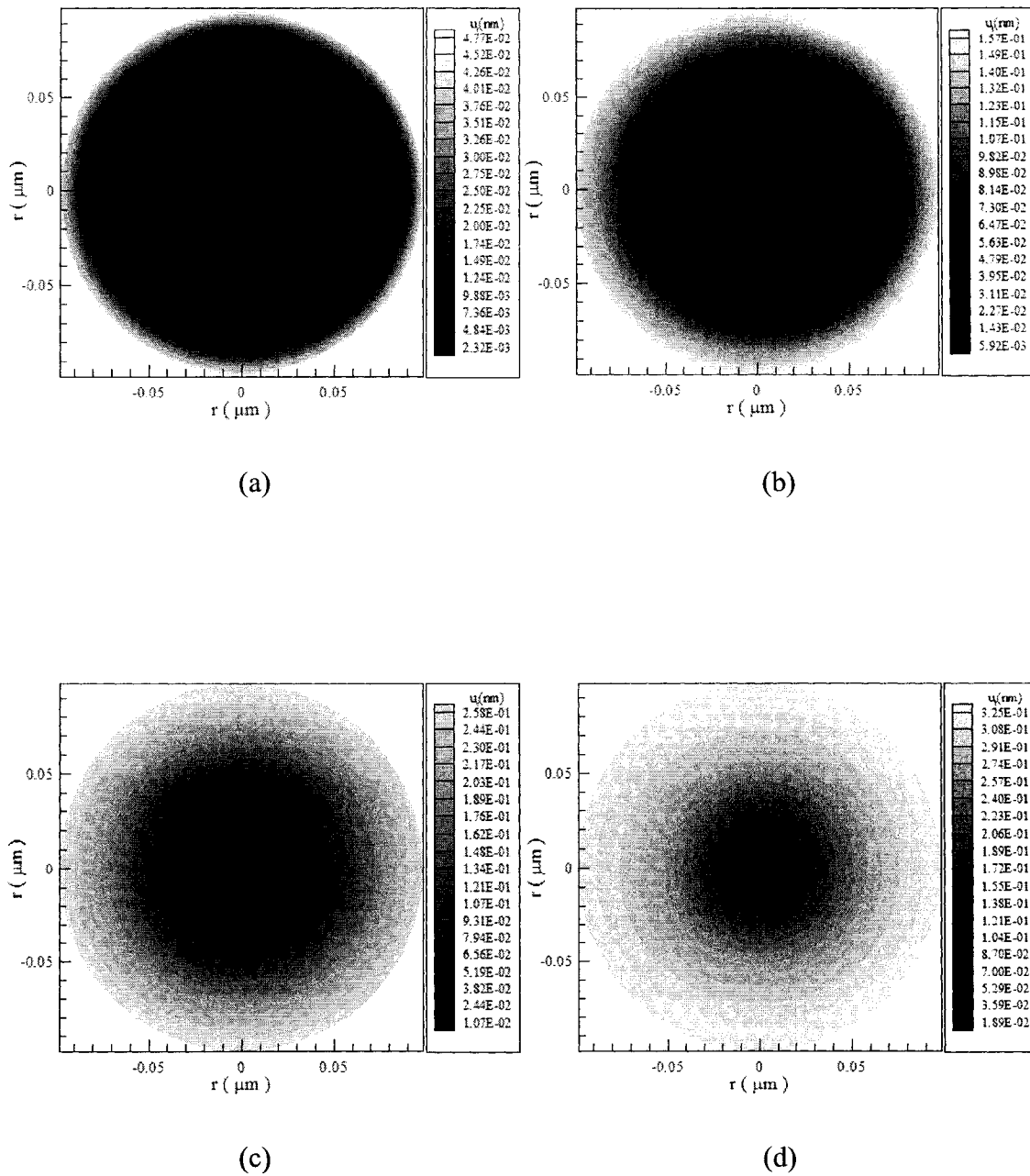


Fig. 5.62 Contours of displacement ( $u_r$ ) distributions in the cross section of  $\theta = 0$  and  $\theta = \pi$  at different times (a)  $t = 5$  ps, (b)  $t = 10$  ps, (c)  $t = 15$  ps, and (d)  $t = 20$  ps with a mesh of  $60 \times 20 \times 20$  and a laser fluence  $J$  of  $500 \text{ J/m}^2$ .



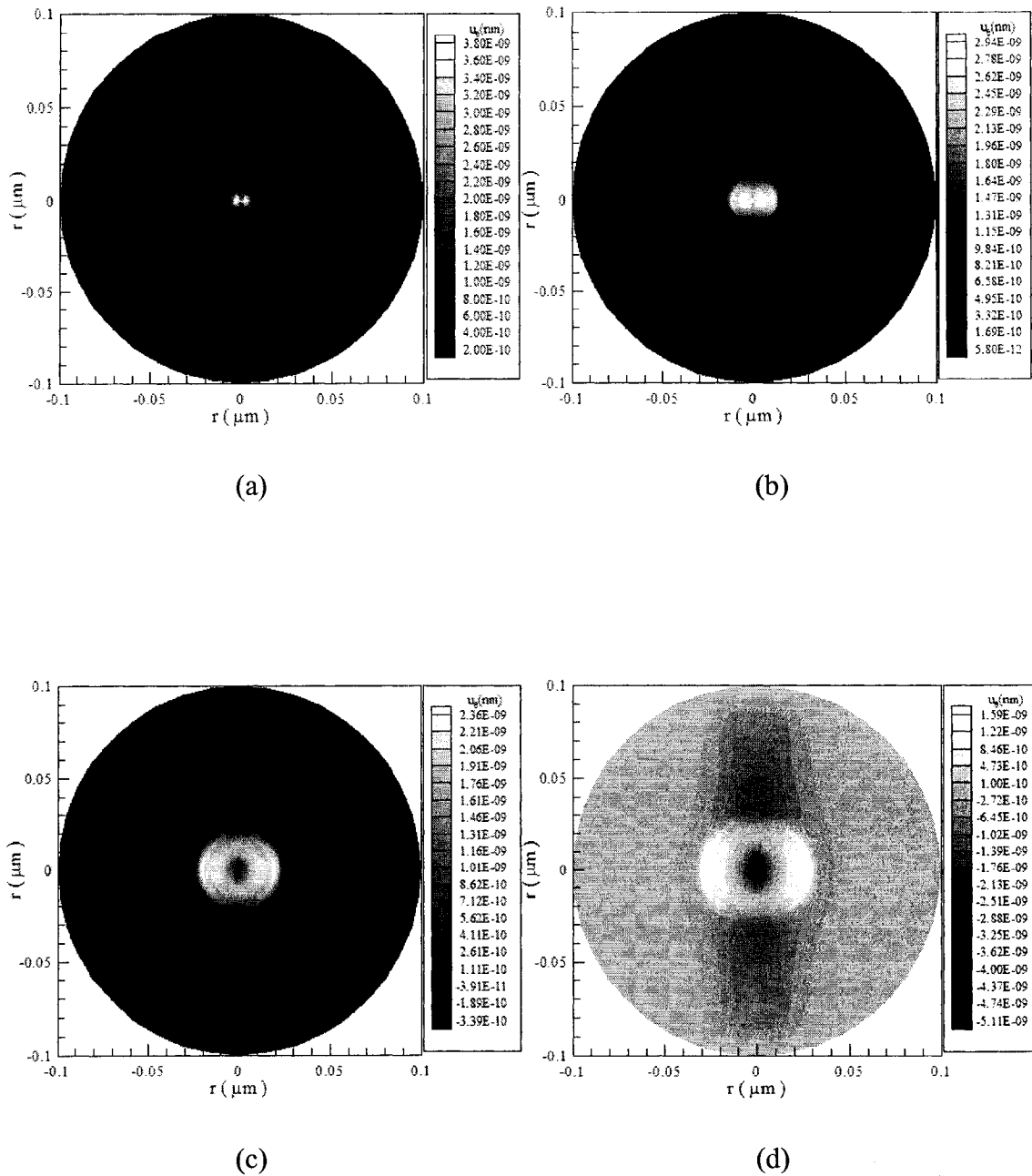


Fig. 5.63 Contours of displacement ( $u_\theta$ ) distributions in the cross section of  $\theta = 0$  and  $\theta = \pi$  at different times (a)  $t = 5$  ps, (b)  $t = 10$  ps, (c)  $t = 15$  ps, and (d)  $t = 20$  ps with a mesh of  $60 \times 20 \times 20$  and a laser fluence  $J$  of  $500 \text{ J/m}^2$ .

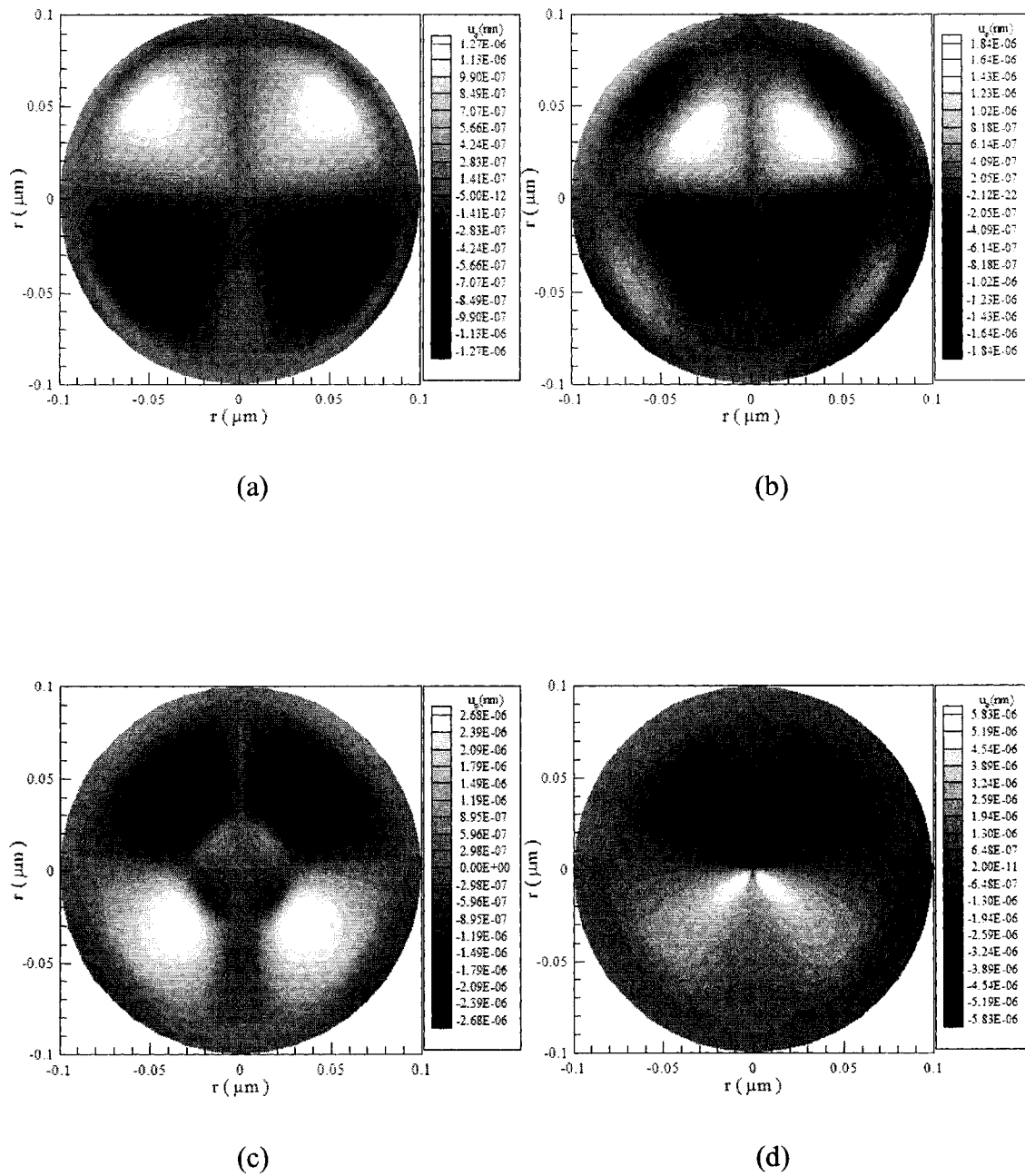


Fig. 5.64 Contours of displacement ( $u_\varphi$ ) distributions in the cross section of  $\theta = 0$  and  $\theta = \pi$  at different times (a)  $t = 5$  ps, (b)  $t = 10$  ps, (c)  $t = 15$  ps, and (d)  $t = 20$  ps with a mesh of  $60 \times 20 \times 20$  and a laser fluence  $J$  of  $500 \text{ J/m}^2$ .

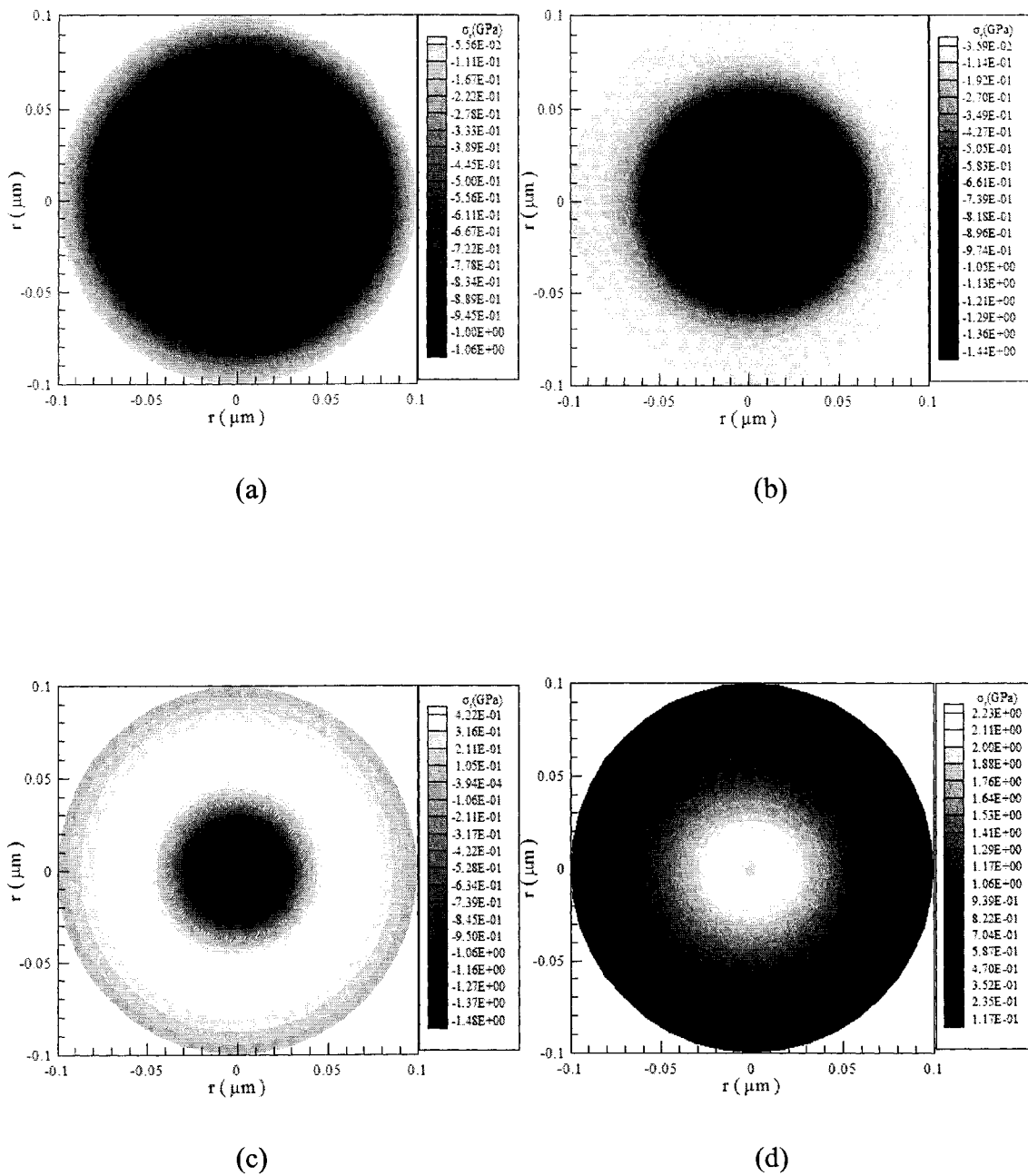


Fig. 5.65 Contours of normal stress ( $\sigma_r$ ) distributions in the cross section of  $\theta = 0$  and  $\theta = \pi$  at different times (a)  $t = 5$  ps, (b)  $t = 10$  ps, (c)  $t = 15$  ps, and (d)  $t = 20$  ps with a mesh of  $60 \times 20 \times 20$  and a laser fluence  $J$  of  $500 \text{ J/m}^2$ .

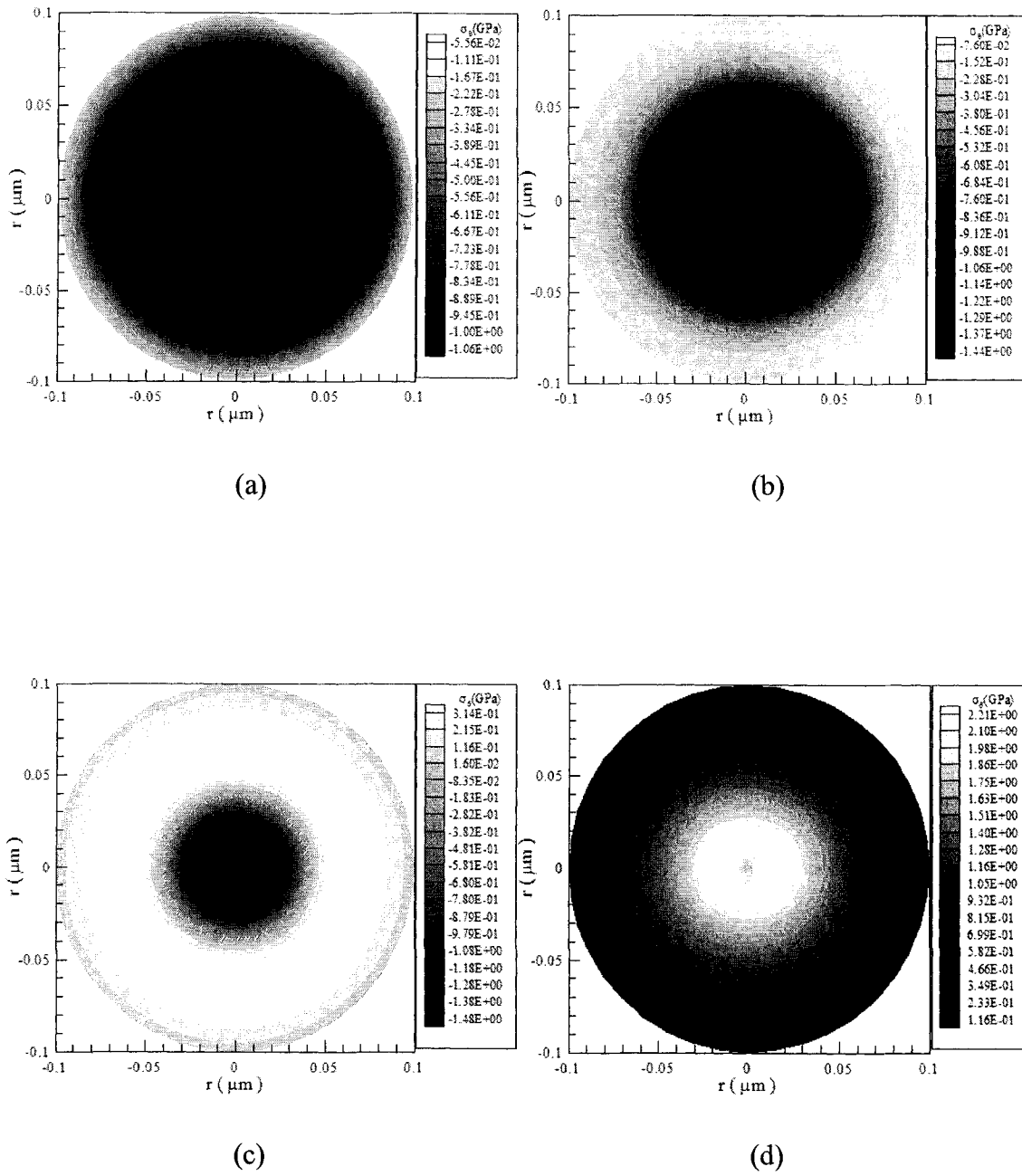


Fig. 5.66 Contours of normal stress ( $\sigma_\theta$ ) distributions in the cross section of  $\theta = 0$  and  $\theta = \pi$  at different times (a)  $t = 5$  ps, (b)  $t = 10$  ps, (c)  $t = 15$  ps, and (d)  $t = 20$  ps with a mesh of  $60 \times 20 \times 20$  and a laser fluence  $J$  of  $500 \text{ J/m}^2$ .

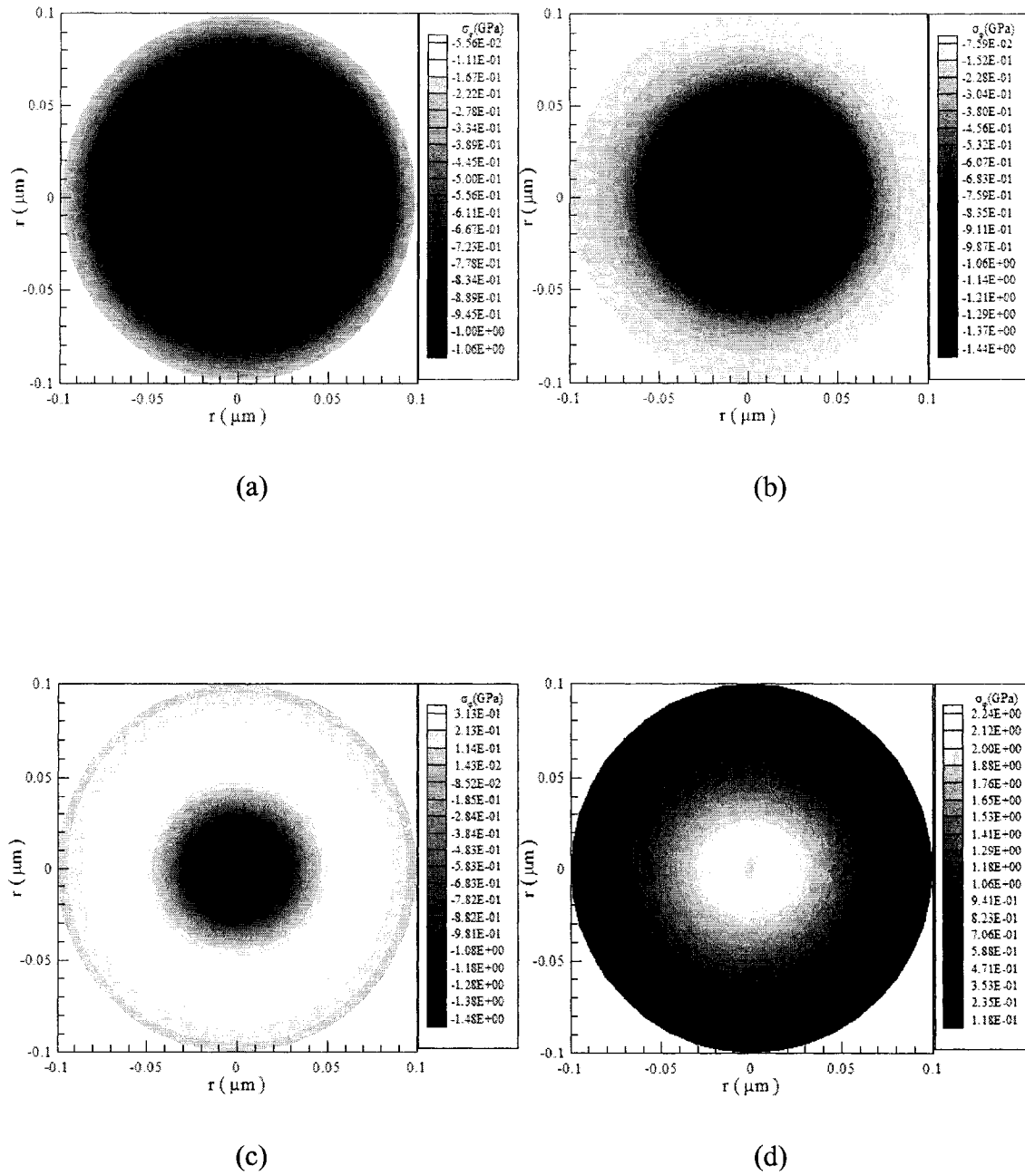


Fig. 5.67 Contours of normal stress ( $\sigma_\varphi$ ) distributions in the cross section of  $\theta = 0$  and  $\theta = \pi$  at different times (a)  $t = 5$  ps, (b)  $t = 10$  ps, (c)  $t = 15$  ps, and (d)  $t = 20$  ps with a mesh of  $60 \times 20 \times 20$  and a laser fluence  $J$  of  $500 \text{ J/m}^2$ .

## **CHAPTER SIX**

### **CONCLUSION**

In this dissertation, we reviewed the fundamentals about the heat transfer for microscale. And then we developed a mathematical model for micro-sphere subjected by ultrashort pulsed lasers in spherical coordinates for studying thermal deformation. The model includes the dynamic equations of motion and the parabolic two-step heat transport equations. We further developed a finite difference scheme based on the developed mathematical model. The scheme was obtained by introducing velocity components to the dynamic equations of motion, and by using a staggered grid, by developing the fourth order compact finite difference for the derivatives of stresses. The model of its numerical method is tested by several numerical examples. Numerical results show that the solutions do not appear non-physical oscillation, and the micro-sphere is expanding when subjected to ultrashort-pulsed lasers.

Further studies will focus on the thermal deformation in a multi-layered micro-sphere since multi-layered micro-sphere is often encountered in engineering.

**APPENDIX**  
**SOURCE CODE OF THE NUMERICAL METHOD**

Source code for the case that the laser irradiates a portion ( $0 \leq r \leq L$ ,  $0 \leq \theta \leq 2\pi$ ,  $0 \leq \varphi \leq \pi/4$ ) with a mesh of  $60 \times 20 \times 20$  and a laser fluence  $J$  of  $500 \text{ J/m}^2$ :

```

c main
  implicit double precision (a-h,l,o-z)
  dimension
t(4010),t1(4010),t2(4010),x(150),y(50),z(50),x1(
150),
  $
x2(150),y1(50),z1(50),a(150),b(150),c(150),beta
(150)

  dimension eto(150,50,50),etn(150,50,50),
  $
lto(150,50,50),ltn(150,50,50),etnmax(150,50,50),
  $
etm(4010),etm1(4010),ltn(4010),ltn1(4010),
  $ u1m(4010),u2m(4010),u3m(4010),
  $
v1m(4010),v2m(4010),v3m(4010),etm2(4010),
  $
xsao(151,51,51),ysao(151,51,51),zsao(151,51,51
),
  $
ssaoxy(151,51,51),ssaioxz(151,51,51),ssaoyz(151
,51,51),
  $
xsao(151,51,51),ysao(151,51,51),zsao(151,5
1,51),
  $
ssaooxy(151,51,51),ssaooxz(151,51,51),ssaooyz(
151,51,51),
  $
xsan(151,51,51),ysan(151,51,51),zsan(151,51,51
),
  $
ssanxy(151,51,51),ssanxz(151,51,51),ssanyz(151
,51,51),
  $
xseo(151,51,51),yseo(151,51,51),zseo(151,51,51
),
  $
sseoxy(151,51,51),sseioxz(151,51,51),sseoyz(151
,51,51),

```

```

  $
xsen(151,51,51),ysen(151,51,51),zsen(151,51,51
),
  $
ssenxy(151,51,51),ssenxz(151,51,51),ssenyz(151
,51,51),
  $
difx(151,51,51),dify(151,51,51),difz(151,51,51),
  $
difxyx(151,51,51),difxyy(151,51,51),difxzx(151
,51,51),
  $
difxzz(151,51,51),difyzy(151,51,51),difyzz(151
,51,51),
  $
v1o(151,51,51),v2o(151,51,51),v3o(151,51,51),
  $
v1n(151,51,51),v2n(151,51,51),v3n(151,51,51),
  $
u1o(151,51,51),u2o(151,51,51),u3o(151,51,51),
  $
u1n(151,51,51),u2n(151,51,51),u3n(151,51,51),
  $ d(151,51,51),gama(151,51,51)

  integer o, counter,l,r

c Lamé constant
  lemta=199.0d+9
c Shear modulus
  cmu=27.0d+9
c Thermal expansion coefficient
  alphas=14.2d-6
  open(unit=62, file='etm.txt')

  pi=3.14159265359
  lx=1.0D-7
  ly=2.0*pi
  lz=1.0*pi
  n=60
  m=20
  r=20
  h1=lx/n
  h2=ly/m
  h3=lz/r

  o=4000
  dt=0.005d-12
  counter=0
  t(1)=0
  x(1)=0
  y(1)=0
  z(1)=0

c initial condition
  print *,t
  k=1

```



```

do l=1,r+1
do j=1,m
do i=1,n+1
eto(i,j,l)=300.0
lto(i,j,l)=300.0
etnmax(i,j,l)=300.0
c print*, eto(i,j,l)
xsao(i,j,l)=0.0
ysao(i,j,l)=0.0
zsao(i,j,l)=0.0
ssaoxy(i,j,l)=0.0
ssaoxz(i,j,l)=0.0
ssaoyz(i,j,l)=0.0

xsaoo(i,j,l)=0.0
ysaoo(i,j,l)=0.0
zsaoo(i,j,l)=0.0
ssaooxy(i,j,l)=0.0
ssaooxz(i,j,l)=0.0
ssaooyz(i,j,l)=0.0

xseo(i,j,l)=0.0
yseo(i,j,l)=0.0
zseo(i,j,l)=0.0
sseoxy(i,j,l)=0.0
sseoxz(i,j,l)=0.0
sseoyz(i,j,l)=0.0
difxyx(i,j,l)=0.0
difxyy(i,j,l)=0.0
difxzx(i,j,l)=0.0
difxzz(i,j,l)=0.0
difzyz(i,j,l)=0.0
difyzz(i,j,l)=0.0
difx(i,j,l)=0.0
dify(i,j,l)=0.0
difz(i,j,l)=0.0
v1o(i,j,l)=0.0
v2o(i,j,l)=0.0
v3o(i,j,l)=0.0
u1o(i,j,l)=0.0
u2o(i,j,l)=0.0
u3o(i,j,l)=0.0

end do
end do
end do

etm(k)=300.0
ltm(k)=300.0
c
do l=2,r+1
z(l)=z(l-1)+h3
z1(l)=z(l-1)+1.0/r
end do
do j=2,m
y(j)=y(j-1)+h2
y1(j)=y1(j-1)+2.0/m
print*, y(j)
end do
do i=2,n+1
x(i)=x(i-1)+h1
x1(i)=(x(i-1)+h1)*1.0d6
x2(i)=-(x(i-1)+h1)*1.0d6
end do

write(*,*) 'start'

do l kt=2,o+1
c
t(k)=t(k-1)+dt

t1(k)=t(k-1)+dt/2.0
t2(k)=(t(k-1)+dt)*1.0d12
c
do l=1,r+1
do j=1,m
do i=1,n+1
xsan(i,j,l)=xsao(i,j,l)
ysan(i,j,l)=ysao(i,j,l)
zsan(i,j,l)=zsao(i,j,l)
enddo
enddo
enddo
c
call
temp(n,m,r,lx,h1,h2,h3,x,y,z,t1(k),dt,lto,ltm,eto,et
n,
$ xsan,ysan,zsan,xsao,ysao,zsao)

tol=1d-12
detuvmax=tol+1d-5
do while (detuvmax.gt.tol)
detuvmax=0.0

c Compute stress

do k=2,r
do j=1,m
do i=2,n

xsen(i,j,k)=(lemta+2.0*cmiu)*xsan(i,j,k)+lemta*
ysan(i,j,k)
$ +lemta*zsan(i,j,k)-
(3.0*lemta+2.0*cmiu)*alphan*(ltn(i,j,k)-300.0)

ysen(i,j,k)=lemta*xsan(i,j,k)+(lemta+2.0*cmiu)*
ysan(i,j,k)
$ +lemta*zsan(i,j,k)-
(3.0*lemta+2.0*cmiu)*alphan*(ltn(i,j,k)-300.0)

```

```

zsen(i,j,k)=lemta*xsan(i,j,k)+(lemta+2.0*cmiu)*
zsan(i,j,k)
  $ +lemta*ysan(i,j,k)-
(3.0*lemta+2.0*cmiu)*alpat*(ltn(i,j,k)-300.0)

  end do
  end do
  end do

  do k=1,r+1
  do j=1,m
  xsen(1,j,k)=xsen(2,j,k)
  ysen(1,j,k)=ysen(2,j,k)
  zsen(1,j,k)=zsen(2,j,k)
  xsen(n+1,j,k)=0.0
  ysen(n+1,j,k)=0.0
  zsen(n+1,j,k)=0.0
  end do
  end do

  do j=1,m
  do i=1,n+1
  zsen(i,j,1)=zsen(i,j,2)
  ysen(i,j,1)=ysen(i,j,2)
  xsen(i,j,1)=xsen(i,j,2)
  zsen(i,j,r+1)=zsen(i,j,r)
  ysen(i,j,r+1)=ysen(i,j,r)
  xsen(i,j,r+1)=xsen(i,j,r)
  end do
  end do
c
  do k=2,r
  do j=1,m
  do i=2,n-1
  ssenxy(i,j,k)=2*cmiu*ssanxy(i,j,k)

  end do
  end do
  end do

  do k=1,r+1
  do j=1,m
  ssenxy(1,j,k)=ssenxy(2,j,k)
  ssenxy(n,j,k)=0
  enddo
  enddo
  do i=1,n-1
  do j=1,m
  ssenxy(i,j,1)=ssenxy(i,j,2)
  ssenxy(i,j,r+1)=ssenxy(i,j,r)
  enddo
  enddo

  do k=2,r-1
  do j=1,m
  do i=2,n-1
  ssenxz(i,j,k)=2*cmiu*ssanxz(i,j,k)
  enddo
  enddo

  do k=1,r
  do j=1,m
  ssenxz(1,j,k)=ssenxz(2,j,k)
  ssenxz(n,j,k)=0
  enddo
  enddo

  do i=1,n-1
  do j=1,m
  ssenxz(i,j,1)=ssenxz(i,j,2)
  ssenxz(i,j,r)=ssenxz(i,j,r-1)
  enddo
  enddo

  do k=2,r-1
  do j=1,m
  do i=2,n
  ssenyz(i,j,k)=2*cmiu*ssanyz(i,j,k)
  enddo
  enddo
  enddo

  do k=1,r
  do j=1,m
  ssenyz(1,j,k)=ssenyz(2,j,k)
  ssenyz(n+1,j,k)=0
  enddo
  enddo

  do i=1,n
  do j=1,m
  ssenyz(i,j,1)=ssenyz(i,j,2)
  ssenyz(i,j,r)=ssenyz(i,j,r-1)
  enddo
  enddo

c  difx-----
  do k=1,r+1
  do j=1,m
  difx(1,j,k)=(xsen(2,j,k)-xsen(1,j,k))/h1
  difx(n,j,k)=(xsen(n+1,j,k)-xsen(n,j,k))/h1
  end do
  end do

  b(2)=0.0
  a(2)=0.416666667
  c(2)=-0.041666667

  do k=1,r+1

```

```

do j=1,m
  d(2,j,k)=(xsen(3,j,k)-xsen(2,j,k))/h1-
0.041666667*difx(1,j,k)
end do
end do

do i=3,n-2
  b(i)=-0.041666667
  a(i)=0.416666667
  c(i)=-0.041666667
  do j=1,m
    do k=1,r+1
      d(i,j,k)=(xsen(i+1,j,k)-xsen(i,j,k))/h1
    end do
  end do
end do

b(n-1)=-0.041666667
a(n-1)=0.416666667
c(n-1)=0

do k=1,r+1
  do j=1,m
    d(n-1,j,k)=(xsen(n,j,k)-xsen(n-1,j,k))/h1-
0.041666667*difx(n,j,k)

  end do
end do

beta(n)=0
do k=1,r+1
  do j=1,m
    gama(n,j,k)=0
  end do
end do

do k1=2,n-1
  i=n-k1+1
  beta(i)=b(i)/(a(i)-c(i)*beta(i+1))
  do j=1,m
    do k=1,r+1

gama(i,j,k)=(d(i,j,k)+c(i)*gama(i+1,j,k))/(a(i)-
c(i)*beta(i+1))
  end do
  end do
end do

do i=2,n-1
  do j=1,m
    do k=1,r+1
      difx(i,j,k)=beta(i)*difx(i-1,j,k)+gama(i,j,k)
    end do
  end do
end do

do i=1,n+1
  a(i)=0.0
  b(i)=0.0
  c(i)=0.0
  beta(i)=0.0
  do j=1,m
    do k=1,r+1
      gama(i,j,k)=0.0
      d(i,j,k)=0.0
    enddo
  enddo
enddo
c  dify-----
do k=1,r+1
  do i=1,n+1
    dify(i,1,k)=(ysen(i,2,k)-ysen(i,1,k))/h2
    dify(i,m,k)=(ysen(i,1,k)-ysen(i,m,k))/h2
  end do
end do

b(2)=0
a(2)=0.416666667
c(2)=-0.041666667

do k=1,r+1
  do i=1,n+1
    d(i,2,k)=(ysen(i,3,k)-ysen(i,2,k))/h2-
0.041666667*dify(i,1,k)
  end do
end do

do j=3,m-2
  b(j)=-0.041666667
  a(j)=0.416666667
  c(j)=-0.041666667
  do i=1,n+1
    do k=1,r+1
      d(i,j,k)=(ysen(i,j+1,k)-ysen(i,j,k))/h2
    end do
  end do
end do

b(m-1)=-0.041666667
a(m-1)=0.416666667
c(m-1)=0

do k=1,r+1
  do i=1,n+1
    d(i,m-1,k)=(ysen(i,m,k)-ysen(i,m-1,k))/h2-
0.041666667*dify(i,m,k)

  end do
end do

beta(m)=0

```

```

do k=1,r+1
do i=1,n+1
gama(i,m,k)=0
end do
end do

do k1=2,m-1
j=m-k1+1
beta(j)=b(j)/(a(j)-c(j)*beta(j+1))
do i=1,n+1
do k=1,r+1

gama(i,j,k)=(d(i,j,k)+c(j)*gama(i,j+1,k))/(a(j)-
c(j)*beta(j+1))
end do
end do
end do

do i=1,n+1
do j=2,m-1
do k=1,r
dify(i,j,k)=beta(j)*dify(i,j-1,k)+gama(i,j,k)
end do
end do
end do
do i=1,n+1
a(i)=0.0
b(i)=0.0
c(i)=0.0
beta(i)=0.0
do j=1,m
do k=1,r+1
gama(i,j,k)=0.0
d(i,j,k)=0.0
enddo
enddo
enddo
c difz-----
do j=1,m
do i=1,n+1
difz(i,j,1)=(zsen(i,j,2)-zsen(i,j,1))/h3
difz(i,j,r)=(zsen(i,j,r+1)-zsen(i,j,r))/h3
end do
end do

b(2)=0.0
a(2)=0.416666667
c(2)=-0.0416666667

do j=1,m
do i=1,n+1
d(i,j,2)=(zsen(i,j,3)-zsen(i,j,2))/h3-
0.041666667*difz(i,j,1)
end do
end do

do k=1,r+1
do i=1,n+1
gama(i,m,k)=0
end do
end do

do k1=2,m-1
j=m-k1+1
beta(j)=b(j)/(a(j)-c(j)*beta(j+1))
do i=1,n+1
do k=1,r+1

gama(i,j,k)=(d(i,j,k)+c(j)*gama(i,j+1,k))/(a(j)-
c(j)*beta(j+1))
end do
end do
end do

do i=1,n+1
do j=2,m-1
do k=1,r
dify(i,j,k)=beta(j)*dify(i,j-1,k)+gama(i,j,k)
end do
end do
end do
do i=1,n+1
a(i)=0.0
b(i)=0.0
c(i)=0.0
beta(i)=0.0
do j=1,m
do k=1,r+1
gama(i,j,k)=0.0
d(i,j,k)=0.0
enddo
enddo
enddo
c difz-----
do j=1,m
do i=1,n+1
difz(i,j,1)=(zsen(i,j,2)-zsen(i,j,1))/h3
difz(i,j,r)=(zsen(i,j,r+1)-zsen(i,j,r))/h3
end do
end do

b(2)=0.0
a(2)=0.416666667
c(2)=-0.0416666667

do j=1,m
do i=1,n+1
d(i,j,2)=(zsen(i,j,3)-zsen(i,j,2))/h3-
0.041666667*difz(i,j,1)
end do
end do

do k=3,r-2
b(k)=-0.0416666667
a(k)=0.416666667
c(k)=-0.0416666667
do i=1,n+1
do j=1,m
d(i,j,k)=(zsen(i,j,k+1)-zsen(i,j,k))/h3
end do
end do
end do

b(r-1)=-0.0416666667
a(r-1)=0.416666667
c(r-1)=0

do j=1,m
do i=1,n+1
d(i,j,r-1)=(zsen(i,j,r)-zsen(i,j,r-1))/h3-
0.041666667*difz(i,j,r)
end do
end do

beta(r)=0
do j=1,m
do i=1,n+1
gama(i,j,r)=0
end do
end do

do k1=2,r-1
k=r-k1+1
beta(k)=b(k)/(a(k)-c(k)*beta(k+1))
do i=1,n+1
do j=1,m

gama(i,j,k)=(d(i,j,k)+c(k)*gama(i,j,k+1))/(a(k)-
c(k)*beta(k+1))
end do
end do
end do

do i=1,n+1
do j=1,m
do k=2,r-1
difz(i,j,k)=beta(k)*difz(i,j,k-1)+gama(i,j,k)
end do
end do
end do

do i=1,n+1
a(i)=0.0
b(i)=0.0
c(i)=0.0
beta(i)=0.0
do j=1,m

```

```

do k=1,r+1
gama(i,j,k)=0.0
d(i,j,k)=0.0
enddo
enddo
enddo
c difxyx-----
do k=1,r
do j=1,m
difxyx(1,j,k)=(ssenxy(2,j,k)-ssenxy(1,j,k))/h1
difxyx(n-1,j,k)=(ssenxy(n,j,k)-ssenxy(n-
1,j,k))/h1
end do
end do

b(2)=0
a(2)=0.416666667
c(2)=-0.0416666667

do k=1,r
do j=1,m
d(2,j,k)=(ssenxy(3,j,k)-ssenxy(2,j,k))/h1
$ -0.041666667*difxyx(1,j,k)
end do
end do

do i=3,n-3
b(i)=-0.0416666667
a(i)=0.416666667
c(i)=-0.0416666667
do k=1,r
do j=1,m
d(i,j,k)=(ssenxy(i+1,j,k)-ssenxy(i,j,k))/h1
end do
end do
end do

b(n-2)=-0.0416666667
a(n-2)=0.416666667
c(n-2)=0.0

do k=1,r
do j=1,m
d(n-2,j,k)=(ssenxy(n-1,j,k)-ssenxy(n-
2,j,k))/h1
$ -0.041666667*difxyx(n-1,j,k)
end do
end do

beta(n-1)=0

do k=1,r
do j=1,m
gama(n-1,j,k)=0
end do
end do

do k1=3,n-1
i=n-k1+1
beta(i)=b(i)/(a(i)-c(i)*beta(i+1))
do k=1,r
do j=1,m
gama(i,j,k)=(d(i,j,k)+c(i)*gama(i+1,j,k))/(a(i)-
c(i)*beta(i+1))
end do
end do
end do

do i=2,n-2
do j=1,m
do k=1,r
difxyx(i,j,k)=beta(i)*difxyx(i-
1,j,k)+gama(i,j,k)
end do
end do
end do

do i=1,n+1
a(i)=0.0
b(i)=0.0
c(i)=0.0
beta(i)=0.0
do j=1,m
do k=1,r+1
gama(i,j,k)=0.0
d(i,j,k)=0.0
enddo
enddo
enddo
c difxyy-----
do k=1,r
do i=1,n
difxyy(i,1,k)=(ssenxy(i,2,k)-ssenxy(i,1,k))/h2
difxyy(i,m,k)=(ssenxy(i,1,k)-
ssenxy(i,m,k))/h2
end do
end do

b(2)=0
a(2)=0.416666667
c(2)=-0.0416666667

do k=1,r
do i=1,n
d(i,2,k)=(ssenxy(i,3,k)-ssenxy(i,2,k))/h2
$ -0.041666667*difxyy(i,1,k)
end do
end do

do j=3,m-2
b(j)=-0.0416666667

```

```

a(j)=0.416666667
c(j)=-0.0416666667
do k=1,r
do i=1,n
d(i,j,k)=(ssenxy(i,j+1,k)-ssenxy(i,j,k))/h2
end do
end do
end do

b(m-1)=-0.0416666667
a(m-1)=0.416666667
c(m-1)=0.0

do k=1,r
do i=1,n
d(i,m-1,k)=(ssenxy(i,m,k)-ssenxy(i,m-
1,k))/h2
$ -0.041666667*difxyy(i,m,k)
end do
end do

beta(m)=0

do k=1,r
do i=1,n
gama(i,m,k)=0
end do
end do

do k1=2,m-1
j=m-k1+1
beta(j)=b(j)/(a(j)-c(j)*beta(j+1))
do k=1,r
do i=1,n
gama(i,j,k)=(d(i,j,k)+c(j)*gama(i,j+1,k))/(a(j)-
c(j)*beta(j+1))
end do
end do
end do

do i=1,n
do j=2,m-1
do k=1,r
difxyy(i,j,k)=beta(j)*difxyy(i,j-
1,k)+gama(i,j,k)
end do
end do
end do

do i=1,n+1
a(i)=0.0
b(i)=0.0
c(i)=0.0
beta(i)=0.0
do j=1,m
do k=1,r+1
gama(i,j,k)=0.0
d(i,j,k)=0.0
enddo
enddo
enddo
c difxzx-----
do k=1,r
do j=1,m
difxzx(1,j,k)=(ssenxz(2,j,k)-ssenxz(1,j,k))/h1
difxzx(n-1,j,k)=(ssenxz(n,j,k)-ssenxz(n-
1,j,k))/h1
end do
end do

b(2)=0
a(2)=0.416666667
c(2)=-0.0416666667

do k=1,r
do j=1,m
d(2,j,k)=(ssenxz(3,j,k)-ssenxz(2,j,k))/h1
$ -0.041666667*difxzx(1,j,k)
end do
end do

do i=3,n-3
b(i)=-0.0416666667
a(i)=0.416666667
c(i)=-0.0416666667
do k=1,r
do j=1,m
d(i,j,k)=(ssenxz(i+1,j,k)-ssenxz(i,j,k))/h1
end do
end do
end do

b(n-2)=-0.0416666667
a(n-2)=0.416666667
c(n-2)=0.0

do k=1,r
do j=1,m
d(n-2,j,k)=(ssenxz(n-1,j,k)-ssenxz(n-
2,j,k))/h1
$ -0.041666667*difxzx(n-1,j,k)
end do
end do

beta(n-1)=0

do k=2,r
do j=1,m
gama(n-1,j,k)=0
end do
end do

```

```

do k1=3,n-1
i=n-k1+1
beta(i)=b(i)/(a(i)-c(i)*beta(i+1))
do k=1,r
do j=1,m
gama(i,j,k)=(d(i,j,k)+c(i)*gama(i+1,j,k))/(a(i)-
c(i)*beta(i+1))
end do
end do
end do

do i=2,n-2
do j=1,m
do k=1,r
difaxz(i,j,k)=beta(i)*difaxz(i-
1,j,k)+gama(i,j,k)
end do
end do
end do

do i=1,n+1
a(i)=0.0
b(i)=0.0
c(i)=0.0
beta(i)=0.0
do j=1,m
do k=1,r+1
gama(i,j,k)=0.0
d(i,j,k)=0.0
enddo
enddo
enddo
c difxzz-----
do i=1,n
do j=1,m
difaxz(i,j,1)=(ssenzz(i,j,2)-ssenzz(i,j,1))/h3
difaxz(i,j,r-1)=(ssenzz(i,j,r)-ssenzz(i,j,r-
1))/h3
end do
end do

b(2)=0
a(2)=0.416666667
c(2)=-0.0416666667

do i=1,n
do j=1,m
d(i,j,2)=(ssenzz(i,j,3)-ssenzz(i,j,2))/h3
$ -0.041666667*difaxz(i,j,1)
end do
end do

do k=3,r-3
b(k)=-0.0416666667
a(k)=0.416666667
c(k)=-0.0416666667
do i=1,n
do j=1,m
d(i,j,k)=(ssenzz(i,j,k+1)-ssenzz(i,j,k))/h3
end do
end do
end do

b(r-2)=-0.0416666667
a(r-2)=0.416666667
c(r-2)=0.0

do i=1,n
do j=1,m
d(i,j,r-2)=(ssenzz(i,j,r-1)-ssenzz(i,j,r-2))/h3
$ -0.041666667*difaxz(i,j,r-1)
end do
end do

beta(r-1)=0

do i=1,n
do j=1,m
gama(i,j,r-1)=0
end do
end do

do k1=3,r-1
k=r-k1+1
beta(k)=b(k)/(a(k)-c(k)*beta(k+1))
do i=1,n
do j=1,m
gama(i,j,k)=(d(i,j,k)+c(k)*gama(i,j,k+1))/(a(k)-
c(k)*beta(k+1))
end do
end do
end do

do i=1,n
do j=1,m
do k=2,r-2
difaxz(i,j,k)=beta(k)*difaxz(i,j,k-
1)+gama(i,j,k)
end do
end do
end do

do i=1,n+1
a(i)=0.0
b(i)=0.0
c(i)=0.0
beta(i)=0.0
do j=1,m
do k=1,r+1

```

```

gama(i,j,k)=0.0
d(i,j,k)=0.0
enddo
enddo
enddo
c difyzy-----
do k=1,r
do i=1,n
difyzy(i,1,k)=(ssenyz(i,2,k)-ssenyz(i,1,k))/h2
difyzy(i,m,k)=(ssenyz(i,1,k)-
ssenyz(i,m,k))/h2
end do
end do

b(2)=0
a(2)=0.416666667
c(2)=-0.0416666667

do k=1,r
do i=1,n
d(i,2,k)=(ssenyz(i,3,k)-ssenyz(i,2,k))/h2
$ -0.041666667*difyzy(i,1,k)
end do
end do

do j=3,m-2
b(j)=-0.0416666667
a(j)=0.416666667
c(j)=-0.0416666667
do k=1,r
do i=1,n
d(i,j,k)=(ssenyz(i,j+1,k)-ssenyz(i,j,k))/h2
end do
end do
end do

b(m-1)=-0.0416666667
a(m-1)=0.416666667
c(m-1)=0.0

do k=1,r
do i=1,n
d(i,m-1,k)=(ssenyz(i,m,k)-ssenyz(i,m-
1,k))/h2
$ -0.041666667*difyzy(i,m,k)
end do
end do

beta(m)=0

do k=1,r
do i=1,n
gama(i,m,k)=0
end do
end do

do k1=2,m-1
j=m-k1+1
beta(j)=b(j)/(a(j)-c(j)*beta(j+1))
do k=1,r
do i=1,n

gama(i,j,k)=(d(i,j,k)+c(j)*gama(i,j+1,k))/(a(j)-
c(j)*beta(j+1))
end do
end do
end do

do i=1,n
do j=2,m-1
do k=1,r
difyzy(i,j,k)=beta(j)*difyzy(i,j-
1,k)+gama(i,j,k)
end do
end do
end do

do i=1,n+1
a(i)=0.0
b(i)=0.0
c(i)=0.0
beta(i)=0.0
do j=1,m
do k=1,r+1
gama(i,j,k)=0.0
d(i,j,k)=0.0
enddo
enddo
enddo
c difyzz-----
do i=1,n
do j=1,m
difyzz(i,j,1)=(ssenyz(i,j,2)-ssenyz(i,j,1))/h3
difyzz(i,j,r-1)=(ssenyz(i,j,r)-ssenyz(i,j,r-
1))/h3
end do
end do

b(2)=0
a(2)=0.416666667
c(2)=-0.0416666667

do i=1,n
do j=1,m
d(i,j,2)=(ssenyz(i,j,3)-ssenyz(i,j,2))/h3
$ -0.041666667*difyzz(i,j,1)
end do
end do

do k=3,r-3
b(k)=-0.0416666667
a(k)=0.416666667

```



```

c(k)=-0.0416666667
do i=1,n
do j=1,m
d(i,j,k)=(ssenyz(i,j,k+1)-ssenyz(i,j,k))/h3
end do
end do
end do

b(r-2)=-0.0416666667
a(r-2)=-0.416666667
c(r-2)=0.0

do i=1,n
do j=1,m
d(i,j,r-2)=(ssenyz(i,j,r-1)-ssenyz(i,j,r-2))/h3
$ -0.041666667*difyzz(i,j,r-1)
end do
end do

beta(r-1)=0

do i=1,n
do j=1,m
gama(i,j,r-1)=0
end do
end do

do k1=3,r-1
k=r-k1+1
beta(k)=b(k)/(a(k)-c(k)*beta(k+1))
do i=1,n
do j=1,m

gama(i,j,k)=(d(i,j,k)+c(k)*gama(i,j,k+1))/(a(k)-
c(k)*beta(k+1))
end do
end do
end do

do i=1,n
do j=1,m
do k=2,r-2
difyzz(i,j,k)=beta(k)*difyzz(i,j,k-
1)+gama(i,j,k)
end do
end do
end do

do i=1,n+1
a(i)=0.0
b(i)=0.0
c(i)=0.0
beta(i)=0.0
do j=1,m
do k=1,r+1
gama(i,j,k)=0.0

```

```

d(i,j,k)=0.0
enddo
enddo
enddo

c
c Calculate velocity
c
c
call
velocity(n,m,r,h1,h2,h3,dt,x,y,z,eto,etn,xseo,yseo,
$ zseo,sseoxy,sseoxz,sseozy,
$ xsen,ysen,zsen,ssenxy,ssenxz,ssenyzy,
$ v1o,v2o,v3o,v1n,v2n,v3n,u1o,u2o,u3o,
$
u1n,u2n,u3n,difx,dify,difz,difxyx,difxyy,difxzx,
difxzz,
$ difyzy,difyzz)

c
c Calculate strain
c
c
do k=2,r
do j=1,m
do i=2,n
xsan(i,j,k)=((v1n(i,j,k)-v1n(i-1,j,k))/h1)
$ *dt+xsao(i,j,k)
c
zsan(i,j,k)=((v1n(i,j,k)+v1n(i-
1,j,k))/2+(v3n(i,j,k)
$ -v3n(i,j,k-1))/h3)*dt/x(i)+zsao(i,j,k)

if (j.eq.1) then
ysan(i,j,k)=((v2n(i,j,k)-
v2n(i,m,k))/h2+(v1n(i,j,k)
$ +v1n(i-
1,j,k))*sin(z(k))/2+(v3n(i,j,k)+v3n(i,j,k-1))
$ *dt/(x(i)*sin(z(k)))+ysao(i,j,k)
else
ysan(i,j,k)=((v2n(i,j,k)-v2n(i,j-
1,k))/h2+(v1n(i,j,k)
$ +(v3n(i,j,k)+v3n(i,j,k-1))
$
*(cos(z(k)))/2)*dt/(x(i)*sin(z(k)))+ysao(i,j,k)

endif
end do
end do
end do

c
c Shear strain
c
do k=2,r
do j=1,m
do i=2,n-1

```



```

lto(i,j,k)=ltn(i,j,k)
xsao(i,j,k)=xsan(i,j,k)
ysao(i,j,k)=ysan(i,j,k)
zsao(i,j,k)=zsan(i,j,k)
ssaoxy(i,j,k)=ssanxy(i,j,k)
ssaoxz(i,j,k)=ssanxz(i,j,k)
ssaoyz(i,j,k)=ssanyz(i,j,k)
xseo(i,j,k)=xsen(i,j,k)
yseo(i,j,k)=ysen(i,j,k)
zseo(i,j,k)=zsen(i,j,k)
sseoxy(i,j,k)=ssenxy(i,j,k)
sseoxy(i,j,k)=ssenxy(i,j,k)
sseoxy(i,j,k)=ssenxy(i,j,k)
v1o(i,j,k)=v1n(i,j,k)
v2o(i,j,k)=v2n(i,j,k)
v3o(i,j,k)=v3n(i,j,k)
u1o(i,j,k)=u1n(i,j,k)
u2o(i,j,k)=u2n(i,j,k)
v3o(i,j,k)=v3n(i,j,k)
end do
end do
end do

etm(k)=etn(61,1,1)
etm1(k)=etn(61,1,21)
ltm(k)=ltn(61,1,1)
ltm1(k)=ltn(61,1,21)
u1m(k)=u1n(31,1,1)
u2m(k)=u2n(31,1,1)
u3m(k)=u3n(31,1,1)

c
c Output intermediate result
c
c
write(62,1020) t2(k), etm(k)
open(unit=71,file='etm2.txt')
write(71,1020) etm(k)
open(unit=8,file='tk.txt')
write(8,1020) t2(k)
open(unit=9,file='ltm2.txt')
write(9,1020) ltm(k)
open(unit=10,file='ltm.txt')
write(10,1020) t2(k), ltm(k)
open(unit=11,file='uu1n.txt')
write(11,1020) t2(k),u1m(k)
open(unit=12,file='uu2n.txt')
write(12,1020) t2(k),u2m(k)
open(unit=13,file='uu3n.txt')
write(13,1020) t2(k),u3m(k)

c the result at time t=15ps
c
c
if (k.eq.3000) then
open(unit=14,file='1etn15.txt')
do i=1,61
write(14,1010) x1(i),etn(i,1,1)
enddo

open(unit=15,file='2etn15.txt')
do i=1,61
write(15,1010) x2(i),etn(i,1,21)
enddo

open(unit=16,file='1ltn15.txt')
do i=1,61
write(16,1010) x1(i),ltn(i,1,1)
enddo

open(unit=17,file='2ltn15.txt')
do i=1,61
write(17,1010) x2(i),ltn(i,1,21)
enddo

open(unit=18,file='1u1n15.txt')
do i=1,60
write(18,1010) x1(i),u1n(i,1,1)
enddo

open(unit=19,file='2u1n15.txt')
do i=1,60
write(19,1010) x2(i),u1n(i,1,21)
enddo

open(unit=20,file='1u2n15.txt')
do i=1,61
write(20,1010) x1(i),u2n(i,1,1)
enddo

open(unit=21,file='2u2n15.txt')
do i=1,61
write(21,1010) x2(i),u2n(i,1,21)
enddo

open(unit=22,file='1u3n15.txt')
do i=1,61
write(22,1010) x1(i),u3n(i,1,2)
enddo

open(unit=23,file='2u3n15.txt')
do i=1,61
write(23,1010) x2(i),u3n(i,1,20)
enddo

```

```

open(unit=24,file='1xsen15.txt')

do i=1,61
write(24,1010) x1(i),xsen(i,1,1)
enddo

open(unit=25,file='2xsen15.txt')
do i=1,61
write(25,1010) x2(i),xsen(i,1,21)
enddo

open(unit=26,file='1ysen15.txt')

do i=1,61
write(26,1010) x1(i),ysen(i,1,1)
enddo

open(unit=27,file='2ysen15.txt')
do i=1,61
write(27,1010) x2(i),ysen(i,1,21)
enddo

open(unit=28,file='1zsen15.txt')

do i=1,61
write(28,1010) x1(i),zsen(i,1,1)
enddo

open(unit=29,file='2zsen15.txt')
do i=1,61
write(29,1010) x2(i),zsen(i,1,21)
enddo

open(unit=30,file='etn15.txt')

do k=1,21
write(30,1010) (etn(i,1,k),i=1,n+1)
enddo

c
open(unit=31,file='ltn15.txt')

do k=1,21
write(31,1010) (ltn(i,1,k),i=1,n+1)
enddo

open(unit=32,file='u1n15.txt')
do k=1,21
write(32,1010) (u1n(i,1,k),i=1,n)
enddo

open(unit=33,file='u2n15.txt')
do k=1,21
write(33,1010) (u2n(i,1,k),i=1,n+1)
enddo

open(unit=34,file='u3n15.txt')
do k=1,21
write(34,1010) (u3n(i,1,k),i=1,n+1)
enddo

c
open(unit=35,file='xsen15.txt')

do k=1,21
write(35,1010) (xsen(i,1,k),i=1,n+1)
enddo

open(unit=36,file='ysen15.txt')

do k=1,21
write(36,1010) (ysen(i,1,k),i=1,n+1)
enddo

open(unit=37,file='zsen15.txt')

do k=1,21
write(37,1010) (zsen(i,1,k),i=1,n+1)
enddo

c
end if

c the result at time t=20ps
c
c
if (k.eq.4000) then
open(unit=38,file='1etn20.txt')

do i=1,61
write(38,1010) x1(i),etn(i,1,1)
enddo

open(unit=39,file='2etn20.txt')
do i=1,61
write(39,1010) x2(i),etn(i,1,21)
enddo

open(unit=40,file='1ltn20.txt')

do i=1,61
write(40,1010) x1(i),ltn(i,1,1)
enddo

open(unit=41,file='2ltn20.txt')

do i=1,61
write(41,1010) x2(i),ltn(i,1,21)
enddo

open(unit=42,file='1u1n20.txt')

do i=1,60

```

```

write(42,1010) x1(i),u1n(i,1,1)
enddo

open(unit=43,file='2u1n20.txt')
do i=1,60
write(43,1010) x2(i),u1n(i,1,21)
enddo

open(unit=44,file='1u2n20.txt')

do i=1,61
write(44,1010) x1(i),u2n(i,1,1)
enddo

open(unit=45,file='2u2n20.txt')
do i=1,61
write(45,1010) x2(i),u2n(i,1,21)
enddo

open(unit=46,file='1u3n20.txt')

do i=1,61
write(46,1010) x1(i),u3n(i,1,2)
enddo

open(unit=47,file='2u3n20.txt')
do i=1,61
write(47,1010) x2(i),u3n(i,1,20)
enddo

open(unit=48,file='1xsen20.txt')

do i=1,61
write(48,1010) x1(i),xsen(i,1,1)
enddo

open(unit=49,file='2xsen20.txt')
do i=1,61
write(49,1010) x2(i),xsen(i,1,21)
enddo

open(unit=64,file='1xsan20.txt')

do i=1,61
write(64,1010) x1(i),xsan(i,1,1)
enddo

open(unit=65,file='2xsan20.txt')
do i=1,61
write(65,1010) x2(i),xsan(i,1,21)
enddo

open(unit=50,file='1ysen20.txt')

do i=1,61
write(50,1010) x1(i),ysen(i,1,1)
enddo

open(unit=51,file='2ysen20.txt')
do i=1,61
write(51,1010) x2(i),ysen(i,1,21)
enddo

open(unit=52,file='1zsen20.txt')

do i=1,61
write(52,1010) x1(i),zsen(i,1,1)
enddo

open(unit=53,file='2zsen20.txt')
do i=1,61
write(53,1010) x2(i),zsen(i,1,21)
enddo

open(unit=54,file='etn20.txt')

do k=1,21
write(54,1010) (etn(i,1,k),i=1,n+1)
enddo

c
open(unit=55,file='ltn20.txt')

do k=1,21
write(55,1010) (ltn(i,1,k),i=1,n+1)
enddo

open(unit=56,file='u1n20.txt')
do k=1,21
write(56,1010) (u1n(i,1,k),i=1,n)
enddo

open(unit=57,file='u2n20.txt')
do k=1,21
write(57,1010) (u2n(i,1,k),i=1,n+1)
enddo

open(unit=58,file='u3n20.txt')
do k=1,21
write(58,1010) (u3n(i,1,k),i=1,n+1)
enddo

c
open(unit=59,file='xsen20.txt')

do k=1,21
write(59,1010) (xsen(i,1,k),i=1,n+1)
enddo

open(unit=60,file='ysen20.txt')

```

```

do k=1,21
write(60,1010) (ysen(i,1,k),i=1,n+1)
enddo

open(unit=61,file='zsen20.txt')

do k=1,21
write(61,1010) (zsen(i,1,k),i=1,n+1)
enddo
c
end if
c

1 end do

c
1010 format(401e15.6)
1020 format(e15.6,2e15.6)
c
end

subroutine
temp(n,m,r,lx,h1,h2,h3,x,y,z,t,dt,lto,ltn,eto,etn,
$ xsan,ysan,zsan,xsao,ysao,zsao)
c
implicit double precision (a-h,l,o-z)
dimension x(150),y(200),z(400)
dimension
eto(150,50,50),etn(150,50,50),lto(150,50,50),
$ ltn(150,50,50),etnmax(150,50,50),
$
ewetn(150,50,50),oldet(150,50,50),oldlt(150,50,
50),
$
xsan(151,51,51),ysan(151,51,51),zsan(151,51,51
),
$
xsao(151,51,51),ysao(151,51,51),zsao(151,51,51)
integer iteration,l,r
c
c
c Lame constant
lemta=199.0d+9
c Shear modulus
cmiu=27.0d+9
c Thermal expansion coefficient
alphan=14.2d-6
c Electron heat capacity
ce0=2.1d+4
c Lattice heat capacity
cl=2.5d+6
c Electron - lattice coupling factor
g=2.6d+16
c Electron thermal conductivity
cke0=315.0
c Laser fluence
flu=500.0
c Laser pulse duration
tp=0.1d-12
c Optical penetration depth
delta=15.3d-9
c Surface reflectivity
sur=0.93
c
iteration=0
d=g*dt/(2.0*cl)
ee=(3.0*lemta+2.0*cmiu)*alphan/cl
c

do k=1,r+1
do j=1,m
do i=1,n+1
oldet(i,j,k)=eto(i,j,k)
oldlt(i,j,k)=lto(i,j,k)
end do
end do
end do

c

tol=1e-3
detmax=tol+0.001
do while (detmax.gt.tol)
c
detmax=0.0

do k=2,r
do j=1,m
do i=2,n

q=0.94*flu*(1.0-sur)/(tp*delta)
$ *exp(-(lx-x(i))/delta)
$ -2.77*(t-2.0*tp)*(t-
2.0*tp)/(tp*tp))*abs(cos(z(k)))

if (k.le.6) then
if (j.eq.1) then
a=ce0*(eto(i,j,k)+oldet(i,j,k))/(2.0*300.0)
b1=cke0*((oldet(i+1,j,k)+oldet(i,j,k))/(oldlt(i+1,j
,k)
$
+oldlt(i,j,k)))/(2.0*h1*h1*x(i)*x(i))*dt*(x(i)+h1/
2)*(x(i)+h1/2)
b2=cke0*((oldet(i-1,j,k)+oldet(i,j,k))/(oldlt(i-
1,j,k)
$
+oldlt(i,j,k)))/(2.0*h1*h1*x(i)*x(i))*dt*(x(i)-
h1/2)*(x(i)-h1/2)
b3=cke0*((oldet(i,j+1,k)+oldet(i,j,k))/(oldlt(i,j+1
,k)

```

```

$ +oldlt(i,j,k))
/(2.0*h2*h2*x(i)*x(i)*sin(z(k))*sin(z(k)))*dt
b4=cke0*((oldet(i,j,k)+oldet(i,m,k))/(oldlt(i,j,k)
$
+oldlt(i,m,k)))/(2.0*h2*h2*x(i)*x(i)*sin(z(k))*si
n(z(k)))*dt
c
c1=cke0*((eto(i+1,j,k)+eto(i,j,k))/(lto(i+1,j,k)
$
+lto(i,j,k)))/(2.0*h1*h1*x(i)*x(i))*dt*(x(i)+h1/2
)*(x(i)+h1/2)
c2=cke0*((eto(i-1,j,k)+eto(i,j,k))/(lto(i-1,j,k)
$
+lto(i,j,k)))/(2.0*h1*h1*x(i)*x(i))*dt*(x(i)-
h1/2)*(x(i)-h1/2)
c3=cke0*((eto(i,j+1,k)+eto(i,j,k))/(lto(i,j+1,k)
$
+lto(i,j,k))
/(2.0*h2*h2*x(i)*x(i)*sin(z(k))*sin(z(k)))*dt
c4=cke0*((eto(i,j,k)+eto(i,m,k))/(lto(i,j,k)
$
+lto(i,m,k)))/(2.0*h2*h2*x(i)*x(i)*sin(z(k))*sin(
z(k)))*dt
ewetn(i,j,k)=(b1*oldet(i+1,j,k)+b2*oldet(i-
1,j,k)
$
+b3*oldet(i,j+1,k)+b4*oldet(i,m,k)
$
+b5*oldet(i,j,k+1)+b6*oldet(i,j,k-1)
$
+g*d*dt*(eto(i,j,k)-lto(i,j,k))/(2.0*(1.0+d))
$
+g*dt*lto(i,j,k)/(2.0*(1.0+d))
$
-((xsan(i,j,k)+ysan(i,j,k)+zsan(i,j,k))
$
-(xsao(i,j,k)+ysao(i,j,k)+zsao(i,j,k)))
$
/(2.0*(1.0+d))
$
+c1*(eto(i+1,j,k)-eto(i,j,k))-c2*(eto(i,j,k)-
eto(i-1,j,k))
$
+c3*(eto(i,j+1,k)-eto(i,j,k))-c4*(eto(i,j,k)-
eto(i,m,k))
$
+c5*(eto(i,j,k+1)-eto(i,j,k))-c6*(eto(i,j,k)-
eto(i,j,k-1))
$
-g*dt*(eto(i,j,k)-
lto(i,j,k))/2.0+q*dt+a*eto(i,j,k)
$
/(a+b1+b2+b3+b4+b5+b6+g*dt/2.0-
g*dt*d/(2.0*(1.0+d)))
else if (j.eq.m) then
a=ce0*(eto(i,j,k)+oldet(i,j,k))/(2.0*300.0)
b1=cke0*((oldet(i+1,j,k)+oldet(i,j,k))/(oldlt(i+1,j
,k)
$
+oldlt(i,j,k)))/(2.0*h1*h1*x(i)*x(i))*dt*(x(i)+h1/
2)*(x(i)+h1/2)
b2=cke0*((oldet(i-1,j,k)+oldet(i,j,k))/(oldlt(i-
1,j,k)

```

```

$
+oldlt(i,j,k)))/(2.0*h1*h1*x(i)*x(i))*dt*(x(i)-
h1/2)*(x(i)-h1/2)
b3=cke0*((oldet(i,1,k)+oldet(i,j,k))/(oldlt(i,1,k)
$
+oldlt(i,j,k))
/(2.0*h2*h2*x(i)*x(i)*sin(z(k))*sin(z(k)))*dt
b4=cke0*((oldet(i,j,k)+oldet(i,j-
1,k))/(oldlt(i,j,k)
$
+oldlt(i,j-
1,k)))/(2.0*h2*h2*x(i)*x(i)*sin(z(k))*sin(z(k)))*
dt
c1=cke0*((eto(i+1,j,k)+eto(i,j,k))/(lto(i+1,j,k)
$
+lto(i,j,k)))/(2.0*h1*h1*x(i)*x(i))*dt*(x(i)+h1/2
)*(x(i)+h1/2)
c2=cke0*((eto(i-1,j,k)+eto(i,j,k))/(lto(i-1,j,k)
$
+lto(i,j,k)))/(2.0*h1*h1*x(i)*x(i))*dt*(x(i)-
h1/2)*(x(i)-h1/2)
c3=cke0*((eto(i,1,k)+eto(i,j,k))/(lto(i,1,k)
$
+lto(i,j,k))
/(2.0*h2*h2*x(i)*x(i)*sin(z(k))*sin(z(k)))*dt
c4=cke0*((eto(i,j,k)+eto(i,j-1,k))/(lto(i,j,k)
$
+lto(i,j-
1,k)))/(2.0*h2*h2*x(i)*x(i)*sin(z(k))*sin(z(k)))*
dt
ewetn(i,j,k)=(b1*oldet(i+1,j,k)+b2*oldet(i-
1,j,k)
$
+b3*oldet(i,1,k)+b4*oldet(i,j-1,k)
$
+b5*oldet(i,j,k+1)+b6*oldet(i,j,k-1)
$
+g*d*dt*(eto(i,j,k)-lto(i,j,k))/(2.0*(1.0+d))
$
+g*dt*lto(i,j,k)/(2.0*(1.0+d))
$
-((xsan(i,j,k)+ysan(i,j,k)+zsan(i,j,k))
$
-(xsao(i,j,k)+ysao(i,j,k)+zsao(i,j,k)))
$
/(2.0*(1.0+d))
$
+c1*(eto(i+1,j,k)-eto(i,j,k))-c2*(eto(i,j,k)-
eto(i-1,j,k))
$
+c3*(eto(i,1,k)-eto(i,j,k))-c4*(eto(i,j,k)-
eto(i,j-1,k))
$
+c5*(eto(i,j,k+1)-eto(i,j,k))-c6*(eto(i,j,k)-
eto(i,j,k-1))
$
-g*dt*(eto(i,j,k)-
lto(i,j,k))/2.0+q*dt+a*eto(i,j,k)
$
/(a+b1+b2+b3+b4+b5+b6+g*dt/2.0-
g*dt*d/(2.0*(1.0+d)))
else
a=ce0*(eto(i,j,k)+oldet(i,j,k))/(2.0*300.0)
b1=cke0*((oldet(i+1,j,k)+oldet(i,j,k))/(oldlt(i+1,j
,k)
$
+oldlt(i,j,k)))/(2.0*h1*h1*x(i)*x(i))*dt*(x(i)+h1/
2)*(x(i)+h1/2)

```

```

    b2=cke0*((oldet(i-1,j,k)+oldet(i,j,k))/(oldlt(i-
1,j,k)
    $
+oldlt(i,j,k)))/(2.0*h1*h1*x(i)*x(i))*dt*(x(i)-
h1/2)*(x(i)-h1/2)
    b3=cke0*((oldet(i,j+1,k)+oldet(i,j,k))/(oldlt(i,j+1
,k)
    $ +oldlt(i,j,k)))
/(2.0*h2*h2*x(i)*x(i)*sin(z(k))*sin(z(k)))*dt
    b4=cke0*((oldet(i,j,k)+oldet(i,j-
1,k))/(oldlt(i,j,k)
    $ +oldlt(i,j-
1,k)))/(2.0*h2*h2*x(i)*x(i)*sin(z(k))*sin(z(k)))*
dt
    c1=cke0*((eto(i+1,j,k)+eto(i,j,k))/(lto(i+1,j,k)
    $
+lto(i,j,k)))/(2.0*h1*h1*x(i)*x(i))*dt*(x(i)+h1/2
)*(x(i)+h1/2)
    c2=cke0*((eto(i-1,j,k)+eto(i,j,k))/(lto(i-1,j,k)
    $ +lto(i,j,k)))/(2.0*h1*h1*x(i)*x(i))*dt*(x(i)-
h1/2)*(x(i)-h1/2)
    c3=cke0*((eto(i,j+1,k)+eto(i,j,k))/(lto(i,j+1,k)
    $ +lto(i,j,k)))
/(2.0*h2*h2*x(i)*x(i)*sin(z(k))*sin(z(k)))*dt
    c4=cke0*((eto(i,j,k)+eto(i,j-1,k))/(lto(i,j,k)
    $ +lto(i,j-
1,k)))/(2.0*h2*h2*x(i)*x(i)*sin(z(k))*sin(z(k)))*
dt
    ewetn(i,j,k)=(b1*oldet(i+1,j,k)+b2*oldet(i-
1,j,k)
    $ +b3*oldet(i,j+1,k)+b4*oldet(i,j-1,k)
    $ +b5*oldet(i,j,k+1)+b6*oldet(i,j,k-1)
    $ +g*d*dt*(eto(i,j,k)-lto(i,j,k))/(2.0*(1.0+d))
    $ +g*dt*lto(i,j,k)/(2.0*(1.0+d))
    $ -
g*dt*ee*((xsan(i,j,k)+ysan(i,j,k)+zsan(i,j,k))
    $ -(xsao(i,j,k)+ysao(i,j,k)+zsao(i,j,k)))
    $ /(2.0*(1.0+d))
    $ +c1*(eto(i+1,j,k)-eto(i,j,k))-c2*(eto(i,j,k)-
eto(i-1,j,k))
    $ +c3*(eto(i,j+1,k)-eto(i,j,k))-c4*(eto(i,j,k)-
eto(i,j-1,k))
    $ +c5*(eto(i,j,k+1)-eto(i,j,k))-c6*(eto(i,j,k)-
eto(i,j,k-1))
    $ -g*dt*(eto(i,j,k)-
lto(i,j,k))/2.0+q*dt+a*eto(i,j,k)
    $ /(a+b1+b2+b3+b4+b5+b6+g*dt/2.0-
g*dt*d/(2.0*(1.0+d)))
c
    endif
    else
    if (j.eq.1) then
        a=ce0*(eto(i,j,k)+oldet(i,j,k))/(2.0*300.0

```

```

    b1=cke0*((oldet(i+1,j,k)+oldet(i,j,k))/(oldlt(i+1,j
,k)
    $
+oldlt(i,j,k)))/(2.0*h1*h1*x(i)*x(i))*dt*(x(i)+h1/2
)*(x(i)+h1/2)
    b2=cke0*((oldet(i-1,j,k)+oldet(i,j,k))/(oldlt(i-
1,j,k)
    $
+oldlt(i,j,k)))/(2.0*h1*h1*x(i)*x(i))*dt*(x(i)-
h1/2)*(x(i)-h1/2)
    b3=cke0*((oldet(i,j+1,k)+oldet(i,j,k))/(oldlt(i,j+1
,k)
    $ +oldlt(i,j,k)))
/(2.0*h2*h2*x(i)*x(i)*sin(z(k))*sin(z(k)))*dt
    b4=cke0*((oldet(i,j,k)+oldet(i,m,k))/(oldlt(i,j,k)
    $
+oldlt(i,m,k)))/(2.0*h2*h2*x(i)*x(i)*sin(z(k))*si
n(z(k)))*dt
    c1=cke0*((eto(i+1,j,k)+eto(i,j,k))/(lto(i+1,j,k)
    $
+lto(i,j,k)))/(2.0*h1*h1*x(i)*x(i))*dt*(x(i)+h1/2
)*(x(i)+h1/2)
    c2=cke0*((eto(i-1,j,k)+eto(i,j,k))/(lto(i-1,j,k)
    $ +lto(i,j,k)))/(2.0*h1*h1*x(i)*x(i))*dt*(x(i)-
h1/2)*(x(i)-h1/2)
    c3=cke0*((eto(i,j+1,k)+eto(i,j,k))/(lto(i,j+1,k)
    $ +lto(i,j,k)))
/(2.0*h2*h2*x(i)*x(i)*sin(z(k))*sin(z(k)))*dt
    c4=cke0*((eto(i,j,k)+eto(i,m,k))/(lto(i,j,k)
    $
+lto(i,m,k)))/(2.0*h2*h2*x(i)*x(i)*sin(z(k))*sin(
z(k)))*dt
    c5=cke0*((eto(i,j,k+1)+eto(i,j,k))/(lto(i,j,k+1)
    $
+lto(i,j,k)))/(2.0*h3*h3*x(i)*x(i)*sin(z(k)))*dt*s
in(z(k)+h3/2)
    c6=cke0*((eto(i,j,k-1)+eto(i,j,k))/(lto(i,j,k-1)
    $
+lto(i,j,k)))/(2.0*h3*h3*x(i)*x(i)*sin(z(k)))*dt*s
in(z(k)-h3/2)
    ewetn(i,j,k)=(b1*oldet(i+1,j,k)+b2*oldet(i-
1,j,k)
    $ +b3*oldet(i,j+1,k)+b4*oldet(i,m,k)
    $ +b5*oldet(i,j,k+1)+b6*oldet(i,j,k-1)
    $ +g*d*dt*(eto(i,j,k)-lto(i,j,k))/(2.0*(1.0+d))
    $ +g*dt*lto(i,j,k)/(2.0*(1.0+d))
    $ -
g*dt*ee*((xsan(i,j,k)+ysan(i,j,k)+zsan(i,j,k))
    $ -(xsao(i,j,k)+ysao(i,j,k)+zsao(i,j,k)))
    $ /(2.0*(1.0+d))
    $ +c1*(eto(i+1,j,k)-eto(i,j,k))-c2*(eto(i,j,k)-
eto(i-1,j,k))

```



```

$ +c3*(eto(i,j+1,k)-eto(i,j,k))-c4*(eto(i,j,k)-
eto(i,m,k))
$ +c5*(eto(i,j,k+1)-eto(i,j,k))-c6*(eto(i,j,k)-
eto(i,j,k-1))
$ -g*dt*(eto(i,j,k)-lto(i,j,k))/2.0+a*eto(i,j,k)
$ /(a+b1+b2+b3+b4+b5+b6+g*dt/2.0-
g*dt*d/(2.0*(1.0+d)))

```

```

else if (j.eq.m) then
  a=ce0*(eto(i,j,k)+oldet(i,j,k))/(2.0*300.0)

```

```

b1=cke0*((oldet(i+1,j,k)+oldet(i,j,k))/(oldlt(i+1,j,
k)

```

```

$
+oldlt(i,j,k))/(2.0*h1*h1*x(i)*x(i))*dt*(x(i)+h1/
2)*(x(i)+h1/2)

```

```

  b2=cke0*((oldet(i-1,j,k)+oldet(i,j,k))/(oldlt(i-
1,j,k)

```

```

$
+oldlt(i,j,k))/(2.0*h1*h1*x(i)*x(i))*dt*(x(i)-
h1/2)*(x(i)-h1/2)

```

```

b3=cke0*((oldet(i,1,k)+oldet(i,j,k))/(oldlt(i,1,k)

```

```

$ +oldlt(i,j,k))
/(2.0*h2*h2*x(i)*x(i)*sin(z(k))*sin(z(k)))*dt

```

```

  b4=cke0*((oldet(i,j,k)+oldet(i,j-
1,k))/(oldlt(i,j,k)

```

```

$ +oldlt(i,j-
1,k))/(2.0*h2*h2*x(i)*x(i)*sin(z(k))*sin(z(k)))*
dt

```

```

  c1=cke0*((eto(i+1,j,k)+eto(i,j,k))/(lto(i+1,j,k)
$

```

```

+lto(i,j,k))/(2.0*h1*h1*x(i)*x(i))*dt*(x(i)+h1/2
)*(x(i)+h1/2)

```

```

  c2=cke0*((eto(i-1,j,k)+eto(i,j,k))/(lto(i-1,j,k)
$ +lto(i,j,k))/(2.0*h1*h1*x(i)*x(i))*dt*(x(i)-
h1/2)*(x(i)-h1/2)

```

```

  c3=cke0*((eto(i,1,k)+eto(i,j,k))/(lto(i,1,k)
$ +lto(i,j,k))

```

```

/(2.0*h2*h2*x(i)*x(i)*sin(z(k))*sin(z(k)))*dt

```

```

  c4=cke0*((eto(i,j,k)+eto(i,j-1,k))/(lto(i,j,k)
$ +lto(i,j-

```

```

1,k))/(2.0*h2*h2*x(i)*x(i)*sin(z(k))*sin(z(k)))*
dt

```

```

  ewetn(i,j,k)=(b1*oldet(i+1,j,k)+b2*oldet(i-
1,j,k)

```

```

$ +b3*oldet(i,1,k)+b4*oldet(i,j-1,k)

```

```

$ +b5*oldet(i,j,k+1)+b6*oldet(i,j,k-1)

```

```

$ +g*d*dt*(eto(i,j,k)-lto(i,j,k))/(2.0*(1.0+d))

```

```

$ +g*dt*lto(i,j,k)/(2.0*(1.0+d))

```

```

$ -

```

```

g*dt*ee*((xsan(i,j,k)+ysan(i,j,k)+zsan(i,j,k))

```

```

$ -(xsao(i,j,k)+ysao(i,j,k)+zsao(i,j,k))

```

```

$ /(2.0*(1.0+d))

```

```

$ +c1*(eto(i+1,j,k)-eto(i,j,k))-c2*(eto(i,j,k)-
eto(i-1,j,k))

```

```

$ +c3*(eto(i,1,k)-eto(i,j,k))-c4*(eto(i,j,k)-
eto(i,j-1,k))

```

```

$ +c5*(eto(i,j,k+1)-eto(i,j,k))-c6*(eto(i,j,k)-
eto(i,j,k-1))

```

```

$ -g*dt*(eto(i,j,k)-lto(i,j,k))/2.0+a*eto(i,j,k)

```

```

$ /(a+b1+b2+b3+b4+b5+b6+g*dt/2.0-

```

```

g*dt*d/(2.0*(1.0+d)))

```

```

else

```

```

  a=ce0*(eto(i,j,k)+oldet(i,j,k))/(2.0*300.0)

```

```

b1=cke0*((oldet(i+1,j,k)+oldet(i,j,k))/(oldlt(i+1,j,
k)

```

```

$
+oldlt(i,j,k))/(2.0*h1*h1*x(i)*x(i))*dt*(x(i)+h1/
2)*(x(i)+h1/2)

```

```

  b2=cke0*((oldet(i-1,j,k)+oldet(i,j,k))/(oldlt(i-
1,j,k)

```

```

$
+oldlt(i,j,k))/(2.0*h1*h1*x(i)*x(i))*dt*(x(i)-
h1/2)*(x(i)-h1/2)

```

```

b3=cke0*((oldet(i,j+1,k)+oldet(i,j,k))/(oldlt(i,j+1,
k)

```

```

$ +oldlt(i,j,k))
/(2.0*h2*h2*x(i)*x(i)*sin(z(k))*sin(z(k)))*dt

```

```

  b4=cke0*((oldet(i,j,k)+oldet(i,j-
1,k))/(oldlt(i,j,k)

```

```

$ +oldlt(i,j-
1,k))/(2.0*h2*h2*x(i)*x(i)*sin(z(k))*sin(z(k)))*
dt

```

```

  c1=cke0*((eto(i+1,j,k)+eto(i,j,k))/(lto(i+1,j,k)
$

```

```

+lto(i,j,k))/(2.0*h1*h1*x(i)*x(i))*dt*(x(i)+h1/2
)*(x(i)+h1/2)

```

```

  c2=cke0*((eto(i-1,j,k)+eto(i,j,k))/(lto(i-1,j,k)
$ +lto(i,j,k))/(2.0*h1*h1*x(i)*x(i))*dt*(x(i)-
h1/2)*(x(i)-h1/2)

```

```

  c3=cke0*((eto(i,j+1,k)+eto(i,j,k))/(lto(i,j+1,k)
$ +lto(i,j,k))

```

```

/(2.0*h2*h2*x(i)*x(i)*sin(z(k))*sin(z(k)))*dt

```

```

  c4=cke0*((eto(i,j,k)+eto(i,j-1,k))/(lto(i,j,k)
$ +lto(i,j-

```

```

1,k))/(2.0*h2*h2*x(i)*x(i)*sin(z(k))*sin(z(k)))*
dt

```

```

  ewetn(i,j,k)=(b1*oldet(i+1,j,k)+b2*oldet(i-
1,j,k)

```

```

$ +b3*oldet(i,j+1,k)+b4*oldet(i,j-1,k)

```

```

$ +b5*oldet(i,j,k+1)+b6*oldet(i,j,k-1)

```

```

$ +g*d*dt*(eto(i,j,k)-lto(i,j,k))/(2.0*(1.0+d))

```

```

$ +g*dt*lto(i,j,k)/(2.0*(1.0+d))

```

```

$ -

```

```

g*dt*ee*((xsan(i,j,k)+ysan(i,j,k)+zsan(i,j,k))

```

```

$ -(xsao(i,j,k)+ysao(i,j,k)+zsao(i,j,k))

```

```

$ /(2.0*(1.0+d))

```



```

dimension x(150),y(200),z(400)
dimension eto(150,50,50),etn(150,50,50),
$
xseo(151,51,51),yseo(151,51,51),zseo(151,51,51
),
$
sseoxy(151,51,51),sseoxz(151,51,51),sseoyz(151
,51,51),
$
xsen(151,51,51),ysen(151,51,51),zsen(151,51,51
),
$
ssenxy(151,51,51),ssenxz(151,51,51),ssenyz(151
,51,51),
$
v1o(151,51,51),v2o(151,51,51),v3o(151,51,51),
$
v1n(151,51,51),v2n(151,51,51),v3n(151,51,51),
$
u1o(151,51,51),u2o(151,51,51),u3o(151,51,51),
$
u1n(151,51,51),u2n(151,51,51),u3n(151,51,51),
$
difx(151,51,51),dify(151,51,51),difz(151,51,51),
$
difxyx(151,51,51),difxyy(151,51,51),difxzx(151,
51,51),
$
difxzz(151,51,51),difzyz(151,51,51),difyzz(151,
51,51)
c
integer l,r
c Density
lou=1.93d+4
c Electron - blast coefficient
tri=70

do k=2,r
do j=1,m
do i=1,n
if (j.eq.1) then
v1n(i,j,k)= dt*difx(i,j,k)
$ /(lou)+dt*difxzz(i,j,k-1)
$ /(lou*(x(i)+h1/2))+dt*difxyy(i,m,k)
$
/(lou*(x(i)+h1/2)*sin(z(k)))+dt*((xsen(i,j,k)+xse
n(i+1,j,k))
$ -(ysen(i,j,k)+ysen(i+1,j,k))/2-
(zsen(i,j,k)+zsen(i+1,j,k))/2
$ +(ssenxz(i,j,k)+ssenxz(i,j,k-
1))*(cos(z(k)))/(2*sin(z(k))))
$
/(lou*(x(i)+h1/2))+dt*tri*(etn(i+1,j,k)*etn(i+1,j,
k)
$ -etn(i,j,k)*etn(i,j,k))/(lou*h1)
else
v1n(i,j,k)= dt*difx(i,j,k)
$ /(lou)+dt*difxzz(i,j,k-1)
$ /(lou*(x(i)+h1/2))+dt*difxyy(i,j-1,k)
$
/(lou*(x(i)+h1/2)*sin(z(k)))+dt*((xsen(i,j,k)+xse
n(i+1,j,k))
$ -(ysen(i,j,k)+ysen(i+1,j,k))/2-
(zsen(i,j,k)+zsen(i+1,j,k))/2
$ +(ssenxz(i,j,k)+ssenxz(i,j,k-
1))*(cos(z(k)))/(2*sin(z(k))))
$
/(lou*(x(i)+h1/2))+dt*tri*(etn(i+1,j,k)*etn(i+1,j,
k)
$ -etn(i,j,k)*etn(i,j,k))/(lou*h1)
endif

u1n(i,j,k)=v1n(i,j,k)*dt+u1o(i,j,k)
end do
end do
end do

do i=2,n
do j=1,m
do k=1,r
if (j.eq.1) then
v3n(i,j,k)= dt*difxzx(i-1,j,k)
$ /(lou)+dt*difz(i,j,k)
$ /(lou*x(i))+dt*difyzy(i,m,k)
$
/(lou*x(i)*sin(z(k)+h3/2))+dt*((zsen(i,j,k+1)
$ +zsen(i,j,k))/2-(ysen(i,j,k+1)+ysen(i,j,k))/2)
$
*(cos(z(k)+h3/2))/sin(z(k)+h3/2)+3*(ssenxz(i-
1,j,k))/2)/(lou*x(i))+dt*tri*(etn(i,j,k+1)
$ *etn(i,j,k+1)-
etn(i,j,k)*etn(i,j,k))/(lou*h3*x(i))
else
v3n(i,j,k)= dt*difxzx(i-1,j,k)
$ /(lou)+dt*difz(i,j,k)
$ /(lou*x(i))+dt*difyzy(i,j-1,k)
$
/(lou*x(i)*sin(z(k)+h3/2))+dt*((zsen(i,j,k+1)
$ +zsen(i,j,k))/2-(ysen(i,j,k+1)+ysen(i,j,k))/2)
$
*(cos(z(k)+h3/2))/sin(z(k)+h3/2)+3*(ssenxz(i,j,k)
$ +ssenxz(i-
1,j,k))/2)/(lou*x(i))+dt*tri*(etn(i,j,k+1)
$ *etn(i,j,k+1)-
etn(i,j,k)*etn(i,j,k))/(lou*h3*x(i))
endif

u3n(i,j,k)=v3n(i,j,k)*dt+u3o(i,j,k)
end do
end do
end do

```

```

do k=2,r
do i=2,n
do j=1,m
  if (j.eq.m) then
v2n(i,j,k)= dt*difxyx(i-1,j,k)
$ /(lou)+dt*difyzz(i,j,k-1)
$ /( dt*dify(i,j,k)
$ /(lou*x(i)*sin(z(k)))+dt*((ssenyz(i,j,k)
$ +ssenyz(i,j,k-1))*(cos(z(k)))
3*(ssenxy(i,j,k)
$ +ssenxy(i-1,j,k))/2)/(dt*tri*(etn(i,1,k)
$ *etn(i,1,k)-
etn(i,j,k)*etn(i,j,k))/(lou*h2*x(i)*sin(z(k)))

  else
v2n(i,j,k)=dt*difxyx(i-1,j,k)
$ /(lou)+dt*difyzz(i,j,k-1)
$ /(dt*dify(i,j,k)
$ /(lou*x(i)*sin(z(k)))+dt*((ssenyz(i,j,k)
$ +ssenyz(i,j,k-1))*(cos(z(k)))
3*(ssenxy(i,j,k)
$ +ssenxy(i-1,j,k))/2)/(dt*tri*(etn(i,j+1,k)
$ *etn(i,j+1,k)-
etn(i,j,k)*etn(i,j,k))/(lou*h2*x(i)*sin(z(k)))
  endif

u2n(i,j,k)=v2n(i,j,k)*dt+u2o(i,j,k)
end do
end do
end do

c
return
end

```

## REFERENCES

- [Al-Nimr 1997a] M.A. Al-Nimr, S. Masoud, Non-equilibrium laser heating of metal films, *ASME Journal of Heat Transfer*, 119 (1997) 188-190.
- [Al-Nimr 1997b] M.A. Al-Nimr, Heat transfer mechanisms during laser heating of thin metal films, *International Journal of Thermophysics*, 18 (1997) 1257-1268.
- [Al-Nimr 1999] M.A. Al-Nimr, V.S. Arpaci, Picosecond thermal pulses in thin metal films, *Journal of applied physics*, 85 (1999) 2517-2521.
- [Al-Nimr 2000a] M.A. Al-Nimr, V.S. Arpaci, The thermal behavior of thin metal films in the hyperbolic two-step model, *International Journal of Heat and Mass Transfer*, 43 (2000) 2021-2028.
- [Al-Nimr 2000b] M.A. Al-Nimr, M. Naji, On the phase-lag effect on the non-equilibrium entropy production, *Microscale Thermophysics Engineering*, 4 (2000) 231-243.
- [Al-Nimr 2000c] M.A. Al-Nimr, M. Naji, V.S. Arpaci, Non-equilibrium entropy production under the effect of the dual-phase-lag heat conduction model, *ASME Journal of Heat Transfer*, 122 (2000) 217-222.
- [Al-Nimr 2001] M.A. Al-Nimr, S. Kiwan, Effect of thermal losses on the microscopic two-step heat conduction model, *International Journal of Heat and Mass Transfer*, 44 (2001) 1013-1018.
- [Al-Nimr 2003] M.A. Al-Nimr, M. Header, M. Naji, Use of the microscopic parabolic heat conduction model in place of macroscopic model validation criterion under harmonic boundary heating, *International Journal of Heat and Mass Transfer*, 46 (2003) 333-339.
- [Antaki 1998] P.J. Antaki, Solution for non-Fourier dual phase lag heat conduction in a semi-infinite slab with surface heat flux, *International Journal of Heat and Mass Transfer*, 41 (1998) 2253-2258.
- [Antaki 2000] P.J. Antaki, Effect of dual-phase-lag heat conduction on ignition of a solid, *Journal of Thermophysics Heat Transfer*, 14 (2000) 276-278.

- [Antaki 2002] P.J. Antaki, Importance of nonequilibrium thermal conductivity on ignition of a solid, *International Journal of Heat and Mass Transfer*, 45 (2002) 4063-4067.
- [Barron 1985] R. Barron, *Cryogenic Systems*, second edition, Oxford Science Publications, New York, 1985.
- [Barron 2005] B.R. Barron, *A FE-FD hybrid scheme for solving parabolic two-step micro heat transport equation in irregular shaped three dimensional double-layered thin films exposed to ultrashort-pulse lasers*, Ph.D Dissertation, Louisiana Tech University, LA, 2005.
- [Barron 2006] B.R. Barron, W. Dai, A FE-FD hybrid scheme for solving parabolic two-step micro heat transport equations in an irregularly shaped three-dimensional double-layered thin film, *Numerical Heat Transfer, Part B*, 49 (2006) 437-465.
- [Brorson 1987] S.D. Brorson, J.G. Fujimoto, and E.P. Ippen, Femtosecond electron heat transfer dynamics in thin gold film, *Physical Review Letter*, 59 (1987) 1962-1965.
- [Bruno 1997] A.B. Bruno, H.W. Jerome, *Theory of thermal stresses*, New Education edition, Dover Publications, 1997.
- [Chen 1999a] J.K. Chen, J.E. Beraun, D.Y. Tzou, A dual-phase-lag diffusion model for interfacial layer growth in metal matrix composites, *Journal of Material Science*, 34 (1999) 6183-6187.
- [Chen 1999b] J.K. Chen, J.E. Beraun, T.C. Carney, A corrective smoothed particle method for boundary value problems in heat conduction, *International Journal of Numerical Methods in Engineering*, 46 (1999) 231-252.
- [Chen 2000a] J.K. Chen, J.E. Beraun, A generalized smoothed particle hydromechanics method for nonlinear dynamic problems, *Computational Methods in Applied Mechanical Engineering*, 190 (2000) 225-239.
- [Chen 2000b] J.K. Chen, J.E. Beraun, D.Y. Tzou, A dual-phase-lag diffusion model for predicting thin film growth, *Semiconductor Science Technology*, 15 (2000) 235-241.
- [Chen 2001] J.K. Chen, J.E. Beraun, Numerical study of ultrashort laser pulse interactions with metal films, *Numerical Heat Transfer, Part A*, 40 (2001) 1-20.
- [Chen 2002a] J.K. Chen, J.E. Beraun, and C.L. Tham, Comparison of one-dimensional and two-dimensional axisymmetric approaches to the thermomechanical response caused by ultrashort laser heating, *Journal of Optics A: Pure Applied Optics*, 4 (2002) 650-661.

- [Chen 2002b] J.K. Chen, W.P. Latham, J.E. Beraun, Axisymmetric modeling of femtosecond-pulse laser heating on metal films, *Numerical Heat Transfer, Part B*, 42 (2002) 1-17.
- [Chen 2002c] J.K. Chen, J.E. Beraun, Thermomechanical response of metal films heated by ultrashort-pulsed lasers, *Journal of Thermal Stresses*, 25 (2002) 539-558.
- [Chen 2003] J.K. Chen, J.E. Beraun, and C.L. Tham, Investigation of thermal response caused by pulse laser heating, *Numerical Heat Transfer, Part A*, 44 (2003) 705-722.
- [Chen 2005] J.K. Chen, D.Y.Tzou, J.E. Beraun, Numerical investigation of ultrashort laser damage in semiconductors, *International Journal of Heat and Mass Transfer*, 48 (2005) 501-509.
- [Chiffell 1994] R.J. Chiffell, *On the wave behavior and rate effect of thermal and thermomechanical waves*, M.S. Thesis, University of New Mexico, Albuquerque, NM, 1994.
- [Dai 1999] W. Dai, R. Nassar, A finite difference method for solving the heat transport equation at microscale, *Numerical Methods for Partial Differential Equations*, 15 (1999) 697-708.
- [Dai 2000a] W. Dai, Y. Zhang, R. Nassar, A Hybrid Finite Element-Alternating Direction Implicit Method for Solving Parabolic Differential Equations on Multi-layers with Irregular Geometry, *Journal of Computational and Applied Mathematics*, 117 (2000) 1-16.
- [Dai 2000b] W. Dai, R. Nassar, A domain decomposition method for solving three-dimensional heat transport equations in double layered thin films with microscale thickness, *Numerical Heat Transfer, Part A*, 38 (2000) 243-256.
- [Dai 2000c] W. Dai, R. Nassar, A compact finite difference scheme for solving a three-dimensional heat transport equation in a thin film, *Numerical Methods for Partial Differential Equations*, 16 (2000) 441-458.
- [Dai 2001a] W. Dai, R. Nassar, A finite difference scheme for solving a three-dimensional heat transport equation in a thin film with micro-scale thickness, *International Journal for Numerical Methods in Engineering*, 50 (2001) 1665-1680.
- [Dai 2001b] W. Dai, R. Nassar, A finite difference method for solving 3-D heat transport equations in a double-layered thin film with microscale thickness and nonlinear interfacial conditions, *Numerical Heat Transfer, Part A*, 39 (2001) 21-33.
- [Dai 2002] W. Dai, R. Nassar, An approximation analytic method for solving dual-phase-lagging heat transfer equations, *International Journal of Heat and Mass Transfer*, 45 (2002) 1585-1593.

- [Dai 2004a] W. Dai, L. Shen, R. Nassar, A convergent three-level finite difference scheme for solving a dual-phase-lagging heat transport equation in spherical coordinates, *Numerical Methods for Partial Differential Equations*, 20 (2004) 60-71.
- [Dai 2004b] W. Dai, G. Li, R. Nassar, L. Shen, An unconditionally stable three-level finite difference scheme for solving parabolic two-step micro heat transport equations in a three-dimensional double-layered thin film, *International Journal for Numerical Methods in Engineering*, 59 (2004) 493-509.
- [Falkovsky 1999] L.A. Falkovsky, E.G. Mishchenko, Electron-lattice kinetics and metals heated by ultrashort laser pulses, *Journal of Experimental and Theoretical Physics*, 88 (1999) 84-88.
- [Fushinobu 1999] K. Fushinobu, L.M. Phinney, Y. Kurosaki, C.L. Tien, Optimization of laser parameters for ultrashort-pulse laser recovery of stiction-failed microstructures, *Numerical Heat Transfer, Part A*, 36 (1999) 345-357.
- [Glass 1985] D.E. Glass, M.N. Ozisik, and D.S. McRae, On the numerical solution of hyperbolic heat conduction, *Numerical Heat Transfer*, 8 (1985) 497-504.
- [Grigoropoulos 1994] C.P. Grigoropoulos, Heat transfer in laser processing of thin films, in: C.L. Tien (Ed), *Annual Review of Heat Transfer*, vol. V, Hemisphere, New York, 1994, 77-130.
- [Herwig 2000] H. Herwig, and K. Becjert, Fourier versus non-Fourier heat conduction in materials with a non-homogeneous inner structure, *Journal of Heat Transfer*, 22 (2000) 363-365.
- [Hoashi 2002] E. Hoashi, T. Yokomine, A. Shimizu, Numerical analysis of ultrafast heat with phase change in a material irradiated by an ultrashort-pulsed laser, *Numerical Heat Transfer, Part A*, 41 (2002) 783-801.
- [Joshi 1993] A.A. Joshi, and A. Majumdar, Transient ballistic and diffusive phonon heat transport in thin films, *Journal of Applied Physics*, 74 (1993) 31-39.
- [Kaye 1973] G.W.C. Kaye, *Tables of Physical and Chemical Constants and some Mathematical Functions*, 14<sup>th</sup> ed., Longman, London, UK, 1973, p.31.
- [Kaba 2004] I. Kaba, "A Numerical Method to Solve the Two-Step Parabolic Heat Transport Equations in a Microsphere Subjected to an Ultrafast Laser Pulse", Ph. D. Dissertation, Louisiana Tech University, LA, 2004.
- [Kaba 2005] I. Kaba, W. Dai, A stable three-level finite difference scheme for solving the parabolic two-step model in a 3D micro-sphere heated by ultrashort-pulsed lasers, *Journal of Computational and Applied Mathematics*, 181 (2005) 125-147.



[Kaganov 1957] M.L. Kaganov, I.M. Lifshitz, and M.V. Tanatarov, Relaxation between electrons and crystalline lattices, *Soviet Physics JETP*, 4 (1957) 173-178.

[Lee 2003] S.H. Lee, J.S. Lee, S. Park, Y.K. Choi, Numerical analysis on heat transfer characteristics of a silicon film irradiated by pico to femtosecond pulse lasers, *Numerical Heat Transfer, Part A*, 44 (2003) 833-850.

[Lee 2005] S.H. Lee, K.G. Kang, Numerical analysis of electronic transport characteristics in dielectrics irradiated by ultrashort-pulsed laser using the nonlocal Fokker-Planck equation, *Numerical Heat Transfer, Part A*, 48 (2005) 59-76.

[Liu 2000] J. Liu, Preliminary survey on the mechanisms of the wave-like behaviors of heat transfer in living tissues, *Forschung im Ingenieurwesen*, 66 (2000) 1-10.

[Lor 1999] W.B. Lor, H.S. Chu, Propagation of thermal waves from a surface or an interface between dissimilar material, *Numerical Heat Transfer*, 36 (1999) 681-697.

[Lor 2000] W.B. Lor, H.S. Chu, Effect of interface thermal resistance on heat transfer in a composite medium using the thermal wave model, *International Journal of Heat and Mass Transfer*, 43 (2000) 653-663.

[Mandelis 1992] A. Mandelis, S.B. Peralta, Thermal wave based materials characterization and nondestructive evaluation of high-temperature superconductors: a critical review, in: R. Kossowsky (Ed.), *Physics and Materials Science of High Temperature Superconductors II*, Kluwer Academic Publishers, Boston, MA, 1992, 413-440.

[Narayan 1991] J. Narayan, V. P. Gosbole, G.W. White, Laser method for synthesis and processing of continuous diamond films on nondiamond substrates. *Science*, 52 (1991) 416-418.

[Opsal 1991] J. Opsal, The application of thermal wave technology to thickness and grain size of aluminum films, in *Metallization: Performance and Reliability Issues for VLSI and ULSI*, SPIE, 1596 (1991) 120-131.

[Ozisik 1994] M.N. Ozisik, and D.Y. Tzou, On the wave theory in heat conduction, *Journal of Heat Transfer*, 116 (1994) 526-535.

[Patanka 1980] S.V. Patanka, *Numerical Heat Transfer and Fluid Flow*, McGraw-Hill, New York, 1980 (Chapter 5).

[Qiu 1992] T.Q. Qiu, C.L. Tien, Short-pulse laser heating on metals, *International Journal of Heat and Mass Transfer*, 35 (1992) 719-726.

- [Qiu 1993] T.Q. Qiu, *Energy dissipation and transport during high-power and short-pulse laser-metal interactions*, Ph. D. Dissertation, University of California, Berkely, CA, 1993.
- [Qiu 1994a] T.Q. Qiu, C.L. Tien, Short-femtosecond laser heating of multi-layer metals I. Analysis, *International Journal of Heat and Mass Transfer*, 37 (1994) 2789-2797.
- [Qiu 1994b] T.Q. Qiu, T. Juhasz, C. Suarez, W.E. Bron, C.L. Tien, Femtosecond laser heating of multi-layer metals II – experiments, *International Journal of Heat and Mass Transfer*, 37 (1994) 2789-2808.
- [Reismann 1980] H. Reismann, P.S. Pawlik, *Elasticity, Theory and Applications*, Wiley, New York, 1980, 135.
- [Shirk 1998] M.D. Shirk, P.A. Molian, A review of ultrashort pulsed laser ablation of materials, *Journal of Laser Application*, 10 ( 1998) 18-28.
- [Swartz 1989] E.T. Swartz, R.O. Pohl, Thermal boundary resistance, *Reviews of Modern Physics*, 61 (1989) 605-668.
- [Smith 1999] A.N. Smith, J.L. Hosterler, P.M. Norris, Nonequilibrium heating in metal films: an analytical and numerical analysis, *Numerical Heat Transfer, Part A*, 35 (1999) 345-357.
- [Tang 1996] D.W. Tang and N. Araki, Non-Fourier heat conduction in a finite medium under periodic surface thermal disturbance, *International Journal of Heat and Mass Transfer*, 39 (1996) 1585-1590.
- [Touloukian 1970a] Y.S. Touloukian, R.W. Powell, C.Y. Ho, and P.G. Klemens, Thermal conductivity, *Thermophysical Properties of Matter*, Vol. 1, IFI/Plenum, New York, 1970.
- [Touloukian 1970b] Y.S. Touloukian, and E.H. Buyco, Specific heat, *Thermophysical Properties of Matter*, Vol. 4, IFI/Plenum, New York, 1970.
- [Tsai 2003] C.S. Tsai, C.I. Hung, Thermal wave propagation in a bi-layered composite sphere due to a sudden temperature change on the outer surface, *International Journal of Heat and Mass Transfer*, 46 (2003) 5137-5144.
- [Timoshenko 1970] S.P. Timoshenko, J.N. Goodier, *Theory of Elasticity*, third edition, McGraw-Hill, 1970.
- [Tzou 1993] D.Y. Tzou, An engineering assessment of the relaxation time in thermal wave propagation, *International Journal of Heat and Mass Transfer*, 117 (1993) 1837-1840.

- [Tzou 1994] D.Y. Tzou, M.N. Ozisik and R.J. Chiffelle, The lattice temperature in the microscopic two-step model, *Journal of Heat Transfer*, 116 (1994) 1034-1038.
- [Tzou 1995a] D.Y. Tzou, A unified field approach for heat conduction from macro- to micro- scales, *Journal of Heat Transfer*, 117 (1995) 1837-1840.
- [Tzou 1995b] D.Y. Tzou, The generalized lagging response in small-scale and high-rate heating, *International Journal of Heat and Mass Transfer*, 38 (1995) 3231-3240.
- [Tzou 1995c] D.Y. Tzou, Experimental support for the lagging behavior in heat propagation, *Journal of Thermophysics and Heat Transfer*, 6 (1995) 686-693.
- [Tzou 1995d] D.Y. Tzou, and Y.S. Zhang, An analytic study on the fast-transient process in small scales, *International Journal of Engineering*, 33 (1995) 1449-1463.
- [Tzou 1997] D.Y. Tzou, *Macro to Microscale Heat Transfer: The Lagging Behavior*, Taylor & Francis, Washington, DC, 1997.
- [Tzou 1999] D.Y. Tzou, Ultrafast heat transport: The lagging behavior, in: *44<sup>th</sup> SPIE's Annual Meeting*, 1999, July 18-22, Denver, Colorado.
- [Tzou 2002a] D.Y. Tzou, Ultrafast transient behavior in microscale heat/mass transport, *Advanced Photon Source Millennium Lecture Series*, Argonne National Laboratories, Chicago, 2000.
- [Tzou 2002b] D.Y. Tzou, Microscale heat transfer and fluid flow, *45<sup>th</sup> SPIE's Annual Meeting*, 2000, July 30-August 4, San Diego, California.
- [Tzou 2001] D.Y. Tzou, and K.S. Chiu, Temperature-dependent thermal lagging in ultrafast laser heating, *International Journal of Heat and Mass Transfer*, 44 (2001) 1725-1734.
- [Tzou 2002] D.Y. Tzou, J.K. Chen, J.E. Beraun, Hot-electron blast induced by ultrashort-pulsed lasers in layered media, *International Journal of Heat and Mass Transfer*, 45 (2002) 3369-3382.
- [Wang 2000] L. Wang, M. Xu, X. Zhou, *Dual-Phase-Lagging Heat Conduction*, Jinan, Shandong University Press, 2000.
- [Wang 2001a] L. Wang, X. Zhou, *Dual-Phase-Lagging Heat Conduction: Problems and Solutions*, Jinan, Shandong University Press, 2001.
- [Wang 2001b] L. Wang, M. Xu, X. Zhou, Well-posedness and solution structure of dual-phase-lagging heat conduction, *International Journal of Heat and Mass Transfer*, 44 (2001) 1659-1669.

- [Wang 2002] L. Wang, M. Xu, Well-posedness of dual-phase-lagging heat conduction equation: higher dimension, *International Journal of Heat and Mass Transfer*, 45 (2002) 1165-1171.
- [Wang 2006a] H. Wang, W. Dai, R. Nassar, R. Melnik, A finite difference method for studying thermal deformation in a thin film exposed to ultrashort-pulsed lasers, *International Journal of Heat and Mass Transfer*, 49 (2006) 2712-2723.
- [Wang 2006b] H. Wang, W. Dai, R. Nassar, R. Melnik, A finite difference method for studying thermal deformation in a double-layered thin film exposed to ultrashort-pulsed lasers, *International Journal of Thermal Sciences*, 45 (2006) 1179-1196.
- [Wang] H. Wang, W. Dai, L.G. Hewavitharana, A finite difference method for studying thermal deformation in a double-layered thin film with imperfect interfacial contact exposed to ultrashort-pulsed lasers, *International Journal of Thermal Sciences*, in press.
- [Wang 2007] H. Wang, “ *A Finite Difference Method for Studying Thermal Deformation in Two-Dimensional Micro Scale Metal Thin Films Exposed to Ultrashort Pulsed Lasers*”, Ph. D. Dissertation, Louisiana Tech University, LA, 2007.
- [Xu 2003] B. Xu, B.Q. Li, Finite element solution of non-Fourier thermal wave problems, *Numerical Heat Transfer, Part B*, 44 (2003) 45-60.